Cape Peninsula
University of Technology

MODELLING AND SIMULATION OF THE CUBE SATELLITE POWER SYSTEMS

by

KHAYA NTUTUZELO DWAZA

Thesis submitted in fulfilment of the requirements for the degree.

Master of Technology: Electrical Engineering

in the Faculty of Engineering & Built Environment

at the Cape Peninsula University of Technology

Supervisor: **Prof. Senthil Krishnamurthy**
Co-supervisor: **Dr. Haltor Mataifa**

Bellville
October 2024

Updated October 2024

DECLARATION

I, Khaya Ntutuzelo Dwaza, declare that the contents of this thesis represent my own unaided work, and that the thesis has not previously been submitted for academic examination towards any qualification. Furthermore, it represents my own opinions and not necessarily those of the Cape Peninsula University of Technology.

Signed **Date: October 2024**

ABSTRACT

The power availability for CubeSat missions critically depends on the efficiency of solar panel power generation, control, and regulation, particularly given the constraints of fitting within a ten cm^3 volume. This thesis focuses on optimizing solar power generation using Maximum Power Point Tracking (MPPT) techniques to maximize the utility of the limited solar panel area available on a CubeSat. A comprehensive comparative analysis of conventional MPPT methods is presented, specifically focusing on the Perturb and Observe (PO) technique chosen for its low computational complexity. The PO MPPT technique was implemented using a DC-DC boost converter and a PV module based on the Azur Space 3G30C datasheet in MATLAB/Simulink. During the implementation, it was observed that without PO MPPT control, the output current, voltage, and power exhibited significant ripple between minimum and maximum levels. With the application of PO MPPT, these outputs stabilized; however, the technique was found to have significant limitations. A critical research gap identified was PO's poor tracking of the Maximum Power Point (MPP) under fast-changing meteorological conditions, coupled with pronounced oscillations around the Global Maximum Power Point (GMPP). The thesis explores advanced MPPT techniques, including a varying step-size PO method, to address these issues, as existing literature suggests. Additionally, the potential of Artificial Intelligence (AI) algorithms—such as Particle Swarm Optimization (PSO), Grey Wolf Optimization (GWO), and Genetic Algorithms (GA)—to enhance PO MPPT performance under varying conditions was investigated. These AI-driven approaches have shown promise in reducing oscillations and improving tracking accuracy at the GMPP. This research introduces a novel hybrid PO-PSO MPPT technique, which combines the simplicity of PO with the global search capability of PSO. Simulation results demonstrated that the hybrid PO-PSO MPPT method significantly mitigates the oscillations at the GMPP, enhances tracking under varying temperature conditions, and stabilizes the output parameters more effectively than conventional methods, including GA-tuned PID controllers and standalone PSO MPPT functions. These findings validate the hybrid PO-PSO approach as a superior solution for optimizing power generation in CubeSat applications, addressing the identified research gaps and providing a robust framework for future small satellite power systems.

Keywords: Maximum Power Point Tracking (MPPT); Perturb and Observe (PO); Maximum Power Point (MPP); Photo Voltaic (PV); Cube Satellite (CubeSat); Pulse Width Modulation (PWM); Proportional Integral derivative (PID) controller; Particle Swarm Optimisation (PSO); integral square error (ISE); integral time absolute error (ITAE); Integral absolute error (IAE); Integral time square error (ITSE); artificial intelligence (AI); global maximum power point (GMPP).

ACKNOWLEDGEMENTS

I wish to thank:

- My Supervisors, Prof S, Krishnamurthy, and Dr. Haltor Mataifa, for their guidance and advice.
- The CPUT Library management and staff for their support and willingness to provide me with the information needed for this study.

The financial assistance of the MerSETA Research Fund and Walter Sisulu study subsidy fund towards this research is acknowledged. Opinions expressed in this thesis and the conclusions arrived at are those of the author and are not necessarily to be attributed to the MerSETA Research Fund and Walter Sisulu study subsidy fund.

DEDICATION

I dedicate this masterpiece of hard work to my late Father and living Mother. Your resiliency is acknowledged. To my wife, thank you for your sacrifice. To my kids, thank you for lending me your TV to be used as an extended screen for this research. To God, our Heavenly Father, thank you for the blessing of knowledge.

For (My parents)

TABLE OF CONTENTS

LIST OF FIGURES

LIST OF TABLES

ABBREVIATIONS AND ACRONYMS

Abbreviation/Acronym

ADCS	Attitude Determination Control system
CubeSat	Cube Satellite
EPS	Electrical Power System
MPPT	Maximum Power Point Tracking
PC&DU	Power Control & Distribution Unit
PV	Photovoltaic
PID	Proportional Integral Derivative
CMC	Command and Data Handling System
PGU	Power Generation Unit
PDM	Power Distribution Module
PCM	Power Control Module
CPP	Consumption Power Profile
MPP	Maximum Power Point
GMPP	Global Maximum Power Point
PO	Perturb and Observe
PSO	Particle Swarm Optimisation
ITAE	Integral Time Absolute Error
ISE	Integral Square Error
IAE	Integral Absolute Error
ITSE	Integral Time Square Error
FOCV	Fractional Open Circuit Voltage
XJT	Next Triple Junction
BOL	Beginning of Life
EOL	End of Life
FSCC	Fractional short circuit current
InC	Incremental conductance

GA	Genetic algorithm
FL	Fuzzy logic
ANFIS	Adaptive Neuro-Fuzzy Inference System
GWO	Grey Wolf Optimisation
OBC	Onboard Computer
TT&C	Telemetry Tracking and Command
TCS	Telecommunication System
Lidar	Light Detection and Ranging
NASA	National Aeronautics and Space Administration
SANSA	South African National Space Agency

List of Mathematical Symbols

I_{ph}	Photovoltaic current
I_o	Diode saturation current
A	Ideality factor of diode
k	Boltzmann constant
E_g	Band gap energy
R_S [Ω]	Series resistance
R_p [Ω]	Shunt resistance
RMSE	Root Mean Square Error
V_{OC}	Open circuit voltage
I_{SC} (*)	Short circuit current
N_s	Number of cells in series
N_p	Number of cells in parallel
V_{mpp} (*)	Maximum power point voltage
I_{mpp} (*)	Maximum power point current
P_{mpp} (*)	Maximum power point power

K_i [A/°C]	Coefficient with temperature of the short circuit current @ STC
T_{ref}	Nominal Temperature

I_{OUT}	Output current
V_{OUT}	Output voltage
V_{OSD}	Desired solar panel output voltage
P_{OS}	Available output power
R	Reliability
T_N	Eclipse period
T_s	Sun period
V_D	Average Voltage
V_d	Discharge Cut-off voltage
η	PV quality factor
η_{ch}	Charge efficiency
X_{b-1}	Redundancy of the battery
A_i	Area of a unit cell
P_{OSD}	Desired solar panel output power
E_f	Efficiency
C	Capacitance
P_N	Required power during an eclipse
G	Solar Irradiance
C	Capacitance

GLOSSARY

Term	Definition
Algorithm	A step-by-step procedure for solving a problem using a computer.
Optimization	A mathematical discipline that concerns the finding of minima and maxima of functions, subject to so-called constraints.
Model	The pursuit of constructing proportionally scaled miniature working representations of the full-sized machine(s).
Modeling and simulation (M&S)	Using a physical or logical representation of a given system to generate data and help determine decisions or make predictions about the system.
PID controller tuning	PID tuning is finding the values of proportional, integral, and derivative gains of a PID controller.
Maximum power point tracking	Maximum PowerPoint Tracking is an algorithm that is included in charge controllers, and it is used for extracting the maximum available power from a PV module.
Direct energy transfer	The energy transfer from a PV panel to the DC-DC converter without using an MPPT algorithm.

CHAPTER 1

THESIS INTRODUCTION AND RESEARCH OBJECTIVES

1.1 Introduction

The smallest Cube Satellite (CubeSat) is a 1U (one unit), and its cubic volume is 10 cm^3. A 1U CubeSat weighs about 1.3 kg. Some of the common 1U extensions are 2U, 3U, and 6U. In a 1U, all satellite subsystems are fitted in a 10 cm^3 cube. The subsystems of a satellite include an electric power system (EPS), attitude determination and control system (ADCS), onboard computer (OBC), telemetry tracking and command (TT&C) system, telecommunication system (TCS), and payload system. The famous CubeSat payload examples are remote sensing (camera/Lidar), Ionosphere characterization, and interplanetary missions. Because of their small size, CubeSats are low-cost and take a short time to develop. Hence, they are used extensively for education, research, and scientific exploration. In 2018, NASA launched a twin CubeSat mission to occult the radio in the Mars atmosphere **(Oudrhiri et al., 2020)**.

CubeSat's electric power system (EPS) ensures robust power delivery and voltage regulation for all other CubeSat subsystems. To design the EPS for a CubeSat, engineers follow one of the two standard architectures: direct energy transfer (DET) or maximum power point tracking (MPPT). Each of the two architectures can be modified to accommodate mission power requirements. The EPS is comprised of power sources (solar panels), power regulation and control (high-frequency switching converters), storage (battery charge regulator and batteries), and loads (subsystems) **(Kumar et al., 2021)**.

A single CubeSat low earth orbit cycle is approximately ninety minutes. The CubeSat experiences a sun and an eclipse period during an orbit cycle. PV power generation, control, and regulation are crucial during the sun period to produce regulated power for charging the batteries and powering all CubeSats subsystems. The battery powers CubeSats subsystems during the eclipse period. The modeling and simulation of the battery charge regulator (BCR) and battery systems are essential for EPS design. However, the work presented in this thesis focuses on PV power generation, control, and regulation for CubeSat power systems. Eliminating the BCR and the battery systems modeling and simulation was done to limit the technical deliverables to four parts. The technical deliverables achieved in this thesis are as follows: PV module modeling, perturb and observe (PO) MPPT, genetic algorithm (GA) PID tunning, particle swarm optimization (PSO) MPPT function, hybrid PO PSO MPPT function for

generated solar power control and regulation implementation for CubeSat power systems. The solar module mounting area is limited to 10 cm^3 for a 1U CubeSat mission. Hence, implementing the MPPT function to extract the maximum solar power generated is crucial for a CubeSat mission. Each module of the Azur space 3G30C module has three cells and produces 2.5V, 0.5A, and 2.5W at MPP when operated under standard test conditions. The standard test conditions are 1367W/M^2 and 28°C. The implemented MPPT design architecture provided a boost converter for each module on each panel side. Each boost converter has its own MPPT controller and is connected either to a 3.3V or a 5V bus line. On each panel side, the Azur space module was connected to the next adjacent module in parallel and had its boost converter. This design paradigm is also beneficial if a single module fails on a particular side while the other module remains functional or is under partial shading conditions (PSC). The remaining functional module connected to a boost converter will produce 5V, 0.223A, and 1W. When both modules on each panel side are functional, they produce 5V, 0.5A, and 2.5W. The direct energy transfer (DET) architecture requires two Azur space modules on each panel side to be connected in series to produce 5V, 0.5A, and 2.5W. This is not an efficient use of available modules. Also, the DET architecture doesn't cater to single module failure on a side or PSC.

1.2 Awareness of the Problem

The problem with solar-generated power is varying irradiation and varying temperature. These varying irradiations and temperatures are inputs of a PV solar array and produce varying DC voltage, current, and power as outputs of a PV solar array. The first worst-case cube orientation pointing towards the sun is when only one of the four adjacent sides points towards the sun. In this first worst case, the expected PV solar array output voltage range is 2V to 3V, the current range is 0.45A ~0.85A, and the power range is ~1.6W to ~2.4W. The second worst-case cube orientation pointing towards the sun is when the top or the bottom side points towards the sun. In this second worst case, the expected PV solar array output voltage range is 2V to 3V, the current range is 0.45A ~1.2A, and the power range is~ 2.4W to ~3.6W (Mahdi et al., 2014). The CubeSat's bus loads voltages are 3.3V and 5V. The bus load impedances will vary for each subsystem connected to the bus lines. A classical solution to a problem of this nature is solved by employing a boost converter between the PV solar arrays and the loads (Fathah et al., 2013).

However, the boost converter's output power oscillates and threatens to damage the feeding electronics. MPPT algorithms improve the maximum power extraction from a solar PV module and dampen the oscillatory output power of boost converters

(Murtaza et al., 2013). Accurate bus voltage levels are problematic to achieve through boost converter's theoretical design equations since converters have power losses. Hence, a GA is used to tune the PID controller-based closed loop boost converter transfer function plant to ensure that bus voltages are achieved. Particle swarm optimization is an alternative algorithm to tune the PID controller-based closed-loop boost converter plant to ensure bus voltages are achieved **(Panduranga Vittal et al., 2021)**. This approach, which uses the PID controller and tuning algorithm like the PSO or the GA, requires the boost converter to be approximated to a transfer function plant and placed before the PID controller. This approximation can be performed through either of the three following methods: linearisation in Simulink, State Space averaging derivation method, or by AC analysis small signal transfer function derivation method. These approximation methods do not accurately represent the nonlinear response of the boost converter.

1.3 Problem Statement

To supply autonomous power for a CubeSat. The EPS subsystem must be designed to efficiently use the PV module's power generation capacity. CubeSat's bus voltage levels must be maintained at 5V and 3.3V independently of PV solar power fluctuations due to space radiation and temperature. CubeSat's bus voltage levels must be maintained at 5V and 3.3V independently of the different load impedances that influence the current demands of load subsystems. The design architecture must cater for PV module partial shading or singular PV module failure on each panel side of the CubeSat.

How can CubeSat's Electrical Power System (EPS) be optimized to maximize power generation efficiency from the PV modules under varying space conditions, such as radiation and temperature fluctuations?

What are the most effective strategies for maintaining stable 5V and 3.3V bus voltage levels in a CubeSat despite fluctuations in PV solar power caused by environmental factors in space?

How do varying load impedances affect the current demands of CubeSat subsystems, and what EPS design architecture best suits these demands while maintaining stable bus voltages?

How can the EPS be designed to maintain optimal power output and voltage levels when the CubeSat experiences partial shading or when a singular PV module fails on any of its panel sides?

What roles do bio-tuning optimization techniques, such as PSO or hybrid algorithms, play in enhancing the resilience of CubeSat's EPS to fluctuations in space radiation and temperature?

How can extreme space radiation and temperature conditions impact the performance of the PV modules and the overall EPS, and how can these impacts be mitigated?

1.4 Research Objectives

Model and simulate the adjacent side of a PV solar panel. Design, model, and simulate a boost converter to control and regulate input and output power. Implement a PO MPPT function to control the duty cycle of the PWM signal controlling the switching element of the boost converter; implement GA PID tuning to a closed loop boost converter plant to approximate the response of a closed loop boost converter plant controlled by MPPT function, Implement PSO PID tuning to a closed loop boost converter plant to approximate the response of a closed loop boost converter plant controlled by MPPT function.

Implement a PSO-based MPPT function to control the duty cycle of the PWM signal controlling the switching element of the boost converter, implement a novel hybrid PO PSO MPPT function to improve the tracking accuracy of both PO MPPT or PSO MPPT functions when implemented unconnectedly, and discus and contrast all the developed MPPT controllers used to control a PV solar module maximum power extraction and regulate the boost coveter output voltage, current and power—benchmark results to existing literature.

1.4.1. Objectives

- Model the Azur space 3G30C PV module using MATLAB/Simulink.
- Design, model, and simulate a boost converter using MATLAB/Simulink.
- Implement PO MPPT function for CubeSat power systems using MATLAB/Simulink.
- Implement GA PID tuning to a closed loop boost converter plant using MATLAB/Simulink.
- Implement PSO PID tuning to a closed loop boost converter plant using MATLAB/Simulink.
- Implement a PSO-based MPPT function using MATLAB/Simulink.
- Implement a novel hybrid PO PSO MPPT function using MATLAB/Simulink.
- Discus and contrast all the developed MPPT controllers and benchmark results to existing literature.

1.5 Hypothesis

This research work is conducted on the presumption that the application of MPPT algorithm or functions will solve the problem of extracting maximum power from a PV module, regulate boost converter output voltage to a fixed bus line level independently of load current demands, and minimize oscillations on the output voltage, current and power produced by boost converters. It also presumes that applying two widely used PID controller tuning optimization techniques, i.e., GA and PSO, will achieve the CubeSat's bus setup voltages for a closed loop boost converter with different optimization response times.

1.6 Delimitation of Research

The study of this project demonstrates the use of a 1U CubeSat model, which can also be adjusted for a 3U CubeSat model. Attitude control is necessary to change the three dimensions of the CubeSat to maximize solar panel sun exposure. The ADCS subsystem performance affects solar power generation. However, this study does not cover attitude correction modeling and simulation as the ADCS subsystem is a master's research field. This study focuses on the EPS subsystem. The modeling and simulation of the battery charge regulator (BCR) and battery systems are essential for EPS design.

However, the work presented in this thesis focuses on PV power generation, control, and regulation for CubeSat power systems. The CubeSat typically has 5V and 3.3V bus lines. However, the design of boost converters, modeling, and simulation only demonstrates 5V implementation. Eliminating the BCR and the battery systems modeling and simulation was done to limit the technical deliverables to four parts. The bio-inspired optimization techniques MATLAB implementation is limited only to GA and PSO for the scope of this thesis. The reason for selecting the GA and the PSO is that they are the most widely used in the available literature. The conventional selected MPPT technique, which is implemented on MATLAB/Simulink modeling and simulation, is limited to the PO technique because of its low computational demand on the OBC microprocessor of the CubeSat compared to FOCV, FSSC, and InC.

1.7. Motivation of the Research

Robust power delivery to other CubeSat subsystems is critical for the longevity of the space mission life cycle. Hence, it is enhanced by applying MPPT techniques to improve PV solar array efficiency**(Solihin et al., 2011)**. The comparative analysis of PID controller tuning optimization techniques applied to a closed loop DC-DC boost converter Simulink model will benchmark future research work where the latest

intelligent controllers and the latest tuning techniques are analyzed in comparative studies**(Garg et al., 2020)**. Table 1.2 shows various intelligent controllers and tuning optimization techniques that can be used with a closed-loop boost converter**(Jayakumaran et al., 2018)**. Regarding bio-tuning optimization techniques shown in this table, the list is not exhaustive of all the methods available in the literature, although it covers several of them (Achiammal, 2017).

Table 1. 1: Intelligent controllers and tuning techniques

Closed Loop Boost Converter		
CubeSat's PV Panel Side Outputs ▪ Voltage: 2V – 3V ▪ Current: ~0.45 – 0.8A ▪ Power: ~1.6W – ~2.4W	**Intelligent controllers**	**PID controllers Tuning with optimization techniques**
	Fuzzy logic controller	Genetic Algorithm (GA)
	Radial basis function neural network	Particle swarm optimization (PSO)
	Probabilistic neural network	Grey wolf optimization
	Adaptive Neuro-Fuzzy Inference System (ANFIS)	Ant-Lion optimisation
	Support vector machine	Whale optimisation
		Bacterial Foraging optimization

1.8. Assumptions

These assumptions are the foundation for the research methodology and analysis, particularly in optimizing power management in CubeSat systems employing MPPT techniques.

- This research assumes that the CubeSat is stabilized with its solar panels facing the Sun. Minimum exposure occurs when at least two sides are exposed to the Sun at any given time (typically one large side if panels are fixed and an adjacent side), and maximum exposure occurs if the CubeSat rotates or its attitude changes; it can expose up to three sides during different parts of the orbit.

- This research assumes that analyzing the two widely used bio-tuning optimization techniques, i.e., GA (Chapter 4) and PSO (Chapters 5 and 6), will provide a benchmark for the expected output signal responses of other latest bio-tuning optimization techniques like GWO, Ant-colony, bee, colony, etc.

- This research assumes that the advantage of PO in terms of low hardware and software complexity will outweigh its reasonable tracking of the GMPP during fast-changing weather conditions. If there is a need to modify the PO function for fast-varying weather conditions, AI algorithms will be investigated for CubeSat implementation in conjunction with the PO. In Chapter 6, tracking of

the global maximum power point (GMPP) by PO is poor under fast-changing temperatures, and combining PO and PSO MPPT improved tracking at fast-changing temperature conditions and oscillations at the GMPP.

- This research assumes that the maximum power demand by any CubeSat subsystem of a 1U to a 3U CubeSat will not exceed 11W, as seen in a paper by Ali et al., 2021. It assumes that the maximum CubeSat's current demand will not exceed 2200mA for any 1U to 3U CubeSats for a 5V bus distribution line, as seen in Table 2.2 of Chapter 2.

- The top and the bottom sides are mounted Spectro lab solar cells, and the output power of the top or the bottom sides is assumed to be the same as one of the adjacent sides (Chapter 2).

These assumptions underpin the research methodology for developing and optimizing MPPT techniques specifically designed for CubeSats, targeting to enhance their operational efficiency and extend mission lifetimes in the challenging environment of space.

1.9. Research Methodology

The diagram in Figure 1.1 shows the development process followed in designing actual models in MATLAB/Simulink. Firstly, the PV array model is modeled in Simulink using the Azur 3G30C datasheet to model the PV power generated by the modules mounted on the four adjacent sides of the cube. Secondly, the boost converter for a 4x1 array side is developed in Simulink. Thirdly, the GA and the PSO tunned PID controllers and the closed loop boost converter transfer function plant are modeled in Simulink, and fourthly, PO, PSO, and hybrid MPPT controllers are designed in Simulink.

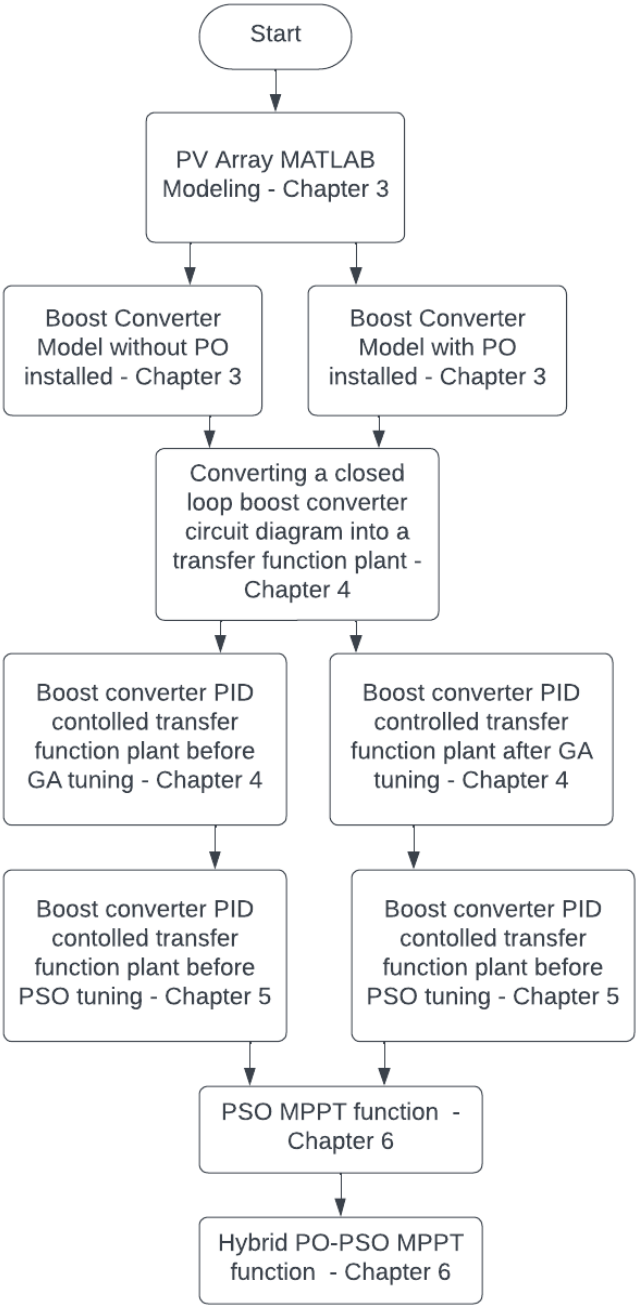

Figure 1. 1: MATLAB/Simulink model's development process

1.9.1. Model development

- The solar PV array modeling and simulation are conducted using Simulink.
- Modelling of the boost converter is conducted using Simulink.
- Modelling of PO MPPT control implementation is conducted using Simulink.

The Simulink Model in Figure 1.2 shows the PV model measurements on the far left, the PV array and the boost converter plant on the bottom, the PO MPPT on the top, and the boost converter outputs on the far left.

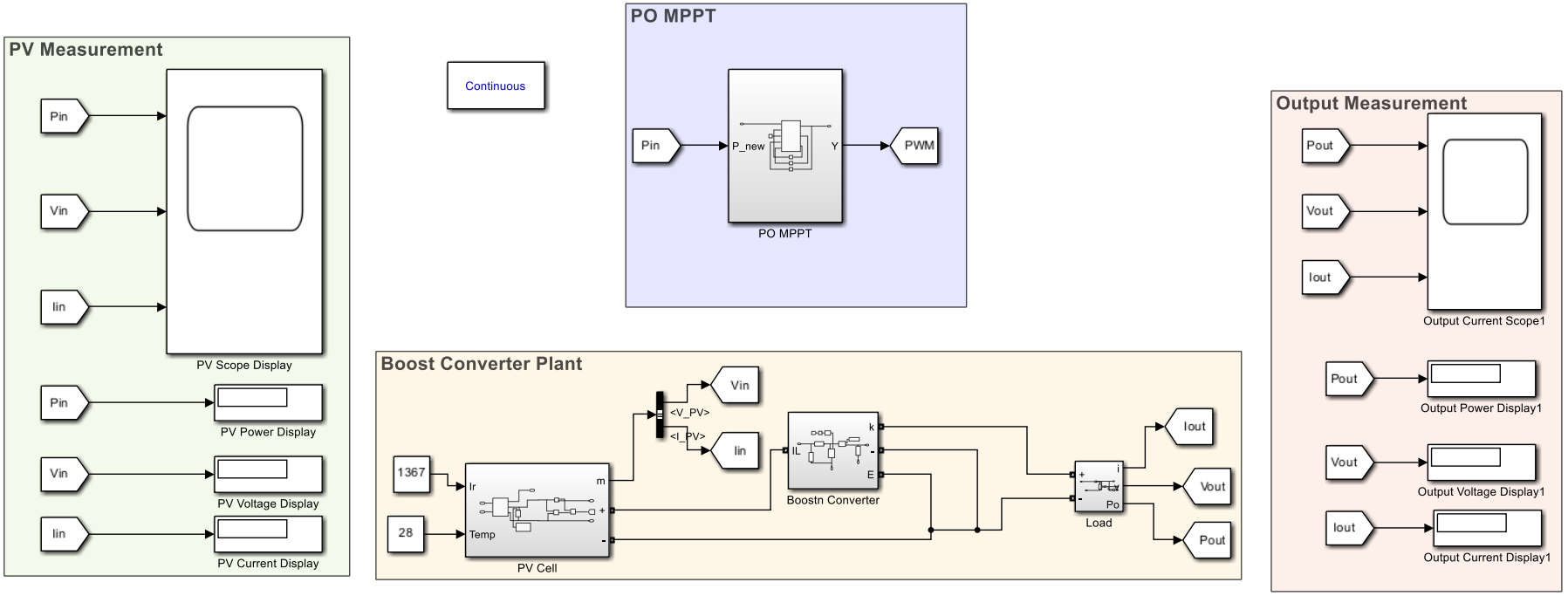

Figure 1. 2: PV array modeling and PO MPPT control modeling

- A closed-loop boost converter transfer function plant was developed using MATLAB/Simulink linearisation for GA/PSO-tuned PID-controlled transfer function closed-loop plant.
- The setup of the GA-tuned PID controlled transfer function closed loop plant was used (substituting the GA algorithm with the PSO algorithm) with the ITAE cost function as the objecting function of the PSO algorithm in a MATLAB script file.

Figure 1.3 shows the GA-tuned PID-controlled transfer function closed loop plant.

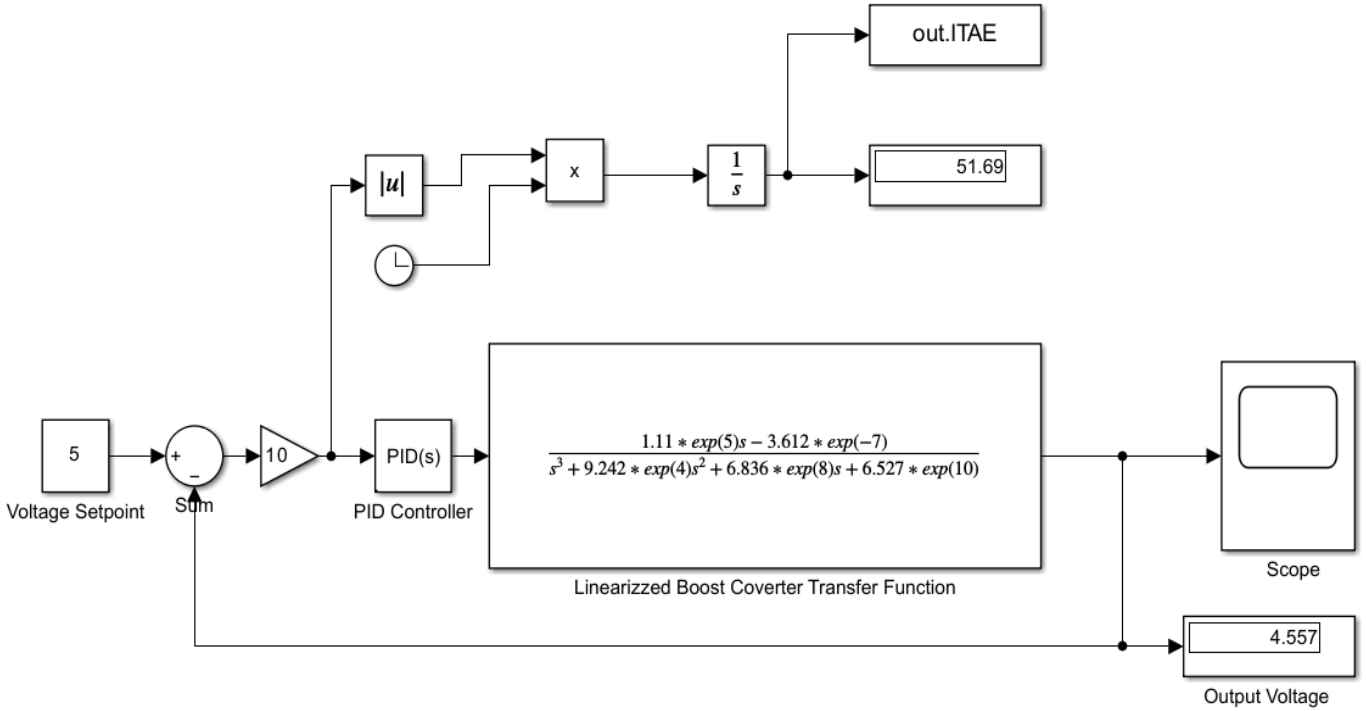

Figure 1. 3: GA-tuned PID controlled transfer function closed loop plant modeling

- PSO MPPT algorithm was implemented as a MATLAB function in the boost converter plant without converting the boost converter into a transfer function in MATLAB/Simulink.
- The hybrid PO PSO MPPT model was developed in MATLAB/Simulink.

Figure 1.4 shows the hybrid PO-PSO MPPT MATLAB/Simulink model, PV model measurements on the far left, the PV array and the boost converter plant on the bottom, the hybrid PO-PSO MPPT on the top, and the boost converter outputs on the far left.

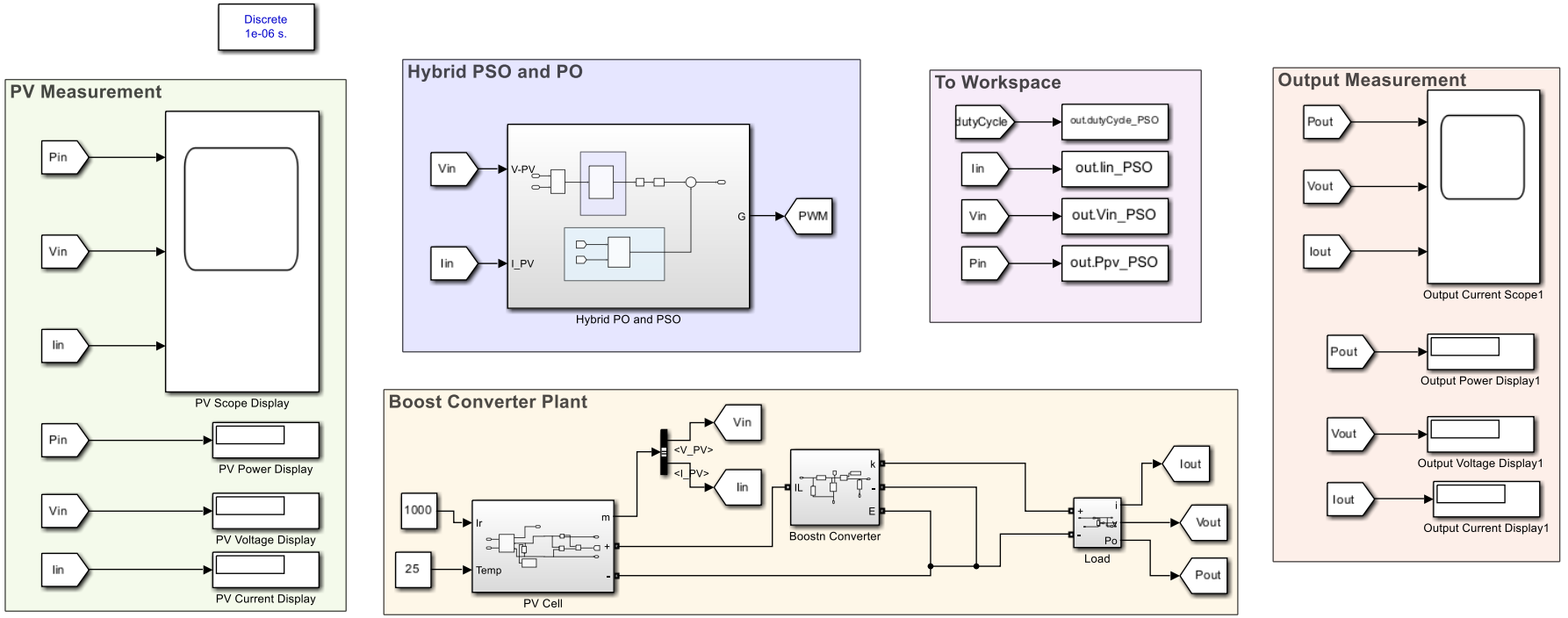

Figure 1. 4: PV array modeling and Hybrid PO PSO MPPT control modeling

1.9.2. Algorithm development

In PO, the duty cycle is perturbed in one direction, and if the PV panel power continues to increase, the perturbing continues in that direction. If the new power is less than the old power, it will perturb in the opposite direction. Once the algorithm reaches the maximum power point (MPP), it oscillates around it. Figure 1.5 shows the PO flowchart, where the delta is the perturbed dutycycle.

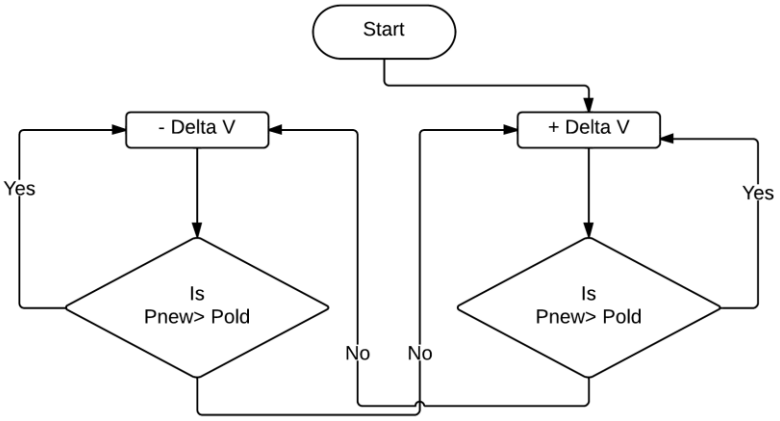

Figure 1. 5: The basic flowchart of the PO MPPT function

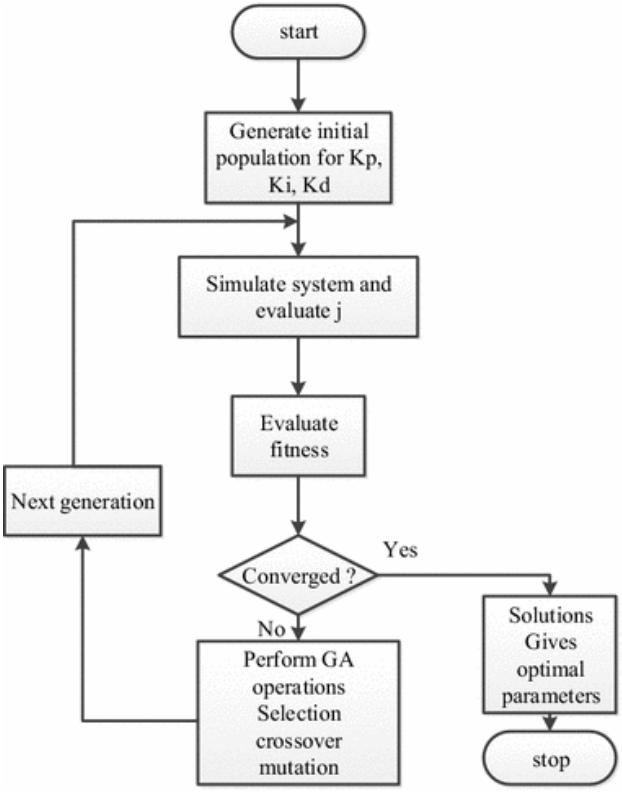

Figure 1.6: The GA and the PSO ITAE flow chart

In Figure 1.6, the GA optimization is implemented using the ITAE performance index as an objective function to minimize an error of the closed loop boost converter plant.

This error is taken before the Simulink model PID controller and sent to the MATLAB script function using the “To workspace” function block. The ITAE objective function is then called to the GA application program for minimization. Similarly, PSO optimization is implemented using the ITAE performance index as an objective function to minimize an error of the closed loop boost converter plant. This error is taken before the Simulink model PID controller and sent to the MATLAB script function using the “To workspace” function block. The ITAE objective function is then called to the PSO script file for minimization.

1.9.3. System simulation and performance analysis

- In the PO MPPT, PSO MPPT, and hybrid PO PSO MPPT, the Simulink models’ simulation is performed by pressing “run” on the Simulink model, and the boost converter output results of voltage, current, and power can be viewed on the output displays and output characteristics curves viewed on the scopes. Also, MPPT can be viewed from the output of the PV array (input of the boost converter) using scopes and displays.

- In the GA and PSO PID tuning, the PID gain values are optimized on the MATLAB script file using the ITAE cost reduction code. The results of the optimized gain values replace the gain variables K(1), K(2), and K(3) on the PID Simulink block. The operator presses run on the Simulink model, and the output results of voltage, current, and power can be viewed on the output displays. Output characteristic curves can be viewed from the scope.

1.10. Main Research Outputs

- Published a paper in the proceedings of the SAPEC 2024 conference; the paper is titled “Application Perturb and Observe Maximum Power Point Tracking Technique for CubeSat Power Systems.” The conference proceeding was published by IEEE Explore as follows:
- K. Dwaza and S. Krishnamurthy, "Application Perturb and Observe Maximum Power Point Tracking Technique for CubeSat Power Systems," 2024 32nd Southern African Universities Power Engineering Conference (SAUPEC), Stellenbosch, South Africa, 2024, pp. 1-5, doi: 10.1109/SAUPEC60914.2024.10445093.
- Compiled a comprehensive literature review on the modeling and simulation of PV solar modules and the modeling and simulation of the power regulation and control system for a CubeSat EPS.

- Modelled and simulated one diode/ two resistors (1D/2R) PV array Simulink mathematical model using 3G30C datasheet.
- The PO MPPT technique was implemented in Simulink, and the percentage increase in the output power yield was assessed by comparing the output of the MPPT-controlled PV array with that without the MPPT controller.
- A closed-loop boost converter transfer function plant model was developed using MATLAB/Simulink linearisation tool. The PID controller was placed before the plant to create a dynamic response and reduce the steady-state error. The PID controller gains were automatically tuned using GA and PSO algorithms to minimize the system's steady-state error.
- PSO MPPT algorithm was implemented as a MATLAB controller function with the boost converter powered by a PV array. The analysis was simulated without converting the boost converter into a transfer function.
- The hybrid PO PSO MPPT model was developed and simulated in MATLAB/Simulink.

1.11. Thesis Outline

Chapter 2 discusses and presents previous work concerning the modeling and simulation of PV solar modules and the modeling and simulation of the power regulation and control system for a CubeSat EPS. The literature reviewed focuses firstly on PV solar module mathematical modeling using Simulink, secondly on the MPPT functions comparison, thirdly on PID controllers used to minimize the steady-state error of a closed-loop boost converter plant, and tuning of those PID controllers using artificial intelligent (AI) techniques like particle swarm optimization (PSO), genetic algorithm (GA), fuzzy logic (FL), etc., Fourthly on MPPT algorithms which use AI algorithms like PSO, and lastly on MPPT enhancement techniques which are implemented as a hybrid combination of the MPPT functions like PO function and AI algorithms like PSO, for a CubeSat EPS.

Chapter 3 implements the Azur Space 3G30C solar module's mathematical modeling in MATLAB/Simulink. One side of the four adjacent sides of the 1U cube is mounted with two modules to form one side panel. One side panel is connected to a PO MPPT controller for maximum power extraction from any PV side panels in the CubeSat architecture. Boost converter designs are implemented for a 3.3V and a 5V bus. At the end of Chapter 3. a comparison of how the power, voltage, and current characteristics respond to the application of the PO function and without it is demonstrated. Chapter 4 is about representing the PV generation, boost converter control, and regulation to maintain the fixed 5V and 3.3V bus lines in the event of boost converter current loads

variation demanded by satellite subsystems by a model with a DC battery, GA-tunned PID controller, a closed loop boost converter transfer function plant and a reference set point bus level of either 5V or 3.3V. A battery replaced the Simulink PV side panel model. The battery is set to the minimum input voltage position of the voltage range. For example, if the PV input voltage range is 2V to 3V, the battery in the boost converter is set to 2V. The approximation of the boost converter into a transfer function is performed using the linearisation in MATLAB/Simulink. The boost converter transfer function plant becomes the controlled device while the PID controller is placed before it to develop a dynamic response and to reduce the steady-state error. The output of the boost converter plant is connected as a negative unity feedback loop. The PID controller gains parameters Kp, Ki, and Kd, which are tuned by the genetic algorithm (GA); the steady-state error is minimized using integral time absolute error (ITAE). The model is simulated in MATLAB/Simulink, and the results are obtained.

Chapter 5 begins with the state space averaging derivation method and AC analysis small signal transfer function derivation method to obtain a transfer function for a closed loop boost converter plant. Then, the theoretically derived state space and transfer functions are compared to the linearisation of Simulink-generated state space and transfer function. Approaching the end of the chapter, the GA tuning in Chapter 4 is replaced by PSO tuning using the same model. At the end of the Chapter, the PSO algorithm is used as the MPPT function in MATLAB/Simulink. The models were simulated, and the results were obtained.

Chapter 6 implements a hybrid MPPT. This hybrid MPPT is comprised of the PO function and the PSO algorithm, and together, they control the duty cycle of the PWM. The PWM is connected to the boost converter's MOSFET. The boost converter is a power regulator that solves the fluctuating PV output voltage, current, and power, which are subject to meteorological conditions; it also solves the load, voltage, current, and energy, which are variable and are subject to the load current demand of each connected subsystem of the CubeSat.

The results of the PO MPPT (implemented in Chapter 3) are compared with the novel hybrid PO PSO MPPT (implemented here in Chapter 6). The results of the GA-tuned PID controlled transfer function closed loop plant (implemented in Chapter 4) are compared with the hybrid PO PSO MPPT (implemented in Chapter 6). Also, the results of the PSO algorithm (implemented in Chapter 5) are compared with the results of the hybrid PO PSO MPPT (implemented in Chapter 6). Chapter 7 briefly discusses the

primary outcomes of this research thesis, as per the projected research outputs as enumerated in Section 1.4, Chapter 1.

1.12. Conclusion

This thesis presents control and regulation strategies used to extract the maximum solar power source for an EPS of a CubeSat. The control and regulation strategies are PO MPPT function, GA/PSO tuned PID controller for a closed loop transfer function plant, PSO MPPT function, and a hybrid PO PSO MPPT function. This chapter conceptualizes the research by stating the problem the study seeks to solve, the research aim, the envisaged research outcomes, and the methodology followed in achieving the research objectives. The following chapter provides an overview of the literature work consulted for the modeling of PV array, mathematical calculation of boost converter component values, state space and transfer function modeling of boost converter, overview performance comparison MPPT algorithms, overview comparison of intelligent PID controllers, and overview comparison PID tuning bio-inspired algorithms.

CHAPTER 2

REVIEW OF THE MODELLING, CONTROL, AND REGULATION OF SOLAR POWER GENERATION FOR CubeSat POWER SYSTEMS

2.1. Introduction

This Chapter aims to discuss and present previous work concerning the modeling of both PV solar modules and power regulation and control of a CubeSat EPS. The literature reviewed focuses firstly on solar panel mathematical modeling using Simulink, secondly on the classical MPPT techniques comparison for application in a CubeSat EPS, thirdly on MPPT enhancement techniques which are implemented using PID controllers in a closed loop boost converter/buck converter, and tuning of those PID controllers using artificial intelligent methods like particle swarm optimization (PSO), genetic algorithm (GA), fuzzy logic (FL), etc. The literature based on battery charge regulator storage systems has not been reviewed since it is outside the scope of the thesis. Subsection 2.2 discusses PV mathematical modeling and simulation in MATLAB/Simulink. Subsection 2.3 discusses power regulation and control using switch power converters. Subsection 2.4 discusses conventional MPPT objective functions, hybrid MPPT techniques, and PID controllers applied to boost converters transfer function plants, and finally, subsection 2.5 discusses various Cube Satellite missions.

2.2. Solar PV Mathematical Modelling and Simulation in MATLAB/Simulink

The modeling of solar PV cell blocks in the Simulink library is crucial. Simulink makes it possible to accurately model the behavior and performance of the solar cell blocks in the library for various irradiations and temperatures (Nair & Linda, 2019). The benefit of mathematical modeling is that it gives access to adjust the performance characteristics of the solar PV cell blocks the same way the manufacturer would create the solar PV cell blocks in Simulink using the manufacturer data sheet specifications. This modeling allows for adjusting solar PV cell block parameters like ideality factor for polycrystalline and mono-crystalline PV cells according to CubeSat manufacturer specifications.

If the number of cells in a series is equal to one and the number of cells in parallel is equal to one, then that is a PV cell. If the number of cells in a series is more significant than one and the number of cells in parallel equals one, then that is a PV module. However, if the number of cells in both series and parallel is more significant than one, we have a PV array (Hoarca, 2021). A gap is identified in the 202a Simulink library, and numerous PV cell blocks are available for various PV cell manufacturers. The dominant PV cell manufacturers for CubeSat applications are Spectrolab and AZUR SPACE, but

neither PV cell block is currently available in the Simulink library. Creating Spectrolab and AZUR SPACE PV cells in the Simulink library will benefit the users doing research and CubeSat space mission applications for education and scientific explorations. Hence, in Chapter 3, the mathematical modeling of the Spectrolab and AZUR SPACE PV cells is modeled using Simulink/MATLAB according to the manufacturer's datasheet. A PV module connects two or more PV cells in series and no cells in parallel. It can be modeled in Simulink using the physics principle of a PN junction **(Weixiang et al., 2011)**.

The IV and the PV characteristic curves of the PV module are nonlinear and vary with the rate of change of the irradiation and the rate of change of the temperature exposed to the sun (Krismadinata et al., 2012). Numerous PV modules are available in the Simulink library, but AZUR space and Spectrolab PV modules are unavailable. Most CubeSat launched in orbit used the AZUR space and Spectrolab PV modules (Rabochová et al., 2018). Hence, the mathematical modeling of the AZUR space and Spectrolab PV modules in Simulink is a research gap addressed in this thesis.

The PV solar cell is modeled from first principles using five algebraic current equations: Photocurrent, Diode saturation current, Reverse saturation current, Shunt Resistor current, and Output current. Photocurrent (Iph) is current directly proportional to the incident solar irradiation from the sun. The diode saturation current (ID) is the forward bias current present only when the photocurrent is present. The reverse saturation current (Irs) is the avalanche current in the reverse bias condition that must not be exceeded. The shunt resistor current (Ish) is the nonideality current that flows through the shunt resistor and represents the slope of the current on the IV characteristic curve.

The output current (I) is the generated nonideality current that flows through the series resistor. It also represents the voltage slopes across the maximum point of the IV characteristic curve **(Hoarca, 2021)**. Table 2.1 shows a summarised previous work reviewed in this thesis. Figure 2. 1 shows the same information in terms of a bar graph. Table 2.2 and Figure 2.2 show the list and the bar graph for the number of publications reviewed for each subsection of Chapter 2: solar PV mathematical modeling and simulation in MATLAB/Simulink, power regulation and control using switch power converters, PID controllers and MPPT functions, and various CubeSat missions **(Kabaca et al., 2015)**.

Table 2.1 summary of the reviewed work

Source	Year of plublication	No. of sources consulted
Mohan	1995	1
Midya et al,	1996	1
Brambilla et al,	1999	1
Kim et al,	2001	1
Dahlquist	2002	1
Park	2003	1
Rashid	2004	1
Esram et al, Cheikh et al	2007	2
Asif, Tsai et al, Liu et al,	2008	3
Larbes et al, Villalva et al	2009	2
Weixiang et al, Solihin, Neji et al, Rai et al, Bazzi et al	2011	5
Ali et al,	2012	1
Murtaza et al, Fathah, Haripriya et al, Krismadinataa et al, Reisi et al, Hemmo, Moradi et al, Chen et al	2013	8
Mahdi et al, Lowe et al, Abdulkadir et al, Jayachitra et al	2014	4
Singh et al, Kabaca et al, Sirin, Sheard, Harrag et al,	2015	5
Shrivastav at al, Viswambaran et al, Waghulde et al, Agarwal et al, Sheik Mohammed et al, Ahmed et al,	2016	6
Achiammal, Guter et al, Lasheen et al, Mohanty et al, Manickam et al, Robles Algarín et al,	2017	6
Jayakumaran et al, Salman et al, Kler et al, Priyadarshi et al, Batarseh et al, Dhieb et al,	2018	6
Sher & Baig, Bani Salim et al, Bjaoui et al, Yang et al, Priyadarshi et al, Bani Salim et al, Acharya et al, Ammar et al,	2019	8
Chen et al, Pathak et al, Garg et al, Yaqoob et al, Oudrhiri et al, Haji et al, Kamran et al, Parvaneh et al, Mirza et al, Garud etal, Erikson, Bollipo et al, Da Rocha et al, Pilakkat et al, Ali et al, Refaat et al, Zečević et al,	2020	17
Routray et al, Hoarcă, Aoughlis et al, Ali et al, Kumar et al, Fathi et al, Saidi et al, Aminnejhad et al, Tao et al, Banakhr et al, Sudharshan et al, Jihad et al, Fahim et al, Villegas-Mier et al, Nkambule et al,	2021	16
Edpuganti et al, Radi et al, Mohammed et al, Shinde et al, Mataifa et al, Yaqoob et al, Devarakonda et al, Priyadarshi et al, Allahabadi et al, Devarakonda et al, Mahfoud et al,	2022	11
Takano et al, Jumshudlu et al, Ibrahim et al, Saleem et al, Mirza et al, Tadj et al, Elmetwaly et al, Manna et al, Kayisli et al, Aguila-Leon et al, Vankadara et al, Aika, Sulthana et al, Katche et al, Hassan et al, Mohamed et al, Wang et al, Sharma et al,	2023	18
Kumar et al, Jasim et al, Radeen et al, Veerasamy et al, Jiang et al 2024, Chandrashekar et al, Oubbati et al , Murugesan et al,	2024	8

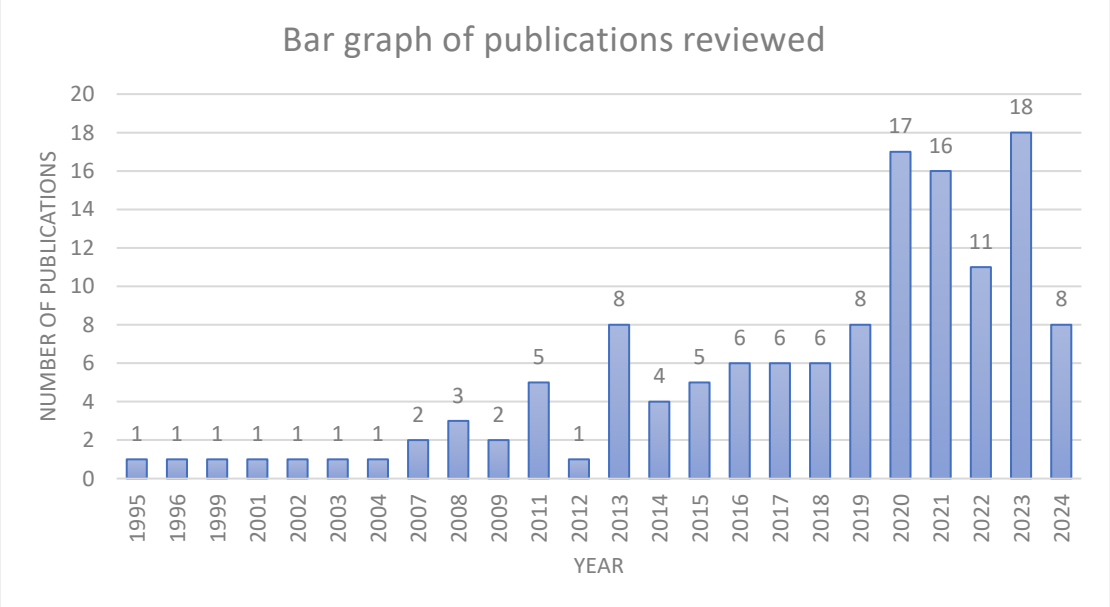

Figure 2.1: Bar graph of the publications reviewed

Table 2.2 shows the list of reviewed papers for each subsection of Chapter 2. The subsections of Chapter 2: solar PV mathematical modeling and simulation in MATLAB/Simulink, power regulation and control using switch power converters, PID controllers and MPPT functions, and various CubeSat missions.

Table 2.2: Number of Reviewed Papers for each subsection of Chapter 2

Source	Number of Sources Reviewed	Subsections
Krismadinata et al (2012), Chek et al (2021), Álvarez (2021), Rabochová (2018), Villalva (2009), Dahbi (2015), Weixiang (2011), Keskin (2015), Essaadi (2016), Hoarcă (2005), Tsai (2008)	11	2.2. Solar PV mathematical modelling and simulation in MATLAB/Simulink
Fathah (2013), Haripriya et al (2013), Kazimierczuk et al (2016), Godina et al (2020), Nguyen et al (2020), Blaabjerg (2019), Tan and Hoo (2015), Al-Baidhani et al (2018), Sarif et al (2018), Mocci et al (2014), Cao (2023)	11	2.3. Power Regulation and Control using Switch Power Converters
Abdulkadir et al (2014), Aguila-Leon et al (2023), Allahabadi et al (2022), Aminnejhad et al (2021), Ammar et al (2019), Aoughlis et al (2021), Moradi (2013), Ali et al (2020), Pilakkat and Kanthalakshmi (2020), Manickam et al, (2017), Mohanty and Subudhi (2017), Chandrashekar et al (2024), Veerasamy et al (2024), Ali et al (2020),	13	2.4. PID controllers and MPPT Functions
Yaqoob et al (2022), Oudrhiri et al (2020), Kumar et al (2021), Nasir et al (2020), Neji et al (2011), Salehinia et al (2017), Park (2003), Hernandez (2015), Siciliano (2022), Hemmo (2013), Ali (2020)	11	2.5. Cube Satellites Missions

Figure 2.2 shows the bar graph for the subsections of Chapter 2.

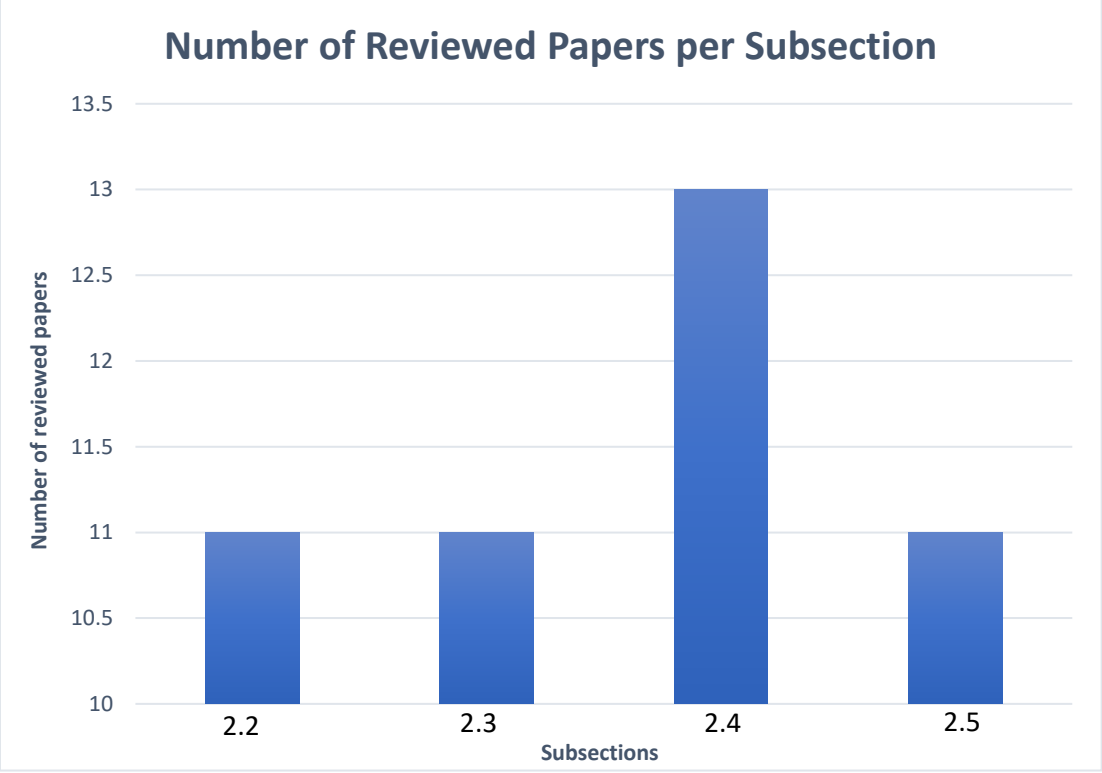

Figure 2.2: Papers Reviewed per subsection of Chapter 2

2.3. Power Regulation and Control using Switch Power Converters

DC-to-DC converters can be used to step up or step down DC voltage. Hence, they are used for voltage regulation. These DC-to-DC converters, also known as choppers, are used for traction motor control in electric automobiles, trolley cars, marine hoists, forklift trucks, and mine haulers. They deliver high efficiency, reasonable acceleration control, fast dynamic response, and are less bulky than linear converters **(Mohamed et al., 2016)**.

To achieve the step-down, the switching component, i.e., power BJT, power MOSFET, GTO, forced commutated thyristor, must be connected in series to the output load resistor and diode connected in parallel to the load to prevent load current from flowing back to the source. To achieve the step-up, the switching component must be connected in parallel to the load resistor and the diode in series to the load to prevent the load current from flowing back to the source voltage. In step up and step down, the duty cycle must be varied between 0 and 1 to control the output voltage (Fathah, 2013).

2.3.1. Recent Developments in DC-DC Converter Technologies

2.3.1.1. Overview of DC-DC Converter Topologies

DC-DC converters are critical components of modern power electronics, providing effective voltage conversion across various applications. The three primary topologies-buck, boost, and buck-boost converters—remain subject to intensive study and development. These converters are critical in delivering controlled voltage levels required for operating a wide range of electronic equipment, from portable gadgets to sophisticated industrial systems.

2.3.1.2. Buck Converter: Advancements and Applications

The buck converter, a step-down regulator, remains widely used due to its efficiency, simplicity, and reliability. Its principle of operation involves the high-frequency switching of a transistor (usually a MOSFET), which controls energy transfer from input to output, with an inductor storing energy when the switch is on and delivering it to the load when the switch is off. Recent studies have highlighted the continuous evolution of buck converters, particularly in terms of reducing size, improving efficiency, and enhancing control strategies.

Recent Advancements:

- Buck Converter Synchronous Rectification: This technique, which replaces the diode with a low-RDS (on) MOSFET, has been shown to reduce conduction losses, thereby improving overall converter efficiency notably **(Wang et al., 2023)**.
- Buck Converter Digital Control Techniques: The change towards digital control methods, such as adaptive on-time control and predictive control, has improved the dynamic response and adaptability of buck converters in several applications **(Albira and Zohdy, 2021)**.
- Integrated Circuits: The integration of multiple components into a single chip has not only reduced the physical size of converters but also enhanced their reliability and performance in high-frequency applications**(Cheon et al., 2024)**

Applications:

Buck converters are important in consumer electronics, electric vehicles, and renewable energy systems' power management systems. They are particularly valued for their ability to provide stable and efficient power conversion in environments where space and energy efficiency are at a premium **(Sharma et al., 2023)**.

2.3.1.3. Boost Converter: Enhancements and Use Cases

The boost converter, reliable for stepping up voltage from input to output, continues to be a research subject due to its importance in applications requiring higher output voltages. The operation involves energy storage in an inductor during the "on" phase and release during a switch's "off" phase.

Key Developments:

- Boost Converter High-Frequency Operation: Recent advancements have focused on increasing the switching frequency, which allows for smaller inductors and capacitors, thereby reducing the overall size and improving the power density of the converters **(Kumar et al., 2024)**.

- Advanced Switching Devices: The use of GaN and SiC transistors has enhanced the performance of boost converters, enabling them to operate at higher efficiencies and temperatures, making them suitable for more demanding applications **(Mehrotra et al., 2024)**.

- Enhanced Control Algorithms: Researchers have developed more sophisticated control algorithms to improve boost converters' stability and

transient response, especially under varying load conditions **(Mohammed, 2024)**.

Applications:

Boost converters are critical in applications such as battery-powered devices, where they ensure that the voltage level is maintained even as the battery discharges, and in renewable energy systems, where they step up the voltage from solar panels to suitable levels for storage or grid connection **(Abdul Zahra et al., 2024)**.

2.3.1.4. Buck-Boost Converter: Versatility and Innovations

The buck-boost converter's capability to either step up or step down the input voltage makes it highly flexible, especially in applications where input voltage can vary significantly. This converter combines the principles of both buck and boost converters and operates by switching a transistor to control the energy transfer through an inductor.

Recent Innovations:

Buck-boost Multi-Mode Operation: Advanced buck-boost converters can dynamically switch between buck, boost, and buck-boost modes, providing greater flexibility and efficiency across a wider range of input conditions **(Salah Hilo Mohammed Al-Attwani et al., 2024)**.

Improved Efficiency: Researchers have developed techniques such as zero-voltage switching (ZVS) and zero-current switching (ZCS) to minimize switching losses, thereby improving the efficiency of buck-boost converters **(Koushki et al., 2024)**.

Integrated Power Modules: The trend towards integrating multiple power stages into a single module has reduced the size and improved the performance of buck-boost converters in compact applications **(Fekik et al., 2024)**.

Applications:

The versatility of buck-boost converters makes them ideal for battery management systems, portable electronic devices, and renewable energy systems where they are required to manage fluctuating input voltages and maintain stable output **(Sharma et al., 2023)**.

2.4. Conventional MPPT, AI MPPT, and PID Controller-based MPPTs

This section will discuss traditional MPPT first, second, AI MPPT, and finally, PID controller-based MPPTs.

2.4.1. Requirements for the Implementation of MPPT Techniques

The output voltage of an AZUR space solar module varies according to temperature and radiation. The 4G32C AZUR space PV solar module, which is 8X4cm, produces 3.025V and 433.5mA at maximum power point (MPP = 1.31W) under the radiation of 1367W/m^2 and 28°C standard test conditions. The change in maximum point voltage per temperature change is -8.4mV/°C at the beginning of life (BOL), and the change in maximum current per temperature change is 0.03mA/°C at the BOL. If the space radiation is kept constant at 1367W/m^2 and the expected space maximum temperature is 125°C, then the maximum point voltage at 125°C is calculated to be 3.84V. Similarly, If the space radiation is kept constant at 1367W/m^2 and the expected space minimum temperature is -65°C, the maximum point voltage is calculated to be 2.24V. These solar modules are connected in parallel so that even when only one module is exposed to the sun, a voltage not under 2V may be expected. Generally, the bus voltages of a CubeSat are 3.3V and 5V, respectively, and the load current demand will vary for each CubeSat subsystem.

Therefore, boost converters must increase the DC PV module output voltage range of 2.24V – 3.84V to 3.3V and 5V bus voltages. The DC PV module output voltage ranges between 2.24mV for -65°C to 3.84mV for 125°C when space radiation is kept constant at 1367W/m^2. The four control and regulation methods extracted from a vast literature study which are implemented in this Thesis are the PO MPPT function, GA/PSO tuned PID controller for a closed loop transfer function plant, PSO MPPT function, and a hybrid PO&PSO MPPT function. It is now clear that two boost converters for the 3.3V bus and the 5V bus must be designed. It is now clear that each module is connected to a 3.3V and 5V boost converters, and all the modules are connected in parallel so that even when only one module is exposed to the sun, a voltage not under 2V may be expected. Table 2. 2 depicts the maximum current demand per CubeSat consulted research paper. According to Table 2. 2, the 3.3V converter must produce a minimum current of 1.304mA and 4.303W, and the 5V converter must produce a minimum current of 2.2A and 11W to support the current demands of all CubeSat subsystems in Table 2.2.

Table 2. 3: Maximum Current demand per CubeSat research paper

CubeSat Research Paper Author(s)	Maximum current (mA) Demand for 5V Bus	Maximum Power Demand for 5V Bus	Maximum current Demand for 3.3V Bus	Maximum Power Demand for 3.3V Bus
(Mahd et al., 2014)	100mA - Payload	0.5W	850mA – TX coms	2.81W
(Kumar et al., 2021)	626.2mA – RF coms	3.131W	1304.1mA – TT&C and OBC	4.303W
(Chen et al., 2021)	600mA – UHF RX	3W	151.5mA - OBC	0.5W
(Agarwal et al., 2016)	750mA – Battery charging	3.75W	300mA - Payload	1W
(A. J. Ali et al., 2021)	2200mA - Coms	11W	-	-
(Acharya et al., 2019)	240mA - ADCS	1.2W	121.2mA - OBC	0.4W
(M. B. O. E. Ali et al., 2021)	245mA - ADCS	1.225W	568mA - Coms	1.874W

All EPS architectures can be divided into two classes from the viewpoint of energy transfer techniques: Maximum Power Point Trackers (MPPT) and Direct Energy Transfer (DET) subsystem (Shekoofa and Kosari, 2013). With certain modifications, these two architectures are implemented based on the satellite project requirements (Kumar et al., 2021). Figure 2. 6 depicts the direct energy transfer architecture. This architecture has four major sections: source, storage, power distribution unit (PDU), and loads. This architecture requires a shunt regulator (SR) and a battery charging regulator (BCR).

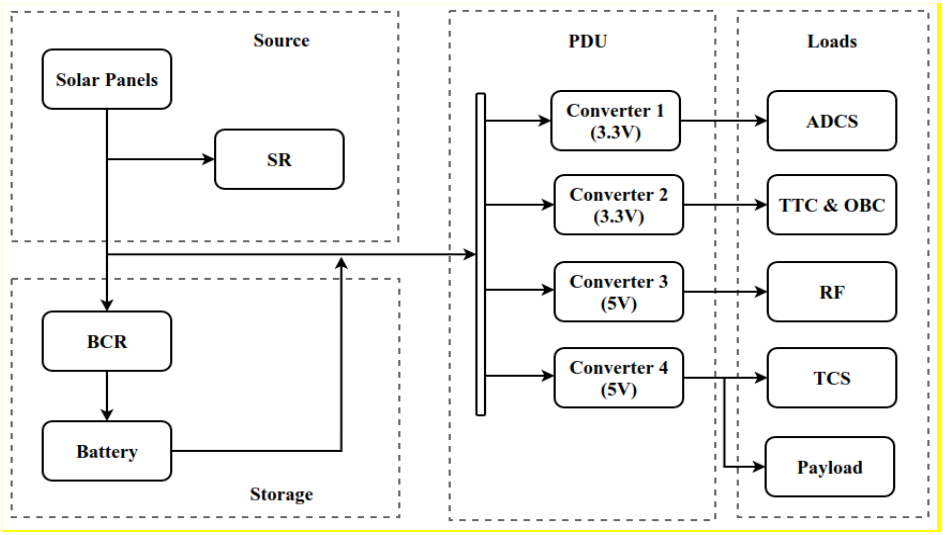

Figure 2.3: DET architecture (adapted from Kumar et al., 2021)

The MPPT architecture (Figure 2.7: MPPT architecture) is also comprised of four primary categories, which are the source, storage, power distribution, and loads, but it doesn't have a shunt regulator. However, it does have a battery charge regulator. Solar photovoltaic (PV) systems are widely utilized; However, their efficiency depends on variables such as irradiation variations, temperature variations, load variations, and

partial shading conditions. MPPT techniques have been developed to address the meteorological and load variability subjectivity of PV modules (Aguila-Leon et al., 2023). The requirement for higher proficiency from the PV system to reap the maximum energy requires MPPT functions **(Banakhr and Mosaad, 2021)**. Tracking the maximum output power of a PV cell is an essential problem in harvesting more energy under different weather and load conditions **(Bani Salim et al., 2019a)**. The research scope is to maintain a constant output voltage from the boost converter despite variations in the boost converter's input voltage derived from the solar PV module and variations of the boost converter loads ((**Mohammed et al., 2022)**.

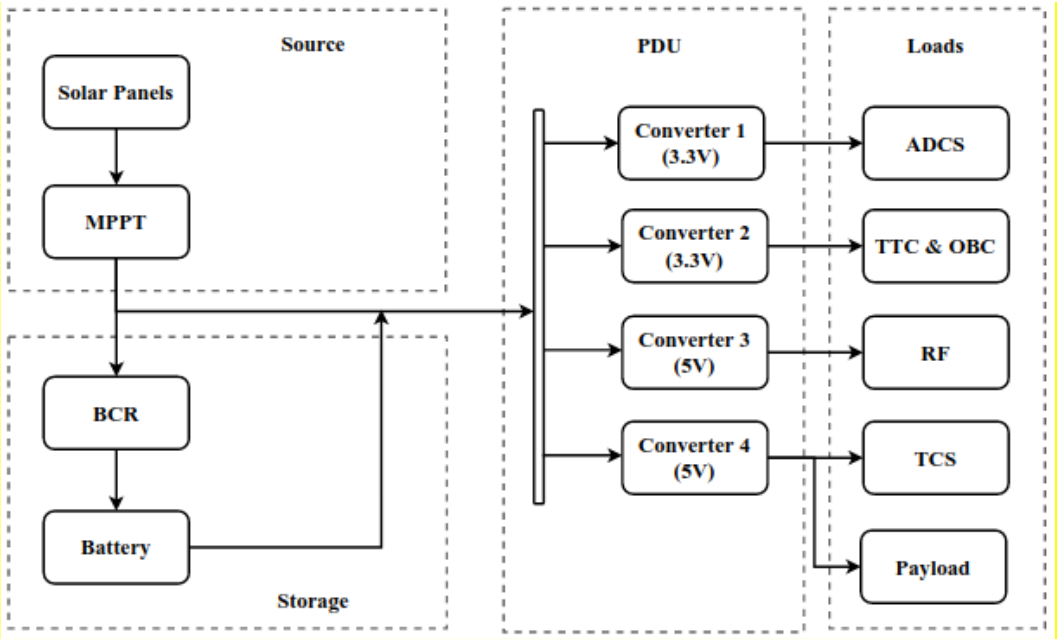

Figure 2.4: MPPT architecture (adapted from Kumar et al., 2021)

2.4.2. Conventional Maximum Power Point Tracking Functions

This sub-section will discuss the application of conventional MPPTs, AI MPPTs, and PID controllers to minimize the steady-state error of the boost converter closed loop and unity feedback loop.

2.4.2.1. Perturb and Observe MPPT Objective Function

The Perturb and Observe (PO) technique is a method used for Maximum Power Point Tracking (MPPT) in photovoltaic (PV) arrays or modules. In this technique, the voltage or the duty ratio of the DC-DC converter that interfaces the PV module to the load is adjusted in one direction. If the power increases, the adjustment continues in that direction. If the power decreases, the adjustment is made in the opposite direction. It involves adjusting the operating voltage or current of the PV array to achieve maximum power output under specific meteorological conditions. PO responds to changes in

irradiance and temperature to optimize power output, adapting to array or module changes over time. It can oscillate around the Maximum Power Point (MPP), and strategies like fuzzy logic control or variable perturbation size are used to optimize tracking under rapid meteorological conditions. PO may struggle with rapid atmospheric changes, but methods like three-point weight comparison or high sampling rates can address this issue **(Larbes et al., 2009)**. Typically, PO requires two sensors for voltage and current measurement, with DSP or microcomputer control commonly used for implementation **(Viswambaran et al., 2017)**.

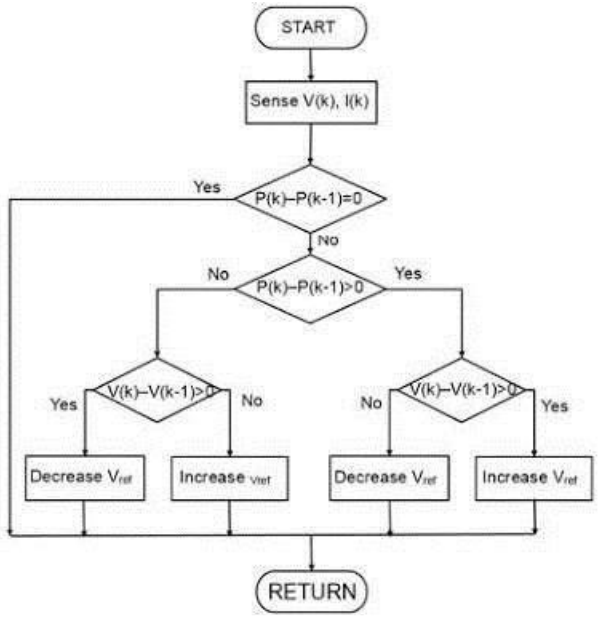

Figure 2.5: Flow Chart of the PO function (Adapted from Jayakumaran, 2018)

2.4.2.2. Incremental Conductance MPPT Objective Function

The Incremental Conductance (Inc) method is used for MPPT in photovoltaic systems. It explains how the algorithm adjusts the reference voltage by analyzing the conductance of the solar panel to accurately track the MPP and optimize system efficiency in changing environmental conditions. This method involves perturbing the insolation for the PV panel to efficiently track the maximum power point by comparing conductance with incremental conductance. It is effective in scenarios with sudden changes in climatic conditions and attempts to optimize power output, although it does not settle precisely at the MPP. It exhibits oscillations at the MPP. The PV power curve has a positive slope on the left side of the MPP, a negative slope on the right side, and a zero slope at the MPP.

$$\frac{I_{pv}}{V_{pv}} + \frac{\Delta I_{pv}}{\Delta V_{pv}} \qquad (2.1)$$

The first term on the left-hand side of Equation (2.1) is instantaneous

conductance, while the second is incremental conductance. The objective of the incremental conductance MPPT function is to drive the sum of the instantaneous conductance and the incremental conductance towards zero and consequently bring the PV module operating point to the MPP **(Reza Reisi et al., 2013)**.

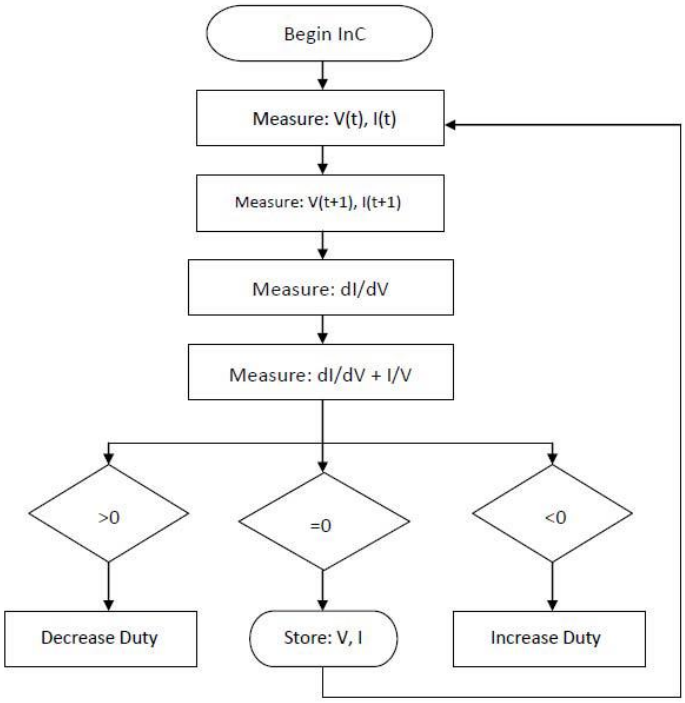

Figure 2.6: Flow Chart of the INC function (Adapted from Jayakumaran, 2018)

2.4.2.3. Fractional Open Circuit Voltage MPPT Objective Function

The close linear relationship between V_{MPP} and V_{OC} of the PV array, under varying irradiance and temperature levels, has ushered in the fractional V_{OC} method.

$$\boldsymbol{V_{MPP} \approx k_1 \times V_{OC}} \quad (2.2)$$

In equation 2.2, k_1 is a constant of proportionality. Since k_1 depends on the characteristics of the PV array being used, it is usually computed beforehand by empirically determining V_{MPP} and V_{OC} for the specific PV array at different irradiance and temperature levels. The factor k_1 has been reported to be between 0.71 and 0.78. Once k_1 is determined, V_{MPP} can be computed using (2.2), with V_{OC} measured periodically by momentarily shutting down the power converter. This incurs some disadvantages, including temporary loss of power. Pilot cells are used to obtain V_{OC} to prevent temporal loss of power. These pilot cells must be carefully chosen to represent the PV array's characteristics closely. It is claimed that the voltage generated by pn-junction diodes is approximately 75% of V_{OC} **(Esram and Chapman, 2007)**.

This eliminates the need to measure VOC and compute V_{MPP}. Once V_{MPP} has been approximated, a closed-loop control on the power converter can reach this desired voltage asymptotically. Since V_{MPP} is only an approximation, the PV module technically never operates at the MPP. Depending on the application of the PV system, this can sometimes be adequate. Even if fractional V_{OC} is not an actual MPPT function, it is straightforward and cheap to implement as it does not necessarily require DSP or microcontroller control. However, k_1 is no longer valid in the presence of partial shading (which causes multiple local maxima) of the PV array, and the PV array voltage is proposed to be swept to update k_1. This adds to the implementation complexity and incurs more power loss **(Wang et al., 2010)**.

2.4.2.4. Fractional Short Circuit Current MPPT Objective Function

Fractional I_{SC} is formulated because, under varying atmospheric conditions, I_{MPP} is approximately linearly related to the short circuit current I_{SC} of the PV module.

$$I_{MPP} \approx k_2 I_{SC} \tag{2.3}$$

k_2 is a proportionality constant. For example, k_2 must be determined according to the PV module used in the fractional VOC function. The constant k_2 is generally found to be between 0.78 and 0.92. Measuring I_{SC} during operation is problematic. An additional switch must be added to the power converter to periodically short the PV array so that I_{SC} can be measured using a current sensor. This increases the number of components and costs. A boost converter can be used, where the converter switch can short the PV array. **(Yuvarajan and Shanguang Xu, 2003)**. Power output is reduced when finding I_{SC}, and the MPP is never perfectly matched. **(Koutroulis et al., 2001)**. A method of compensating k_2 is proposed so that the MPP can be better tracked while atmospheric conditions change. **(Noguchi et al., 2000)**.

To guarantee proper MPPT in multiple local maxima, periodically sweeping the PV array voltage from open circuit to short-circuit to update k_2 must be done. Most PV systems in the literature using fractional I_{SC} use a DSP. In some cases, a simple current feedback control loop is used instead.

2.4.2.5. Previous Research Heritage of Implemented Conventional MPPT Objective Functions

Table 2.4.: sources reviewed from the literature that implemented conventional MPPTs' objective functions, summarising how those conventional MPPTs' objective functions were implemented.

Table 2. 4: Previous Research Heritage of Implementation of Conventional MPPT Objective Functions

Source	The principal focus of the work	Method(s) Used to Implement the Objective Function	Objective Function Implemented	Comments
(Bollipo et al., 2020)	Discusses the application of constant voltage (CV) in uniform irradiation conditions and **neglects** the effect of both irradiation/insolation and temperature.	This technique requires measuring the Voc at regular intervals. Moreover, this technique applies to conditions where temperature variation is low. Leedy et al. did hardware implementation of this technique using TL494IN from Texas Instruments for PWM generation.	Constant Voltage (CV)	This CV technique estimates MPP a bit far away from the genuine MPP. Thus, the working point does not coordinate the MPP, and considering different topographical positions is necessary for the optimum reference voltage to decrease the error value. The method is simple, fast, and easy to implement but has limited precision.
(Devarakonda et al., 2022)	Discusses the application of perturb and observe (PO) under various irradiation levels, loads, and temperatures.	If the operating voltage is perturbed and if the power is increased ($dp/dv > 0$), then we can see that the point is now moving towards the MPP, whereas if it decreases ($dp/dv < 0$), then the direction of perturbation is reversed. The process will continue until the MPP is reached at every point. Based on the previous duty ratio, the following duty ratio is calculated by checking the differences between the power and voltage values.	Perturb and Observe (PO)	Owing to its simple design and ease of operation and execution, the perturbation and observation technique is the most widely used technique. However, the P&O algorithm doesn't track the MPP under rapidly varying atmospheric changes. It uses both voltage and current sensors.

(Hassan et al., 2023)	Fractional open circuit voltage (FOCV) is founded on estimating the K_V value. Hence, it is most appropriate for low voltage, high current applications.	If the value of K_v is known and the V_{oc} of the PV array can be measured using a voltage sensor, V_{MPP} can easily be calculated from $V_{MPP} = K_v.V_{oc}$. K_v is somewhere in the range of 0.7–0.8 and can be known with the help of the data sheet provided by the manufacturer.	Fractional Open Circuit Voltage (FOCV)	It is a simple and fast way of tracking MPP. However, it is still looking for the exact MPP. As the operation of this method depends on the estimation, it is viable for uniform irradiation conditions.
(Fahim et al., 2021)	FSCC is founded on the estimation of the *k* value. Hence, it is most appropriate for low-current and high-voltage applications.	This method works on the principle that the current at the maximum power point is equal to the short circuit current time k., where k is a constant of proportionality that depends on the characteristics of the PV panels. k ranges between 0.75 and 0.9. if k is known, the current at MPP can be calculated by $I_{mpp} = k * I_{sc}$. It is measured using a current sensor.	Fractional Short Circuit Current (FSCC)	It is a simple and fast way of tracking MPP. However, it is still looking for the exact MPP. As the operation of this method depends on the estimation, it is viable for uniform irradiation conditions.
(Katche et al., 2023)	The technique uses the current and voltage of the PV modules to find the MPP and can track the MPP with varying weather conditions.	The derivative of the output power, P, concerning the panel voltage, V, is equivalent to zero at the MPP. If the ratio of the increment in conductance is higher than the negative conductance, the reference voltage is increased to track MPP. If the ratio of the increment in conductance is less than the negative conductance, the reference voltage is decreased to track MPP.	Incremental Conductance (InC/IC)	This strategy tracks more quickly than P&O and tracks under dynamic weather conditions. Yet, it cannot discover global MPP in nearby MPPs like P&O. The basic microcontroller is good enough to execute this technique. Both voltage and current sensors are utilized, as in the case of P&O.
(Lasheen et al., 2017)	Proposes an Adaptive Reference Voltage (ARV) MPPT technique to improve the performance of the constant voltage (CV) technique by making it adaptable to changing weather conditions.	The reference voltage (RV) for MPPT is adapted according to the measured radiation and temperature levels. The operating range of the radiation at a given temperature is divided into several divisions, and the corresponding RV is recorded off-line in a truth table. The difference between the reference and measured voltages is compensated using a proportional-integral controller to generate a suitable duty ratio that controls the pulse width of the boost converter.	Adaptive Reference Voltage (ARV)	Adaptive Reference Voltage (ARV) improves the time response and MPPT efficiency, damps oscillation, and provides better power source stability.
(Esram et al., 2007)	Ripple correlation control (RCC) correlates the time derivative of the time-varying PV array power	If *v* or *i* is increasing (dv > 0 or di > 0) and *p* is increasing (dp > 0), then the operating point is below the MPP (V	Ripple correlation control (RCC).	Simple and inexpensive analog circuits can be used to implement RCC. RCC accurately and quickly tracks the MPP, even under

	(p)˙ with the time derivative of the time-varying PV array current˙(i) or voltage (v) to drive the power gradient to zero, thus reaching the MPP.	<V_{MPP} or I < I_{MPP}). On the other hand, if *v* or *i* is increasing and *p* is decreasing (dp < 0), then the operating point is above the MPP (V >V_{MPP} or I > I_{MPP}). Combining these observations, we see that ˙ dp.dv or dp.di are favorable to the left of the MPP, negative to the right of the MPP, and zero at the MPP.		varying irradiance levels. The time taken to converge to the MPP is limited by the power converter's switching frequency and the RCC circuit's gain. Another advantage of RCC is that it does not require prior information about the PV array characteristics, making its adaptation to different PV systems straightforward.
(Ali et al., 2012)	It is designed to work with a PV system that is connected in parallel with an AC system line.	The current going in the inverter increases the power coming out of the boost converter and consequently increases the power out of the PV array. While the current increases, the voltage V_{link} can be kept constant as long as the power required by the inverter does not exceed the maximum power available from the PV array. If that is not the case, V_{link} starts drooping. Right before that point, the current control command I_{peak} of the inverter is at its maximum, and the PV array operates at the MPP.	DC-link capacitor droop control	DC-link capacitor droop control does not require the computation of the PV array power. However, its response deteriorates when compared to a method that detects the power directly; this is because its response directly depends on the reaction of the DC-voltage control loop of the inverter. This control of the scheme can be easily implemented with analog operational amplifiers and decision-making logic units.

2.4.2.6. Discussion of Conventional Objective MPPT Functions

The significant drawbacks of the conventional objective MPPT functions are the low velocity of convergence, poor tracking of the global maximum power point (GMPP) under rapid irradiation changes, rapid load changes and rapid temperature changes, oscillation at MPP, inability to find a GMPP but finding multiple local maxima and a general low tracking velocity because of constant/fixed step size **(Jately et al., 2021)**.The benefits of the conventional objective MPPT functions are that they are simple to implement and implement with analog and logic decision circuits. Another advantage of the FOCV and FSCC is that they have low computation requirements and don't require a microprocessor to implement them **(Ilyas et al., 2015)**. Early improvements of the traditional MPPTs were variable step size hill climbing techniques like variable step size PO and variable step size InC **(Malathy and Ramaprabha, 2013)**. The current hybrid techniques are tabulated in Table 2. 4, where in formulating the hybrid MPPT, conventional MPPTs are combined with AI techniques, or two AIs are combined to form a hybrid.

2.4.3. AI MPPT Algorithms

The AI algorithms tune PID controllers and minimize the steady-state error of power converter transfer function plants. In some applications, AI Algorithms are used as MPPT functions solely to optimize the duty ratio of the PWM in power converters. Sometimes, AI algorithms are combined with conventional true-seeking objective functions like perturb and observe (PO), incremental conductance (INC), fractional open circuit voltage (FOCV), and fractional short circuit current (FSCC) to optimize the duty ratio of the PWM in power converters. The reason for combining the conventional objective MPPT functions and artificial intelligence (AI) is to improve the drawbacks of the true-seeking traditional methods, such as low tracking speed, power oscillation at MPP, and improper search during rapidly varying environmental conditions.

AI techniques, which are computationally intelligent and bioinspired MPPT algorithms, often offer quicker responses and greater accuracy. However, the quasi-seeking/AI algorithms are complex in such that they have a high computing load and, consequently, require expensive high-performance computing devices. In addition, specialized knowledge, extensive sensory gadgets, and large amounts of historical data are needed to model, train, test, and develop the AI MPPT systems. In some literature consulted, two AI techniques are combined to form a hybrid technique instead of improving the conventional objective MPPT function by introducing an AI technique **(Sulthan et al., 2023)**.

2.4.3.1. The PSO Algorithm

The PSO algorithm introduced by J. Kennedy and R.C. Eberhart in 1995 is widely used to optimize system performance. A modified PSO was introduced in 1998 to improve the performance of the original PSO. A linearly decreasing inertia weight (ω) is added to the enhanced PSO during each iteration. Clerc reported another widely used PSO. In this thesis, the PSO used is the 1998 PSO (Aoughlis et al., 2021). A PSO is a stochastic, population-based evolutionary algorithm search method. It is modeled after the behavior of a bird swarm or a fish school **(Abdulkadir and Yatim, 2014)**. The algorithm's methodology focuses on the attitude of a swarm of birds or a school of fish when searching for food.

In the PSO, a particle represents a potential solution to a problem. Particles imitate the success of neighboring particles and their own achieved success. Therefore, the position of a particle is influenced by the position of the best particle (P_{best}) in a neighborhood, as well as the best solution found by all the particles in the entire population (G_{best}). Each particle is treated as a point in a D-dimensional space. The i^{th} particle is represented as XI= (x_{i1}, x_{i2}, …, x_{iD}). The best previous position giving the minimum fitness value of any particle is recorded and described as PI= (p_{i1}, p_{i2}, …, p_{iD}); this is called P_{best}. The position of the best particle among all particles in the population is called G_{best}. The velocity for the particle i^{th} is represented as V_I = (v_{i1}, vi_2, …, v_{iD}). The particle position, x_i, is adjusted using equation 2.3.:

$$\boldsymbol{X_{k+1}^{i}} = \boldsymbol{X_{k}^{i}} + \boldsymbol{V_{k+1}^{i}} \times \Delta \boldsymbol{t} \qquad (2.4)$$

where the velocity component represents the step size v_i. The velocity is calculated using equation 2.4.

$$\boldsymbol{v_{k+1}^{i}} = \boldsymbol{\omega} * \boldsymbol{v_{k}^{i}} + \boldsymbol{c_1} \times \boldsymbol{rand_1} \times \frac{(\boldsymbol{p^i} - \boldsymbol{x_k^i})}{\Delta \boldsymbol{t}} + \boldsymbol{c_2} \times \boldsymbol{rand} \times \frac{(\boldsymbol{P_k^g} - \boldsymbol{x_k^i})}{\Delta \boldsymbol{t}} \qquad (2.5)$$

Where: i = 1, 2, …… N

Where: $\boldsymbol{X_{k+1}^{i}}$ denotes the i^{th} particle position; the velocity of the i^{th} particle is represented by $\boldsymbol{v_{k+1}^{i}}$; The number of iterations is denoted by k; the inertia weight is defined by ω; $rand_1$ and $rand_2$ are uniformly distributed random variables within [0, 1]; the cognitive and social coefficients are denoted by c_1 and c_2, respectively. In the velocity equation, $\boldsymbol{c_1} \times \boldsymbol{rand_1} \times \frac{(\boldsymbol{p^i} - \boldsymbol{x_k^i})}{\Delta \boldsymbol{t}}$ is called the cognitive part, representing the particle's personal experience or individual memory that brings it back to the most satisfying place it

passed through in the past. The term $c_2 \times rand \times \frac{(P_k^g - x_k^i)}{\Delta t}$ reflects social behavior. It makes each particle follow the best position found by its neighbors.

2.4.3.2. The GA Algorithm Tuning PID Controllers

The application of Genetic Algorithms (GAs) for PID tuning has been extensively studied and is a focal point in control system optimization. Genetic Algorithms are preferred for efficiently searching and optimizing PID parameters, overcoming the limitations of traditional tuning methods such as Ziegler-Nichols or manual tuning. Recent literature highlights various enhancements and applications of GAs for PID tuning:

- Improved Genetic Algorithm advances include modifications to avoid premature convergence and maintain population diversity. Techniques such as local stochastic search capabilities and dynamic adjustment strategies have been introduced to accelerate convergence and improve search stability **(Chen et al., 2021)**.

- Hybrid Approaches, which combine GAs with other optimization techniques like Particle Swarm Optimization (PSO), have shown promising results. By leveraging the strengths of different methods, these hybrid algorithms significantly enhance tuning performance and robustness in various industrial applications.

- Specific studies have shown that GA-tuned PID controllers offer practical benefits in specific applications, such as controlling brushless DC (BLDC) motors, hydraulic servo systems, and automatic voltage regulators. These studies demonstrate GA-tuned PID controllers' superior performance and stability compared to conventional methods.

- Metaheuristic comparison reviews comparing GAs with other metaheuristic algorithms, such as Ant Colony Optimization (ACO) and Bacterial Foraging Optimization (BFO), highlight each method's unique advantages and limitations in PID tuning contexts **(Mohamed et al., 2023)**.

2.4.3.3. Ant Colony Optimisation (ACO) Tuning PID Controllers

Ant Colony Optimization (ACO) for PID tuning is a notable research area that has garnered significant attention. This approach leverages the foraging behavior of ants to optimize the PID controller parameters, enhancing the controller's performance in various applications. A comprehensive summary of the current literature on the subject:

- PID Controller Tuning for Load Frequency Control: ACO has been employed to tune PID controllers in load frequency control problems for interconnected thermal power systems with renewable energy sources. The results demonstrate that ACO can effectively improve the stability and performance of these systems **(Murugesan et al., 2024)**.

- Ant Colony Optimization for Induction Motors: A study applied ACO to optimize PID controllers for induction motors to minimize speed ripple and harmonics. The optimization process was validated using MATLAB/Simulink, showing enhanced motor performance compared to conventional methods **(Yin et al., 2018)**.

- Direct Torque Control for Doubly Fed Induction Motors: A hybrid ACO-based PID tuning method was developed for doubly fed induction motors' direct torque control (DTC). The approach improved torque and speed control, reducing overshoots and torque ripples **(Mahfoud et al., 2022)**.

- Comparative Studies and Hybrid Approaches: Recent reviews have highlighted the integration of ACO with other optimization techniques and its application in various fields, including electrical machine control and power system stabilization. These studies underscore the robustness and effectiveness of ACO in PID tuning **(Wang et al., 2023)**.

- Theoretical and Practical Implementations: The theoretical foundations of ACO, such as its global optimization capabilities and robustness, have been extensively documented. The practical implementations in PID tuning not only demonstrate the algorithm's ability to handle non-linear systems and complex optimization problems but also provide valuable insights for real-world applications **(Yin et al., 2018)**.

2.4.3.4. Adaptive Fuzzy Logic Control for MPPT

Fuzzy Logic Control (FLC) is a dependable choice for MPPT in PV systems with its widely recognized robustness and adaptability. Power converters, the usual regulators of these systems, ensure efficient energy conversion and stable power supply under varying environmental conditions. FLC utilizes a set of rules and membership functions to handle the non-linear and uncertain nature of PV systems. FLC does not require a precise mathematical model, which is advantageous in dynamic environments. Adaptive fuzzy logic controllers adjust the membership functions and rules based on real-time data.

This provides better performance under varying irradiance and temperature conditions compared to conventional MPPT techniques like Perturb and Observe (PO) **(Refaat et al., 2020)**. Studies demonstrate that FLC-based MPPT systems, modeled in environments like MATLAB/Simulink, show improved efficiency, reduced power loss, and faster response times than traditional methods like INC. **(Robles Algarín et al., 2017)**. Comparative studies indicate that FLC significantly reduces the oscillations at the maximum power point and improves the overall system stability and reliability.

2.4.3.5. Artificial Neural Networks-Based MPPT Techniques

Among various MPPT techniques, Artificial Neural Networks (ANNs) have shown significant promise due to their ability to handle nonlinear relationships and adapt to varying meteorological conditions. ANNs are used to model the PV characteristics and predict the MPP under different irradiance and temperature conditions. The ANN-based MPPT algorithms can quickly adapt to changes in the environment, providing accurate tracking of the MPP with minimal oscillations around the MPP. **(Zečević and Rolevski, 2020)**. Hybrid algorithms combining ANN with other techniques, such as Fuzzy Logic (FL) or Particle Swarm Optimization (PSO), enhance the performance of MPPT systems. These hybrid methods leverage the strengths of each approach to improve convergence speed and tracking accuracy. **(Villegas-Mier et al., 2021)**. The effectiveness of ANN-based MPPT algorithms depends on the training dataset and the neural network's architecture. A well-trained ANN can generalize unseen data well, ensuring robust performance across different environmental conditions. Techniques such as supervised learning are commonly used to train the ANNs with historical weather and PV performance data. **(Sharma et al., 2023)**. Listed below are the key performance advantages of using ANN MPPT:

- Efficiency: ANN-based MPPT systems demonstrate high efficiency, with studies reporting an average performance of around 98% under uniform conditions. The ability of ANNs to learn and predict the optimal MPP voltage and current under varying conditions is a critical factor in their superior performance **(Villegas-Mier et al., 2021)**.

- Speed and Accuracy: Compared to traditional MPPT techniques, ANN-based methods exhibit faster convergence to the MPP and fewer oscillations around the MPP. This results in more stable and reliable energy extraction from PV systems **(Nkambule et al., 2021)**. Adaptability: ANNs can be trained to account for partial shading conditions and other non-ideal scenarios that typically challenge conventional MPPT objective functions.

- This adaptability ensures consistent and fixed performance even under suboptimal conditions, enhancing the overall reliability of the PV system **(Nkambule et al., 2021)**.

2.4.3.6. Previous Research Heritage of Implementation of AI MPPTs' Algorithms

Table 2.5.: sources reviewed from the literature that implemented AI MPPTs' Algorithms, and it summarises how those algorithms were implemented.

Table 2. 5: Previous Research Heritage of Implementation of AI MPPTs' Algorithms

Source	The principal focus of the work	Method(s) Used to Implement the Objective Function &/ Algorithm	Objective Function Implemented &/ Algorithm	Comments
(Abdulkadir and Yatim, 2014)	Partial shading prohibits conventional InC from finding global maxima. Thus, PSO is employed in traditional InC to find global maxima. The advantage of using InC with PSO is that it narrows the search space for PSO and reduces the response time of the hybrid MPPT compared to the response time when PSO is used alone.	In the first stage, the incremental conductance method is employed to search for the first local maximum quickly. In the second stage, the PSO is activated to search for the global maximum point.	Incremental Conductance (InC) + particle swarm optimization (PSO)	Simulation results show that the proposed hybrid method can track the global maximum point without difficulty, has a faster response time, and has a better dynamic response than the plain PSO method.
(Moradi et al., 2013)	A robust hybrid is proposed to mitigate irradiance, poor sensitivity, and decreasing convergence speed when the battery is not connected or has sizeable internal resistance of the first MPPT they developed.	In the first stage, the MPP is estimated using analytical equations and a model of the PV system while considering ambient temperature, irradiation, and load model (set point tuning). The classic perturbation and observation (P&O) method will follow the maximum power point in the second phase.	Sensors, analytical equations, a model of the PV system, and Thevenin model of the load + Perturb and observe (PO).	In the first phase, the influence of temperature and light intensity on MPP was formulated, and the effects of load and battery characteristics modeled by equivalent Thevenin circuits were considered. Therefore, the MPP approximated in this phase is robust regarding load changes and battery conditions.
(Ammar et al., 2019)	The PV and the DC-DC converter are nonlinear, so fractional order calculus describes the nonlinearity of the PV and converter system in this	In the 1st case study, irradiation is set to 800W/m^2, the temperature is set to 25°C, and a performance comparison of plane InC, variable step InC, FO-InC fixed step + PSO, FO-InC fixed	Incremental Conductance (InC) and Fractional Order (FO)	The efficiency of the eight different MPPT techniques under testing was compared, and it was revealed that the plane InC has the worst efficiency of 75.9%, and

	fractional order incremental conductance (FO-InC) technique.	step + ACO, FO-InC fixed step + ALO, FO-InC variable step + PSO, FO-InC variable step + ACO, FO-InC variable step + ALO is done. In the 2nd case study, the irradiation is increased to 1000W/m2, and the performance comparison is repeated.		the best efficiency is that of the variable step FO-InC + ALO, with the efficiency of 98.1%.
(Aguila-Leon et al., 2023)	These four metaheuristic algorithms, the Grey Wolf Optimizer algorithm, Wolf Optimizer Algorithm, Simulated Annealing, and Particle Swarm Optimization, are compared to the Perturb and Observe and Incremental Conductance algorithms.	The MPPT techniques are analyzed for the transient state and full-day operation scenarios for constant and variable irradiations, temperatures, and loads.	Grey Wolf Optimizer (GWO) + Discrete PID MPPT Controller + InC	The comparative results show that the Maximum Power Point Tracking controller optimized by the Grey Wolf Optimizer algorithm has superior performance, giving an average 6% output power higher than the other controllers under the test scenarios evaluated.
(Allahabadi et al., 2022)	Proposes an artificial neural network in the 1st stage to estimate the GMPP and uses a hill climbing method, PO/InC, in the second stage to accurately track the GMPP.	It doesn't use the voltage and current sensors but samples the IV curve at specific points for training data (reflecting changes in temperature and irradiation) of the ANN for stage 1 of the MPPT. A feed-forward ANN estimates the position of the GMPP, and the 2nd stage hill-climbing technique tracks the exact location of the global MPP.	ANN+Hill Climbing (PO/InC)	The results showed that the proposed ANN-based tracker provides accurate tracking even under complicated partial shading patterns and is about 1.7−7.9 times faster than the methods compared with them. The proposed method is an excellent fit for vehicle-integrated PV (such as cars, buses, and boats) subjected to complicated and rapidly changing partial shading conditions.
(Aminnejhad et al., 2021)	A robust sliding-mode controller with quantized inputs is proposed for MPPT in photovoltaic power generation systems.	The PV panel's output current and voltage are inputs for the QISMC. Sliding surface, control law, and hysteresis quantizer comprise the QISM controller design. The controller's output is then applied to the boost converter PWM.	Adaptive sliding mode controller with quantized hysteresis inputs (QISM)	Using hysteresis quantized inputs, the chattering phenomena, as the main weakness of the sliding mode controllers, is removed. Also, the external disturbances, model uncertainties, and environmental and load variation effects are attenuated in the proposed controller scheme.
(Aoughlis et al., 2021)	Proposes an MPPT technique that ends oscillations at MPP of PO MPPT technique by employing a PID controller tuned by PSO technique	The PSO tunes the PID controller gains using the integral square error performance index as an objective function that calculates the difference between theoretical and generated power. In the 1st structure, the PID	PO+PID+PSO	The second structure can extract the maximum energy from the TEG for each temperature gradient change more efficiently. The second structure is more stable

		controller is used to tune the step size of the PO algorithm by observing at each sample time the difference between the maximum TEG Power and the actual power generated. The PO tunes the duty cycle of the boost converter PWM. In the 2nd structure, the PSO tunes the step size of the PO, then tunes the PID gains using the tuned step size, and then the PID drives the duty cycle of the PWM.		and more precise than the first structure.
(Larbes et al., 2009)	Proposed an improved fuzzy logic controller tuned by a genetic algorithm, and its performance is compared to that of the PO technique under varying weather conditions.	FLC doesn't require knowledge of the exact model. The FLC has two inputs, i.e., error (E) and change of error CE, computed at sample time k, and the output is the duty cycle that drives the PWM of the boost converter.	Improved FLC using GA	The enhanced algorithm is compared to the PO technique. Compared to the PO technique, the FLC demonstrates improved rise and settling time for a fast solar irradiance increase from 500 to 100W/m2.
(Kamran et al., 2020)	The proposed algorithm confines the search space of the power curve to a 10% area that contains the MPP and starts perturbation and observation within that limited search space.	Enslin et al. (1997) and Huynh and Dunnigan (2016) state that the VMPP is about 76% of the open circuit voltage. It first measures the voltages V1 and V2 to find the MPP-containing region to restrict the operating point of the solar panel to 10% of the power curve and then starts perturbation and observation. In a few perturbations, MPP is achieved and maintained. Under uniform weather conditions, it sticks to the maximum power point, while as the irradiance changes, it finds new local maxima in the same way described for the constant irradiance and then maintains it.	PO + sun tracker + V_1 and V_2 Calculator.	The confinement of the algorithm's search space lessened the response time to the changing weather conditions, decreasing the steady-state oscillations at the MPP. Integrating the solar tracker and improved P&O MPPT algorithm provides better quality and conditioned electricity for the load. The proposed system was experimentally steered, whose results verified the effectiveness of the proposed P&O algorithm. According to the simulation results, the oscillations at the MPP have not been eliminated.
(Banakhr and Mosaad, 2021)	The paper proposes an adaptive MPPT of a stand-alone PV system using an updated PI controller optimized by harmony search (HS).	A lookup table is formed for the temperature and irradiance with the corresponding voltage at MPP (VMPP). This is the updated reference voltage required for MPP at each temperature and irradiance. A comparator computes the error between the measured PV and	PI + Hill climbing + Harmony search (HS)	Compared to IC and PO, the fluctuations at the MPP are eliminated by the proposed PI-HS MPPT—the proposed adaptive technique performed better than P&O and IC techniques regarding system efficiency.

		updated reference voltage. This error is minimized using HS optimization. The HS finds the optimized gains for the PI controller, and the PI controller tunes the duty cycle of the PWM of the DC-DC converter.		
(Bani Salim et al., 2019b)	The main goal of the Roburst direct adaptive controller (RDAC) is that the Boost converter (main plant) output $y_p(t)$ will follow the reference plant output $y_m(t)$ by use of the adaptive gains.	The proposed RDAC uses only the boost converter inputs and outputs and does not need any estimations or identification of boost converter parameters. The RDAC comprises a reference model, a compensator, and three adaptive gains (K_e, K_x, K_u). K_e is the adaptive gain of the error, K_x is the adaptive gain of the states, and K_u is the adaptive gain of the input. To implement the RDAC, the plant Gp(s) has to be almost strictly positive real (ASPR), and if the plant Gp(s) is not ASPR, then a compensator Gc(s) has to be added in the feedforward path to the plant so that the new plant, called augmented plant Ga(s), becomes ASPR.	Robust direct adaptive controller (RDAC)	The results show that the response time for the adaptive controller is less than 0.3 s, which is fast. Also, the adaptive controller can track the MPP for various irradiance values. During the steady-state operation, some prominent peaks occur in the duty cycle because of the high steady-state at the beginning of the RDAC operation. The controller can adapt to the changes within the boost converter parameters, i.e., the algorithm presented in this paper can be used with different MPPT types, leading to a stable system and maximum output power values.
(Mohammed et al., 2022)	This paper presents the design of a maximum power point tracking-based (MPPT) DC converter controller.	The PSO algorithm tunes the PID controller to find optimum PID gain values through the integral time square error cost function performance index. The incremental Conductance (IC) algorithm has been employed as an MPPT with an optimized PID.	InC MPPT + PID + PSO	The results illustrated that the voltage, current, and power system responses with the proposed controller under different disturbances had less overshoot, lower steady-state error, and shorter settling time compared with the optimized PID controller, noticing that the results were obtained by using the same optimization technique for the two controllers. The effectiveness of the proposed controller has been tested by implementing different disturbances, including variable temperature, variable irradiation, and load change disturbances.

(Saidi et al., 2021)	The paper proposes a Neural Network Estimator-based MPPT controller that calculates the position of the MPP based on open circuit voltage (V_{OC}) and uses the PO technique to search for the GMPP within the estimated region.	The system comprises a Neural Network Estimator (NNE), a conversion coefficient, and an optimal duty cycle calculation stage. The proposed NNE technique, implemented in MATLAB/Simulink, calculates the ratio of open circuit voltage (VCO) corresponding to each solar radiation for various temperature values to the standard open circuit voltage. A regularisation coefficient is determined, which estimates the voltage corresponding to the MP directly from the open circuit voltage for each solar radiation. Finally, the optimal duty cycle is evaluated from the input/output equation of the boost converter.	PO + NNE	It is demonstrated that this controller can achieve almost 99% of the real PV maximum power. The Simulation results indicate that optimizing the P&O MPPT control with an NNE algorithm provides better results and performance regarding accuracy and complexity.
(Harrag and Messalti, 2015)	It presents a new modified PO MPPT algorithm with an adaptive duty cycle step using a PID controller tuned by a genetic algorithm.	The reference power of a closed-loop feedback system is derived from the PV cell or module. The output power produced by the DC-DC converter is the negative feedback power compared to the reference power at the summation point. The output of the summing point produces an error that is used as an objective function of the GA algorithm. A performance index is applied to the error as a cost function to be reduced by the GA algorithm. The GA algorithm minimizes the cost function by finding the optimum gain values of the PID controller and placing them into the workspace. The optimized PID controls the step size of the PO MPPT and, thus, improves its adaptability and response time.	GA+ PID+PO	The efficiency and improvements of the proposed algorithm in transient, steady-state, and dynamic responses, especially under rapidly changing atmospheric conditions, have been demonstrated by measuring the related ripple, overshoot, and response time. Algorithm robustness was verified using different schemes for temperature and insolation, proving its ability to track MP in random and fast-changing atmospheric conditions.
(Ahmed and Salam, 2016)	Proposes an adaptable step size of the PO and sets a tracking boundary for the PO, and that boundary reduces convergence speed.	It modifies the PO step size by calculating the locus of the MPP as a function of open circuit voltage. The step size is reduced at positions closer to the MPP and increased at	Modified PO MPPT+PID	The proposed method is validated experimentally using a buck-boost converter fed by a solar PV array simulator. Based on the EN 50530 dynamic irradiance tests, the

		positions further to the MPP. The MPP is estimated using open circuit voltage.		proposed method achieved an average MPPT efficiency of almost 1.1% higher than the conventional PO when irradiance changes slowly and about 12% higher under fast-change irradiance.
(Da Rocha et al., 2020)	It proposes combining the Bat-based algorithm with traditional algorithms (P&O, IC, and Beta) To overcome oscillations at the MPP due to partial shading conditions and find GMPP under partial shading.	The proposed MPPT algorithms, named in this paper as Bat-P&O, Bat-Beta, and Bat-IC, are evaluated and compared using a DC-DC Boost converter. Finally, experimental and simulation results assess the performance and effectiveness of the Bat-based MPPT techniques.	BAT algorithm + Hill climbing MPPT traditional/classical algorithms	The proposed Bat-P&O, Bat-Beta, and Bat-IC MPPT algorithms presented the best overall performance compared to other MPPT algorithms. The comparison tests also evaluated the algorithms considering a scenario with three different patterns of solar irradiance and temperature, which included a slight variation in solar irradiance and the transition from STC to partial shading condition. In particular, the Bat-Beta MPPT algorithm improved performance for all test conditions.
(Mohanty et al., 2017)	It proposes a new MPPT algorithm combining grey wolf optimization (GWO). It perturbs & observes (P&O) technique for efficient extraction of MP from a PV system subjected to rapid variation of solar irradiance and partial shading conditions.	GWO handles the initial stages of MPPT, followed by applying the PO algorithm at the final stage for faster convergence with the GMPP. This MPPT thus overcomes the computational overhead encountered in the case of a GWO-based MPPT algorithm reported earlier by Mohanty et al. The idea behind using the hybrid technique is to scale down the search space of GWO, which will help speed up convergence toward the GMPP. The proposed MPPT algorithm is first implemented using MATLAB/Simulink, and subsequently, an experimental setup is prepared for practical implementation.	GWO + PO	The results confirmed that the proposed hybrid GWO-PO MPPT provides superior tracking performance in weather conditions compared to both GWO and PSO+PO-based MPPT algorithms.
(Ali et al., 2020)	Proposes an online grid-connected PV-inverter system. Its MPPT is controlled by an SMC whose parameters are	To compare the proposed method with PO MPPT, InC MPPT, and Fuzy logic controller MPPT, the setup takes the output from the DC-DC converter through a negative feedback loop and	Sliding mode controller (SMC) + θ Modified Krill herd algorithm	Results show desirable limitation of oscillations at GMPP and an efficiency of 99.5% in tracking the MPP.

	optimized using a modified Krill herd method.	compares it to PV reference power. The comparator's output error (difference between power output and power PV) is fed to the SMC, whose coefficients (K_a, K_b, K_c, K_d, and K_e) are optimized by the θ Modified Krill herd algorithm.		
(Pilakkat and Kanthalakshmi, 2020)	Proposes an online grid-connected PV system that has two parts. The first part is an Artificial Bee Colony PO MPPT installed between the PV and Boost converter output power. The second part is the DC–AC inverter, LC filter, and Phase Locked Loop (PLL) to synchronize with the grid. The system is tested under PSC and varying meteorological conditions.	The first stage of the Artificial Bee Colony algorithm + PO MPPT is to determine the minimum change in irradiation using the ABC algorithm. If the condition of minimum change in irradiation is satisfied, then the PO starts the search for the GMPP using a small step size. The primary benefit of the ABC algorithm is eliminating convergence during partial shading conditions at the local maximum power point.	Artificial Bee Colony algorithm + PO MPPT	Even though the ABC-PO algorithm contributes to more excellent performance and precision in tracking GMPP, its complexity in real-time implementation remains a demerit of this method.
(Manickam et al., 2017)	Proposes a PSC detection scheme to eliminate power loss caused by unnecessary broad search under uniform irradiance. This paper proposes a scheme for detecting the type of irradiation, viz., uniform or non-uniform.	This partial shading detection scheme is implemented in a GMPPT control strategy combining the conventional PO algorithm and the Fireworks Algorithm (FWA). Under uniform irradiation conditions, the PO algorithm is used owing to the lower magnitude of power oscillations during tracking than the FWA. On the other hand, under partial shading conditions, the FWA is employed due to its global search and fast-tracking capability.	PO + Fireworks algorithm	Global maximum power point tracking (GMPPT) strategies for photovoltaic systems are effective under non-uniform irradiation conditions but cause unnecessary power loss due to broad search under uniform irradiance.
(Sheik Mohammed et al., 2016)	Proposes an enhanced PO MPPT that combines conventional PO algorithm and Learning Automata (LA) optimization. A unique PV system model is designed to evaluate the proposed algorithm for several scenarios with various weather conditions.	Initially, Learning Automata identifies the zone for the given temperature and irradiation value and selects the optimal duty cycle of the corresponding zone. Next, the PO increased the duty cycle and reached the MPP in a few steps. But, in the case of conventional P&O MPPT, the duty cycle value rises from 0.1 until it reaches MPP.	PO +Learning Automata (LA)	The results demonstrate that the proposed MPPT method has significantly improved the tracking performance, response to fast-changing weather conditions, and Also, there is less oscillation at MPP than at the conventional PO MPPT and Modified P&O MPPT.

2.4.3.7. Discussion of AI MPPT Algorithms

High accuracy, fast tracking speed, ease of implementation, and the ability to track the Global Maximum Power Point (GMPP) even under partial shading conditions (PSC) are the most essential and desirable features. Yet, they are complementary features of any individual MPPT technique because high accuracy is typically associated with slow tracking speed, as in the Perturb and Observe (PO) objective function. Most single or individual MPPT techniques achieve one or two desirable features while failing to reach the others. As a result, Hybrid MPPT techniques are produced, which combine two separate MPPT techniques to achieve the overall benefits of one while removing the shortcomings of the other. The hybrid MPPT techniques improve settling time and overall PV system response time **(Batarseh and Za'ter, 2018)**. Hybrid methods aim to reduce the oscillation at MPP, accelerate the convergence speed, improve the tracking accuracy, reduce the power loss, and improve the conversion efficiency of the PV system **(Fan et al., 2021)**.

2.5. Various Cube Satellite missions

Table 2. 6: Various Cube Satellite missions

Mission Name	Year	Organization	Purpose	References
Artemis 1 CubeSats	2022	NASA	Multiple lunar and deep space exploration	https://www.nasa.gov/
REAL	2021	Dartmouth College	Characterise particle loss from Earth's Van Allen belts	https://www.nasa.gov/
LunIR	2022	Lockheed Martin	Moon surface mapping and composition characterization	https://www.space.com/
OMOTENASHI	2022	JAXA	Demonstrate lunar landing and measure surface radiation	https://www.space.com/
NEA Scout	2022	NASA	Near-Earth asteroid reconnaissance	https://www.space.com/
EQUULEUS	2022	JAXA and the University of Tokyo	Study Earth's plasmasphere and radiation environment	https://www.space.com/
BioSentinel	2022	NASA Ames	Study the effects of deep-space radiation on yeast cells	https://www.space.com/
RainCube	2018	NASA JPL	Relay data from the Mars InSight lander	https://science.nasa.gov/
Mars Cube One (MarCO)	2018	NASA JPL	Relay data from the Mars InSight lander	https://science.nasa.gov/

Q-PACE	2021	University of Central Florida	Study collisions in protoplanetary disks	https://science.nasa.gov/
PREFIRE Mission	2023	NASA	A pair of CubeSats designed to study how much heat is radiated from Earth's polar regions into space. Polar Radiant Energy in the Far-InfraRed Experiment (PREFIRE)	https://www.jpl.nasa.gov/news/nasa-launches-second-small-climate-satellite-to-study-earths-poles
TROPICS Constellation	2023	NASA	Time-Resolved Observations of Precipitation structure and storm Intensity with a Constellation of Smallsats mission.	https://scitechdaily.com/nasa-tropics-constellation-rocket-lab-successfully-launches-final-cubesat-duo/
VISORS Mission	2024	University of Illinois,	The Virtual Super-Resolution Optics with Reconfigurable Swarms (VISORS) will use a formation of CubeSats to image the solar corona.	https://scitechdaily.com/nasa-announces-latest-candidates-for-cubesat-space-missions/

CubeSat missions, in Table 2.5, represent a range of objectives, from deep space exploration to studying Earth's atmosphere. They highlight small satellites' versatility and importance in advancing our understanding of space.

2.6. Conclusion

The advantages that the hybrid MPPT offers are as follows: tracking of the global maximum power point (GMPP) even under partial shading conditions and fast-changing weather conditions, damping of oscillations around the GMPP, increased efficiency of PV power extraction, fast response time and fast convergence time and generally decrease power losses. In the hybrid MPPT, faster response time is proportional to huge oscillations around the MPP and inversely proportional to the tracking efficiency of the GMPP.

The disadvantages of the hybrid MPPT techniques are high computation complexity since they employ bio-inspired AI algorithms, and hardware implementation of hybrid includes additional hardware components such as PID controllers and slide mode controllers; thus, hardware complexity is increased. Increased hardware and software complexities are non-ideal for CubeSat applications with limited volume and mass. The absence of a dedicated microprocessor for EPS is another limitation to implementing hybrid MPPTs for a CubeSat application. Hence, a low-complexity classical MPPT such as PO is desirable to be combined with a low-complexity AI technique.

CHAPTER 3

PV MODULE MODELLING AND PO MPPT CONTROL IMPLEMENTATION FOR A CUBE SATELLITE POWER SYSTEM

3.1. Introduction

This Chapter begins with the mathematical modeling of a PV module using the Azur Space 3G30C solar module datasheet. The module model uses the single-diode PV model method as opposed to the double-diode PV method. The model is implemented in MATLAB/Simulink using the five algebraic equations labeled in the single-diode PV model circuit diagram in Figure 3.2. An orthographic drawing showing an exploded two-dimensional view of how two Azur space 3G30C solar modules are connected in parallel in each X-configuration side panel or Y-configuration side panel is depicted in Figure 3.3 of this chapter. Also, Figure 3.3 illustrates a two-dimensional view of the four Spectrolab solar cells in each Z-configuration side panel connected in parallel. Subsections 3.2 and 3.3 describe the mathematical modeling of the Azur Space 3G30C solar module in MATLAB/Simulink.

The X and Y-configuration side panels are connected to an MPPT controller for maximum power extraction from the PV side panels in the CubeSat architecture shown in Figure 3.1. Subsection 3.4 begins with a comparative analysis of the four conventional MPPT functions. The comparative analysis reveals how each conventional MPPT function performs under standard test conditions (STC) and varying irradiation or temperature. The PO function was implemented because of its low complexity demand in the CubeSat microprocessor power (one OBC). At the end of subsection 3.4. a comparison of how the power, voltage, and current characteristics respond to the application of the PO function and without it is demonstrated.

3.2. Photovoltaic Solar Module Mathematical Modelling Requirements

The PV solar module is modeled using five algebraic current equations from the first principles. A single-diode PV equivalent solar cell circuit is depicted in Figure 3.1. The five current equations are labeled on the equivalent circuit in Figure 3.1. The equivalent circuit in Figure 3.1 concerns the solar PV panel part. The reviewed literature on PV modeling generally agrees that the single-diode model (Figure 3.2) suffices for representing the electrical characteristics of the PV solar cell (Mataifa, 2015). Table 3.1 shows values of the parameters used on the five mathematical equations of a PV solar cell as well as values of inputs as per Azur Space 3G30C solar cell datasheet.

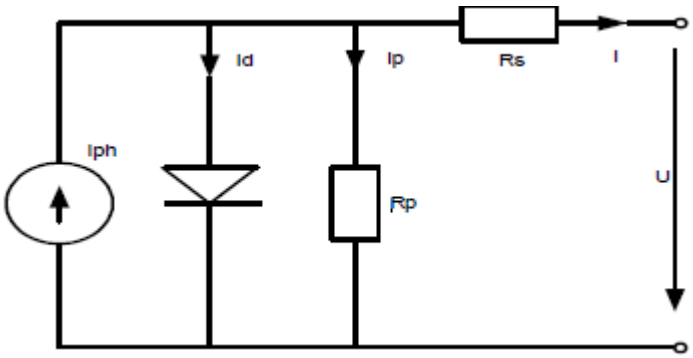

Figure 3. 1: PV solar model of 1D/2R cell (Adapted from Hoarca, 2005)

To calculate the output current of the one diode/two resistor (1D/2R) PV model shown in Figure 3.2, five parameters must be predetermined using measured experimental data and data provided by the manufacturers. These five parameters are photovoltaic current (I_{ph}), diode saturation current (I_S/I_o), diode ideality factor (A), series resistance (R_S), and parallel resistance (R_P). In this thesis, the parameters obtained by Alvarez et al., 2021, where a 1D/2R model equivalent circuit was analytically fitted to I-V curves corresponding to data from Azrur Space 3G30C solar cells datasheet. Numerically fitting demands the I-V curve to have enough large number of points for it to be accurate, whereas analytical fitting uses the characteristic points (, I_{sc}), (V_{mpp}, I_{mpp}), (V_{oc}, 0) and the maximum power point where; $-\frac{I_{mpp}}{V_{mpp}}$ to find the values of the five parameters listed in Table 3.1. Alvarez et al., 2021 also numerically fitted to I-V curves corresponding to data from Azrur Space 3G30C solar cells datasheet and obtained distinct values of the five parameters. However, this thesis does not use the numerically fitted values to model the Azur 3G30C solar PV cell mathematically **(Álvarez et al., 2021)**.

Table 3. 1: Parameters of mathematical equations (Alvarez, 2021)

Parameter	Parameter full name	Parameter value at (STC)
I_{ph} (*) [A]	**Photovoltaic current**	**457mA**
T	Operating Temperature	–65 ºC to +125 ºC at LEO
I_o (*) [A]	**Diode saturation current**	**5.012e-28**
q	Electron charge	1.6e-19C
A	**Ideality factor of diode**	**0.56**
k	Boltzmann constant	1.38e-23 J/K
E_g	Band gap energy	1.1eV
R_S [Ω]	**Series resistance**	**0.653**
R_p [Ω]	**Shunt resistance**	**160.7**
V_t	Thermal Voltage	**0.0257V**

The electrical data of the solar module used on the four adjacent sides of the 1U cube satellite is provided in Table 3.2.

Table 3. 2: Electrical data of the Azur Space 3G30C module BOL (Alvarez, 2021)

Parameter	Parameter name	Parameter value
V_{OC} (*)	Open circuit voltage	2.7V
I_{SC} (*)	Short circuit current	457mA
N_s	Number of cells in series	3
N_p	Number of cells in parallel	1
V_{mpp} (*)	Maximum point voltage	2.411V
I_{mpp} (*)	Maximum point current	442.8mA
Ki [A/°C]	Coefficient with temperature of the short circuit current @ STC	3.2e-4 BOL
T_n	Nominal Temperature	28°C, at STC
G	Solar irradiance	1367W/m^2 at STC

Symbols listed with (*) imply that values of the quantities at standard test conditions (STC) also apply.

3.3. Mathematical Equations of a PV solar module

Based on the single diode/ two resistor (1D/2R) model (Figure 3.1), a five-parameter determination of the solar module listed in Table 3.1., the mathematical expressions of the PV module were derived:

The photovoltaic current ($\boldsymbol{I_{ph}}$) depends on the irradiance and temperature of the cell:

$$\boldsymbol{I_{ph} = [I_{SC} + k_i(T - 301)] \times \frac{G}{1367}} \quad (3.1)$$

The module reverse saturation current $\boldsymbol{I_{s,r}}$:

$$\boldsymbol{I_{rs} = \frac{I_{sc}}{exp\left(\frac{q \times V_{OC}}{N_s \times k \times A \times T}\right) - 1}} \quad (3.2)$$

The saturation/diode saturation current of the cell $\boldsymbol{I_s / I_o}$ varies with the temperature:

$$\boldsymbol{I_s = I_{rs}\left[\frac{T}{T_n}\right]^3 exp\left[\frac{q \times E_g}{A \times K}\left(\frac{1}{T_n} - \frac{1}{T}\right)\right]} \quad (3.3)$$

The current through the parallel resistance or the shunt resistor:

$$I_P = \left[\frac{V+IR_S}{R_P}\right] \quad (3.4)$$

The current through the diode I_d given by the following equation:

$$I_d = I_S\left[exp\left(\frac{V+I\times R_s}{A\times\frac{k\times T}{q}}\right)-1\right] \quad (3.5)$$

The following equation gives the output current of the PV array:

$$I = I_{ph} - I_d - I_s\left[exp\left(\frac{q(V+IR_s)}{AkN_sT}\right)\right] \quad (3.6)$$

Photocurrent (I_{ph}) is current directly proportional to the incident solar irradiation and temperature from the sun. The diode saturation current (I_D) is the forward bias current present only when the photocurrent is present. The reverse saturation current (I_{rs}) is the avalanche current in the reverse bias condition that must not be exceeded. The shunt resistor current (I_{sh}) is the nonideality current that flows through the shunt resistor and represents the slope of the current on the IV characteristic curve. The output current (I) is the generated nonideality current that flows through the series resistor, and it also represents the voltage slopes across the maximum point of the IV characteristic curve. Each side of the cube satellite is fitted with two Azur Space 3G30C solar modules connected in series to form one large panel on each side. All large panels on opposite sides will be connected in parallel to form two groups: the (+X, -X) group and the (+Y, -Y) group.

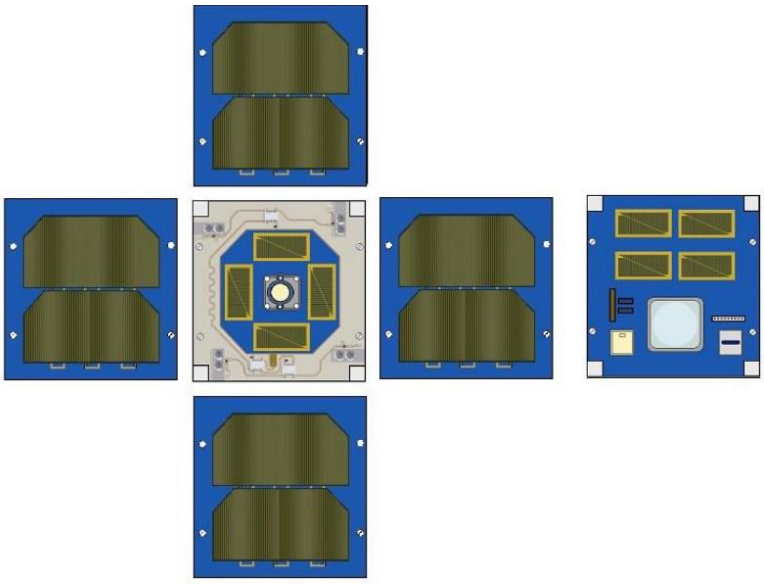

Figure 3. 2: Exploded view of a 1U CubeSat exterior design (Mahdi et al., 2014)

An exploded view of the six sides, including the top and bottom sides, is depicted in Figure 3.3. Each Azur Space 3G30C module MPP outputs: 2411mV, 442.8mA, operated under STC (1367W/m^2, 28°C). Each panel side in the X-configuration or the Y-configuration is fitted with two Azur Space 3G30C modules that are connected in parallel and give a voltage output of 2411mV, a total current output of 885.6mA, at MPP. The opposite panel sides in the X-configuration are connected in parallel and form a (+X, -X) group, and the opposite panel sides in the Y-configuration are connected in parallel and form a (+Y, -Y) group. All eight small Spectrolab TASC cells on the top and bottom sides will be connected parallel to form a (+Z, -Z) group. The Z-configuration's top or bottom side gives a voltage output of 2.2V, a total current of 112mA, at MPP. The (+Z, -Z) group gives a voltage output of 2.2V and a total current of 224mA.

3.4. Photovoltaic Solar module modeling in MATLAB Simulink.

Depicted Figure 3.3 is the photovoltaic current model: $\boldsymbol{I_{ph} = \left[I_{sc} + K_i(T - 301)\frac{G}{1367}\right]}$

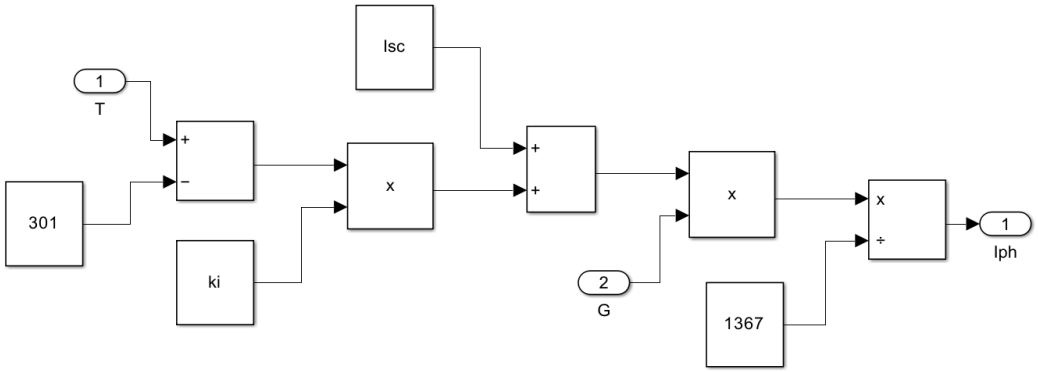

Figure 3. 3: Photocurrent model

Figure 3.3 shows the photocurrent (I_{ph}), which is modeled based on the incident solar irradiance (G) and temperature (T). The photocurrent equation is given by equation 3.1., where $\boldsymbol{I_{sc}}$is the short-circuit current, $\boldsymbol{K_i}$ is the temperature coefficient of the short-circuit current, $\boldsymbol{T}$ is the cell temperature and $\boldsymbol{G}$ is the solar irradiance. This model is fundamental as it establishes the initial current generated by the PV cell when exposed to sunlight. Figure 3.4 is the saturation/diode saturation current model, and it depends on the temperature and is modeled by equation 3.3. $\boldsymbol{I_{rs}}$ is the reverse saturation current, $\boldsymbol{T}$ is the cell temperature, $\boldsymbol{q}$ is the electron charge, $\boldsymbol{E_g}$ is the bandgap energy, $\boldsymbol{k}$ is Boltzmann's constant, and $\boldsymbol{n}$ is the diode ideality factor. This model is crucial for understanding the temperature-dependent behavior of the diode's saturation current. Figure 3.5 is the saturation current model. Ohm's law gives the current through the shunt resistor (Ish) in equation 3.4. V is the output voltage, R_s is the series resistance, and R_{sh} is the shunt resistance. This model captures the losses due to leakage current in the PV cell.

Figure 3.6 is the reverse saturation current model. The reverse saturation current (I_{rs}) is modeled as equation 3.2. where V_{oc} is the open-circuit voltage, and N_s is the number of cells in series. This model is integral for characterizing the behavior of the diode under reverse bias conditions. Figure 3.7 is the Output Current Model. The PV module's output current (I) is derived by combining the models of equations 3.1. to 3.5, thereby forming equation 3.6. This equation consolidates the contributions of photocurrent, diode current, and shunt current to yield the net output current of the PV cell. Figures 3.8 and 3.9 show the combined subsystems of the solar PV cell. These figures illustrate the integration of the sub-models into a unified PV cell model. The final subsystem takes irradiance and temperature as inputs. It outputs the I-V and P-V characteristics, which are essential for simulating the performance of the PV module under various conditions.

Figure 3.10 depicts the I-V curve, which represents the relationship between the output current (I) and the PV module's output voltage (V). It is characterized by the short-circuit current (Isc) at V=0 and the open-circuit voltage (Voc) at I=0. The curve exhibits a non-linear behavior where the maximum power point (MPP) is located at the knee of the curve, indicating the optimal operating point for maximum power extraction. Figure 3.11 depicts the P-V curve and plots the output power (P) against the output voltage (V). The peak of this curve corresponds to the MPP, where the product of current and voltage yields the maximum possible power. This characteristic curve is crucial for MPPT algorithms to adjust the operating point to maximize energy harvest dynamically. The technical description of each model emphasizes the importance of each model and characteristic curves for simulating the performance of photovoltaic systems.

Figure 3.4 is the saturation/diode saturation current model: $I_s = I_{rs}\left[\frac{T}{T_n}\right]^3 exp\left[\frac{q.E_{g0}\left(\frac{1}{T_n}-\frac{1}{T}\right)}{nK}\right]$

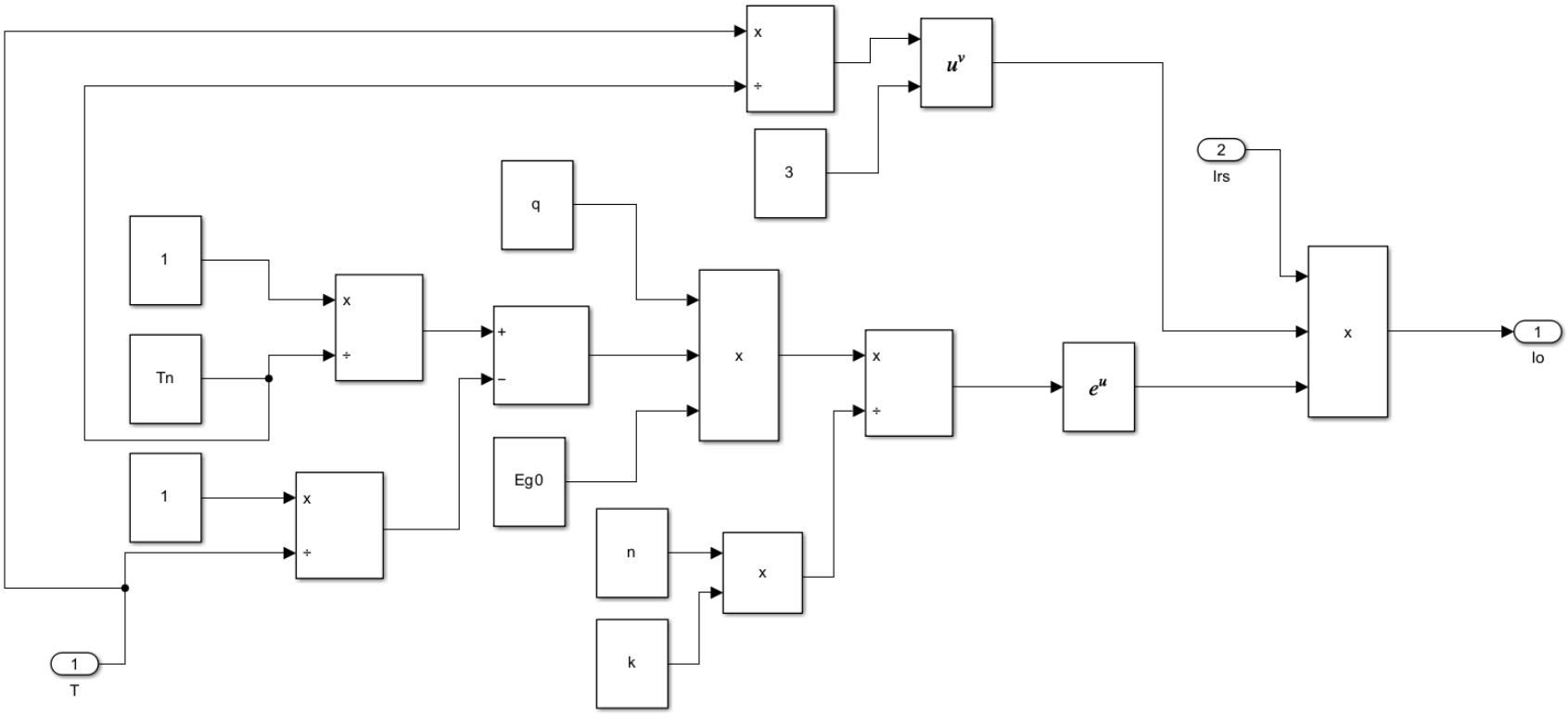

Figure 3. 4: Saturation current model

Depicted Figure 3.5 is the parallel/shunt resistor current model: $\boldsymbol{I_{sh}} = \left[\frac{V+IR_S}{R_{sh}}\right]$

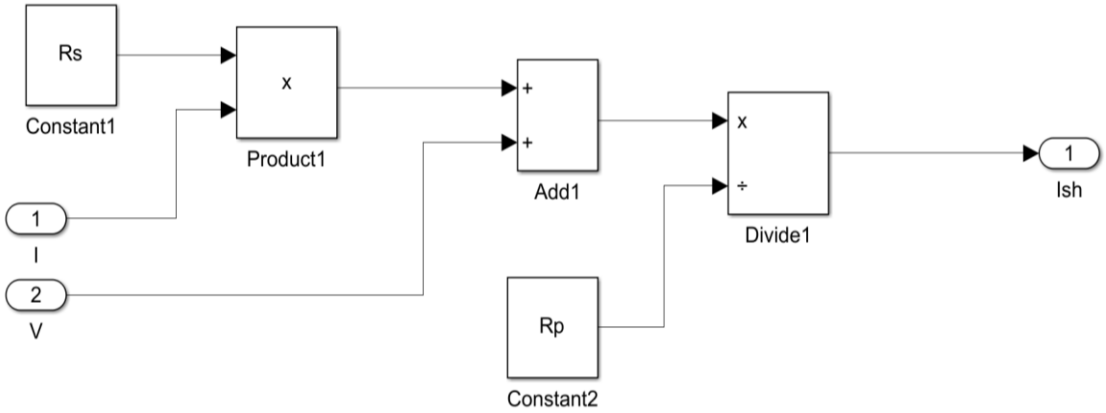

Figure 3. 5: Shunt resistor current model

Depicted Figure 3.6 is the Reverse saturation current model: $\boldsymbol{I_{rs}} = \frac{I_{sc}}{exp\left[\frac{q.V_{OC}}{nN_SKT}-1\right]}$

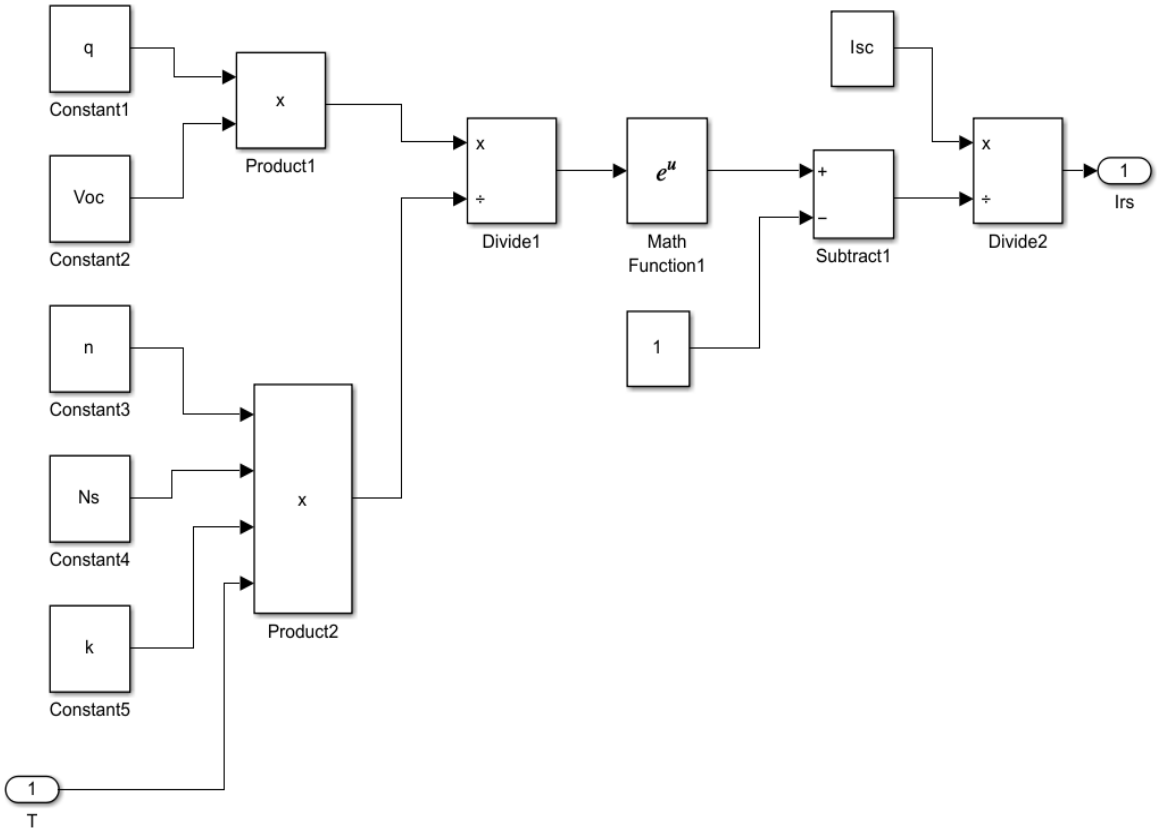

Figure 3. 6: Reverse saturation current model

Depicted Figure 3.7 is the output current model: $\boldsymbol{I = I_{ph} - I_D\left[exp\left(\frac{q(V+IR_s)}{nKN_sT}\right) - 1\right] - I_{sh}}$

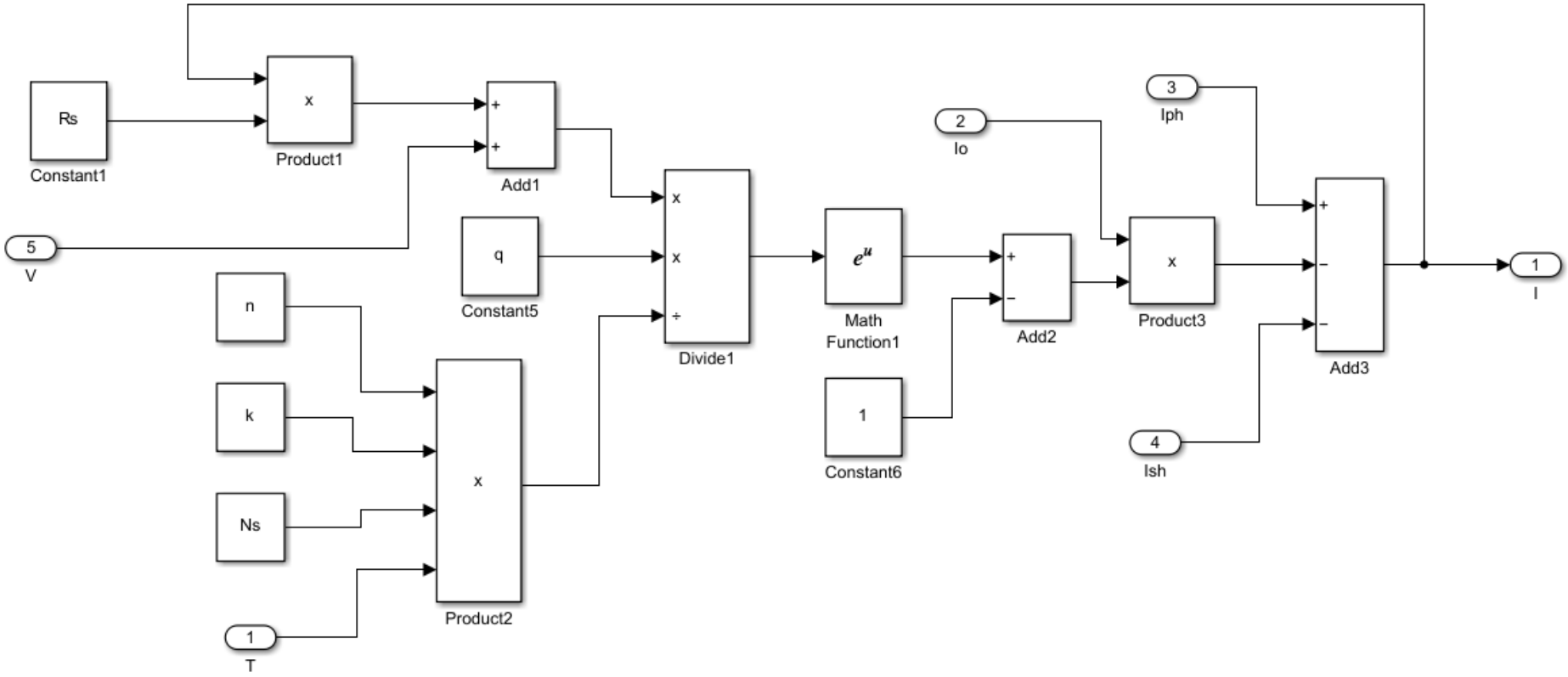

Figure 3. 7: Output current model

When drawing the mathematical models on Simulink, one begins with a single equation, creates a subsystem, and moves on to the following equation. The process is iterated until all the equations are represented. Depicted Figure 3.9 is the combined subsystems of the PV model of a solar cell.

Figures 3.3 to 3.7 show the subsystems of the five current equations and the far right constant, and blocks are added to convert Celsius input temperature to Kelvin value.

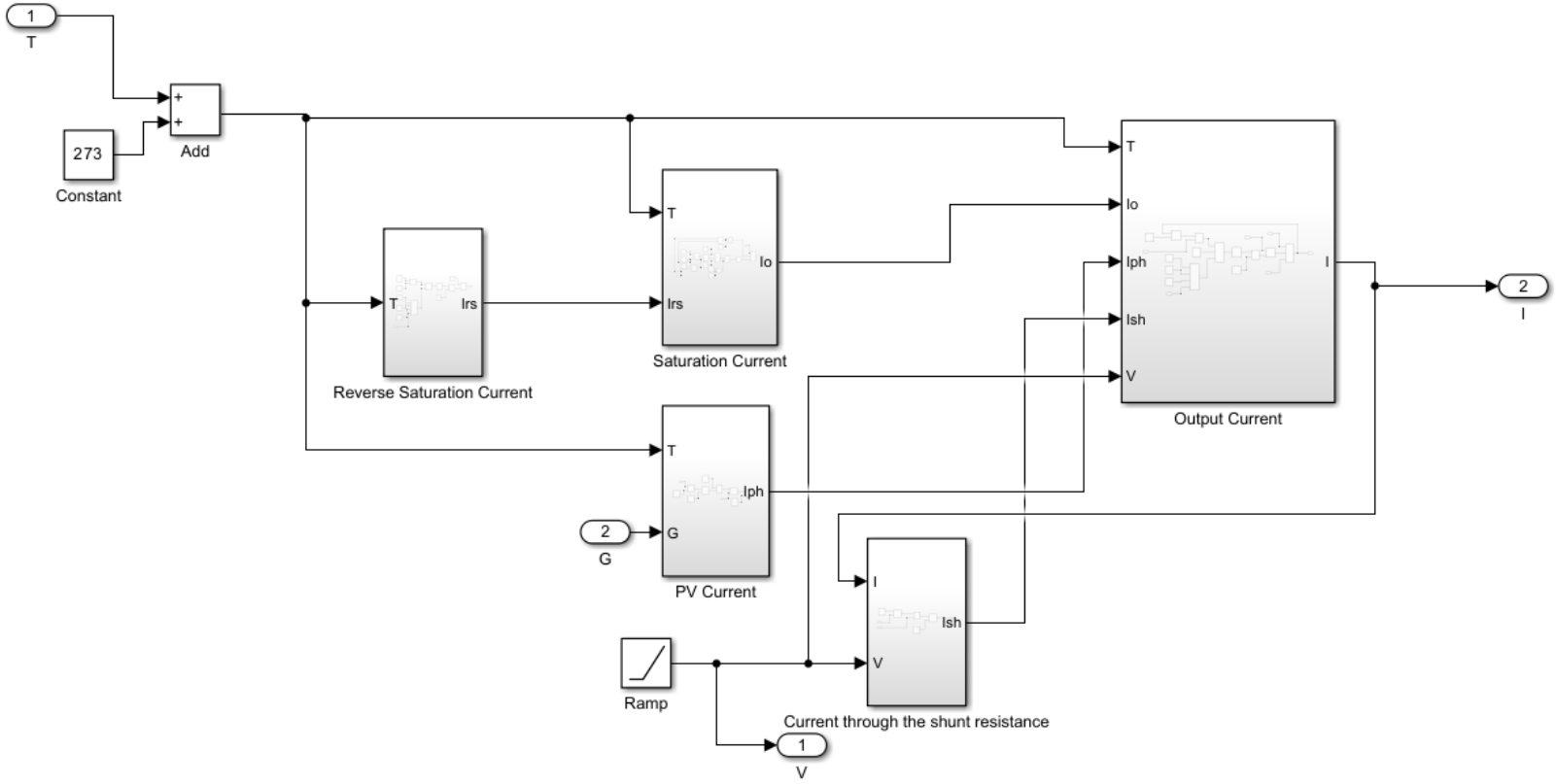

Figure 3. 8: Combined subsystems of the solar PV cell

The final step is to create a single subsystem of the combined subsystems. Temperature and irradiation are placed as inputs of the final PV model, and the IV graph and PV graphs are outputs of the final PV model. The final PV model is depicted in Figure 3.9.

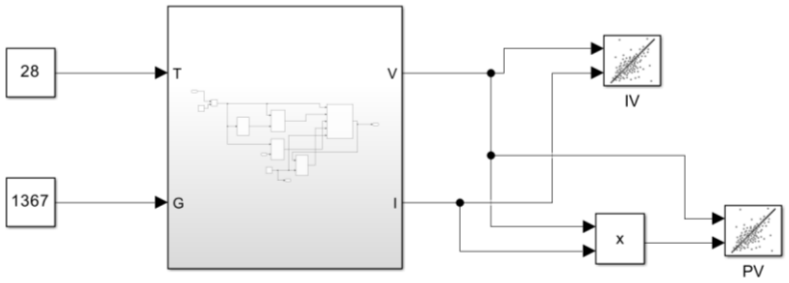

Figure 3.9: Final PV model

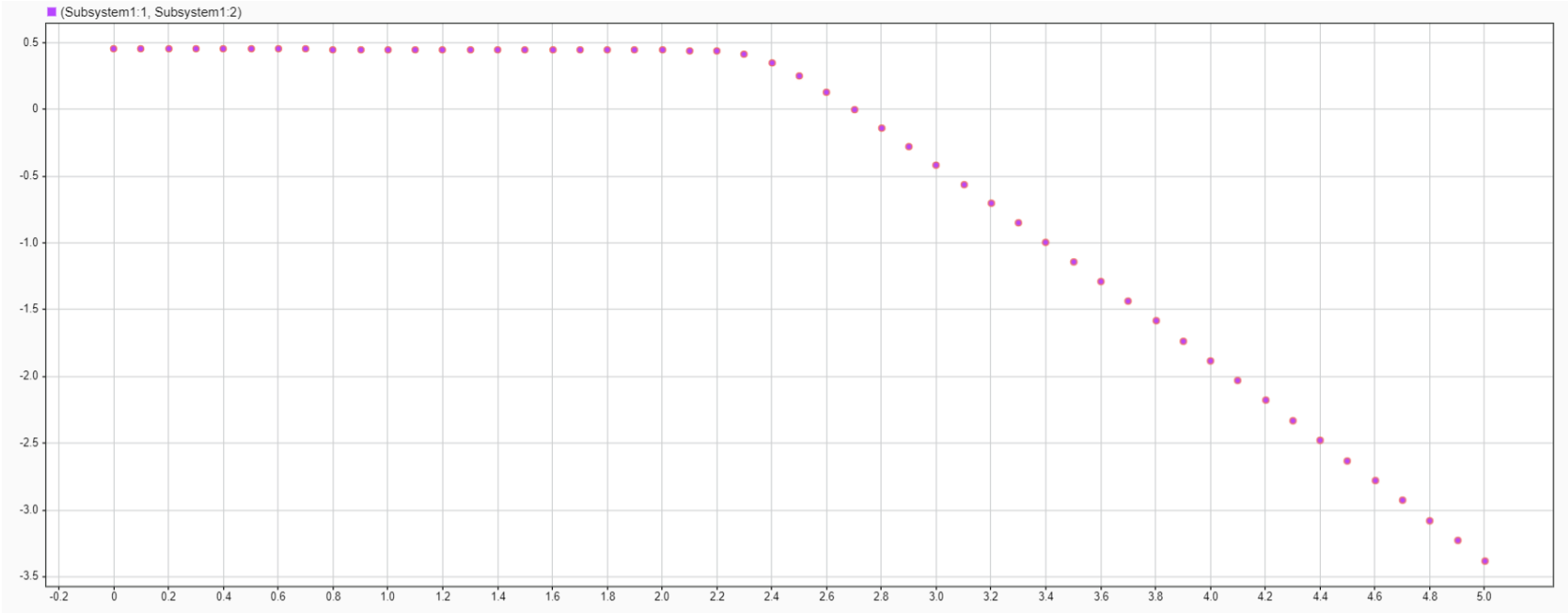

Figure 3. 10: IV curve of the 3G30C PV module

For the model to execute without errors, one needs to go to the model properties, look under callbacks, click the initialization function, and preset all the constant values according to the values outlined in Tables 3.1 and 3.2.

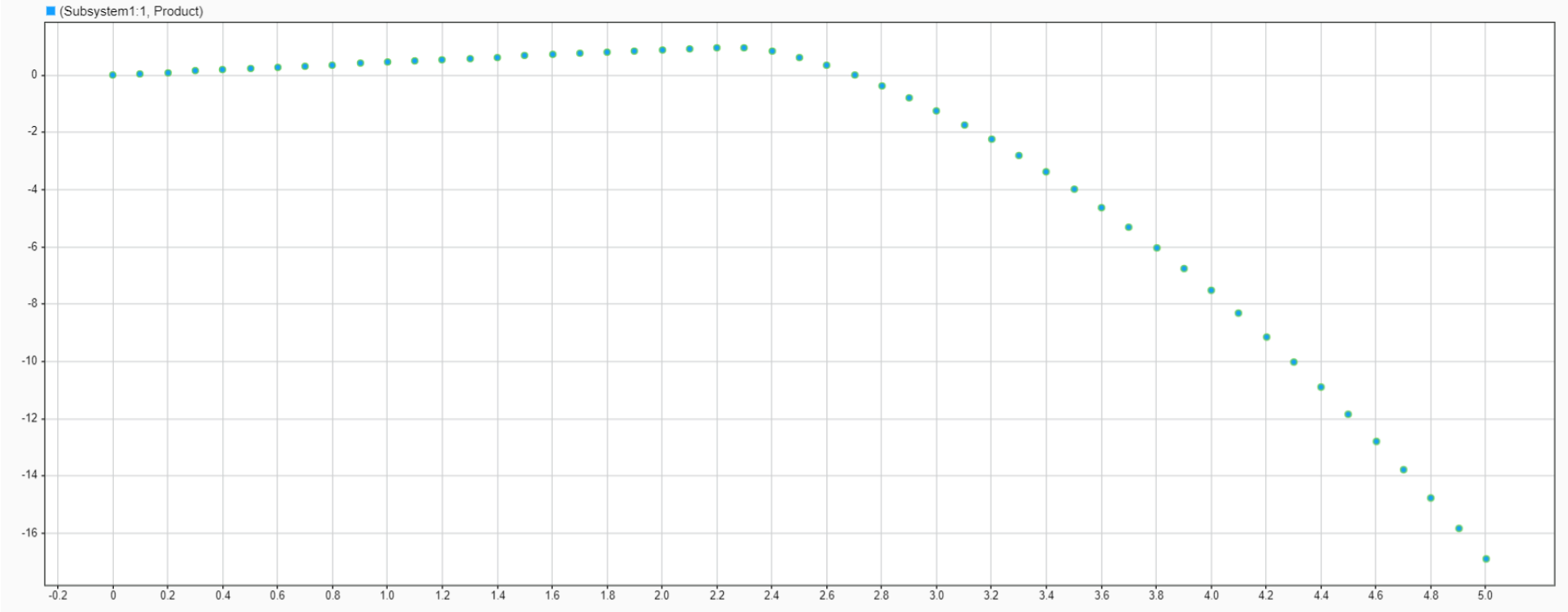

Figure 3. 11: PV curve of the 3G30C PV module

Figure 3.10 depicts the simulation results of the IV model, where the x-axis starts from zero to V_{OC}, equal to 2.7V, and the Y-axis starts from zero to I_{SC}, equal to 0.457A. Figure 3.11 depicts the simulation results of the PV model, where the x-axis starts from zero to V_{OC}, equal to 2.7V, and the Y-axis starts from zero to Pmax, equal to 1.23W. The shunt resistance: $\boldsymbol{R_s = \frac{V_{OC-}V_{mp}}{I_{mp}} = 0.653\Omega}$; Thermal Voltage: $\boldsymbol{V_t = \frac{nkT}{q} = 0.0257V}$; Shunt Resistance: $\boldsymbol{R_{sh} = \frac{V_{mp}}{I_{sc}-I_{mp}} = 160.7\Omega}$

3.5. Conventional MPPT Techniques Comparisons for Implementation in CubeSat Power Systems

There are four conventional MPPT objective functions, namely, perturb and observe (PO), fractional short circuit current (FSCC), fractional open circuit voltage (FOCV), and incremental conductance (IC). Research continuously improves upon these four basic conventional techniques using artificial intelligence (AI) techniques like fuzzy logic neural networks and adaptive neuro-fuzzy Inference systems (ANFIS). It has been found that under steady-state weather conditions, the incremental conductance (IC) performs the best in terms of efficiency and power losses. Under positive increasing temperature incremental conductance (IC), convergence to the maximum power point is faster than all other objective functions, followed by the fractional open circuit voltage (FOCV) technique. However, under negative decreasing temperatures, FOCV finds the maximum point faster than all other techniques followed by the IC technique. Fractional open circuit voltage (FOCV) finds the maximum point fast in dynamic conditions because the open circuit voltage doesn't change rapidly with temperature changes. However, the saturation current that the fractional short circuit current (FSCC) technique depends on changes drastically under dynamic weather conditions. Hence, the FSCC performs poorly under dynamic weather conditions.

The least efficient technique under dynamic weather conditions is PO because of its sampling rate, which doesn't keep up with fast-changing weather. The PO is the easiest to implement in terms of hardware and software complexity. IC is the most complex to implement in terms of software and requires two sensors (voltage and current) in terms of hardware. FOCV and FSCC are easy to implement at the software level but require additional hardware arrangements for installing voltage or current sensors (Murtaza et al., 2013). Also, the FOCV and FSCC use the approximation methods to determine the k-constant. Hence, they are not genuinely seeking MPP functions.

Table 3. 3: Summary of the comparison of MPPT techniques (Murtaza et al., 2013)

Parameters	Perturb and Observe (PO)	Incremental Conductance (IC)	Fractional open Circuit Voltage (FOCV)	Fractional Short Circuit Current (FSCC)
Prior tunning	No	No	Yes	Yes
Dynamic Tracking	Reasonable	High	High	Medium
Steady Tracking	Reasonable	High	Medium	Medium
Algorithm complexity	Low	High	Low	Low
Hardware complexity	Low	Low	Medium	Medium
Sensors	V&I	V&I	V	I

Therefore, for a CubeSat application, the PO will be selected for advantages like no prior tuning, low Algorithm complexity, and low hardware complexity. Table 3.5 gives a summary of the comparison of MPPT objective functions.

3.6. Requirements for designing the 5V and the 3.3V Boost converter

The boost converter's output voltage is more than the input voltage. DC-DC converters are smaller in mass than linear converters. Hence, they are highly efficient and cheap to construct.

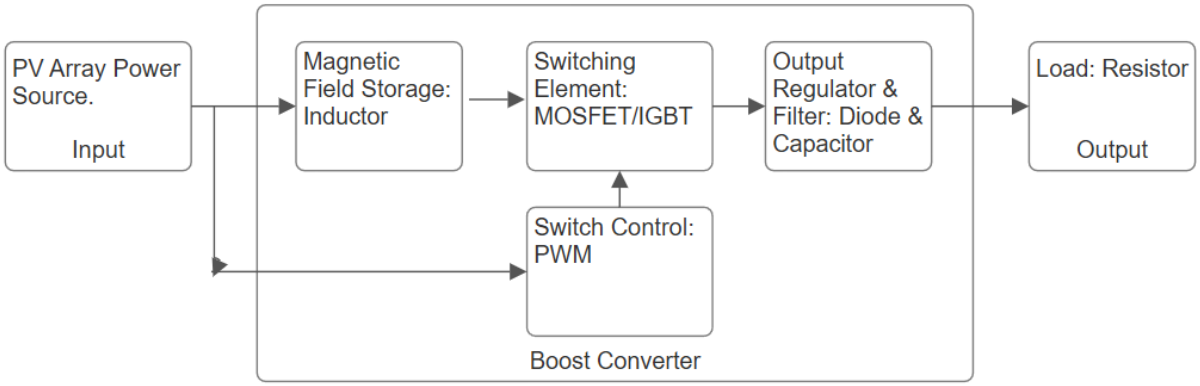

Figure 3. 12: Boost Coveter Basic Block Diagram

The solar PV panel voltage is the source voltage and will change proportionally to solar irradiance and temperature. It is in the left block of Figure 3.12. The input inductor acts as a magnetic field storage device and is at the bottom of Figure 3.12. The MOSFET acts as a switching element driven on and off by the pulse width modulator (PWM), right on top of the magnetic field storage (inductor) in Figure 3.12. The diode acts as an output regulator, and the output capacitor acts as an output filter, and they are at the right of Figure 3.12. In Figure 3.13, the desired inductor ripple current and desired ripple output voltage are inversely proportional to inductance and capacitance, which means the smaller the desired ripples, the larger the inductor and capacitor values.

The boost converter has two modes, i.e., mode one is when the MOSFET is on, and mode two is when the MOSFET is off. The MOSFET is switched on and off by a square wave of the Pulse Width Modulator (PMW). The duty cycle of the switching square wave is determined by input and output voltages, as shown in equation (3.7), and the duty cycle is inversely proportional to the output voltage. When designing a boost converter, the values of inductor ripple current and capacitor ripple voltage, square wave switching frequency, load voltage, load resistance or load current, and solar PV panel output voltage range are preselected and kept constant. Then, boost converter design equations are used to calculate the input inductor and output capacitor values.

(Fathah, 2013). The DC-DC step-up components calculations are for the worst-case design scenario of the CubeSat. The worst-case situation is when two sides of the CubeSat point towards the sun, which means four modules are active.

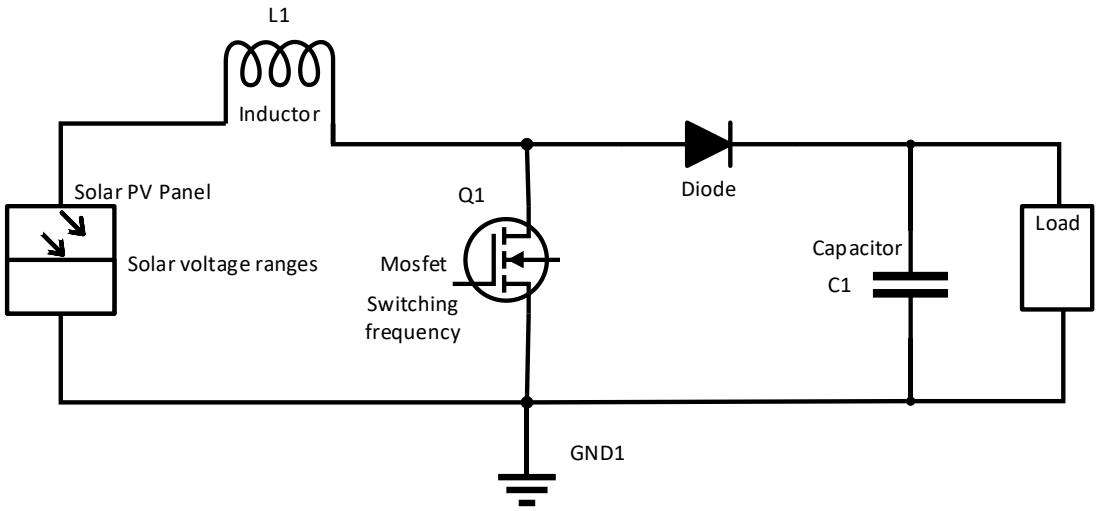

Figure 3. 13: Boost Converter Circuit Diagram

The DC-DC step-up components calculations are for the worst-case design scenario of the CubeSat. The worst-case situation is when two sides of the CubeSat point towards the sun. A configuration where two sides of the CubeSat are pointed to the sun is simulated by the (+X, +Y) or (-X, -Y) groups. The (+X, +Y) or (-X, -Y) group gives a voltage output of 2.4V and a total current of 1.8A. The solar Array will have four modules connected in parallel. This array is an input of the boost converters. The desired outputs of the boost converters are 3.3V and 5V, as determined by the desired bus load voltages. Each (+X, +Y) or (-X, -Y) group (two adjacent sides) is connected to either a 5V boost converter or a 3.3V boost converter.**(Guter et al., 2017)**.

3.7. The Design Calculations of the 5V Boost Converter

These design calculations are for the worst-case scenario when two sides of the one-unit CubeSat are exposed to the sun:

Table 3. 4: PV Array parameters (Adapted from Guter et al., 2017)

Specification of parameters	Description of parameters
$V_{MPP} = 2.4V$	Maximum power point voltage of the PV array.
$V_{oC} = 2.7v$	The Open circuit voltage.
$I_{SC} = 457mA$	Short circuit current of the PV array.
$N_S = 3$	Number of cells in series
$N_p = 4$	Number of cells in parallel
$I_{MPP} = 422.8mA$	PV array maximum power point.

Table 3. 5: Boost Converter Specification (Adapted from AZUR SPACE, 2010)

Specification of parameters	Description of parameters

$V_{in} = 2V - 3V$	Input voltage range of the boost converter
$V_o = 5v$	Output voltage of the boost converter
$\Delta V = 1\%$	Ripple voltage across the capacitor of the boost converter
$\Delta I = 5\%$	Ripple current through the inductor of the boost converter.
$f_s = 5kHz$	Boost converter switching frequency.

Boost converter input Voltage (V_{in}) and Current (I_{in}):

Let's assume that the boost converter operates at the maximum power point of the PV array.

$$V_{in} = V_{MPP} = 2.4V \quad (3.7)$$

$$I_{in} = I_{MPP} \times N_P = 422.8 \times 10^{-3} \times 4 = 1.6912A \quad (3.8)$$

$$P_{in} = V_{in} \times I_{in} = 2.4V \times 1.6912A = 4.059W \quad (3.9)$$

Let's assume that the boost converter operates at 90% efficiency:

$$I_{out} = \frac{0.90 \times 4.059W}{5V} = 0.7306A \quad (3.10)$$

The ripple current is 5% of the input current:

$$\Delta I_L = 0.05 \times I_{in} = 0.05 \times 1.6912A = 0.08456A \quad (3.11)$$

$$L = \frac{V_{in} \times (V_{out} - V_{in})}{\Delta I_L \times f_s \times V_{out}} \quad (3.12)$$

$$L = \frac{2.4V \times (5V - 2.4V)}{0.08456 \times 5kHz \times 5V} = 2.95mH \quad (3.13)$$

The ripple voltage is 1% of the output voltage:

$$\Delta V = 0.01 \times V_{out} = 0.01 \times 5V = 0.05V \quad (3.14)$$

$$D = 1 - \frac{V_{in}}{V_{out}} = 1 - \frac{2.4V}{5V} = 0.52V \quad (3.15)$$

$$C = \frac{I_{out} \times D}{\Delta V \times f_s} \quad (3.16)$$

$$C = \frac{0.7306 \times 0.52}{0.05 \times 5000Hz} = 1520\mu F \quad (3.17)$$

$$R_{out} = \frac{Vout}{Iout} = \frac{5V}{0.7306A} = 6.8\Omega \quad (3.18)$$

Summary of Calculated Values:

- Inductance: 2.95 mH
- Capacitance: 1520 µF

3.8. The 5V Boost converter MATLAB/Simulink model without PO installed

The boost converter MATLAB/Simulink model without Perturb and Observe installed is shown in Figure 3.14. The model is comprised of a PV array and a boost converter. The model is not operating at MPP. The model is tested at STC: 28°C and 1367W/m2. The PV array is set for the worst-case scenario: two sides of the 1U Cube are exposed to the sun, i.e., four modules are active and connected in parallel.

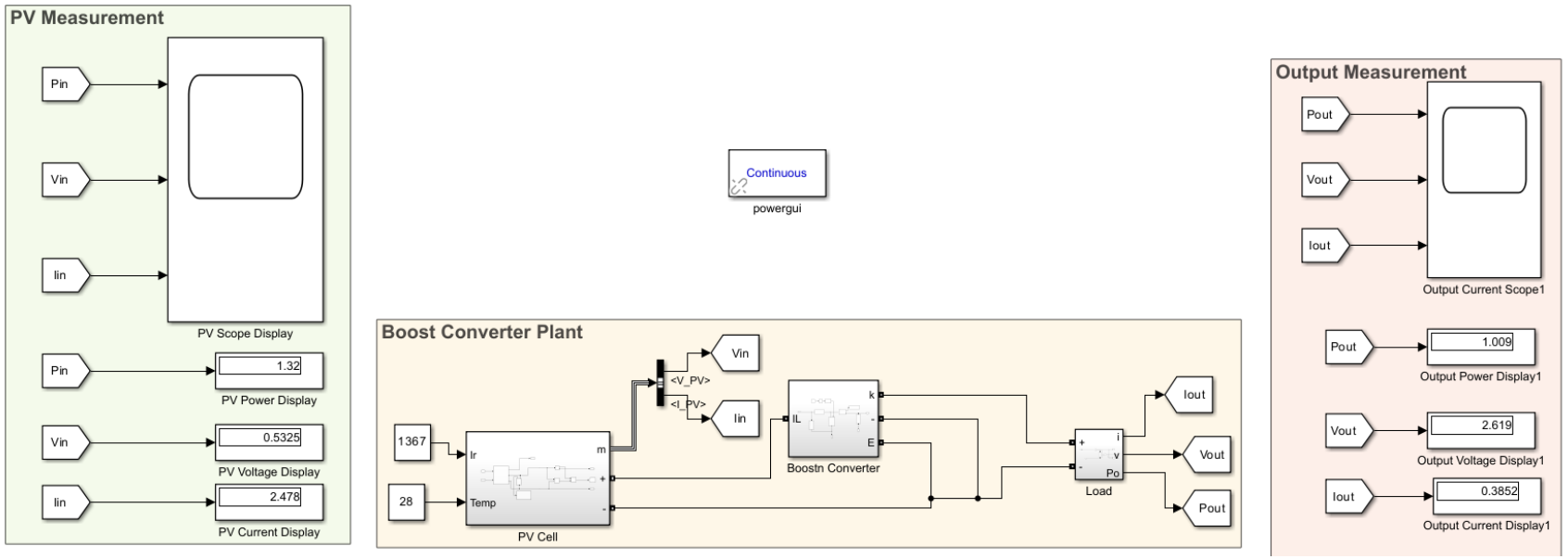

Figure 3. 14: 5V Boost Converter MATLAB/Simulink model without PO installed

To analyze the effect of the perturb and observe the (PO) maximum power point tracking (MPPT) technique, let's first look at the MATLAB/Simulink simulation results of the output current, voltage, and power depicted in Figure 3.15 without PO installed. It can be seen from the displays that the input power is 1.32W, and the output power is 1.009W; there are some power losses from switching elements and system impedances.

Figure 3.15 shows the MATLAB/Simulink simulation results for the output current, voltage, and power without the installed PO.

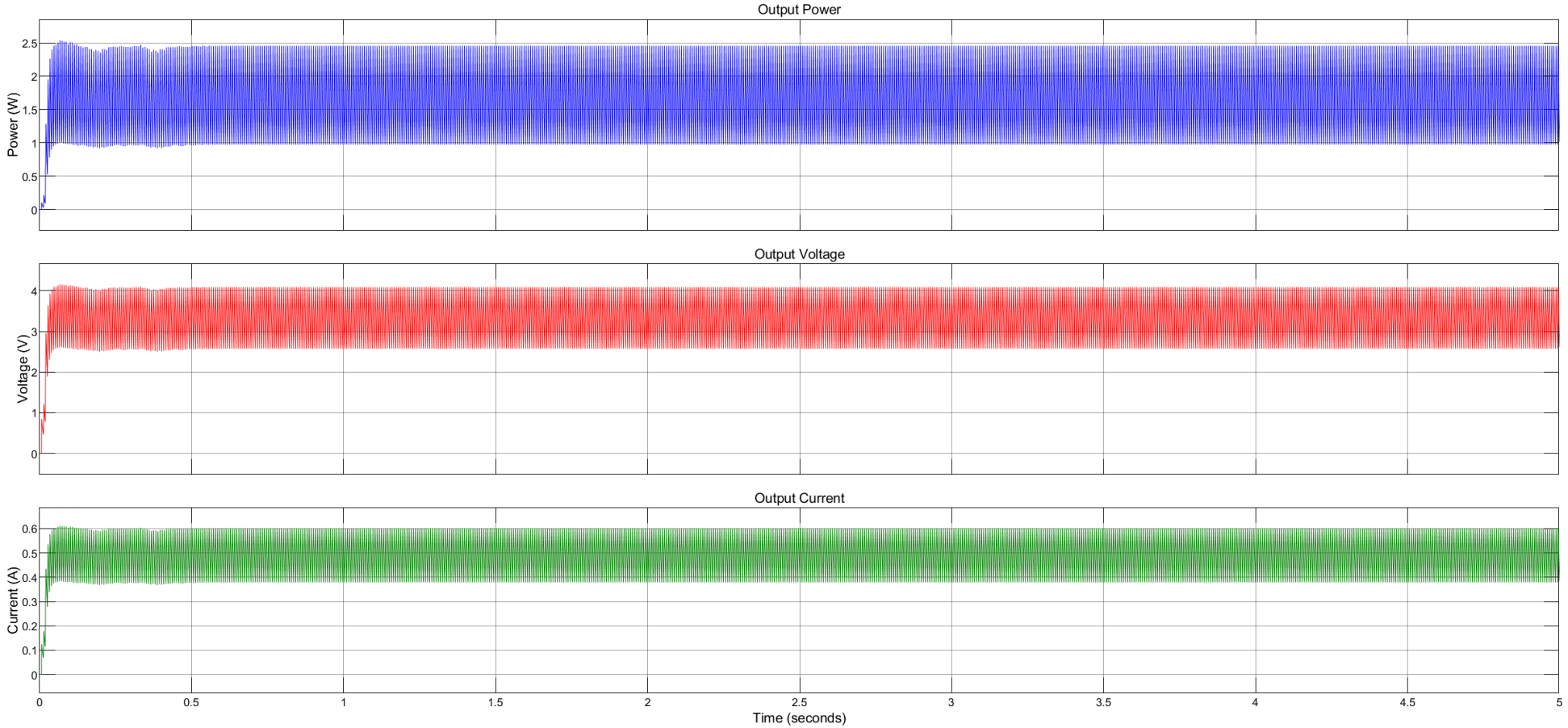

Figure 3. 15: 5V Boost Converter MATLAB/Simulink model simulation results without PO installed

From Figure 3.15, it can be deduced that the output power oscillates between a minimum value of 1.009W to 2.5W, the output current oscillates between a minimum of 0.3852A to 0.6A, and the output voltage oscillates between a minimum of 2.619V and 4.1V.

3.9. The 5V Boost converter MATLAB/Simulink model with PO installed

The PO algorithm objective function and the boost converter take their input power directly from the PV panel, as shown in Figure 3.16. A transient current capacitor filter is installed before the input inductor. The PO objective function uses its sample rate to shift the duty cycle up and down until it finds the MPP and gives its output duty cycle to the input of the PWM. The model is operating at MPP. The model is tested at STC: 28°C and 1367W/m2. The PV array is set for the worst-case scenario: two sides of the 1U Cube are exposed to the sun, i.e., four modules are active and connected in parallel.

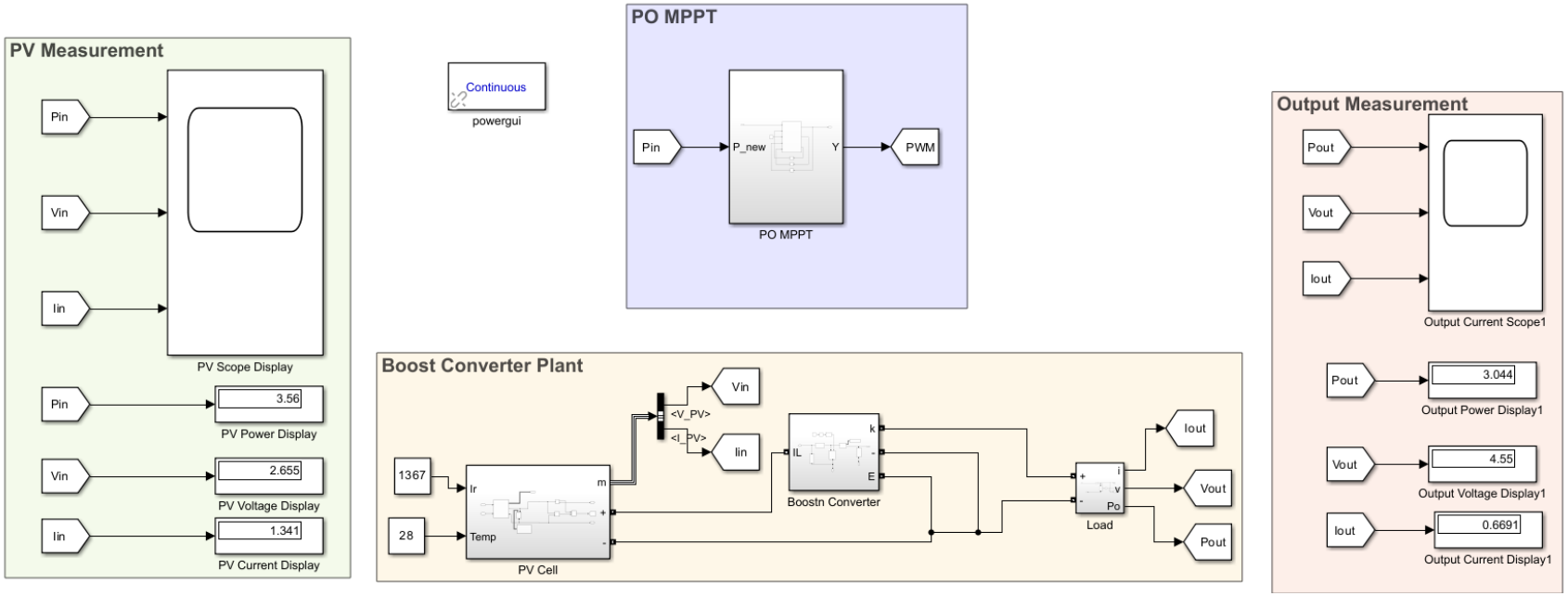

Figure 3. 16: 5V Boost converter MATLAB/Simulink model with PO installed

From Figure 3.16, it can be deduced that the output power is 3W, the output current oscillates between a minimum of 0.7A, and the output voltage is 4.6V.

Figure 3.17 shows MATLAB/Simulink simulation results of the output current, voltage, and power with PO installed.

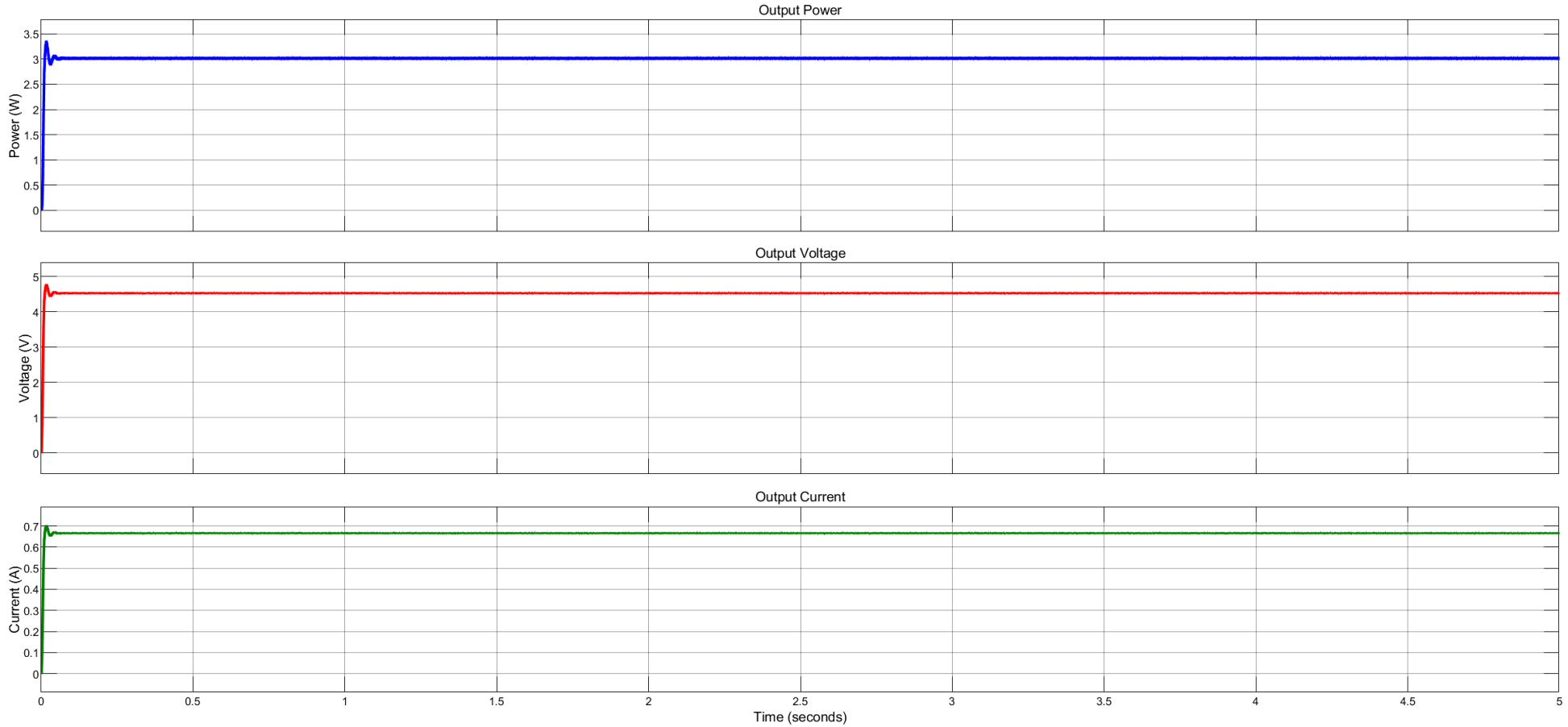

Figure 3. 17: 5V Boost converter MATLAB/Simulink model simulation results with PO installed

It can be seen from Figure 3.16 that the PO objective function will cause the PV array to reach a maximum PV power of 3.6 W and will continue to oscillate around the maximum power PV voltage of 2.7V and a maximum current of 1.34A. The duty cycle will settle around 0.52. It can be seen from Figure 3.17 that the boost converter output power overshoots and dampens at 3.044W, voltage is 4.6V, and current is 0.7A. Hence, applying the PO MPPT improves the output power of the boost converter. All the CubeSat research projects covered in Table 2.2 for a 5V bus can be supplied by the power system EPS modeled in Figure 3.16, except one research project by Agarwal et al., 2016. The power system in Figure 3.16 comprises a 1U CubeSat, and it is assumed that only two sides are exposed to the sun under STC conditions. Even in the mission of Agarwal et al., 2016 all other subsystems of the satellite can be powered by the system modeled in Figure 3.16 except the charging part of the EPS.

3.10. The Design Calculations of the 3.3V Boost Converter

These design calculations are for the worst-case scenario when two sides of the one-unit CubeSat are exposed to the sun:

Table 3. 6: Boost Converter Specification

Specification of parameters	Description of parameters
$\boldsymbol{V_{in} = 2V - 3V}$	Input voltage range of the boost converter
$\boldsymbol{V_o = 3.3v}$	Output voltage of the boost converter
$\boldsymbol{\Delta V = 1\%}$	Ripple voltage across the capacitor of the boost converter
$\boldsymbol{\Delta I = 5\%}$	Ripple current through the inductor of the boost converter.
$\boldsymbol{f_s = 5kHz}$	Boost converter switching frequency.

Boost converter input Voltage ($\boldsymbol{V_{in}}$) and Current ($\boldsymbol{I_{in}}$):

Let's assume that the boost converter operates at the maximum power point of the PV array.

$$\boldsymbol{V_{in} = V_{MPP} = 2.4V} \quad (3.19)$$

$$\boldsymbol{I_{in} = I_{MPP} \times N_P = 422.8 \times 4 = 1.6912A} \quad (3.20)$$

$$\boldsymbol{P_{in} = V_{in} \times I_{in} = 2.4V \times 1.6912A = 4.059W} \quad (3.21)$$

Let's assume that the boost converter operates at 90% efficiency:

$$\boldsymbol{I_{out} = \frac{0.90 \times 4.059W}{3.3V} = 1.1070A} \quad (3.22)$$

The ripple current is 5% of the input current:

$$\Delta I_L = 0.05 \times I_{in} = 0.05 \times 1.6912A = 0.08456A \quad (3.23)$$

$$L = \frac{V_{in} \times (V_{out} - V_{in})}{\Delta I_L \times f_s \times V_{out}} \quad (3.24)$$

$$L = \frac{2.4V \times (3.3V - 2.4V)}{0.08456 \times 5kHz \times 3.3V} = 1.55mH \quad (3.25)$$

The ripple voltage is 1% of the output voltage:

$$\Delta V = 0.01 \times V_{out} = 0.01 \times 3.3V = 0.033V \quad (3.26)$$

$$D = 1 - \frac{V_{in}}{V_{out}} = 1 - \frac{2.4V}{3.3V} = 0.2727V \quad (3.27)$$

$$C = \frac{I_{out} \times D}{\Delta V \times f_s} \quad (3.28)$$

$$C = \frac{1.1070 \times 0.2727}{0.033 \times 5000Hz} = 1830\mu F \quad (3.29)$$

$$R_{out} = \frac{Vout}{Iout} = \frac{3.3V}{1.1070A} = 2.98\Omega \quad (3.30)$$

Summary of Calculated Values:

- Inductance: 1.55 mH
- Capacitance: 1830 µF

3.11. The 3.3V Boost converter MATLAB/Simulink model without PO installed – worst case scenario.

The boost converter MATLAB/Simulink model without Perturb and Observe installed is shown in Figure 3.18. The model is comprised of a PV array and a boost converter. The model is not operating at MPP. The model is tested at STC: 28°C and 1367W/m2. The PV array is set for the worst-case scenario: two sides of the 1U Cube are exposed to the sun, i.e., four modules are active and connected in parallel.

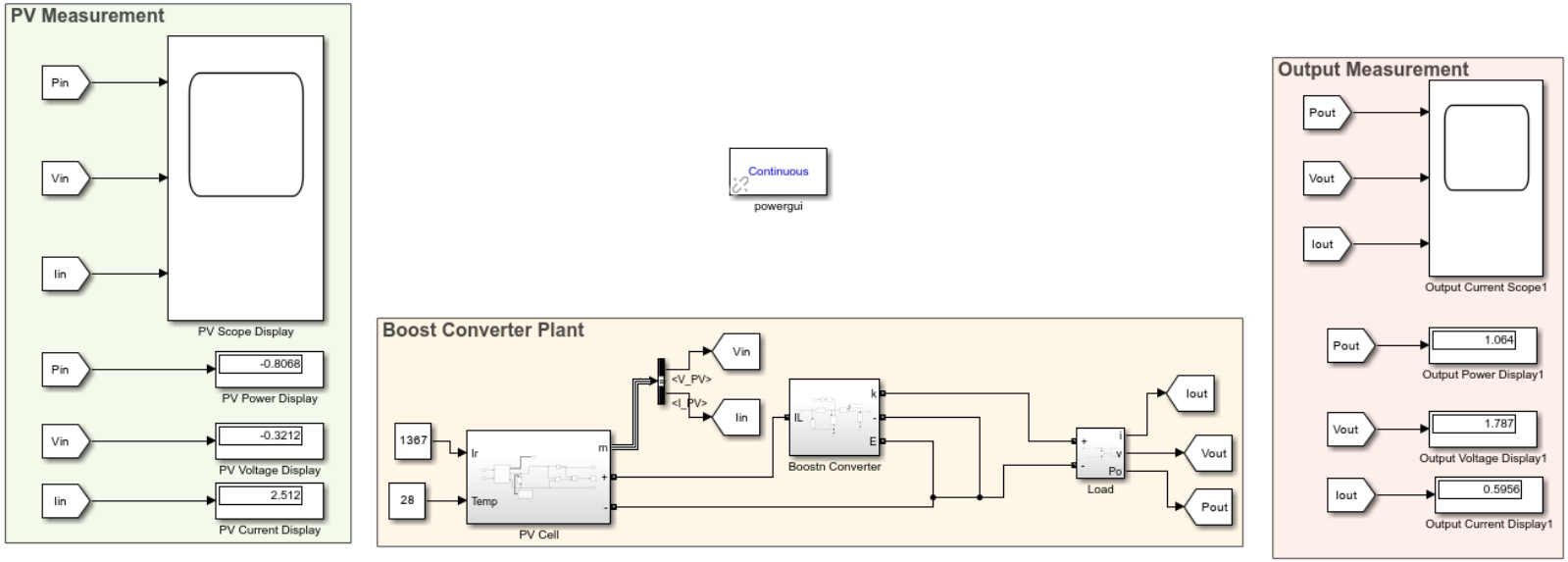

Figure 3. 18: 3.3V Boost Converter MATLAB/Simulink model without PO installed

To analyze the effect of the PO MPPT objective function, let's first look at the MATLAB/Simulink simulation results of the output current, voltage, and power that is depicted in Figure 3.19 without PO installed. It can be seen from the displays that the output power is 1.064W, the output voltage is 1.787V, and the output voltage is 0.6A.

Figure 3.19 shows MATLAB/Simulink simulation results of the output current, voltage, and power without PO installed.

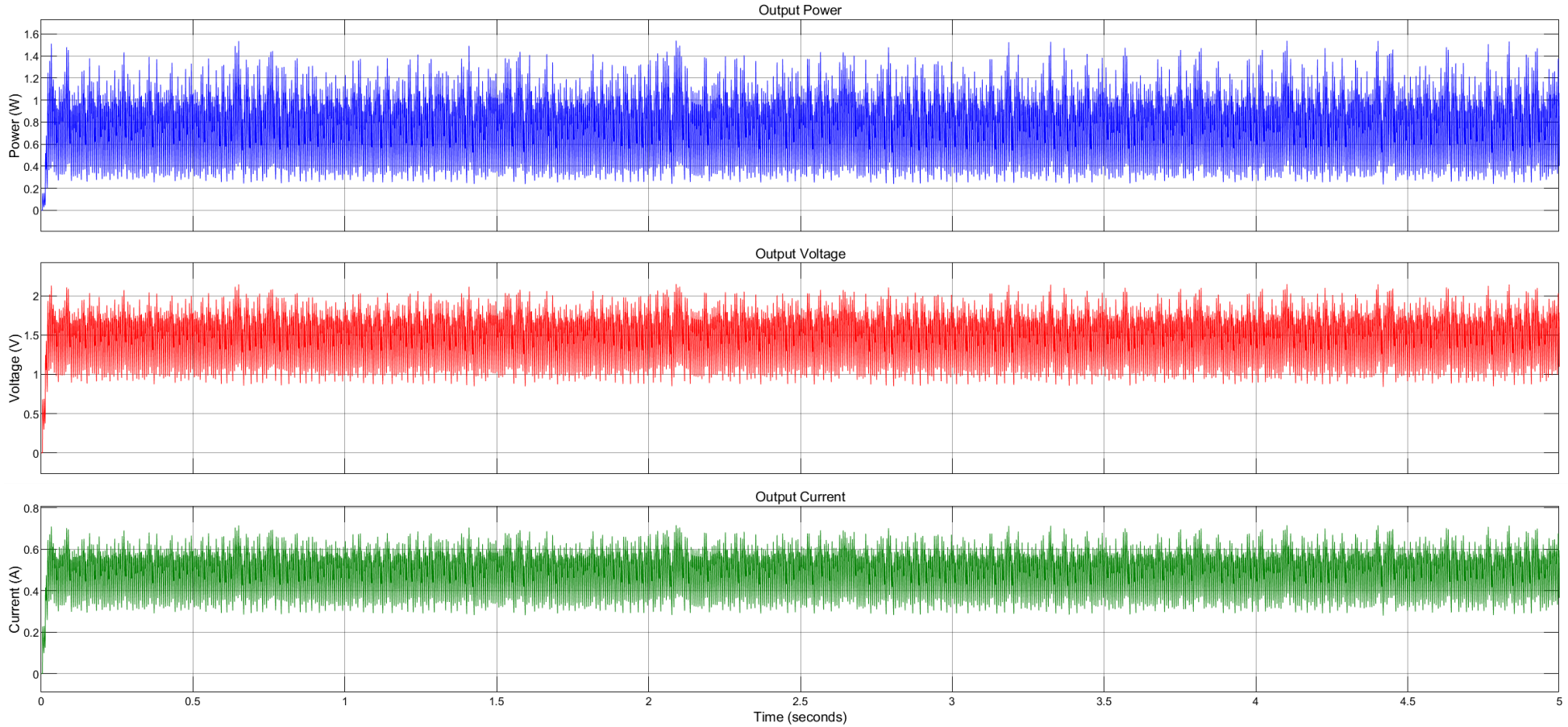

Figure 3. 19: 3.3V Boost Converter MATLAB/Simulink model simulation results without PO installed

From Figure 3.19, it can be deduced that the output power oscillates between a minimum value of 0.4W to 1.064W, the output voltage oscillates between a minimum of 1A to 1.787V, and the output current oscillates between a minimum of 0.4A and 0.6A.

3.12. The 3.3V Boost converter MATLAB/Simulink model with PO installed – worst case scenario.

The PO algorithm objective function and the boost converter take their input power directly from the PV panel as shown in Figure 3.20. A transient current capacitor filter is installed before the input inductor. The PO objective function uses its sample rate to shift the duty cycle up and down until it finds the MPP and gives its output duty cycle to the input of the PWM. The model is operating at MPP. The model is tested at STC: 28°C and 1367W/m2. The PV array is set for the worst-case scenario: two sides of the 1U Cube are exposed to the sun, i.e., four modules are active and connected in parallel.

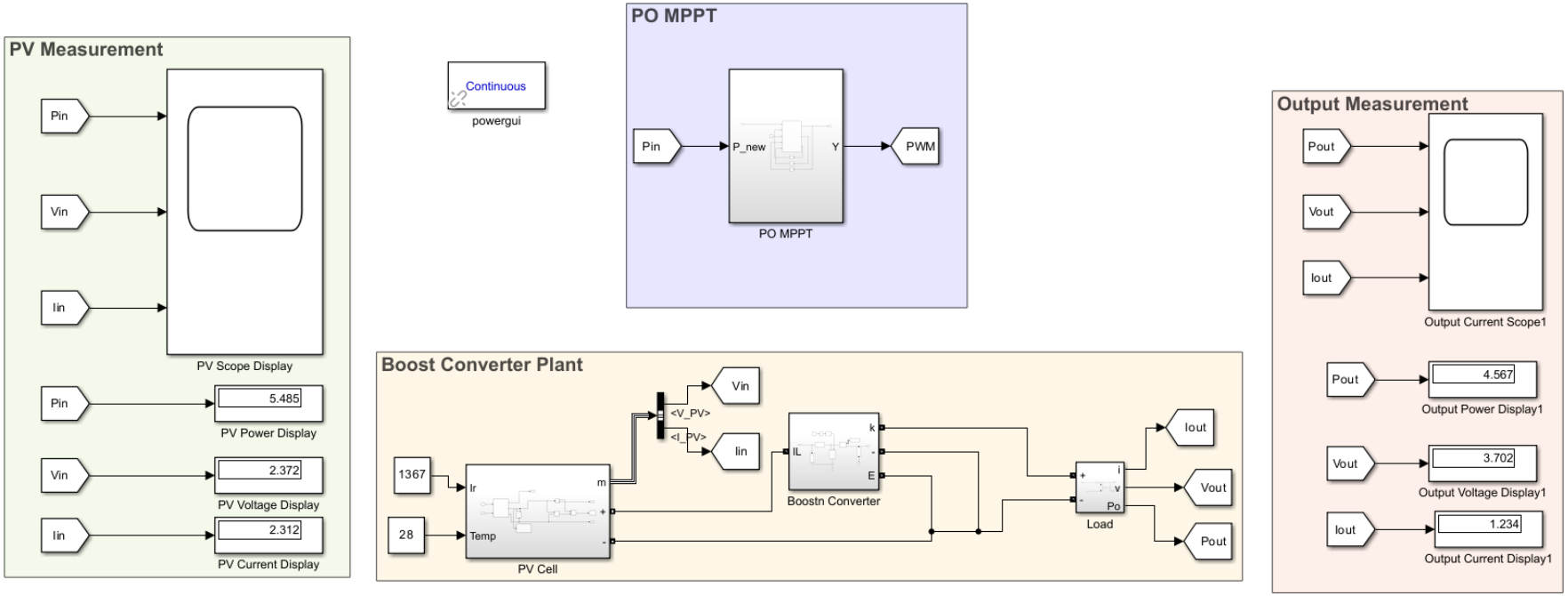

Figure 3. 20: 3.3V Boost converter MATLAB/Simulink model with PO installed

Figure 3.16 shows that the output power oscillates about 4.6W, the output current oscillates about 1.2A, and the output voltage oscillates about 3.7V.

Figure 3.21 shows MATLAB/Simulink simulation results of the output current, voltage, and power with PO installed.

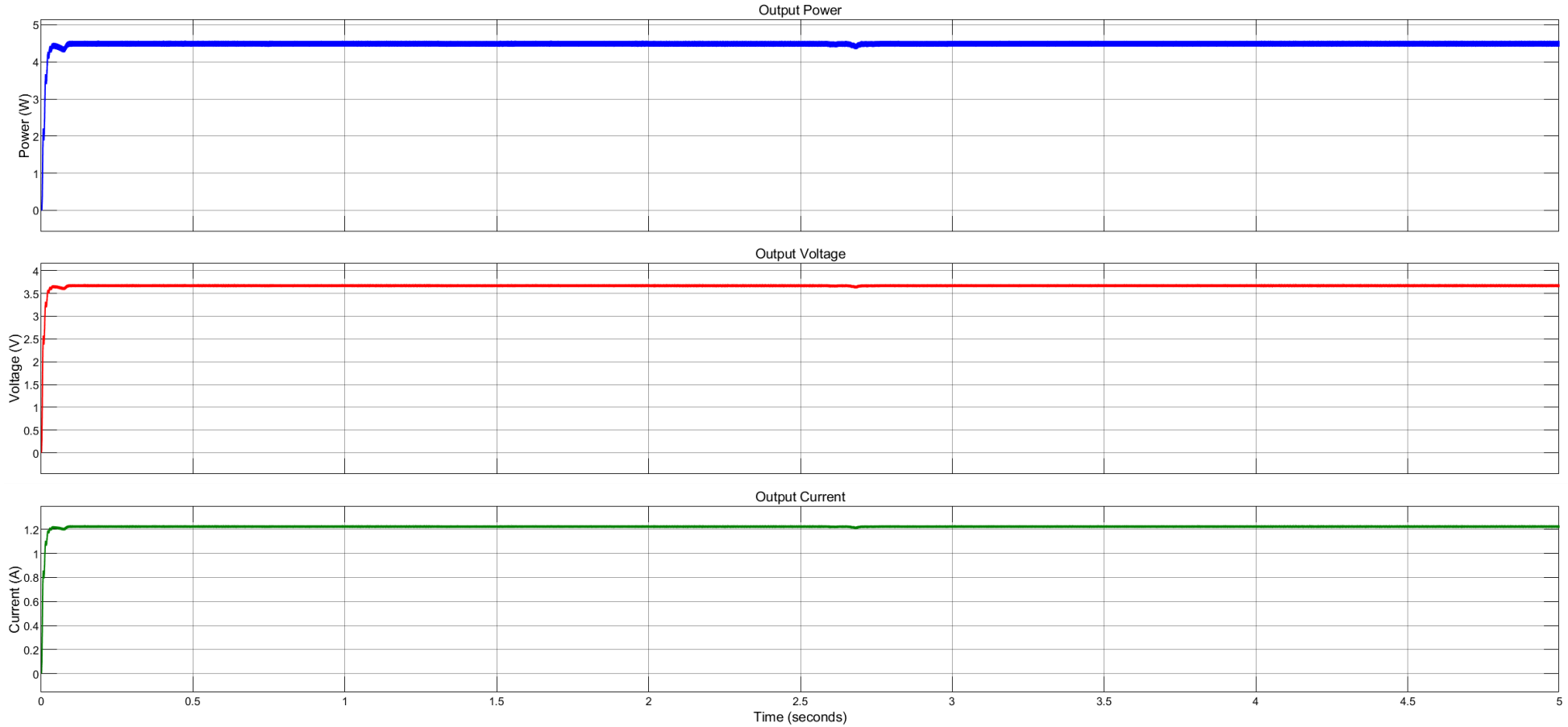

Figure 3. 21: 5V Boost converter MATLAB/Simulink model simulation results with PO installed

It can be seen from Figure 3.20 that the PO objective function will cause the PV array to reach a maximum PV power of 5.5W and will continue to oscillate around the maximum power—a maximum PV voltage of 2.4V and a maximum current of 2.3A. The duty cycle will settle around 0.2727.

It can be seen from Figure 3.21 that the boost converter output power overshoots and dampens at 4.7W, voltage is 3.7V, and current is 1.2A. Hence, applying the PO MPPT improves the output power of the boost converter. All the CubeSat research projects covered in Table 2.2 for a 3.3V bus can be supplied by the power system EPS modeled in Figure 3.20. The power system in Figure 3.20 comprises a 1U CubeSat, and it is assumed that only two sides are exposed to the sun under STC conditions.

3.13. Conclusion

Each (+X, +Y) or (-X, -Y) group (two adjacent sides) is connected to either a 5V boost converter or a 3.3V boost converter. Each (+X, +Y) or (-X, -Y) group (two adjacent sides) produces an output power of 3W, an output current of 0.7A, and an output voltage of 4.6V when connected to a 5V bus. Each (+X, +Y) or (-X, -Y) group (two adjacent sides) produces an output power of 4.6W, an output of 1.2A, and an output voltage of 3.7V. For theoretical demonstration, an assumption that two sides are exposed to the sun is made, and the design of a boost converter for that particular scenario is designed and simulated for implementation with and without PO MPPT. In practice, each side must be connected to its boost converter, and the boost converters must be connected in parallel for maximum power extraction in all practical possible combinations of sides exposed to the sun. In practice, the cube will tumble in space, and it cannot be predicted which side will be exposed to the sun at which time.

The results show 4.6V instead of 5V in the 5V Boost converter model and 3.7V instead of 3.3V in the 3.3V model. Also, if a closer look inside the output graphs with PO applied in the boost converters, there are oscillations in the MPP. The results obtained in this chapter can be improved using AI algorithms that can tune the results to accurate bus voltages and minimize oscillations in the MPP.

CHAPTER 4

GENETIC ALGORITHM IMPLEMENTATION for CubeSat POWER SYSTEMS

4.1. Introduction

It is essential to ensure that the power supplied contains minor ripples and is closest to the desired bus voltages. The reason is that the IC technology may run to uncertain conditions and misinterpret analog voltage, representing a high as a low. In Chapter 3, the results show 4.6V instead of 5V in the 5V Boost converter model and 3.7V instead of 3.3V in the 3.3V model. Also, a closer look at the output graphs with PO applied in the boost converters shows there are oscillations in the maximum power point (MPP). These results obtained in Chapter 3 can be improved using AI algorithms that can tune the results to accurate bus voltages and minimize oscillations about the MPP for CubeSat applications since low voltage is supplied to all CubeSat subsystems.

In control systems, the nonlinear response of the PV-supplied boost converter can be converted into a transfer function plant. The transfer function plant becomes the controlled device while the PID controller is placed before it to develop a dynamic response and minimize the controlled plant's steady-state error. The setpoint will be a 5V bus and a 3.3V bus, respectively. This solution approach ensures that the bus voltages are tuned to their targets. However, converting a PV-supplied boost converter into a transfer function plant is an approximated process, whether using linearisation, state-space averaging method, or control to output small signal method.

Subsection 4.2 discusses the linearisation MATLAB/Simulink method of converting the PV-supplied boost converter into a transfer function plant. Subsection 4.3 implements the linearization method using Matlab/Simulink. Subsection 4.5 explains the tuning process of the PID using GA. Subsection 4.7 implements the GA tuning of a Simulink model. Subsection 4.8 discusses the results of the implemented GA-tuned PID controller-based boost converter transfer function plant.

4.2. PV-supplied Boost Converter Conversion into a Transfer Function Plant Requirements

In some recent literature, the Simulink PV module model has been replaced by a battery. The battery is set to the minimum input voltage position of the voltage range. For example, if the PV input voltage range is 2V to 3V, the battery in the boost converter is set to 2V. Then, the boost converter closed loop plant is approximated into a transfer function using a state space averaging method (Achiammal, 2017). In this chapter, the approximation of the boost converter into a transfer function is performed using the

linearisation in MATLAB/Simulink. The boost converter transfer function plant becomes the controlled device while the PID controller is placed before it to develop a dynamic response and minimize the steady-state error. The output of the boost converter plant is connected as a negative unity feedback loop, as depicted in Figure 4.1.

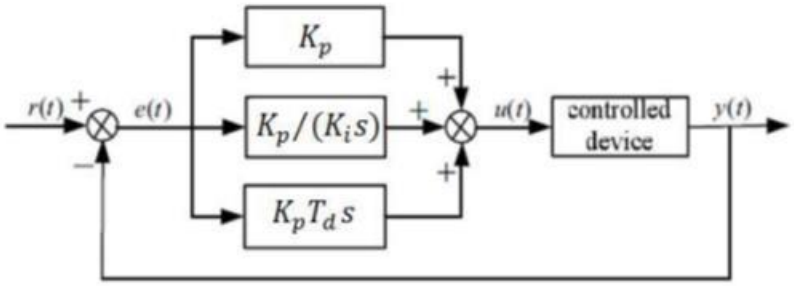

Figure 4. 1: Schematic diagram of a PID controller (Adapted from Achiammal, 2017)

The PID controller gains parameters which are Kp, Ki, and Kd, are tuned by the bio-inspired optimization algorithms such as PSO algorithm, genetic algorithm (GA), BAT algorithm, ANT colony algorithm, Artificial Bee Colony (ABC) algorithm, artificial neural network (ANN) algorithm, grey wolf optimization (GWO) algorithm, and fireworks algorithm (FWA), to name a few **(Aoughlis et al., 2021)**. This approach, which uses the PID controller and tuning algorithm like the GA, requires the boost converter to be approximated to a transfer function plant and placed before the PID controller.

This approximation can be performed through either of the three following methods: linearisation in Simulink, State Space averaging derivation method, or by AC analysis small signal transfer function derivation method. These approximation methods do not accurately represent the nonlinear response of the boost converter. However, in this chapter, the MATLAB/Simulink linearization of the boost converter into a transfer function is tested, and a closed-loop PID system is tuned using a GA algorithm. A GA algorithm tunes the PID controller gains parameters Kp, Ki, and Kd to minimize the steady-state error of the feedback control system. The steady-state error is minimized using a performance index like ITAE.

As mentioned before, applying GA tuning of a PID controller requires the controlled plant to be in a transfer form. Hence, the first step is linearising the PV-supplied boost converter to convert it to a transfer function plant. The linearized transfer function model must mimic the non-linear behavior of the original PID controller-based closed-loop boost converter Simulink model. The boost converter circuit model is shown in Figure 4.2 and simulated in Figure 4.3 to preserve the response curve shape. So that the transfer function model response curve can be compared to the circuit model curve.

Figure 4.2 shows the boost converter circuit model in MATLAB/Simulink. The proportional gain is randomly set to 1, the integral gain is randomly set to 1, and the derivative is randomly set to 0. The input voltage is 2.4V and is equal to V_{MMP}. The output voltage is 1.6V.

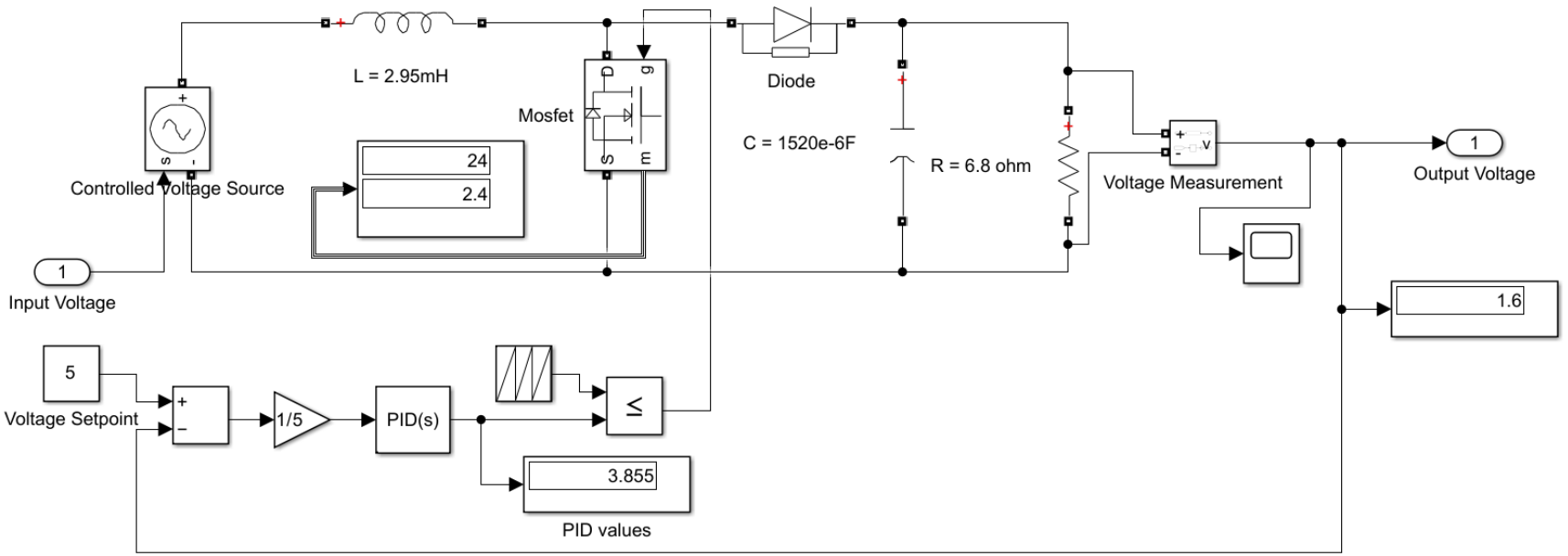

Figure 4.2: The boost converter circuit model in MATLAB/Simulink

Figure 4.3 shows the boost converter circuit model simulation scope waveform in MATLAB/Simulink. The proportional gain is randomly set to 1, the integral gain is randomly set to 1, and the derivative is randomly set to 0. The input voltage is 2.4V and is equal to V_{MMP}. The output voltage is 1.6V.

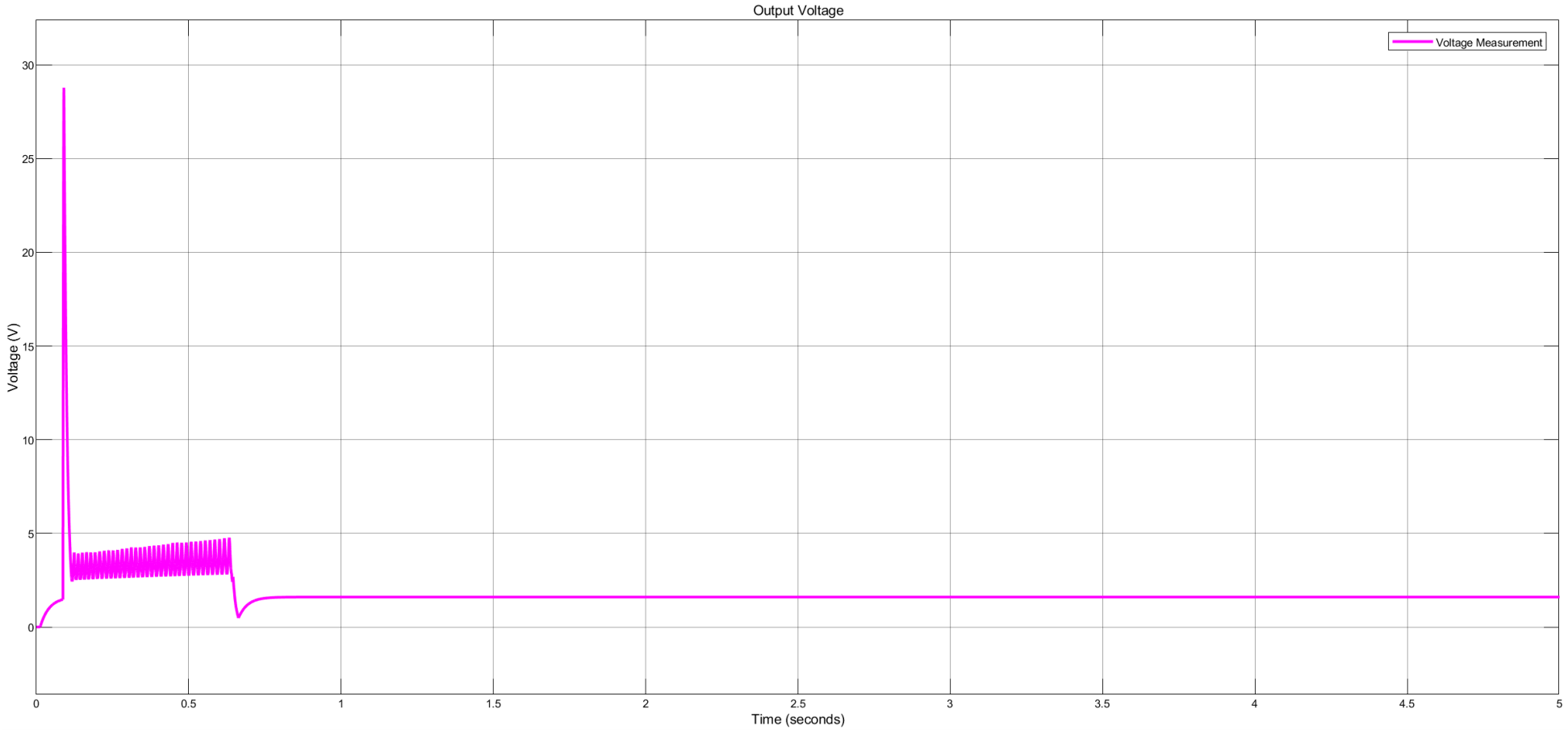

Figure 4.3: The boost converter circuit model output scope simulation results in MATLAB/Simulink

4.3 Conversion of a Circuit Model into a Transfer Function Model

Identify the major components in your Simulink model of a boost converter. The boost converter must be converted into a subsystem in Simulink. The input voltage is set to input port 1, and the PWM signal that goes into the gate of the MOSFET is set to input port 2. The output voltage measurement is set to output port 1. Figure 4.4 shows this step.

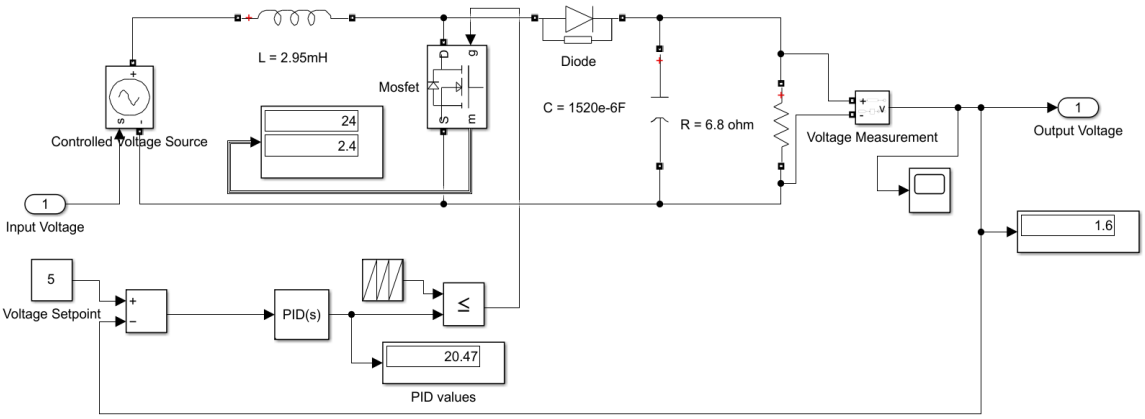

Figure 4. 4: Schematic diagram of the boost converter plant

Now, the schematic will look like it is in Figure 4.5. Right-click on the connecting wire between inputs and the subsystem, select linear analysis points, set it to “Open-loop Input for both inputs,” repeat the process on the connecting wire between the output port and the subsystem, and set it to “Open-loop Output.”

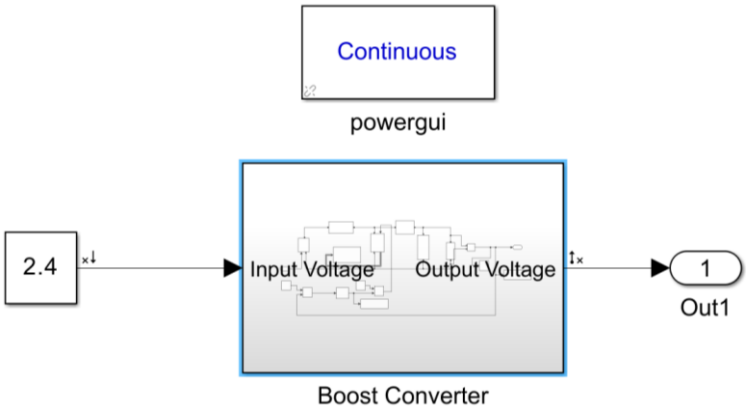

Figure 4. 5: Setting Open-loop Inputs and Open-loop Output

Right-click on the boost converter subsystem block, select linear analysis, and then select linearize block. Linearization is critical for producing a transfer function that accurately captures the system's behavior under the intended operating circumstances. Once the linear analysis tool opens, click on results viewer, then click step function.

Linearization results detail block will open a state space equation, change display linearization results to transfer function, and extract the transfer function.

State Space:

General Information:

Operating point: Model initial condition

Size: two inputs, one output, three states

Linearization Result:

$$A = \begin{matrix} -8.4 \times 10^4 & -0.03697 & -0.03697 \\ 327.3 & -98.06 & -1.316 \\ 2 \times 10^6 & -7999 & -7999 \end{matrix}$$

$$B = \begin{matrix} 339 & 0 \\ 0 & 0 \\ 0 & 0 \end{matrix}$$

$$C = \begin{matrix} 0 & 1 & 0 \end{matrix}$$

$$D = 0$$

Name: Linearization at model initial condition, Continuous-time state-space model.

State Names:

x1 - State-Space (1)

x2 - State-Space (2)

x3 - State-Space (3)

Input Channel Names:

u1 - Boost Converter/1

u2 - Boost Converter/2

Output Channel Names:

y1 - Boost Converter/1

Transfer function:

From input "u1" to output "y1":

$$TF = \frac{1.11 \times 10^5 s - 3.612 \times 10^{-7}}{s^3 + 9.242 \times 10^4 s^2 + 6.836 \times 10^8 s + 6.527 \times 10^{10}}$$

Now that the transfer function is obtained, a unity feedback system comprising a setpoint, PID controller, transfer function plant, output scope, and summing point can be constructed in Simulink.

A boost converter is a DC-DC converter that increases the input voltage to produce a higher, regulated output voltage. In the above section, the boost converter has been converted into a transfer function so that it can be controlled by a PID to reach a set point voltage equivalent to a bus voltage of 5V. However, tuning the PID parameters is critical for achieving peak performance. This chapter implements GA, a bio-inspired optimization algorithm to tune a PID controller to reach 5V bus voltage, resulting in better performance metrics than trial and error tuning or using the Ziegler–Nichols tuning method. The PID controller is a well-known control approach for improving a system's dynamic response while reducing steady-state error (Achiammal, 2017).

The controller alters the control signal based on the difference between the desired setpoint and the actual output. The PID controller consists of three components: proportional (P), integral (I), and derivative (D), each of which contributes to the control signal in a unique way. The transfer function of a PID controller is often stated in terms of these three components, and setting the PID parameters (Kp, Ki, and Kd) is crucial to system performance. The goal is to determine the best combination of these characteristics for stability, response time, and error minimization. The gain block between the sum block and the PID scales the feedback signal to match the desired reference level. This is particularly common in circuits where the output voltage needs to be regulated within specific limits **(Solihin et al., 2011)**.

Simulink's PID controller is commonly built with the "PID Controller" block, which allows for the definition of proportional (Kp), integral (Ki), and derivative (Kd) gains. This step aims to tune these settings to minimize the steady-state error while assuring system stability and optimal transient response. After determining the PID controller parameters, the next step is to simulate the closed-loop system and evaluate the controller's performance. In Simulink, this is accomplished by attaching the PID controller block to the boost converter transfer function model and establishing a unity feedback loop that compares the output voltage to a reference value. The steady-state error, the difference between the desired and actual outputs after the system has settled, is a critical metric in this analysis. In more complex systems, the MATLAB/Simulink optimization toolbox can be used to improve the tuning process. Particle Swarm Optimisation (PSO) and Genetic Algorithms (GA) can be used with the Simulink model to automate searching for the best PID settings. These strategies are especially beneficial for dealing with the nonlinearities and complexities found in boost converters. MATLAB/Simulink offers a comprehensive framework for designing, implementing, and optimizing PID controllers to reduce steady-state error in boost converter systems **(Jaen-Cuellar et al., 2013)**.

4.4. PID-based Boost Converter Transfer Function Plant System before Ga Tuning

The voltage setup voltage of 5V, summation point, PID controller, scope, negative unity feedback, and output voltage display are shown in Fig 4.4. The PID's proportional value is set to a random value of 1; the integral is set to a random value of 1, and the derivative is set to 0. The output voltage before GA: 0.05664V.

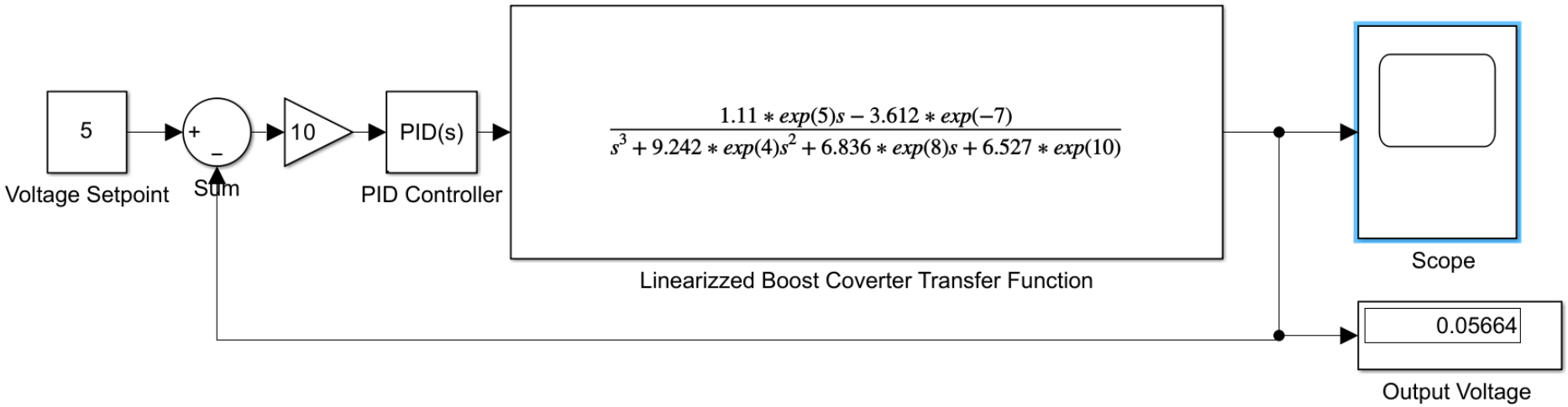

Figure 4. 6: PID-based Boost Converter Transfer Function Plant System before Ga Tuning

Figure 4.7 shows the PID controller-based boost converter transfer function plant system's simulation results before applying a genetic algorithm tuning program. The PID's proportional value is set to a random value of 1; the integral is set to a random value of 1, and the derivative is set to 0.

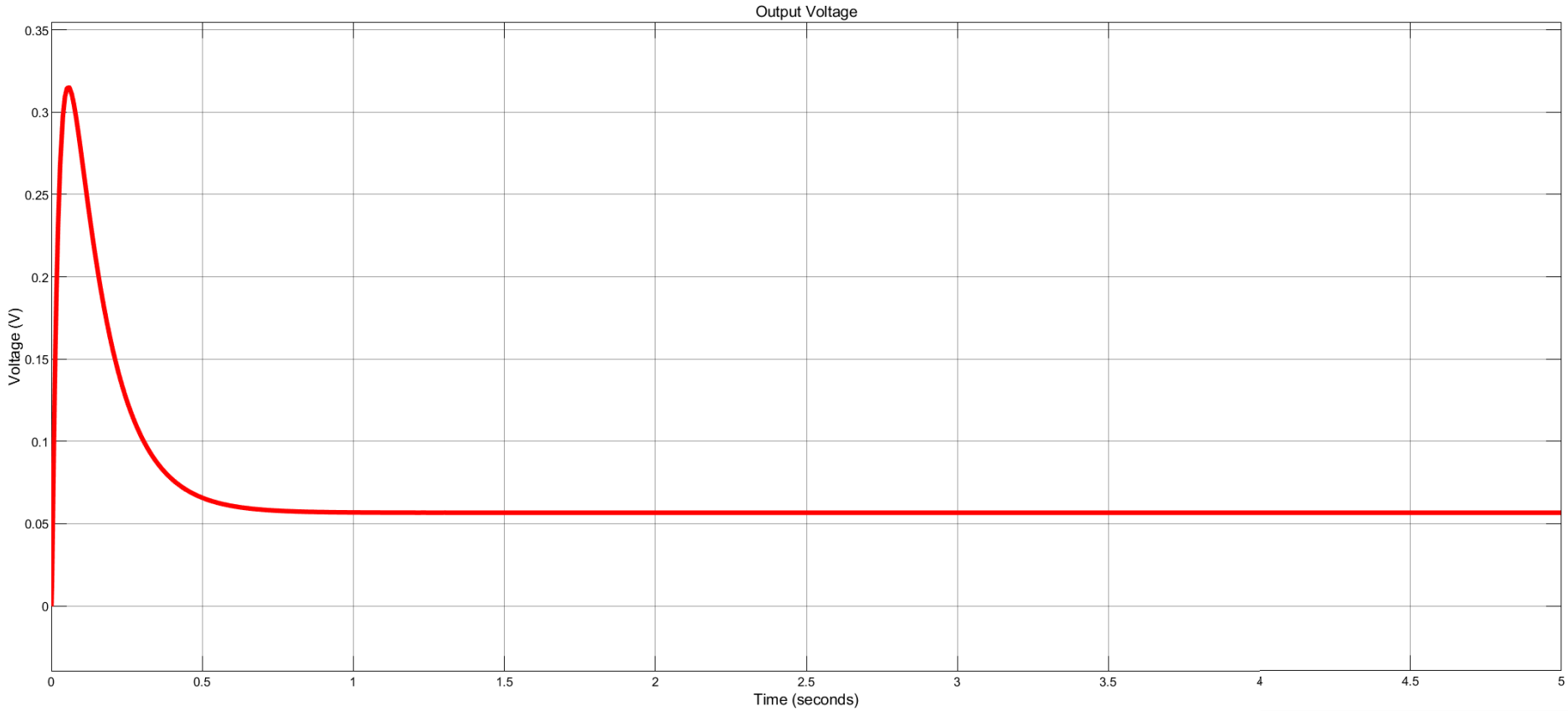

Figure 4. 7: Simulation Results of the PID-based Boost Converter Transfer Function Plant System before Ga Tuning

The amplitude spikes to a maximum value of 3.2e-1V and settles at 6.6e-2V. The settling voltage target is 5V, and the current settling voltage is far off the target. The average output voltage is 0.07V, as shown in the display.

4.5. PID Tuning with a Genetic Algorithm (GA) Steps

Genetic algorithms (GA) replicate the natural selection process to stabilize PID controller parameters (proportional, integral, and derivative gains). A PID parameter setting population is produced randomly or using previous knowledge. Each set is evaluated with a fitness function, such as Integral Time Absolute Error (ITAE), to minimize the system steady-state error. The best-performing sets are chosen to create offspring via crossover and mutation, which adds diversity while preventing premature convergence. This selection, reproduction, and mutation cycle continues for generations until the algorithm finds the best PID settings. The final solution is the PID parameter set that delivers the highest performance according to the fitness function. This strategy is beneficial for controlling the complexity and nonlinearities of the boost converter transfer function **(Meena and Devanshu, 2017)**.

4.5.1. Genetic Algorithm (GA) program Steps

1. Generate the PID parameters:
The genetic algorithm represents the PID controller parameters (Proportional, Integral, and Derivative gains (K_p, K_i, K_d) as genes. It makes a chromosome using these genes to produce a potential solution to the PID tuning problem.

2. Define the Objective Function (Fitness Function):
A definition of fitness function is necessary to measure how well the system works when controlled by specific PID parameters. The fitness function is typically based on a performance statistic such as Integral Time Absolute Error (ITAE), Integral Squared Error (ISE), or another applicable metric.

3. Generate an Initial Population of PID Parameter Sets (Chromosomes):
Create an initial population of PID parameter sets (chromosomes). These are generated at random or may be based on existing knowledge.

4. Evaluate Fitness:
Assess the fitness of each chromosome in the population by applying the PID controller to the system with the appropriate settings and computing the fitness using the given objective function.

5. Selection:
Choose individuals from the population to be the next generation's parents. Everyone's fitness determines the likelihood of selection.

6. Crossover (Recombination):

The process of creating new individuals (offspring) by merging the DNA of two parents. This is usually accomplished through crossover (recombination) processes.

7. Mutation:
To maintain genetic diversity in the population, modest random changes (mutations) to the genomes of some individuals should be introduced.

8. Replace Old Population:
Establish a new population by replacing the old one with newly created individuals (offspring).

9. Repetition:
Repeat steps 4–8 for a predetermined number of generations or until a convergence condition is fulfilled.

10. Final Solution:
According to the fitness function, the final solution corresponds to the PID parameters that produce the best performance.

Figure 4.8 shows the steps of PID tuning using GA in a flow chart:

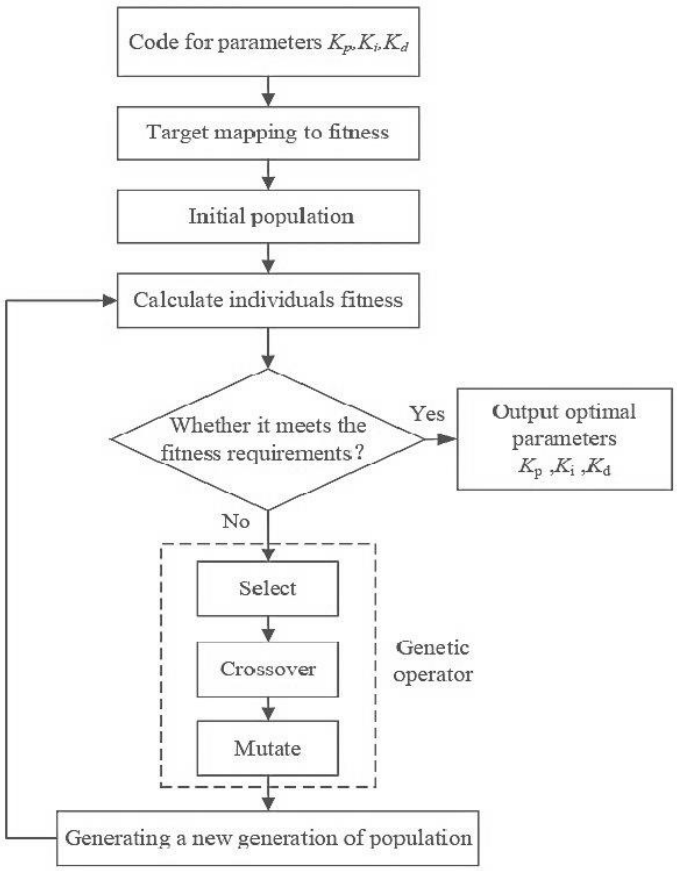

Figure 4. 8: PID Tuning with a Genetic Algorithm (GA) Flowchart

The flowchart in Figure 4.8 can be explained as follows: Code for parameters K_p, K_i, K_D: The first step is to define GA parameters like the number of variables, which in the PID case is equal to three. Define upper and lower bounds, define population size, define maximum number of generations, and define crossover and mutation rates. Target mapping to fitness: define the fitness function based on a performance statistic such as Integral Time Absolute Error (ITAE), Integral Squared Error (ISE), or another applicable metric. Initial population: Initialize the population based on population size and upper and lower bounds using a random number generation function. Calculate individual fitness:

Assess the fitness of each PID variable in the population by applying the PID controller to the system with the appropriate settings and computing the fitness using the given objective function. “Whether it meets the fitness requirements”: checks if the objective function minimization is achieved and if it does, the PID optimum gains have been achieved. If not, “select,” “crossover,” and “mutate” functions are executed. “Generating a new generation of population:” Establish a new population by replacing the old one with newly created individuals (offspring). After this step, the program jumps back to calculate individual fitness, and the loop iterates until objective function requirements are met.

4.6. Genetic Algorithm Fitness Function (Objective Function)

The PID controller gain parameters are tuned using various performance indicators or fitness functions. PID tuning commonly uses the following performance indices

- Integral Time Absolute Error (ITAE):

$$\boldsymbol{ITAE} = \int_{\boldsymbol{0}}^{\infty} \boldsymbol{t} \times |\boldsymbol{e}(\boldsymbol{t})|\, \boldsymbol{dt} \qquad (4.1)$$

The Integral Time Absolute Error (ITAE) emphasizes error reduction during the initial transient reaction and penalizes higher errors for longer. This criterion is appropriate for applications requiring a quick response and short settling time.

- Integral Squared Error (ISE):

$$\boldsymbol{ISE} = \int_{\boldsymbol{0}}^{\infty} [\boldsymbol{e}(\boldsymbol{t})]^{\boldsymbol{2}}\, \boldsymbol{dt} \qquad (4.2)$$

Due to the squaring of error values, Integral Square Error (ISE) prioritizes minimizing significant errors over minor errors. This criterion may result in a quick response, additional control effort, and wear on the motor and other components.

- Integral Time Squared Error (ITSE):

$$\boldsymbol{ITSE} = \int_{\boldsymbol{0}}^{\infty} \boldsymbol{t} \times [\boldsymbol{e}(\boldsymbol{t})]^{\boldsymbol{2}}\, \boldsymbol{dt} \qquad (4.3)$$

ITSE combines parts of ISE and ITAE, penalizing more significant faults during the initial transient reaction. This criterion balances response time and control effort but may produce more extraordinary oscillatory behavior.

- Integral Absolute Error (IAE):

$$\boldsymbol{IAE} = \int_{\boldsymbol{0}}^{\infty} |\boldsymbol{e}(\boldsymbol{t})|\ \boldsymbol{dt} \qquad (4.4)$$

Integral Absolute Error (IAE) assigns equal weight to all errors, regardless of magnitude. This criterion produces a smoother response and requires less control effort, although it may respond slower than other criteria. ITAE or ISE may be better appropriate for quick response and settlement time. If one aims for a smooth response and minimum control effort, IAE may be a better option (Deif, 2023). Optimization techniques employ these indices as objective functions when tuning the PID parameters. Typically, the goal is to minimize these indices, suggesting improved control performance. The Integral Time Absolute Error is selected for its quick response and settling time as the fitness function or objective function of choice for GA PID tuning in the work presented in this chapter. Integral time absolute error is expressed mathematically in equation (4.5):

$$\boldsymbol{ITAE} = \int_{\boldsymbol{=0}}^{\boldsymbol{t=final}} |\boldsymbol{\mu}| \times \boldsymbol{t}\, \boldsymbol{dt} \qquad (4.5)$$

Equation 4.5 is written as a MATLAB code in appendix B. Line 1: "*function cost = tuning(k)"* defines a function named "tuning" that takes a vector k as an input and returns a scalar cost. The vector k represents the PID controller parameters K_p, K_i, and K_d in the Simulink boost converter model that uses a PID controller. Line 2: "*assignin('base','k',k)":* uses the assigning function to assign the value of k to the variable k in the base workspace.

This step is necessary if the Simulink model named "*GA_PID.slx*" that will be simulated uses the PID parameters defined in the base workspace. Line 3: *sim('GA.slx')*: simulates the Simulink model named "*GA_PID.slx*." Line 4: *cost= ITAE(length(ITAE))*: After the simulation is complete, the code calculates a cost based on the Integral Time Absolute Error (ITAE) metric. It extracts the ITAE values from the simulation results and assigns the last values of the ITAE vector to the variable cost. These values are then used as the genetic algorithm's cost or objective function. The steady-state error point connects the summing point and the PID controller in Figure 4.6.

This point must be connected to the objective function equation. The objective function is implemented as a MATLAB code in a dot m script file. The aim of the ITAE function equation is also implemented in Simulink using the clock, absolute error mathematical function, product, integrator, display, and “To Workspace” blocks. The “To Workspace” block connects the “dot m script file code” and the Simulink ITAE objective function equation. The PDI gain parameters (Kp, Ki, Kd) in the Simulink PID block are represented as k(1), k(2), and k(3). The integral time absolute error objective function takes the steady-state error of the model.

It is placed in the MATLAB workspace matrix space so that it can be accessed by the GA script file code for optimization of the Pid gain variables: K_p, K_i, K_D. The integral time absolute error objective function in Figure 4.9 is implemented by the math function, time, product integral, display, and the “To Workspace” blocks. The PID is used in the time domain setting, and the gains are set as variables k(1), k(2), and k(3). A unity feedback loop compares the actual output with the reference 5V, and the gain block between the sum block and the PID scales the feedback signal to match the desired reference level. Table 4.1 shows the optimized PID gain values for the fiftieth generation, the last generation, and the best solution PID gain values between the first and final generations. The maximum number of generations that were set for the algorithm was fifty.

Table 4.1: PID gain values manual and automatic tuning

	PID Gain values automatic Tuning		
Generation	Kp	Ki	Kd
Fiftieth generation	35.7116785741896	47.8438001602993	7.63555477239597
Best Solution Generation	895.1708	997.6162	996.1347

The best-of-all solution gain values of Kp, Ki, and Kd are copied and placed inside the PID Simulink block. The Simulink model in Figure 4.9 is simulated with the best solution PID gains and displayed in Figure 4.11.

Figure 4.9 shows the ITAE objective function in MATLAB

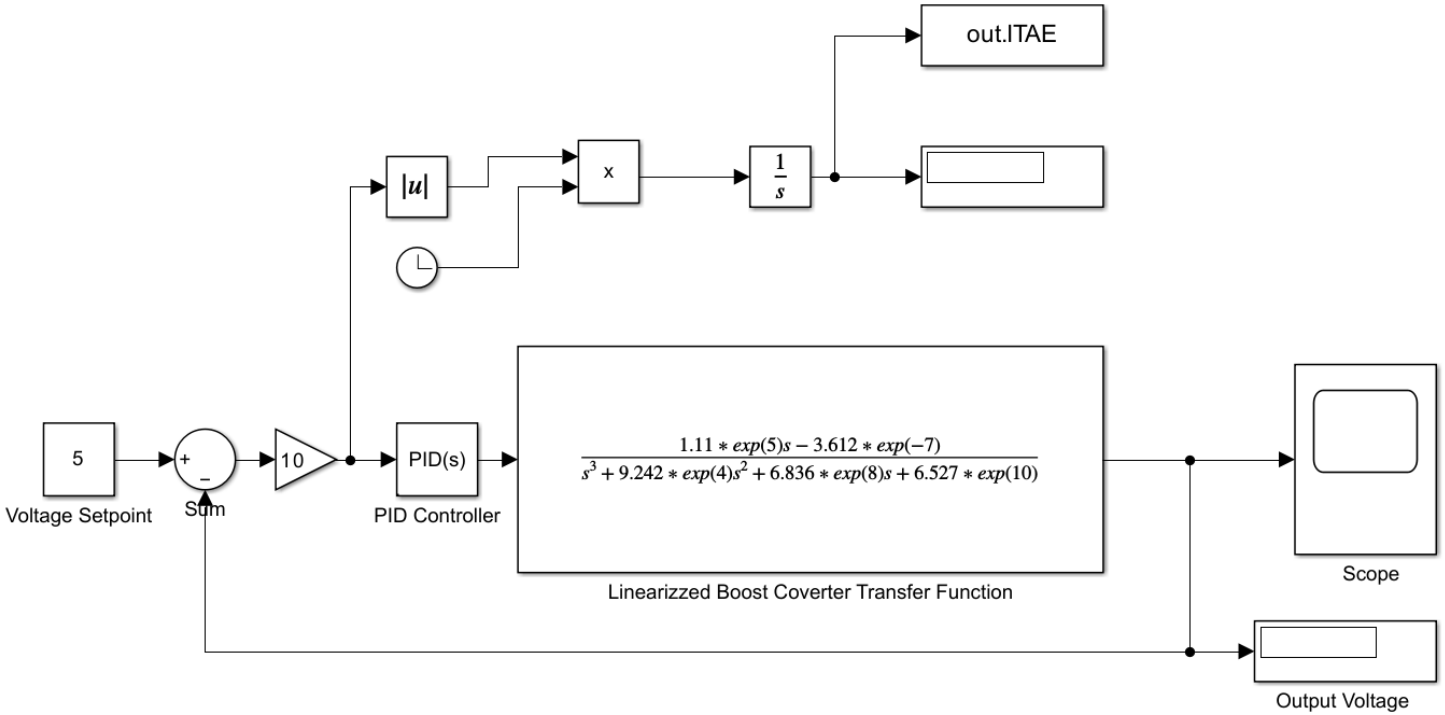

Figure 4. 9: The ITAE objective function

4.7. The Genetic Algorithm (GA) applied as a MATLAB script

In this section of the Thesis, the genetic algorithm that tunes the Simulink model named: "GA_Tuned_PID_Boost_C" is saved in a MATLAB script named "Searching." The subsequent steps explain the "Searching" MATLAB script file code. Also, the "Searching" MATLAB script file code is included in Appendix D.

Step 1: Defining the Genetic Algorithm Parameters

'nVar' - specifies the number of variables to optimize (K_p, K_i, K_d for the PID controller).
'ub' and 'lb' - define the upper and lower bounds for the variables.
'popSize' - specifies the number of individuals in the population.
'maxGenerations' – specifies the maximum number of generations to run the algorithm.
'crossRate' and 'mutRate' – specifies the rates for crossover and mutation operations.
The variables from "Upper Bound" down to "Mutation Rate" are adjustable and unique to user preferences.

Step 2: Objective Function

"fobj" - Handle to the objective function saved in the script file named "Minie," which evaluates the performance of the PID parameters.

Step 3: Population Initialization

'population' - Randomly initialize the population within the given bounds.
'fitness' - Array to store population fitness values.

Step 4: Main GA Loop

Loop through each generation up to the maximum number of generations.

Step 5: Fitness Evaluation

Evaluate everyone's fitness in the population using the 'Minie' objective function.

Step 6: Selection

Sort the population based on fitness values and select the best individuals.

Step 7: Crossover

Perform crossover between pairs of individuals to create offspring.

Step 8: Mutation

Introduce random mutations to maintain diversity in the population.

Step 9: Replacement

Replace the old population with the new population.

Step 10: Display Best Fitness

Display the best fitness value of the current generation.

Step 11: Best Solution

Display the best PID parameters found after all generations and place the best solution PID gains from the workspace into the Simulink PID block.

Step 12: Plot Fitness Curve

Plot the fitness values over generations.

In Figure 4.11, the fitness curve indicates a good evolutionary trend in the genetic algorithm. Initially, the population's fitness was low, but the algorithm successfully found and implemented superior solutions as generations passed. While there were times of stagnation, indicating possible local optima, the overall trajectory suggests good optimization. The final fitness value is noticeably high, indicating that the algorithm arrived at a near-optimal solution. Figure 4.13 illustrates the output voltage of a system over time. The x-axis represents time in seconds, and the y-axis represents the voltage in volts. The graph starts with the output voltage at a value different from the setpoint (5 volts). This is signaled by the over and undershoots at initial conditions. The graph exhibits overshoot (exceeding the setpoint) and undershoot (falling below the setpoint) during the transient response. The PID controller gains influence these behaviors. As the GA iterates, the output voltage gradually converges towards the setpoint. However, it doesn’t reach the exact setpoint voltage. The final value of the output voltage should ideally be very close to the set point. A difference indicates a steady-state error.

4.8. The Optimisation Results of Genetic Algorithm

The maximum number of generations that were set for the algorithm was fifty. The best of all solutions was displayed after the fifty iterations were executed. These gain values of K_p, K_i, and K_d are copied and placed inside the PID Simulink block, and the Simulink model is simulated with these optimized gain values.

Figure 4.11 shows the fitness plotted against the generation. The best individual's fitness (or the population's average fitness) improves over successive generations. The x-axis represents the generation number, while the y-axis represents the fitness value, where lower fitness values generally correspond to better performance or lower error.

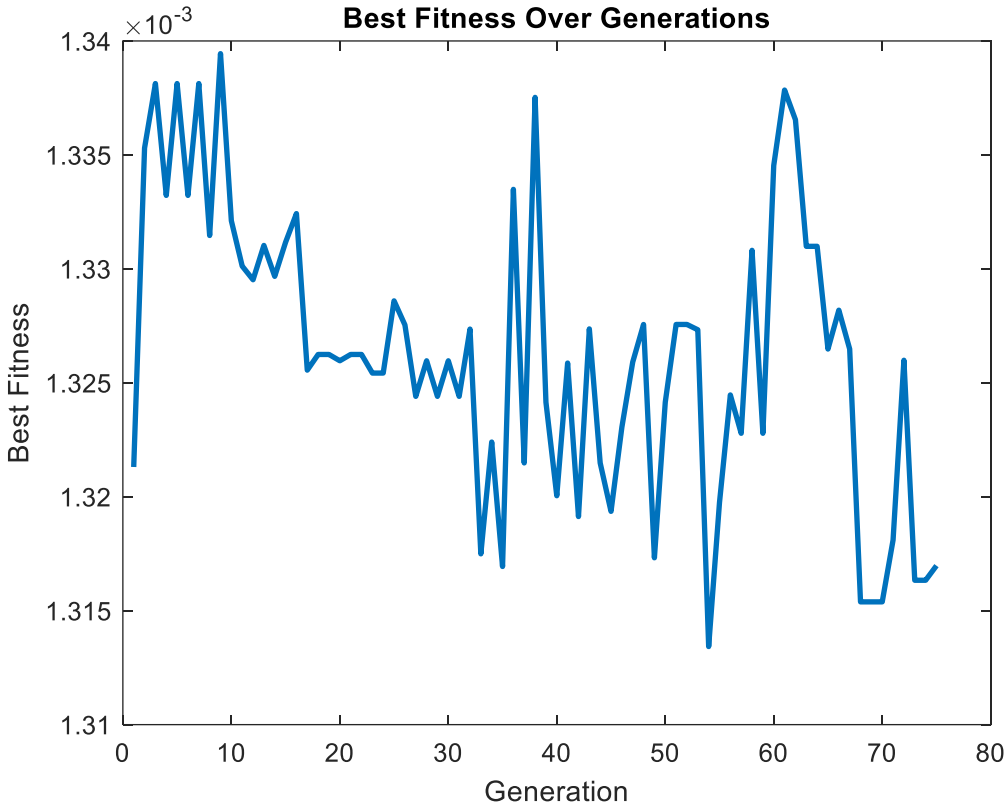

Figure 4. 10: The fitness curve

The fitness value starts relatively high at the beginning of the curve (early generations). This indicates that the initial population (randomly generated set of PID parameters) may not be optimal, but a few individuals might already show some promise. Over successive generations, the fitness values tend to decrease steadily. This suggests that the genetic algorithm effectively explores the search space and refines the PID parameters to minimize the error performance. The fitness curve shows a gradual improvement (decrease in the fitness value) over the generations, starting from a higher value of around 1.34×10^{-3} and eventually reaching around 1.31×10^{-3} by the end of the optimization process. The curve begins to flatten around the 60th generation, which indicates that the algorithm has converged, with no significant improvement in the best fitness value after this point. This suggests that the GA has effectively optimized the PID parameters up to a certain level and is no longer making substantial progress. There is a flat section around 30 to 40 generations where fitness does not improve significantly. This could imply that the GA had difficulty exploring better solutions during this phase, possibly due to local optima. By the last generation, the best fitness reaches approximately 1.31×10^{-3}, indicating the minimum error the GA was able to achieve.

The Simulink model with the best solution PID gains is simulated, and the simulation results are displayed in Figure 4.13. The simulation time is set to 0.1s to show the transient response of the systems simulated with the best PID gain values. The average DC voltage settles at 4.966V.

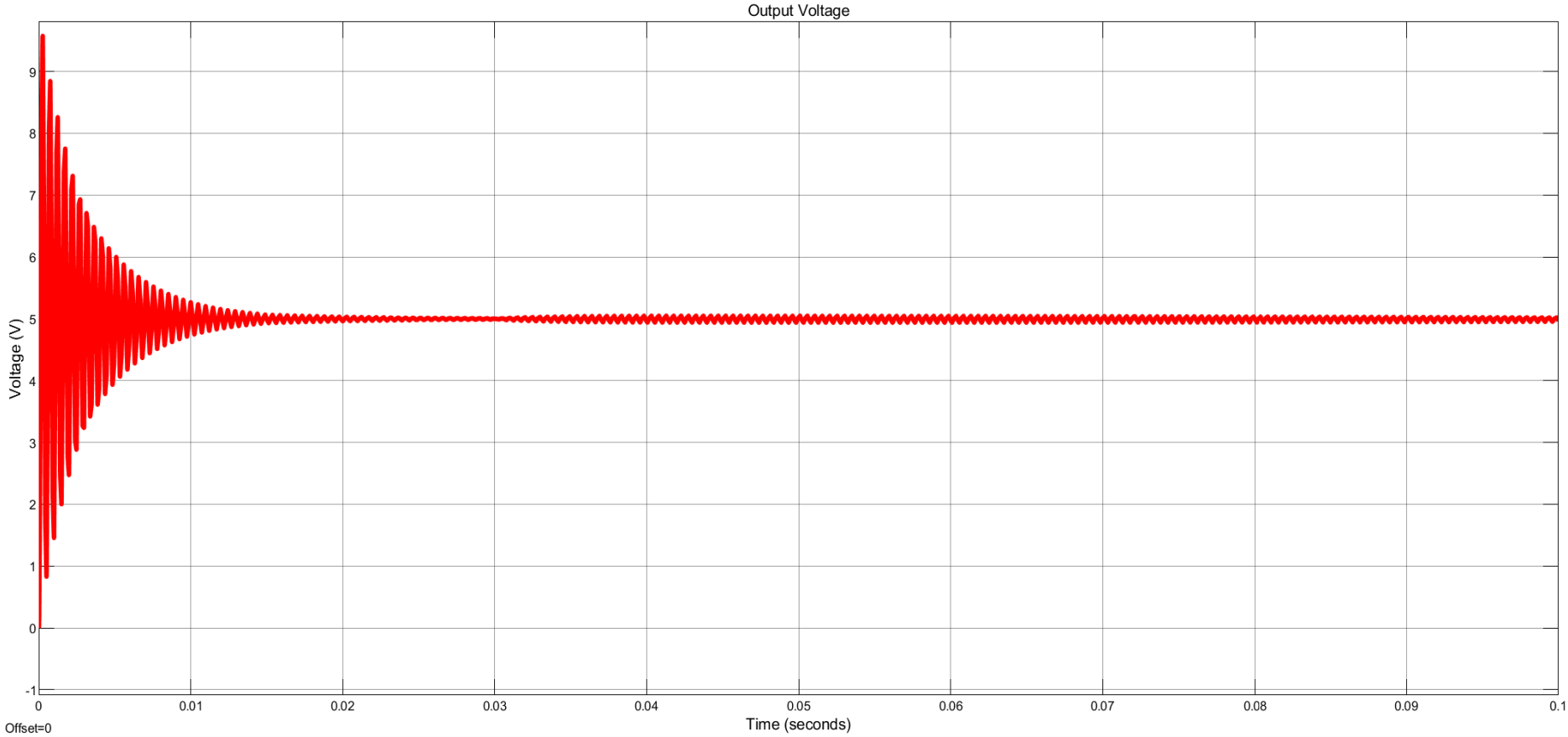

Figure 4. 12: Simulated model with best solution values scope results

Figure 4.14 shows the pronounced oscillations in the GMPP after the GA tuning. The peak-to-peak of these oscillations is 3.66e-2V.

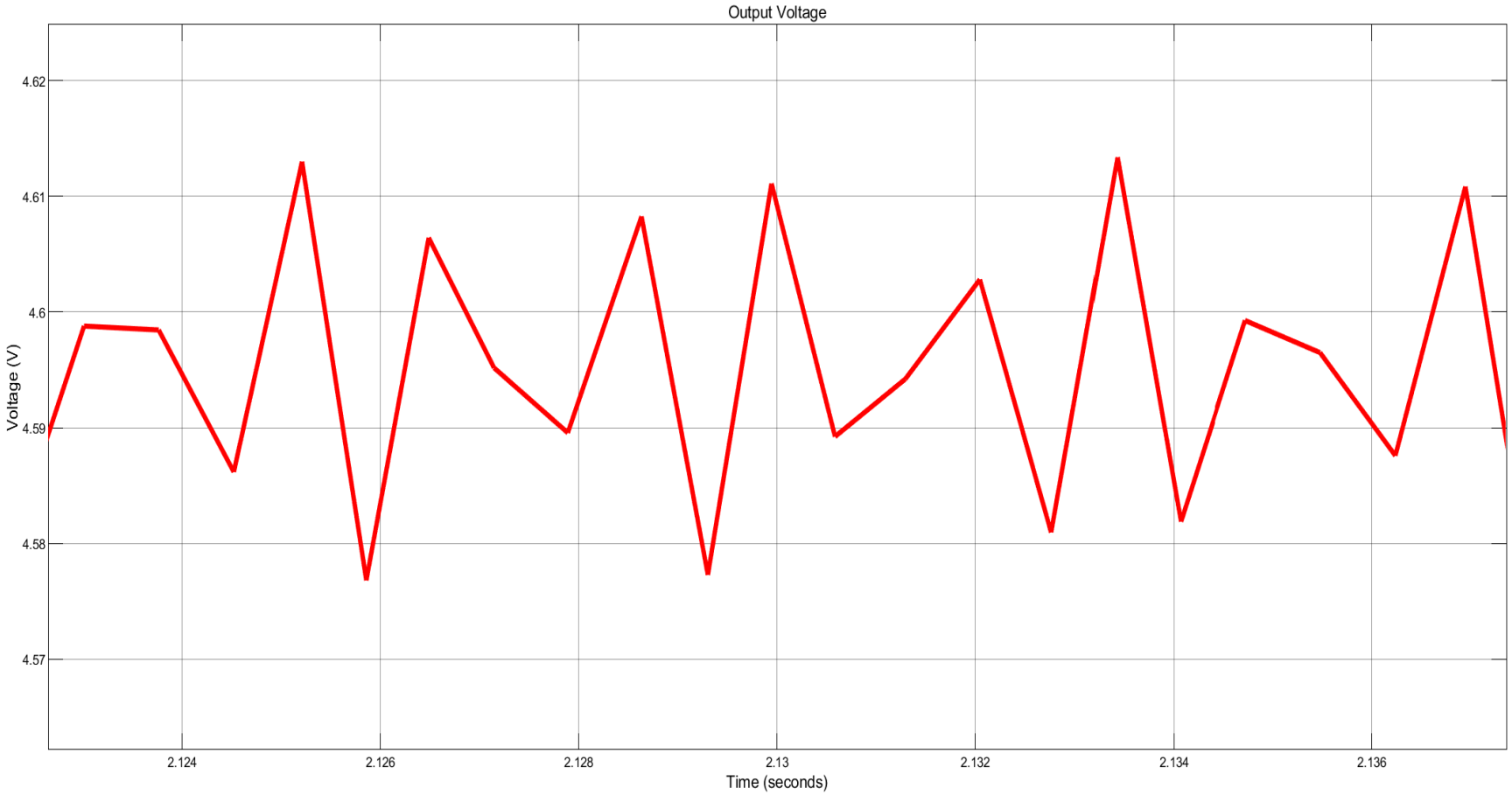

Figure 4.13: The pronounced oscillations in the GMPP after the GA tuning.

4.9. Conclusion

The GA-tuned PID-based boost converter transfer function plant is analyzed in the time domain. The PV array supply of the boost converter before conversion to a transfer function is replaced by a battery with a voltage of 2.4, which is equal to V_{MPP}. The boost converter modeled and simulated in this Chapter is the 5V design of Chapter 3. The 3.3V design is assumed to behave in a similar response but with an adjusted reference voltage of 3.3V. The PID's proportional value is set to a random value of 1; the integral is set to a random value of 1, and the derivative is set to 0. In Figure 4.2, the output voltage without the MPPT installed is 1.6V and far from the 5V target. In Figure 4.3, the scope output waveform overshoots and settles at 1.6V.

Linearization is applied to the boost converter circuit to convert it to a transfer function so that a PID controller can control the transfer function to tune the output voltage to match it to a reference voltage of 5V. The PID controller gains are still set to a proportional value of 1, an integral value of 1, and a derivative value of 0. As seen in Figure 4.7, the amplitude spikes to a maximum value of 3.2e-1V and settles at an amplitude of 6.6e-2V. The settling voltage target is 5V, and the current settling voltage is far off the target. The average output voltage is 0.07V, as shown in the display in Figure 4.6.

GA is applied to the transfer function PID-controlled model, and the best solution values for the PID controller are obtained. The simulation is executed with the best solution values. The output voltage is optimized to a value of 4.6V, close to the 5V bus voltage. This approach in this Chapter is an s-domain analysis, and with it, the output current may not be known, and thus, the output power cannot be calculated. Its practical implementation is non-feasible. However, future research can be conducted to find ways to use the optimized PID values with the original boost convert circuit model. Chapter Five implements the small signal transfer function derivation approach to obtain the boost converter's audio susceptibility transfer function and the control-to-output transfer function. The State Space averaging derivation method and AC analysis small signal transfer function derivation method are theoretical methods that complement the MATLAB/Simulink linearisation method used to convert the boost converter closed loop plant into a transfer function plant. Chapter five uses the same MATLAB/Simulink generated transfer function of the closed loop boost converter. It uses the same integral time absolute error objective function. However, it uses PSO tuning of the PID controller rather than GA tuning.

CHAPTER 5

PARTICLE SWARM OPTIMISATION IMPLEMENTATION of the BOOST CONVERTER for CubeSat POWER SYSTEMS

5.1. Introduction

The chapter implements the small signal transfer function derivation approach to obtain the boost converter's audio susceptibility equation and the control-to-output transfer function. The State Space averaging derivation method and AC analysis small signal transfer function derivation method are theoretical methods that complement the MATLAB/Simulink linearisation method used to convert the boost converter closed loop plant into a transfer function plant, as mentioned in Chapter 4, also presented in this chapter is the averaging method of state space representation of the boost converter. The averaging method of state space is performed to derive the transfer function from the state space. The linearization method mentioned in Chapter 4 produces the boost converter's state space representation and transfer function representation. Hence, this Chapter compares the theoretically derived state space and transfer functions to the linearization Simulink-generated state space and transfer function. Also, the control-to-output transfer function is compared to the linearization Simulink-generated transfer function.

Subsection 5.2 discusses the background of optimization methods used in fine-tuning the PID-controlled boost converter transfer function plant. Subsection 5.3 explains the small signal analysis of the boost converter operation for deriving the audio susceptibility equation and the control-to-output transfer function. Subsection 5.4 discusses the State-Space averaging method used to calculate the state-space equations of a boost converter small signal circuit model. The state-space equations are then converted to a transfer function. The transfer function obtained from the state-space averaging method is compared to the Simulink-generated transfer function using the linearization method.

Subsection 5.5 explains the implementation of the PSO-tuned PID controller that controls the boost converter transfer function plant. The Simulink-generated transfer function by linearization method compares the PSO-tuned PID controller that controls the boost converter transfer function plant with the GA-tuned PID controller that controls the boost converter transfer function plant. Subsection 5.6 discusses the results and the conclusion.

5.2. Optimization Methods Used in Fine-Tuning the PID-Controlled Boost Converter Transfer Function Plant.

Tuning PID controllers for boost converter systems is an essential field of research since it helps preserve system stability, improve response times, and ensure efficient operation under changing load conditions. Several optimization strategies have been investigated in recent literature to achieve optimal PID parameter choices, focusing on dealing with boost converters' nonlinear and dynamic character.

5.2.1. Common Optimization Methods

5.2.1.1. Particle Swarm Optimization (PSO)

PSO is extensively used to optimize PID controllers in boost converters since it is simple and effective. PSO uses the social behavior of birds flocking or fish schooling to search the solution space efficiently. Studies have demonstrated that PSO can successfully optimize PID settings to reduce the integral of time-weighted absolute error (ITAE) and other performance indices. This approach guarantees speedy convergence and robustness in variations in operating conditions. **(Momani et al., 2019)**.

5.2.1.2. Genetic Algorithms (GA)

Genetic Algorithms are another popular choice for PID tuning. GAs simulate the process of natural selection by creating, evaluating, and evolving a population of potential solutions. Combining crossover, mutation, and selection operations allows GAs to effectively explore complex, multi-modal solution spaces. GA-tuned PID controllers have significantly improved dynamic response and stability for boost converters. **(Mohammed et al., 2022)**.

5.2.1.3. Ant Colony Optimization (ACO)

Ants' foraging behavior inspires ACO. It employs a population-based search strategy in which artificial ants create solutions and iteratively refine them using a pheromone updating process. ACO has been effectively used for PID tuning, providing advantages in discovering global optima and coping with nonlinearities in boost converter systems. **(Mohammed et al., 2022)**.

5.2.1.4. Cuckoo Search Algorithm (CSA)

CSA is a nature-inspired optimization technique based on the brood parasitism of some cuckoo species. It is beneficial for handling continuous optimization problems. It has

been used to tune PID controllers by exploiting its ability to balance exploration and exploitation in the search space. This method guarantees excellent accuracy and convergence speed in PID parameter optimization **(Momani et al., 2019)**.

Optimization techniques such as PSO, GA, ACO, and CSA are beneficial for fine-tuning PID controllers in boost converter applications. These algorithms handle the issues given by boost converters' nonlinear and dynamic behavior, resulting in excellent performance and robustness. Recent research has shown that these strategies improve system stability, response time, and overall efficiency, making them valuable tools for engineers and researchers working on power electronics and control systems. In section 5.2, standard PID tuning algorithms are explored. The PID controls the boost converter transfer function plant. In the subsequent section, 5.3, a theoretical derivation of a Control-to-Output Transfer Function from a boost converter small signal circuit is carried out.

5.3. Control-to-Output Transfer Function derivation of the Boost Converter

The control-to-output transfer function of a boost converter, a key element in system design, describes the powerful relationship between the control input (duty cycle, D) and the output voltage (Vout). The small-signal analysis derives this transfer function and assumes that the converter operates in continuous conduction mode (CCM). The derivation involves linearizing the converter's equations around an operating point, neglecting higher-order terms, and taking the Laplace transform. The resulting transfer function is often expressed as a first-order system with a pole and a zero. This transfer function, emphasizing control, provides valuable insights into the system's dynamic response and can be used to design controllers to achieve desired performance characteristics.

Depicted in Figure 5.1 is the small signal circuit of the boost converter.

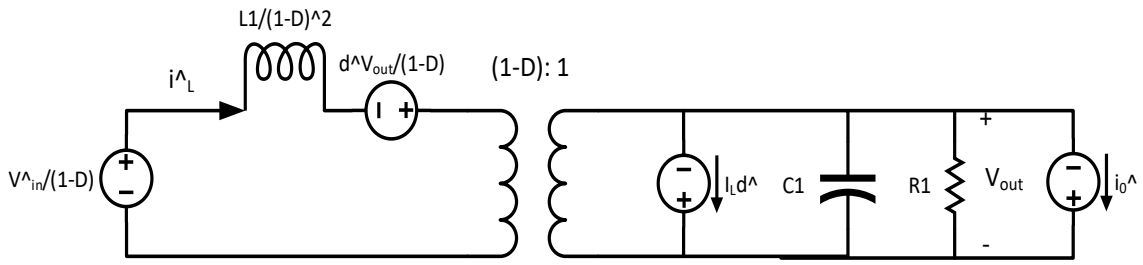

Figure 0.1: Small Signal Circuit of the Boost Converter

We can derive the audio susceptibility transfer function from the small signal circuit and the control-to-output transfer function.

Table 5.1 Critical parameters of the boost converter small signal model circuit.

Symbol	Description	Values of Parameters
V_g	Input voltage	2.4V
V_o	Output voltage	5V
D	Duty Cycle	0.52
$\hat{d}$	small perturbation in the duty cycle	0.1
L	Inductor	2.95mH
C	Capacitor	1520µF
i_L	Inductor current	1.69A
R	Resistor	6.8Ω

Inductor voltage of the boost converter for a small-signal model circuit:

$$\boldsymbol{v_L = L\frac{di_L}{d_t}} \quad (5.1)$$

Capacitor current of the boost converter for a small-signal model circuit:

$$\boldsymbol{i_C = C\frac{dv_C}{dt}} \quad (5.2)$$

The small-signal equivalent circuit equations:

$$\boldsymbol{\tilde{v}_o = \tilde{V}_o - \tilde{v}_c} \quad (5.3)$$

$$\boldsymbol{\tilde{v}_L = L\frac{d\tilde{i}_L}{dt} = \tilde{V}_g d' - \tilde{v}_o D} \quad (5.4)$$

$$\boldsymbol{i_C = C\frac{d\tilde{v}_o}{dt}} \quad (5.5)$$

The small signal perturbations:

$$\boldsymbol{v_L = \tilde{V}_g d' - \tilde{v}_o D} \quad (5.6)$$

Where: $\boldsymbol{d' = 1 - D}$

The control-to-output transfer function relates the change in duty cycle to the change in output voltage:

$$\boldsymbol{G_{vd}(s) = \frac{\bar{V}_o(s)}{\bar{D}(s)}} \quad (5.7)$$

$$\boldsymbol{\tilde{V}_o(s) = \left(\frac{V_g}{D'(sL+r_c)}\right)} \quad (5.8)$$

$$\boldsymbol{G_{vd}(s) = \frac{V_o}{D}\left(\frac{R}{sL(1-D)^2+R}\right)} \quad (5.9)$$

$$\boldsymbol{G_{vd}(s) = \frac{5}{0.52}\left(\frac{6.8}{s(2.95\times10^{-3})\times(1-0.52)^2+6.8}\right)} \quad (5.10)$$

$$\boldsymbol{G_{vd}(s) = \frac{9.615}{9.995\times10^{-5}s+1}} \quad (5.11)$$

The audio susceptibility transfer function relates the change in input voltage to the change in output voltage:

$$\boldsymbol{G_{vg}(s) = \frac{\bar{V}_o(s)}{\bar{V}_g(s)}} \quad (5.12)$$

$$\boldsymbol{\tilde{V}_o(s) = \left(\frac{D'}{(sL+r_c)}\right)\tilde{V}_g(s)} \quad (5.13)$$

$$G_{vg}(s) = \left(\frac{D'R}{sL(1-D)^2+R}\right) \quad (5.14)$$

$$G_{vg}(s) = \left(\frac{0.48\times6.8}{s(2.95\times10^{-3})\times(1-0.52)^2+6.8}\right) \quad (5.15)$$

$$G_{vg}(s) = \frac{0.48}{9.995\times10^{-5}s+1} \quad (5.16)$$

The control-to-output transfer function must differ from the audio susceptibility transfer function because it monitors different variations. The subsequent subsection uses the averaging method to determine the state-space equations of the boost converter circuit. Then, the following section converts the state-space equations into a transfer function.

5.4. State-Space of the Boost Converter Using Averaging Method

The boost converter has two operation modes: closed/on and open/off. In the closed/on mode, the MOSFET/IGBT is switched on; the diode is switched off, the inductor stores energy, and the capacitor releases energy. Figure 5.2 shows the: closed/on mode.

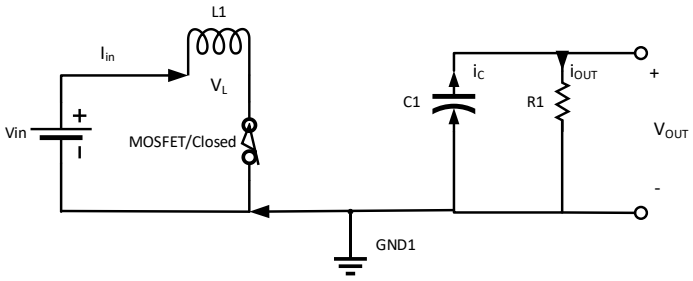

Figure 0.2: Closed/On mode of the Boost Converter

In the open/off mode, the MOSFET/IGBT is switched off; the diode is switched on, the inductor releases energy, and the capacitor stores energy. Figure 5.3 shows the: open/off mode of the boost converter.

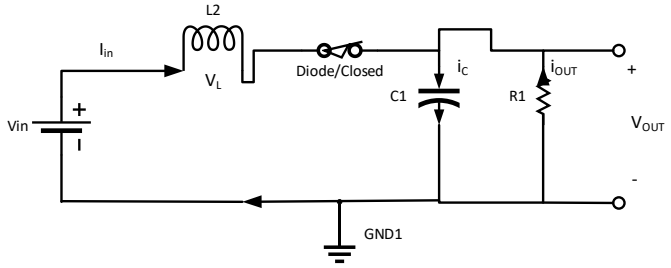

Figure 0.3: Open/Off mode of the Boost Converter

The inductor element creates energy balance, also known as volt-second balance. Volt-second balance means that input power is equal to output power.

$$P_{in} = P_{out} \quad \textbf{(5.17)}$$

The capacitor element creates charge balance. Charge balance means that the input charge is equal to the output charge.

$$Q_{in} = Q_{out} \quad \textbf{(5.18)}$$

A boost converter produces an output voltage of more than an input voltage because the duty cycle must be selected to be less than one (d < 1) in equation 5.3. If d = 0, the output voltage will equal the input voltage. If d > 1, then the output voltage will be negative. If d = 1, then the equation 5.3 is undefined.

$$V_{out} = \frac{V_{in}}{1-d} \quad \textbf{(5.19)}$$

On State (MOSFET closed, diode open):

$$L\frac{di_L}{dt} = V_{in} - V_L \quad (5.20)$$

$$C\frac{dv_C}{dt} = i_C = 0 \quad (5.21)$$

Where: $V_L = v_C$ and $i_C = 0$

Off State (MOSFET open, diode closed):

$$L\frac{di_L}{dt} = V_{in} - V_L \quad (5.22)$$

$$C\frac{dv_C}{dt} = i_C = 0 \quad (5.23)$$

Where: $V_L = v_C + V_{out}$ and $i_C = i_L - \frac{v_C}{R}$

The duty cycle (D) indicates how long the switching period is until the switch is closed. As a result, the state equations over a single switching period (T_s) can be averaged as follows:

$$L\frac{di_L}{dt} = D(V_{in} - v_C) + (1-D)(V_{in} - v_C - V_{out}) \quad (5.24)$$

$$C\frac{dv_C}{dt} = D(0 - i_L) + (1-D)\left(i_L - \frac{v_C}{R}\right) \quad (5.25)$$

Following are the simplified averaged equations:

$$L\frac{di_L}{dt} = V_{in} - (1-D)V_{out} - v_c \quad (5.26)$$

$$C\frac{dv_C}{dt} = -\frac{D}{R}v_c + i_L(1-D) \quad (5.27)$$

The State-Space Representation:

$$\begin{bmatrix} L\frac{di_L}{dt} \\ C\frac{dv_C}{dt} \end{bmatrix} = \begin{bmatrix} 0 & -\frac{1}{L} \\ \frac{1}{C} & \frac{-D}{(RC)} \end{bmatrix} \begin{bmatrix} i_L \\ v_c \end{bmatrix} + \begin{bmatrix} \frac{V_{in}}{L} \\ 0 \end{bmatrix} + \begin{bmatrix} \frac{-(1-D)V_{out}}{L} \\ \frac{i_L(1-D)}{C} \end{bmatrix} \quad (5.28)$$

Output equation:

$$v_{out} = v_C \quad (5.29)$$

Converting the state space into the transfer function:

To convert the state-space representation to a transfer function, we must take the Laplace transform and solve for the output over the input:

$$sX(s) = AX(s) + BU(s) \quad (5.30)$$

Where: $\boldsymbol{X(s)}$Is a state vector in the Laplace domain, A is a system matrix, B is the input matrix, and U is the input in the Laplace domain.

$$\boldsymbol{X(s) = (sI - A)^{-1} + BU(s)} \quad (5.31)$$

$$\boldsymbol{V_{out}(s) = CX(s)} \quad (5.32)$$

$$\boldsymbol{G_{vd}(s) = \frac{V_{out}(s)}{V_{in}(s)} = \frac{(1-D)}{Ls^2+\frac{(1-D)}{R}s+\frac{(1-D)^2}{L}}} \quad (5.33)$$

$$\boldsymbol{G_{vd}(s) = \frac{V_{out}(s)}{V_{in}(s)} = \frac{(1-0.52)}{2.95\times10^{-3}s^2+\frac{(1-0.52)}{6.8}s+\frac{(1-0.52)^2}{2.95\times10^{-3}}}} \quad (5.34)$$

$$\boldsymbol{G_{vd}(s) = \frac{V_{out}(s)}{V_{in}(s)} = \frac{0.48}{0.00295s^2+0.0705882s+78.13555932}} \quad (5.35)$$

The linearisation transfer function is given subsequently for comparison with the state space transfer function:

$$\boldsymbol{TF = \frac{1.11\times10^5 s - 3.612\times10^{-7}}{s^3+9.242\times10^4 s^2+6.836\times10^8 s+6.527\times10^{10}}} \quad (5.36)$$

The difference between the control-to-output transfer function and the state-space transfer function calculated via the averaging method for a boost converter stems from the differing approaches and assumptions utilized in their derivation. The control-to-output transfer function is frequency domain analysis, employing techniques such as Laplace transforms. It considers the small-signal perturbations around a steady-state operating point. It uses the small-signal model to linearize the nonlinear equations of the boost converter. In this method, certain parasitic elements, high-order effects, and non-idealities may need to be addressed to simplify the model. **(Erickson and Maksimović, 2020)**.

The state-space averaging method models the converter in the time domain by averaging its behavior during a switching cycle. This method provides a complete description of the converter's dynamics by considering the instantaneous behavior of the inductor current and capacitor voltage. Non-idealities, such as a capacitor and inductor equivalent series resistance (ESR), can be included in using this method. The difference between the linearisation transfer function obtained using MATLAB/Simulink and the transfer function acquired via the averaging method using the same boost converter component values is due to intrinsic variations in the methodologies utilized to construct these functions.MATLAB/Simulink represents the entire system's dynamics, including higher-order effects, parasitic elements, and interactions that simplistic models may not reveal. When a model is linearised in Simulink, it considers all the states and their interactions at a specific operational point. This frequently yields a higher-order transfer function because it accounts for all the dynamics in the model, including those introduced by switching actions, control loops, and parasitics. Simulink

also incorporates the dynamics of any model-included control and measurement systems, which might introduce new poles and zeros into the transfer function. **(Erickson and Maksimović, 2020)**. The state-space averaging method simplifies the converter operation by averaging states throughout a switching interval. This method typically focuses on the underlying dynamics of inductor current and capacitor voltage, yielding a second-order model of a boost converter. While the averaging method produces a simpler model that is easier to analyze, the full Simulink model provides a more accurate representation for simulation and design (Mohan et al., 1995).

5.5. Implementing PSO to the Simulink-Generated Plant Transfer Function

MATLAB/Simulink model represents the entire system's dynamics, including higher-order effects, parasitic elements, and model-included control and measurement systems, which might introduce new poles and zeros into the transfer function. Hence, the PSO algorithm is applied to it and not to the control-to-output transfer function or the averaging method transfer function. There are two ways discovered in the literature to apply PSO. Firstly, A similar approach to that applied in Chapter 4 using the GA-tuned PID to control the bus voltage setpoint for a boost converter transfer function plant can be applied, and the GA algorithm is replaced with the PSO.

Secondly, the boost converter circuit can implement a PSO algorithm as a MATLAB MPPT function. It was discovered in Chapter 4 that the transfer function plant approach is a theoretical analysis and has no practical utilization in the CubeSat EPS design and implementation. This section explains the first implementation approach that uses the boost converter's frequency domain transfer function plant with PSO tuning of the PID. A similar approach to the genetic algorithm GA is adopted to implement the PSO to tune the PID controller gain parameters. Again, ITAE is selected for its fast response time and settling time as an objective function to minimize the steady-state error. ITAE MATLAB function named “tunning2” is used to evaluate the performance of the PSO-tuned PID-controlled boost converter transfer function closed loop plant with PID gain parameters K(1), K(2), and K(3).

5.5.1. ITAE function execution steps

1. The function receives K, a set of parameters to be tuned for the Simulink model.
2. It assigns K to the base workspace so the Simulink model can access and use these parameters during its simulation.
3. It runs the Simulink model named “PSO_to_theory.slx” with the current parameters K.

4. the cost is calculated using the ITAE value after the simulation. The cost measures how well the model performs with the current parameters.

The ITAE cost function is used as the objecting function of the PSO algorithm in a MATLAB script file. The ITAE function MATLAB code is included in Appendix E.

5.5.2. The Particle Swarm Algorithm MATLAB code steps

To explain the PSO MATLAB code, which is used to minimize the steady-state error of a Simulink model that represents the nonlinear characteristic response of the boost converter plant, which is in the form of a transfer function and is controlled by a PID controller using an ITAE objective function as a minimization performance index, a step-by-step format is explained below:

Step 1: Initialize the MATLAB environment

Clear all variables, close all figures, and clear the command window.

Step 2: Define Problem Details

Set the number of variables (nVar), upper bounds (ub), lower bounds (lb), and the objective function (fobj).

Step 3: Set the PSO Parameters

Define the number of particles (noP), maximum iterations (maxIter), and various PSO parameters, including inertia weights (wMax, wMin), cognitive and social coefficients (c1, c2), and velocity limitations (vMax, vMin).

Step 4: Initialise Particles

Initialize each particle's position, velocity, personal best (PBEST), and global best (GBEST).

Step 5: Run the PSO Main Loop

Iterate over the specified number of iterations.

Step 6: Calculate the Objective value for each particle

Evaluate the objective function for each particle's current position. Update personal best (PBEST) and global best (GBEST) if the current objective value improves.

Step 7: Update Velocity and Position

Compute the inertia weight for the current iteration. Update each particle's velocity and position based on inertia, cognitive, and social components. Ensure velocities and positions are within bounds.

Step 8: Display Iteration Results

Display the current iteration number and the global best objective value. Store the global best objective value for plotting.

Step 9: Plot Convergence Curve

Plot the convergence curve showing the global best objective value at each iteration.

5.5.3. MATLAB/Simulink Model of the PSO-Tuned PID Controller for a PV-Supplied Boost Converter Transfer Function Model

Figure 5.4 shows the MATLAB/Simulink model of the PSO-tuned PID controller for a PV-supplied boost converter transfer function model. The model of the plant is linearised for STC (28°C and 1367w/m^2) PV input condition, and the control action is targeted at matching the output to the 5V reference point. Figure 5.4 model is tuned using PSO with 50 particles, and for 1 iteration, the PID gains adjusted from random: P = 1, I =1, and D=0 to new values: P=7.111285511803252e+02, I=6.245729169933086e+02, and D=5.906086529196359e+02, and yielded an output of 4.331V just after a single PSO iteration. This is a significant improvement from an output voltage of 0.05664V achieved before GA tuning in Chapter 4: Figure 4.6.

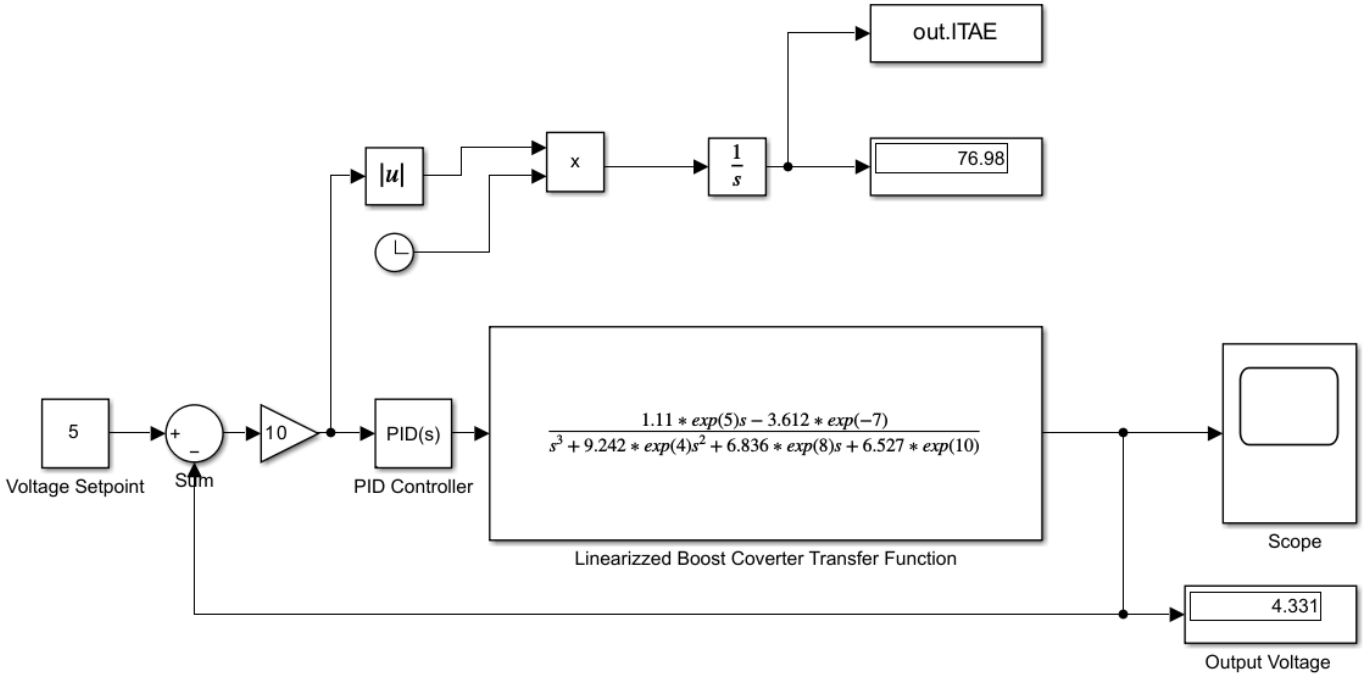

Figure 5.4: PSO tuning of the parameters of the PID after the first iteration

Figure 5.5 shows the scope of the PSO tuning of the parameters of the PID after the first iteration.

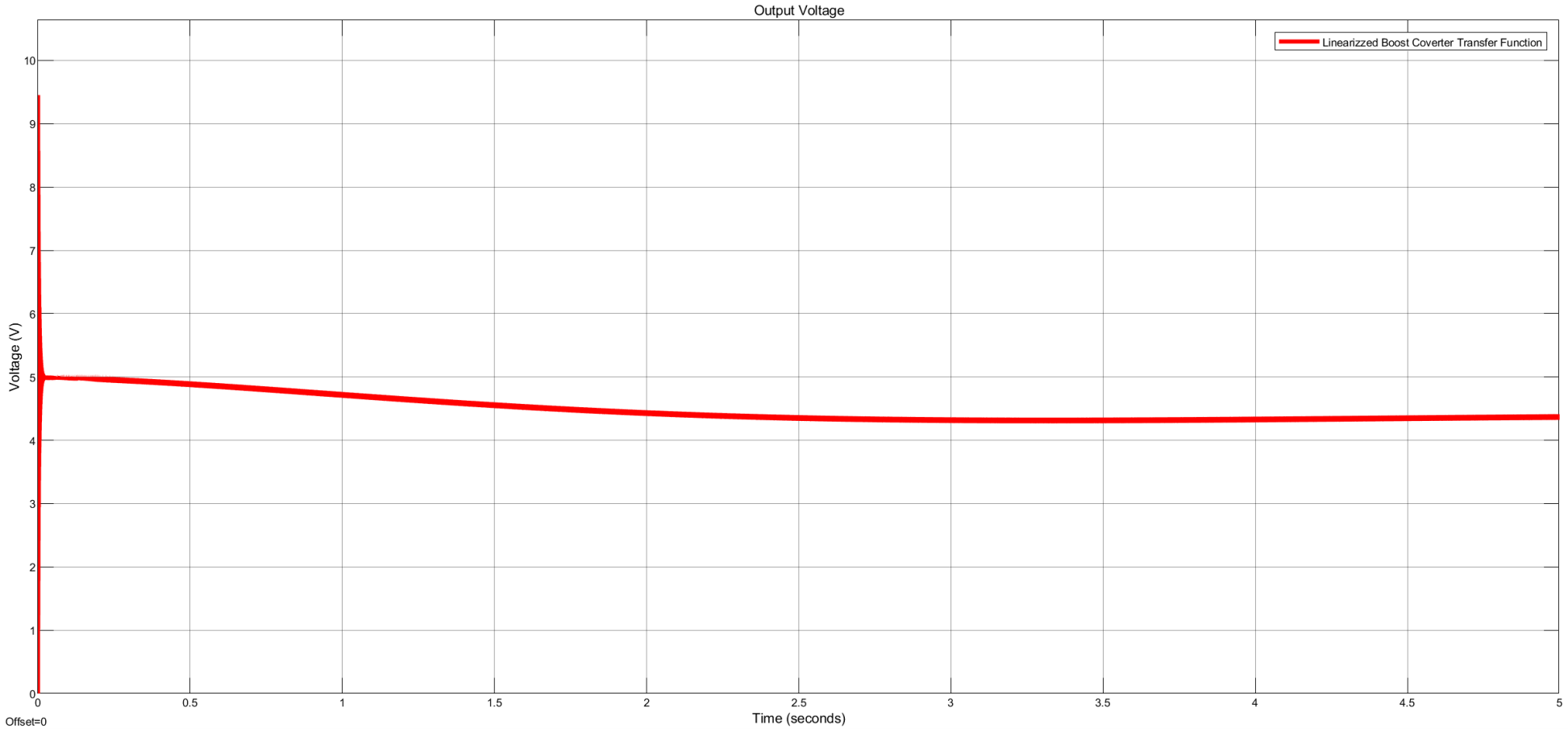

Figure 5.5: PSO tuning of the parameters of the PID after the first iteration

The output waveform shows in Figure 5.5 that the bus voltage of 5V is not achieved; there are pronounced overshoots and undershoots at the initial time of the simulation, but they rapidly dampen.

Figure 5.6 shows the pronounced oscillations about the GMPP after the first iteration of running the PSO tuning code. The peak-to-peak Amplitude of these oscillations is 9.36e-2V.

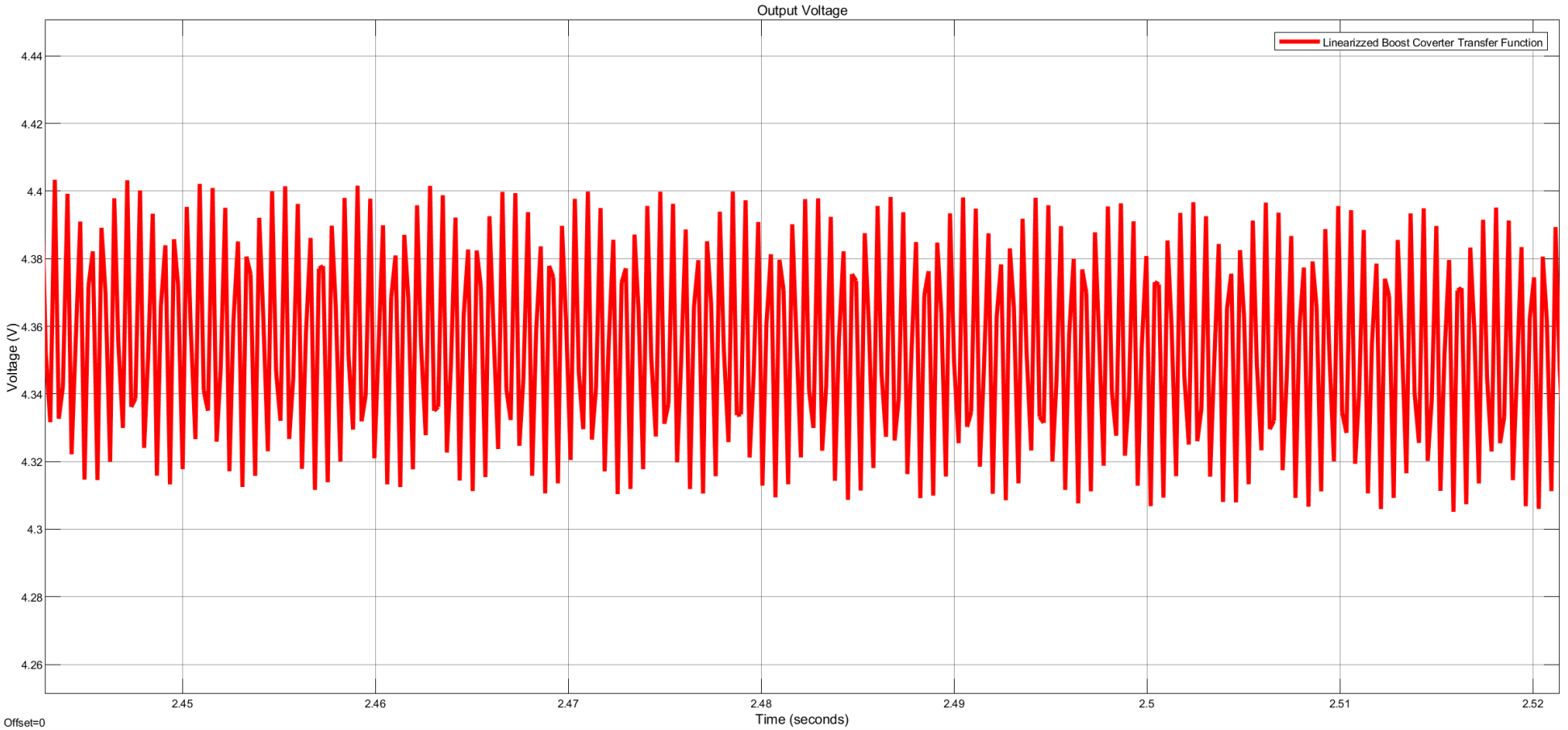

Figure 5.6: The pronounced oscillations about the GMPP after the first iteration of the PSO tuning application

Figure 5.7 is the model of the PSO tuning of the parameters of the PID after the 50 iterations using 50 particles. The average DC output voltage produced by the best-found PID values is 4.7V. The Best PID parameters were K_p: 0, K_i: 1000, and K_d: 495.0556.

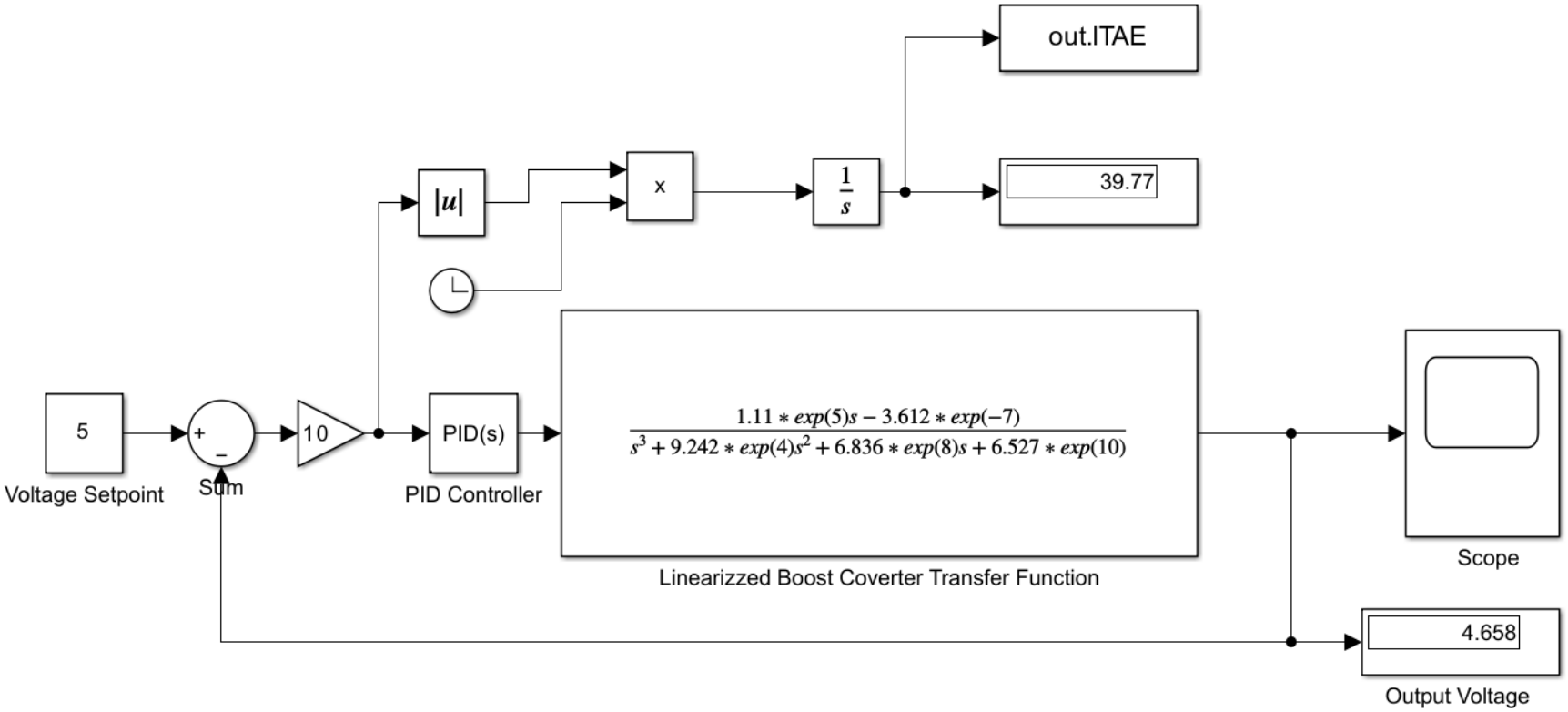

Figure 5.7: PSO tuning of the parameters of the PID after the fifty iterations.

The maximum iterations that were set for the algorithm were fifty iterations. When the fifty iterations were executed, the best gains of all solutions were displayed. These gain values of k_p, k_i, and k_d are automatically sent from the workspace to the Simulink model's PID block, and the Simulink model is simulated with these optimized gain values. Figure 5.8 shows the MATLAB windows with fifty iterations simulated and the best solution displayed.

Pseudocode for the PSO tuning of the PID controller for the PV-supplied boost converter transfer function plant.

1. Clear all variables, close all figures, and clear command window.

2. Initialize problem parameters:
   - Define `nVar` as the number of variables (3 in this case).
   - Set `ub` as the upper bound for the variables [1000, 1000, 1000].
   - Set `lb` as the lower bound for the variables [0, 0, 0].
   - Define `fobj` as the objective function (in this case, a function called `tunning2`).

3. Initialize PSO parameters:
   - Set `noP` as the number of particles (50).
   - Set `maxIter` as the maximum number of iterations (50).
   - Define inertia weight `wMax` as 1 and `wMin` as 0.1.
   - Set cognitive and social acceleration coefficients `c1` and `c2` as 2.
   - Define `vMax` as 20% of the range between the upper and lower bounds (`ub - lb`).
   - Define `vMin` as the negative of `vMax`.

4. Initialize the particle swarm:
   For each particle `k` from 1 to `noP`:
   - Randomly initialize the particle's position `X` within the bounds `[lb, ub]`.
   - Initialize the particle's velocity `V` as a zero vector.
   - Initialize the particle's personal best position `PBEST.X` as a zero vector.
   - Set the particle's personal best objective value `PBEST.O` to infinity.
   - Initialize the global best position `GBEST.X` as a zero vector.
   - Set the global best objective value `GBEST.O` to infinity.

5. Main loop for PSO:
   For each iteration `t` from 1 to `maxIter`:

   5.1 Evaluate the objective function for each particle:

- For each particle `k`, calculate the objective value using the function `fobj` (evaluates `tunning2` for the particle's current position `X`).

- Update the personal best (`PBEST`) for each particle if the current objective value `O` is better than the personal best.

- Update the global best (`GBEST`) if the current objective value `O` is better than the global best.

5.2 Update the particles' velocity and position:

- Calculate the inertia weight `w` based on the current iteration (linearly decreasing from `wMax` to `wMin`).

- Update the velocity `V` of each particle using the PSO formula:

- Velocity depends on inertia, cognitive component (towards personal best), and social component (towards global best).

- Ensure velocities stay within the bounds `[vMin, vMax]`.

- Update the position `X` of each particle by adding the velocity `V`.

- Ensure positions stay within the bounds `[lb, ub]`.

5.3 Display the current iteration number and global best objective value.

5.4 Store the global best objective value at the current iteration for plotting later.

6. After the main loop:

- Display the best PID parameters found (`Kp`, `Ki`, and `Kd`) based on `GBEST.X`.

- Plot the convergence curve showing the global best objective value over iterations.

7. Define the objective function `tunning2`:

- Simulate a PID controller using the parameters `P` (the particle's position).

- Extract the `ITAE` (Integral of Time-weighted Absolute Error) from the simulation output.

- If `ITAE` data is valid, return the final value as the cost; otherwise, return infinity.

In Figure 5.9, there are still undershoots and overshoots at the initial time of the waveform, but they rapidly dampen. The waveform forms a sinusoid that momentarily reaches its positive peak at the 5V DC line. We couldn't tell after the first iteration that the waveform would form a sinusoid along the timeline after the five-second simulation.

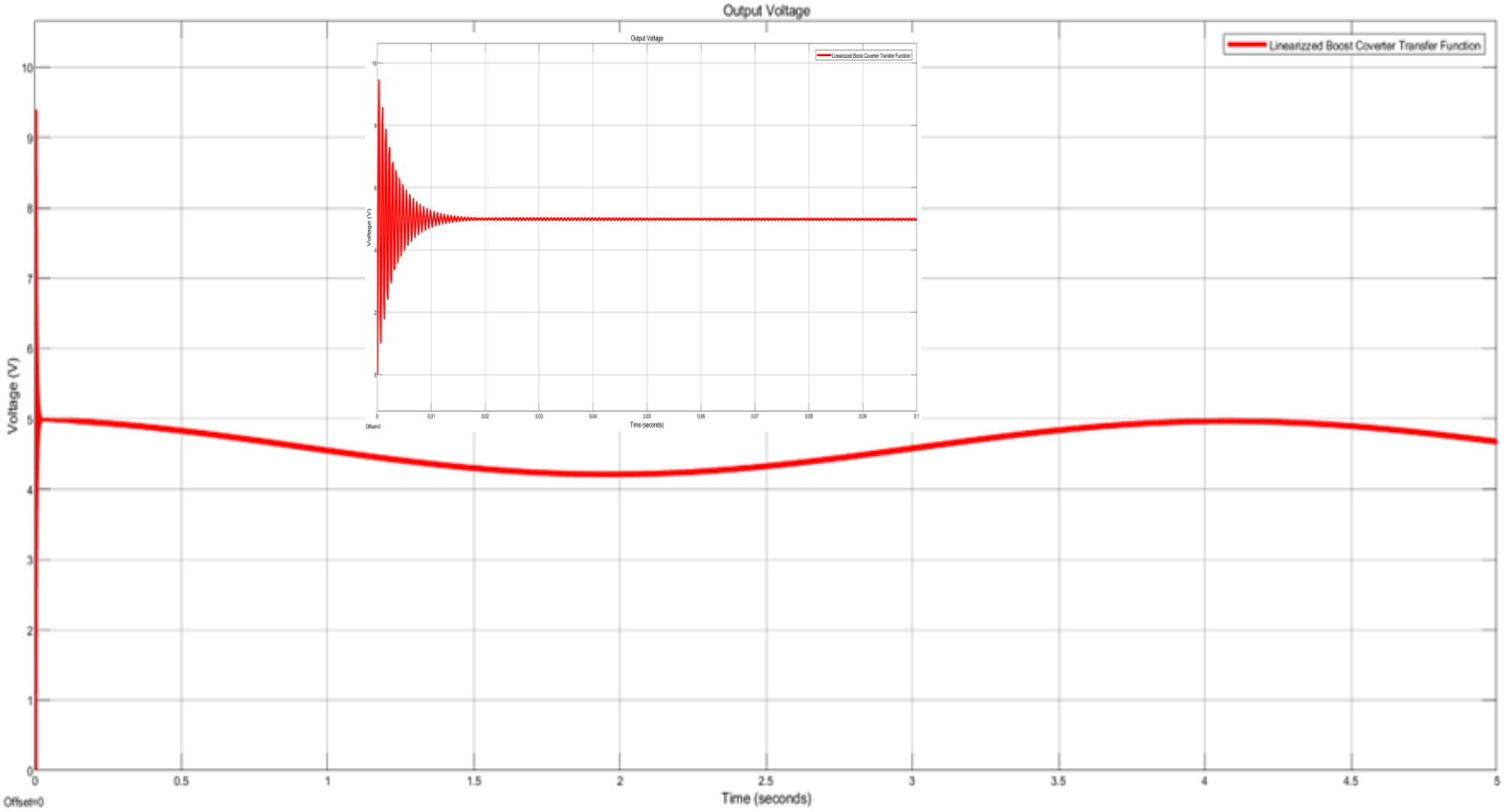

Figure 5.8: PSO Tuning of the Parameters of The PID after the Fiftieth Iteration

Figure 5.10 shows that the pronounced oscillations about the GMPP after the fiftieth iteration reduced amplitude by 13mV. The peak-to-peak of these oscillations is 8.06e-2V.

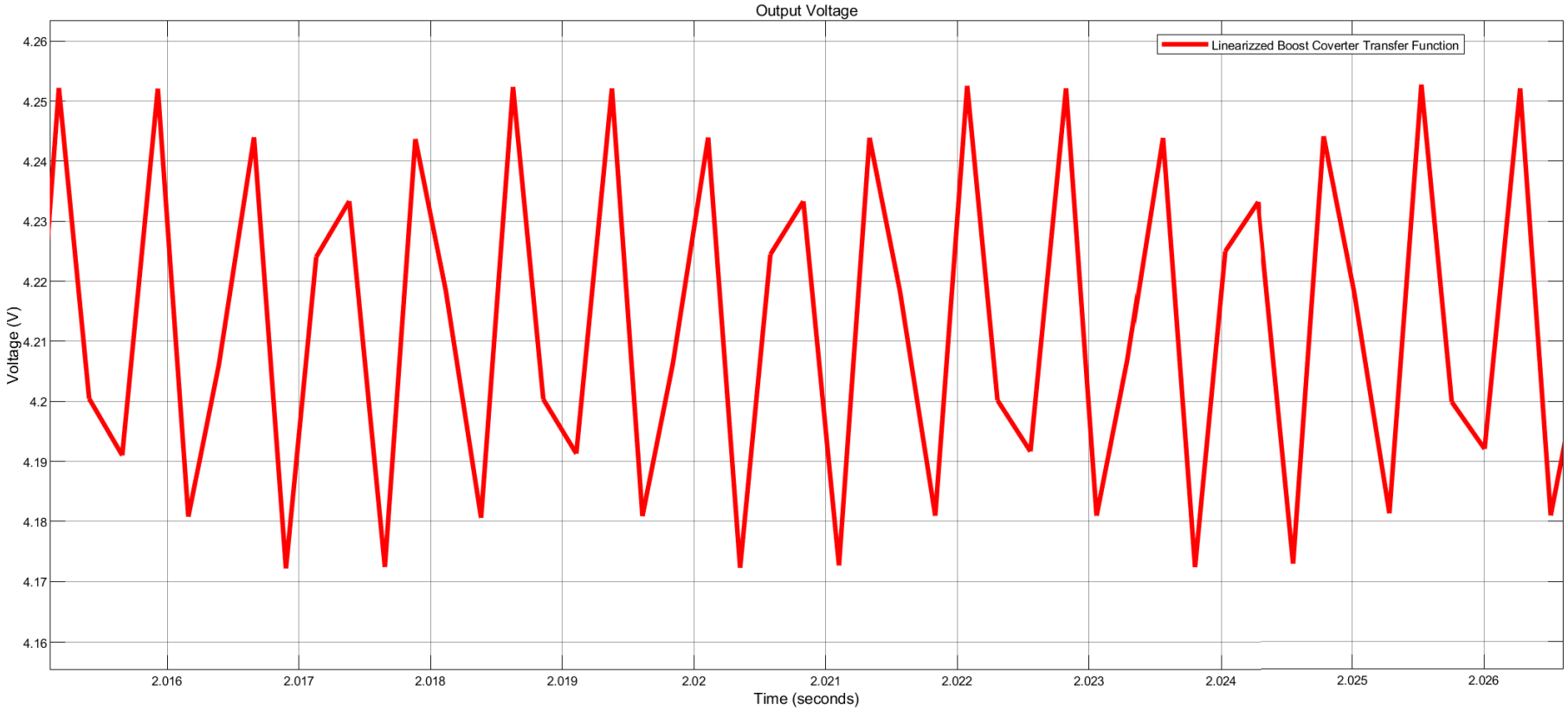

Figure 5.9 Oscillations at the GMPP after the fiftieth iteration

Figure 5.11 shows the convergence curve and how the global best objective value related to minimizing the error metric, the ITAE PID performance index, changes across iterations. The global best objective value steadily improves with iterations. At the start of the PSO process, the objective value fluctuates at higher values of 1.33×10^{-3}, but as iterations progress, it gradually decreases. At the fifty-eighth iteration, the global best value achieves a minimum of 1.2923×10^{-3}. This indicates that the PSO algorithm was able to find a near-optimal solution at this point. Beyond this iteration, the curve flattens out, implying that the optimization has converged, and further iterations do not significantly improve the solution.

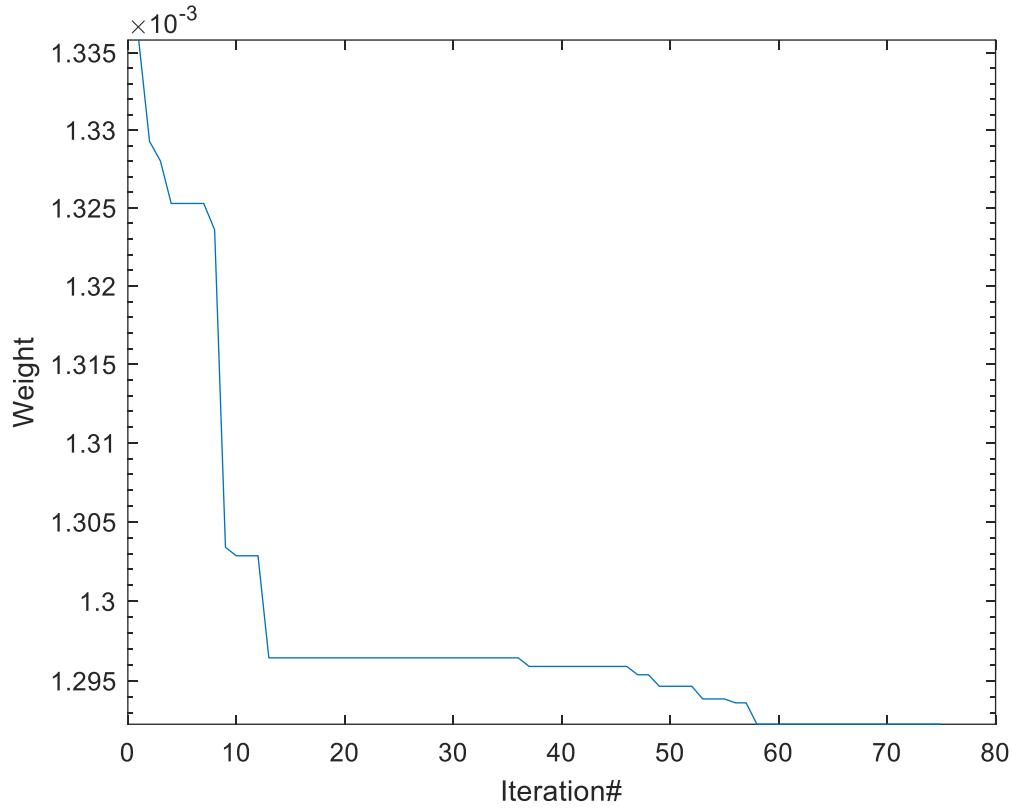

Figure 5.10: The Plot Convergence Curve

5.6. Conclusion

After tuning the PID, which controls the closed loop boost converter transfer function plant with GA, the best solution's average DC output voltage is 4.557V, and after tuning the PID, which controls the closed loop boost converter transfer function plant with PSO, the average DC output voltage produced by the best-found PID values using PSO is 4.658V. The PSO's average DC output voltage is closer to the 5V DC voltage by 101mV. The GA-tuned and PSO-tuned scope simulation results waveforms take a similar curvature. Initially, they over and undershoot, rapidly dampen, and pursue the setpoint voltage. However, the PSO curve intermittently touches the setpoint voltage by its peak positive amplitudes, whereas the GA curve is a continuous sawtooth waveform below the setpoint voltage. The GA oscillation's peak-to-peak amplitude

about the GMPP after 50 generations of tuning is 3.66e-2V, and the PSO oscillation's peak-to-peak amplitude about the GMPP after 50 iterations of tuning is 8.06e-2. There is a difference of 44mV, so the GA is smoother than the PSO by a value of 44mV. Chapter six implements a hybrid technique combining the PO and PSO MPPT to mitigate the PO’s poor tracking under rapid weather conditions.

CHAPTER 6

Hybrid Perturb and Observe Particle Swarm Optimisation Maximum Power Point Tracking Model for Implementation in the CubeSat Power Systems

6.1. Introduction

To mitigate the PO's poor tracking under rapid weather conditions, a hybrid technique that combes the PO and PSO MPPT is implemented in this Chapter. This hybrid MPPT is comprised of the PO function and the PSO algorithm, and together, they control the duty cycle of the pulse width modulated control signal (PWM). The perturb and observe (PO) maximum power point tracking (MPPT) function, which is implemented in Chapter 3, tracks the global maximum power point (GMPP) poorly under rapid weather conditions. The particle swarm optimization (PSO) algorithm implemented in Chapter 5 quickly finds the local maximum power point.

The PWM signal controls the switching duty cycle of the MOSFET in the boost converter circuit, and the duty cycle of the boost converter regulates the output voltage gain. In this Chapter, the target is to design a hybrid controller that will regulate the output voltage of the boost converter at a 5V level under varying photo voltaic weather conditions. The 3.3V boost converter is assumed to respond similarly to 5V but with a different boost converter output voltage of 3.3V.

The MPPT controllers presented in this Chapter work in the time domain. The PV input voltage, current, power, and boost converter output voltage, current, and power are monitored in real-time. The simulations in this Chapter will continue using the assumption of the worst-case scenario where two sides of the 1U CubeSat face the sun. This means the array is made of four parallel connected modules.

Subsection 6.2 provides an overview of how the PO function works, how the PSO MATLAB function works, and how they are combined in the MATLAB/Simulink function to form the hybrid script file code. Subsection 6.3 explains the PSO algorithm in generic terminology. Also included in subsection 6.3 is a PSO algorithm step-by-step process explanation as it is implemented as a MATLAB function in Simulink. Subsection 6.4 depicts the simulation results of the Simulink model that implements the hybrid PO PSO MPPT. Subsection 6.5 discusses the hybrid PO PSO MPPT convergence time in tracking the GMPP, system oscillation at the GMPP, and how the system responds to standard testing conditions (STC) and low earth orbit (LEO) thermal conditions. Subsection 6.6 is the conclusion and benchmarks the results achieved in this Chapter.

6.2. The Overview of the Hybrid PO PSO MPPT Model

The Simulink design of the novel hybrid PO PSO MPPT function that controls the PWM's duty cycle of the boost converter is shown in Figure 6.1. The hybrid code combines the global search capabilities of PSO with the fine-tuning capability of PO. When the system approaches the optimum (minor fluctuations in power), the PO algorithm takes control. Otherwise, the PSO algorithm investigates a wide range of solutions. The size of the power output change determines whether the PO function or the PSO algorithm is used. The hybrid technique addresses the problem of poor GMPP tracking in dynamic situations.

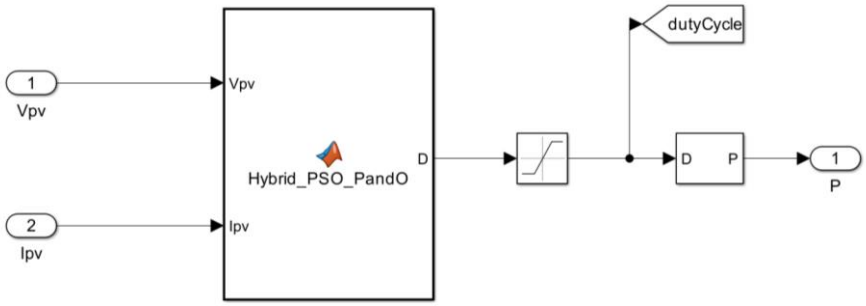

Figure 6. 1: PO MPPT and the PSO MPPT duty cycle computation

The PO MPPT measures both the voltage and the current produced by the PV module and computes the input power of the PO function. The PO function perturbs the power in one direction, and if the power continues to increase, then the PO keeps on perturbing in the same direction. If the perturbed new power value is less than the old one, it will perturb in the opposite direction. One of the drawbacks of the PO function when it is used alone is the oscillation at the maximum power point. Additionally, the PO function tracks the maximum power point (MPP) poorly under rapidly changing weather conditions. Depicted in Figure 6.2 is the flowchart of the PO MPPT function. On the left is a negative perturbation, and on the right is a positive perturbation.

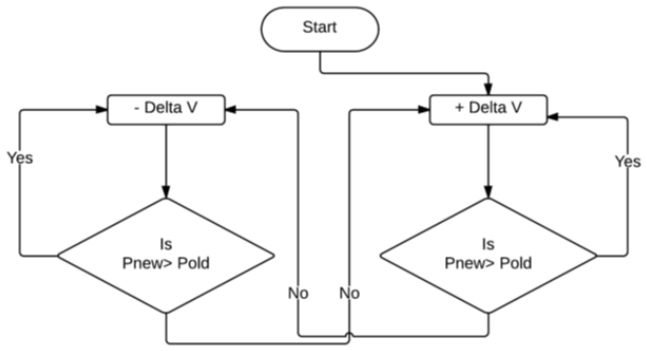

Figure 6. 2: The basic flowchart of the PO MPPT function

The PSO algorithm also uses the measured values of both PV voltage and current to calculate the power of each particle. The current value of the power of each particle is

then compared with the previous value. If the current value is better than the previous value, then the last value is updated. A detailed explanation of the PSO code is explained in subsection 6.3. The novel hybrid PO PSO MPPT overall system comprises a PV power source array, a boost converter, a load, a PO function, and a PSO function, as shown in Figure 6.3.

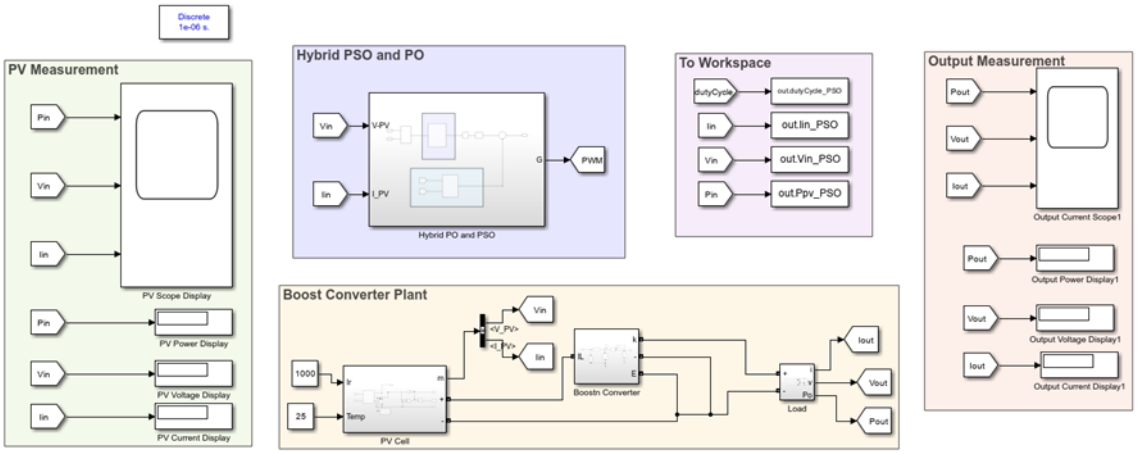

Figure 6. 3: The Hybrid PO-PSO MPPT Model

This design uses a PSO algorithm and a PO objective function because this research Thesis seeks to compare the results of the PO MPPT (implemented in Chapter 3) with the novel hybrid PO PSO MPPT (implemented here in Chapter 6). The comparison is performed using performance indicators: convergence time in tracking the GMPP, the measure of oscillations at the GMPP, and the system's response at standard test conditions (STC) and in low earth orbit (LEO) thermal conditions. Subsection 6.3 explains the PSO algorithm in generic terminology and describes it as implemented as a MATLAB function.

6.3. PSO algorithm for the implementation as a MATLAB MPPT function

Subsection 6.3.1. explains the PSO algorithm in generic terminology.

6.3.1. The Overview of the PSO Algorithm

The PSO algorithm introduced by J. Kennedy and R.C. Eberhart in 1995 is widely used to optimize system performance. A modified PSO was introduced in 1998 to improve the performance of the original PSO. A linearly decreasing inertia weight (ω) is added to the enhanced PSO during each iteration. Clerc reported another widely used PSO. In this thesis, the PSO used is the 1998 PSO (Aoughlis et al., 2021). A PSO is a stochastic, population-based evolutionary algorithm search method. It is modeled after the behavior of a bird swarm or a fish school. (Abdulkadir and Yatim, 2014). The algorithm's methodology focuses on the attitude of a swarm of birds or a school of fish

when searching for food. In the PSO, a particle represents a potential solution to a problem. Particles imitate the success of neighboring particles and their own achieved success. Therefore, the position of a particle is influenced by the position of the best particle (Pbest) in a neighborhood, as well as the best solution found by all the particles in the entire population (Gbest).

Each particle is treated as a point in a D-dimensional space. The i^{th} particle is represented as XI= (x_{i1}, x_{i2},…,x_{iD}). The best previous position giving any particle's minimum/maximum fitness value is recorded and described as PI= (p_{i1}, p_{i2},…,p_{iD}); this is called Pbest. The position of the best particle among all particles in the population is called Gbest. The particle (i) velocity is represented as VI= (v_{i1}, v_{i2},…, v_{iD}). The particle position, xi, is adjusted using:

$$\boldsymbol{x_i^{t+1} = x_i^t + v_i^{t+1}} \quad (6.1)$$

where the velocity component represents the step size v_i. The velocity is calculated by:

$$\boldsymbol{v_i^{t+1} = \omega v_i^t + c_1 r_1 (pbest, i - x_i^t) + c_2 r_2 (gbest - x_i^t)} \quad (6.2)$$

Where: $\boldsymbol{i = 1, 2, \ldots \ldots N}$

Where x_i denotes the ith particle position; the velocity of the ith particle is represented by v_i; the number of iterations is denoted by t; the inertia weight is defined by ω; r_1 and r_2 are uniformly distributed random variables within [0, 1]; and the cognitive and social coefficients are denoted by C_1 and C_2 respectively. In the velocity equation, $\boldsymbol{c_1 r_1 (pbest, i - x_i^t)}$ is called the cognitive part, representing the particle's personal experience or individual memory that brings it back to the most satisfying place it passed through in the past. The term $\boldsymbol{c_2 r_2 (gbest - x_i^t)}$ reflects social behavior. It makes each particle follow the best position found by its neighbors.

6.3.2. PSO Algorithm in MATLAB MPPT function

The MATLAB MPPT function code implements a PSO algorithm for adjusting the duty cycle D of the boost converter based on the input voltage Vpv and current Ipv of a PV array. The goal is to maximize the power output of the boost converter by finding the optimal duty cycle D using the PSO algorithm.

Step 1: Particle Initialization

The '**persistent**' is used to retain the values of the variables between function calls, allowing the algorithm to maintain state and progress over multiple iterations.

The variables ***'u,' 'dcurrent,' 'pbest,' 'p,' 'dc,' 'v,' 'counter,'*** and ***'gbest'*** are initialized on the first function call.

- counter: Tracks the number of iterations.
- dcurrent: Stores the current duty cycle.
- gbest: Stores the global best duty cycle.
- p, v, pbest, dc: Arrays to store particle positions, velocities, personal best positions, and duty cycles.

Table 6.1: PSO algorithm MATLAB MPPT Function variables description

Symbol	Description	Parameters Values
u	Iteration counter	1 to 4
$dcurrent$	Current duty cycle	0.5
$pbest$	Personal best duty cycle for each particle	0[3,1]
p	Personal best power for each particle	0[3,1]
$dc(1)$	The duty cycle for each particle 1	0.2
$dc(2)$	The duty cycle for each particle 2	0.4
$dc(3)$	The duty cycle for each particle 3	0.7
v	Velocity for each particle	0[3,1]
$Counter$	Iteration delay counter	1 to 300
$gbest$	Global best duty Cycle	0.5
dc	Duty Cycle	0[3,1]

Initial duty cycles for each particle **('dc(1)', 'dc(2)', 'dc(3)')** are set to 0.2, 0.4, and 0.7, respectively.

Step 2: Delay Mechanism

The function uses a counter to delay the execution of the PSO algorithm by returning the current duty cycle without modification until a certain number of iterations ('**counter'** reaches 300) have passed.

Step 3: Fitness Evaluation

The fitness of each particle is calculated as the power output*:* $V_{pv} \times I_{pv}$

If the current power output is greater than the previous best: *'**pbest'**,* the best position of the particle is updated to the current duty cycle.

Step 4: Particle Update

The function cycles through each particle (***'u'*** ranging from 1 to 4) to update their duty cycles (***'D'***), velocities, and positions.

If ***'u'*** reaches 4, the algorithm finds the particle with the highest power output (***'gbest'***), updates the global best duty cycle, and recalculates the velocities and positions of the particles.

Step 5: Velocity and Duty Cycle Update

The velocity of each particle is updated using the PSO velocity update formula:

v_final = w * v + c1 * rand() * (pbest - d) + c2 * rand() * (gbest - d)

Where:

- v_final: Updated velocity
- w: Inertia weight
- v: Current velocity
- c1, c2: Cognitive and social parameters
- pbest: Personal best position
- d: Current duty cycle
- gbest: Global best position

The duty cycle is updated based on the new velocity, ensuring it remains within the bounds [0, 1].

d_final = max(0, min(1, d + v_final))

where:

- d_final: Updated duty cycle
- d: Current duty cycle
- v_final: Updated velocity

Step 6: Final output

After all updates, the final duty cycle (‘D’) is returned.

The control action of the PSO method used for MPPT is summarised in Figure 6.5. Also, it puts the steps 1 to 6 covered in subsection 6.2.3 into a flowchart diagram. The PSO algorithm in this function iteratively updates particle positions and velocities based on their fitness values to find the optimal duty cycle that maximizes the power output of the boost converter. The flowchart in Figure 6.4 outlines a Particle Swarm Optimization (PSO) algorithm for tuning a boost converter's duty cycle (D) to maximize output power. The process begins by initializing variables and then iteratively calculates power output for each particle. If the current power is greater than the personal best, the particle's personal best position and power are updated. After a pre-defined number of iterations, the global best duty cycle is determined based on the maximum power achieved by any particle. The particle’s velocities and duty cycles are then updated using the PSO equations. This iterative process continues until a termination condition is met, and the final optimized duty cycle is returned as the optimum result.

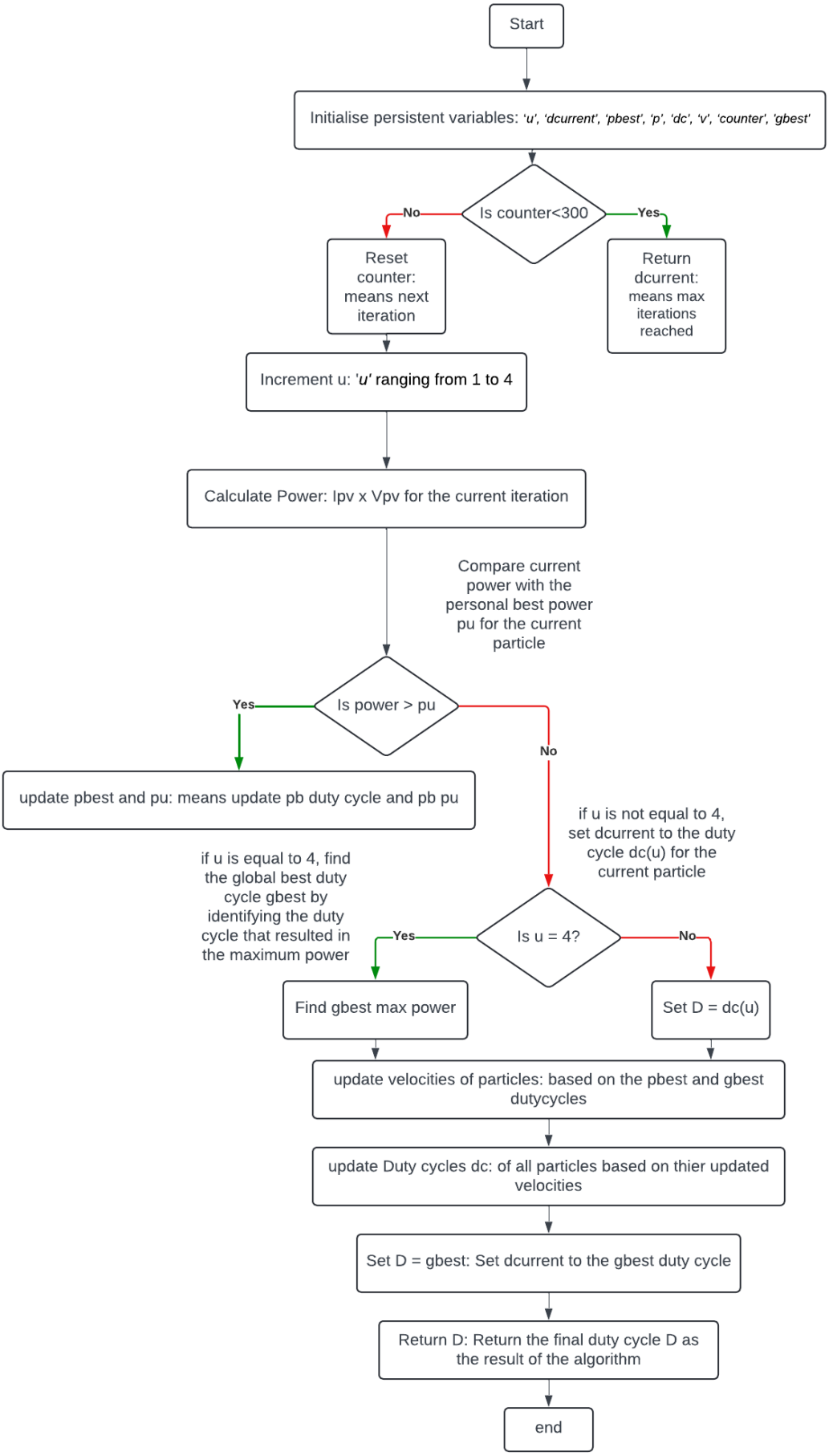

Figure 6.4: The PSO method used for MPPT Flowchart

6.4. The Hybrid PO PSO MPPT Model Implementation

The performance of the PO MPPT at standard testing conditions (STC) is discussed in subsection 6.4.1. Subsection 6.4.2. PO MPPT under rapidly changing space weather conditions. Subsection 6.4.3. discusses the performance of the PSO MPPT at STC. Subsection 6.4.4. PSO MPPT under rapidly changing space weather conditions. Subsection 6.4.5. discusses the performance of the hybrid PO PSO MPPT at STC. Subsection 6.4.6. hybrid PO PSO MPPT under rapidly changing space weather conditions. Azur Space solar cell standard testing conditions, the temperature is 28°C, and the radiation is 1367W/m^2 (Guter et al., 2017). In low earth orbit (LEO), the temperature can change rapidly from -100°C to +125°C, and radiation varies depending on the satellite's distance to the sun from 1322W/m2 to 1414W/m2 (Boushon, 2018).

The worst-case situation is when two sides of the CubeSat point towards the sun. A configuration where two sides of the CubeSat are pointed to the sun is simulated by the (+X, +Y) or (-X, -Y) groups. The (+X, +Y) or (-X, -Y) group gives a voltage output of 2.4V and a total current of 1.8A. The solar Array will have four modules connected in parallel. This array is an input of the boost converters. The desired outputs of the boost converters are 3.3V and 5V, as determined by the desired bus load voltages. However, for practical demonstration in this section, the 5V bus boost converter design of Chapter 3 is utilized, and it is assumed that the 3.3.V bus will behave similarly but with setpoint voltage focused at 3.3V.

6.4.1. Perturb and Observe MPPT at Standard Testing Conditions

The PO MPPT Simulink model is shown in Figure 6.6; at the far left are the PV array measurements. The PV output power, voltage, and current are connected to the scope and the display for displaying average DC levels. At the top center is the PO MPPT MATLAB/Simulink function, which tunes the PWM duty ratio to maximize power extraction. At the bottom center is the boost converter model, which regulates the load voltage. At the far right are the load measurements, where load power, voltage, and current are connected to the scope and displays. The first objective is to measure the time it takes to settle at the GMPP at STC. The second objective is to measure the oscillation amplitude at the global maximum power point (GMPP) at STC. The third objective is to measure the average DC voltage at a small sampling time for PO MPPT, PSO MPPT, and the hybrid MPPT. The fourth objective is to graphically visualize the PO MPPT, PSO MPPT, and hybrid MPPT waveforms at that small sampling point.

Figure 6.6 depicts the PO MPPT Simulink Model. At STC, the irradiation is set to 1367W/m^2 and the temperature to 28°C. The PV output power is 3.56W, the voltage is 2.655V, and the current is 1.341A. The boost converter load power is 3.044W, the voltage is 4.55V, and the current is 0.6691A.

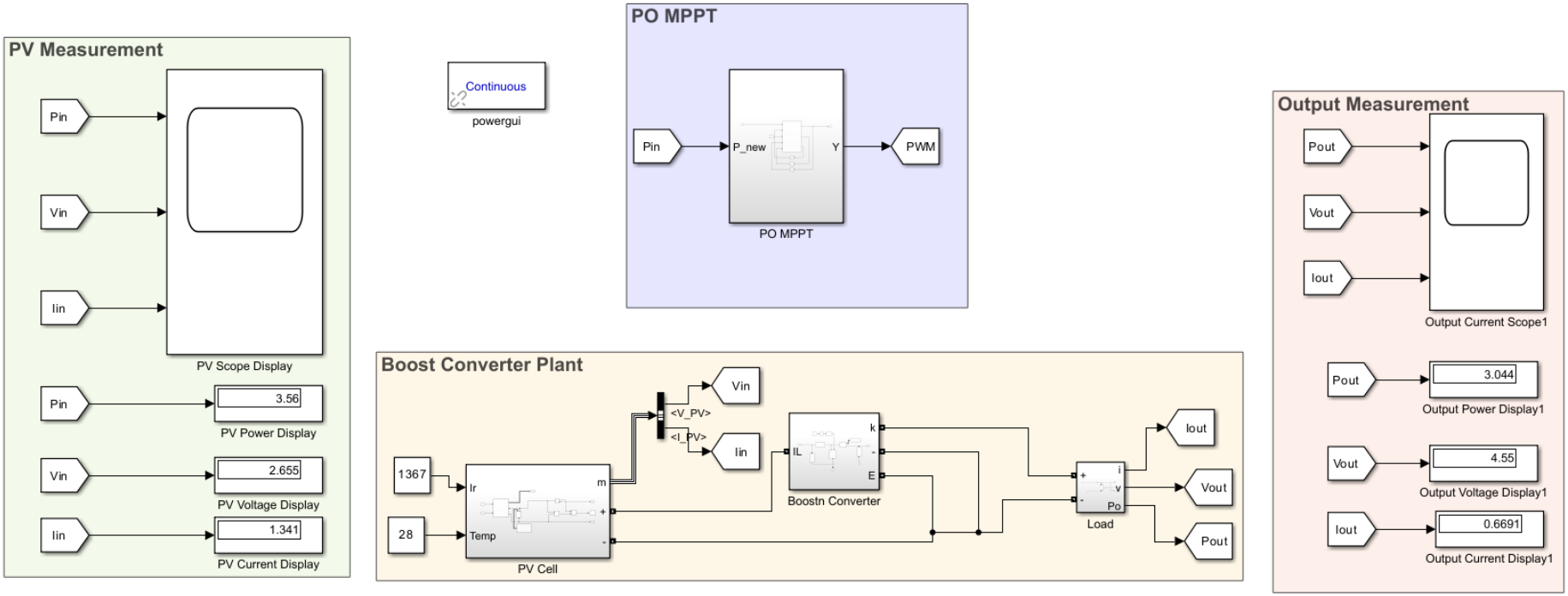

Figure 6. 5: PO MPPT Simulink Model at STC

Figure 6.7 depicts the PO MPPT Simulink Model simulation waveforms for load power, voltage, and current signals. At STC, the irradiation is set to 1367W/m2 and the temperature to 28°C. The PV output power is 3.56W, the voltage is 2.655V, and the current is 1.341A. The boost converter load power is 3.044W, the voltage is 4.55V, and the current is 0.6691A.

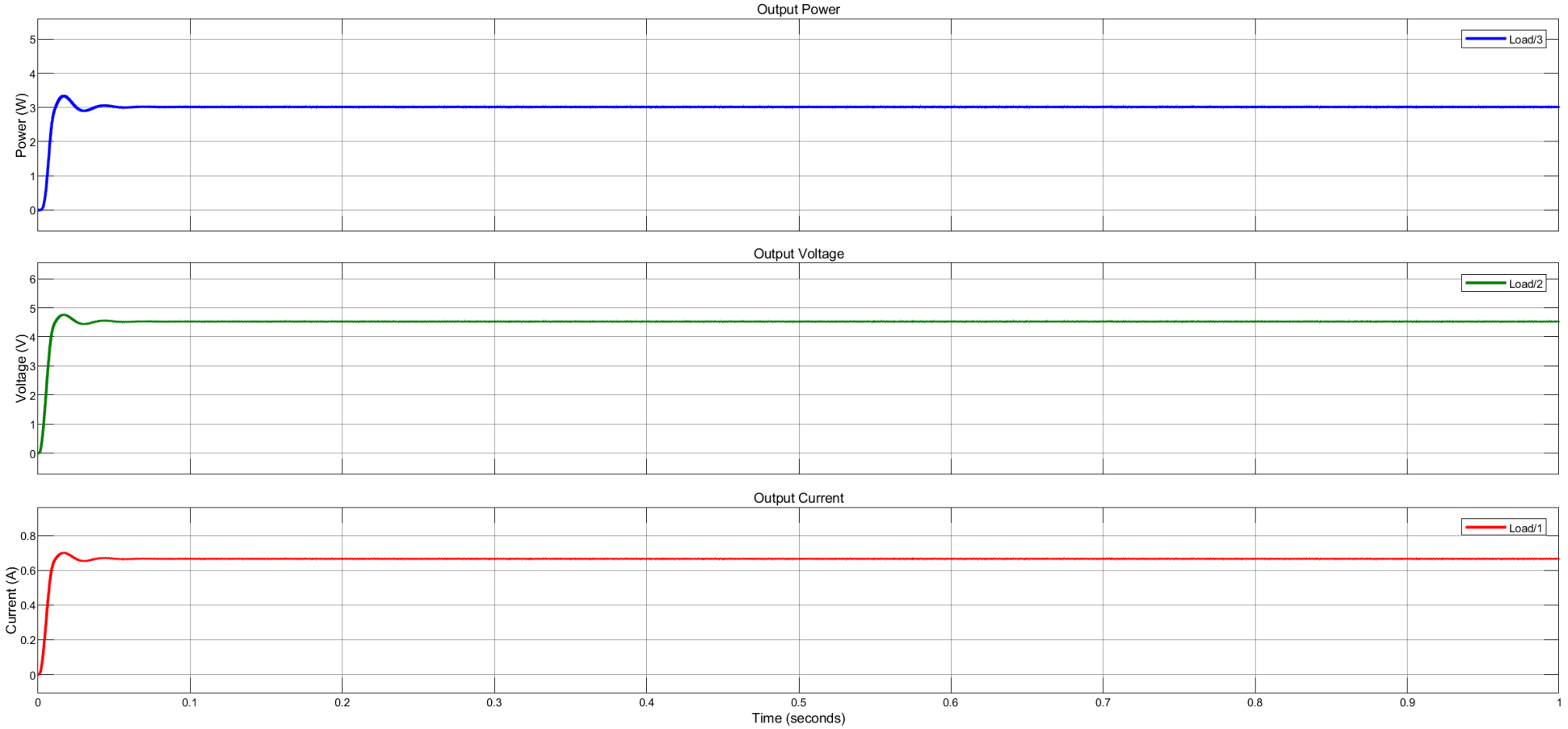

Figure 6. 6: PO MPPT Simulink Model Simulation Waveforms at STC

To measure the settling time of the output power for the PO MPPT at STC, the blue-line graph of Figure 6.7. which represents the output power is enlarged in Figure 6.8. The settling time is 0.05 seconds.

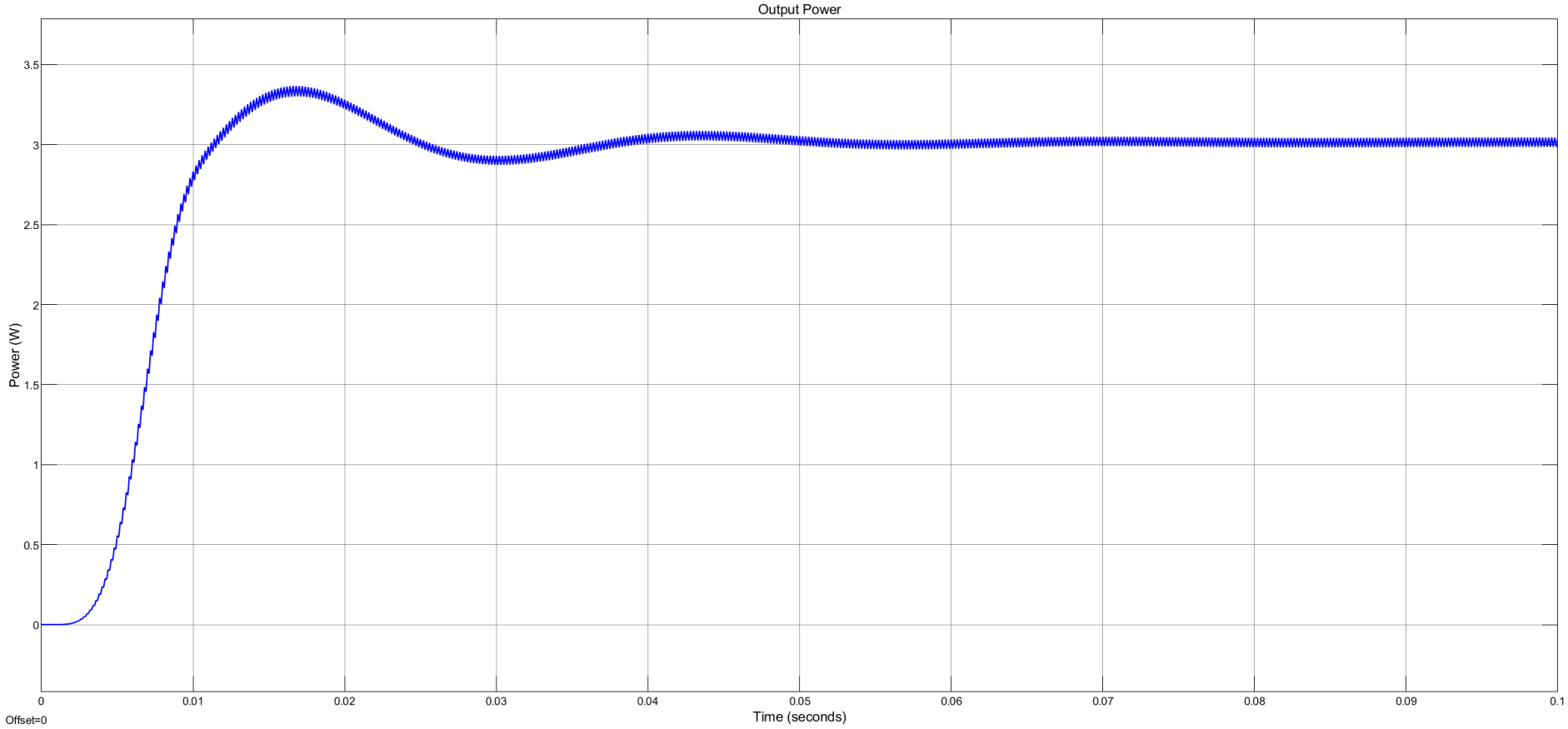

Figure 6. 7: The settling Time of the Boost Converter Load Power

To measure the oscillations at the GMPP at STC, the blue line output power graph of Figure 6.8 is zoomed in between 0.05 seconds and 0.06 seconds, and a sample of pulses at GMPP is taken. The amplitude at GMPP of the sample of pulses is 6.4e-2W.

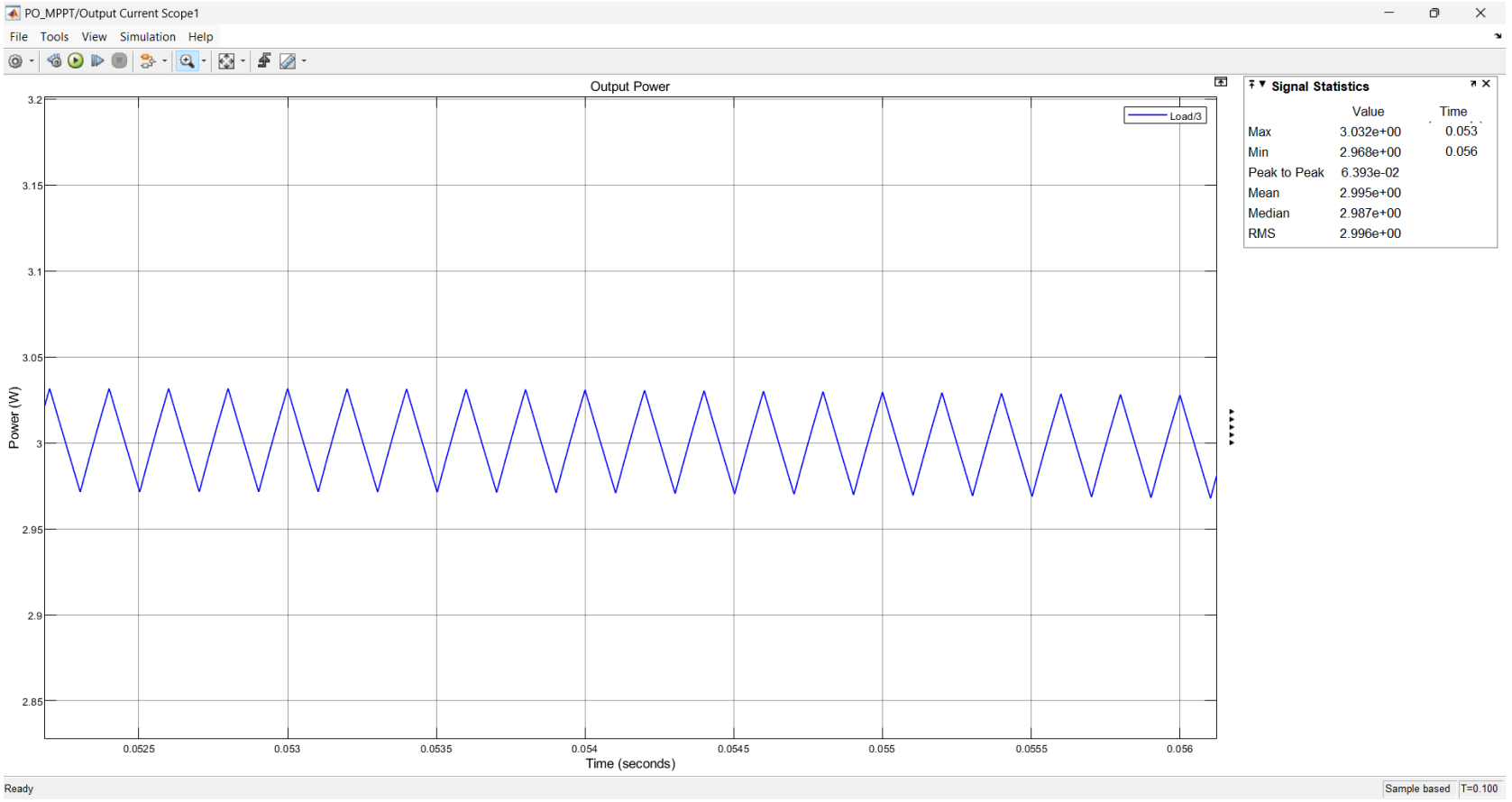

Figure 6. 8: The oscillations at the GMPP at STC

6.4.2. Perturb and Observe MPPT at Varying Testing Conditions

To measure the average DC voltage at a small sampling time for PO MPPT, PSO MPPT, and the hybrid MPPT, the sampling time is set to 0.1s, and the simulation time is 1s. The average DC voltage for PO MPPT is 3.89V in the given simulation time of one second, as seen in the output measurements displayed in Figure 6.10. To design a Simulink dynamic input that simulates varying temperatures between -100°C and +120°C, a random number block and a gain block to scale the random input to your desired temperature range and a summation block are used in MATLAB/Simulink shown in Figure 6.9. The formula that is implemented in Simulink is $\boldsymbol{T = -100 + 220 \times Random\ number.}$

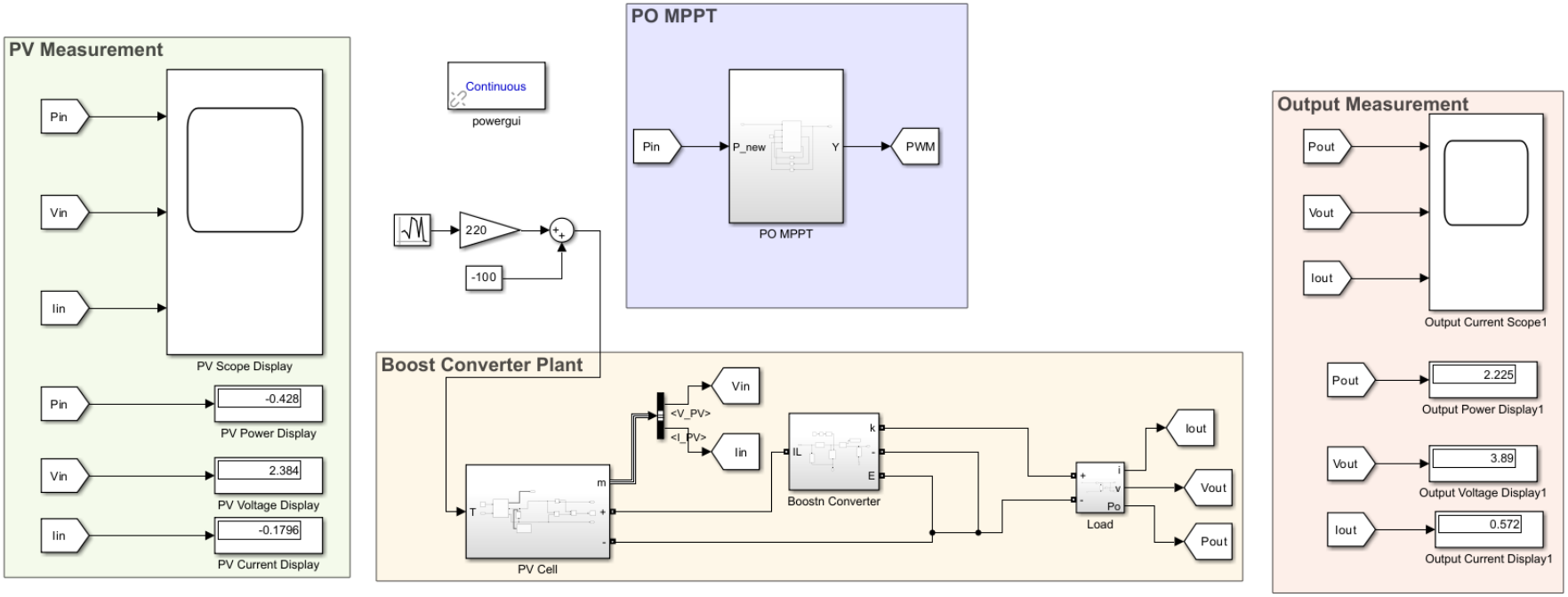

Figure 6. 9: The PO MPPT Average DC Voltage at a Small Sampling Time

The green line graph in Figure 6.10 is the output voltage of the boost converter load. 5V is the target bus voltage, and as the sampling time changes rapidly within the one-second simulation time, the voltage deviates significantly from the targeted voltage. This significant deviation results in an average harvested voltage within the one-second simulation time reducing to 3.89V.

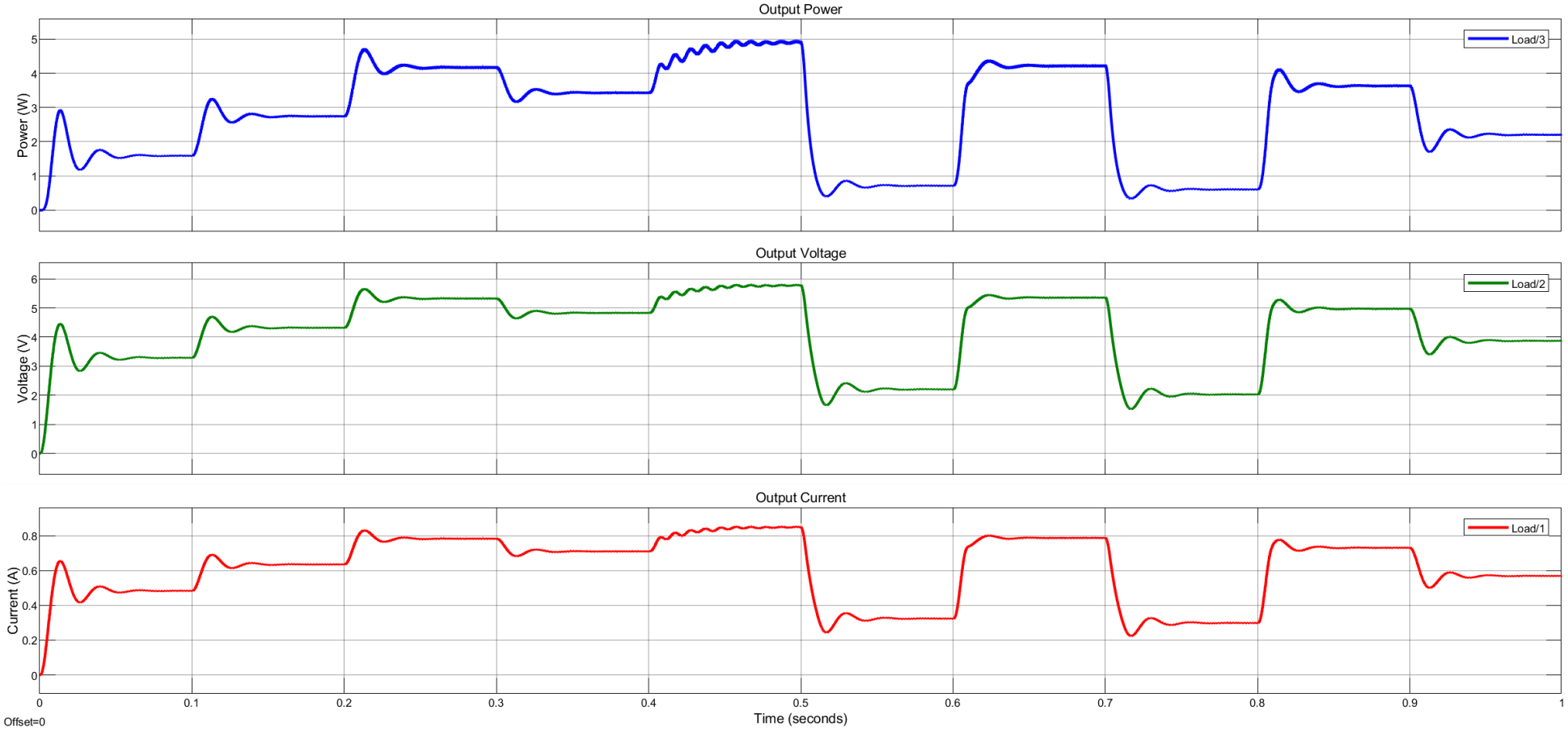

Figure 6. 10: The PO MPPT Output Waveforms at a Small Sampling Time

Figure 6.10 shows the results of the PO MPPT under dynamic temperature conditions implemented in Simulink using the following mathematical formula. $\boldsymbol{T = -100 + 220 \times Random\ number.}$ The gain block is set to 220, representing the maximum space temperature, and the constant block is set to -100, representing the minimum space temperature. The random number block is set to a sampling time of 0.1s to change the temperature randomly every 0.1s. Hence, every 0.1 seconds, the PV temperature will change to a random value within the range of -100 to 220 degrees. The PO MPPT will find the maximum power point at this current temperature. As the temperature of a PV module increases, the open-circuit voltage of the PV module decreases, which typically shifts the MPP to a lower point. Conversely, the open circuit voltage increases as the temperature decreases, shifting the MPP to a higher voltage.

However, the PV module's current output is relatively less sensitive to temperature but may slightly increase with a temperature rise. The PV module's MPP shifts every time the temperature changes (every 0.1 seconds). The P&O algorithm reacts by adjusting the operating duty ratio in small steps. If the power increases with the perturbation, the duty ratio is perturbed further in the same direction. If the power decreases, the algorithm reverses the perturbation direction. There are periods when the algorithm briefly loses track of the MPP, mainly when the temperature changes rapidly. This leads to transient oscillations or overshoots in the power curve as the system recovers and realigns itself with the new MPP. The constant perturbation and adjustment process is evident in the power fluctuations as the system seeks the MPP under the influence of temperature. The results of the PSO MPPT in Figure 6.16 do not show the overshoot after every 0.1 seconds, indicating that the algorithm doesn’t briefly lose the MPP. However, the oscillations around the MPP are pronounced as those of the PO MPPT. The hybrid PO PSO MPPT results in Figure 6.22 show no overshoot after every 0.1 seconds and show reduced oscillations around the MPP.

6.4.3. Particle Swarm Optimisation MPPT at Standard Testing Conditions

The PSO MPPT Simulink model is shown in Figure 6.12, and the PV array measurements are at the far left. The PV output power, voltage, and current are connected to the scope and the display for displaying average DC levels. At the top center is the PSO MPPT MATLAB/Simulink function, which tunes the PWM duty ratio to maximize PV power extraction, and next to it is the 'To Workspace' function, which takes the PV voltage and current from the model to the workspace so that the PSO MATLAB function can use them to calculate power. At the bottom center is the boost converter model, which regulates the load voltage. At the far right are the load measurements, where load power, voltage, and current are connected to the scope and displays.

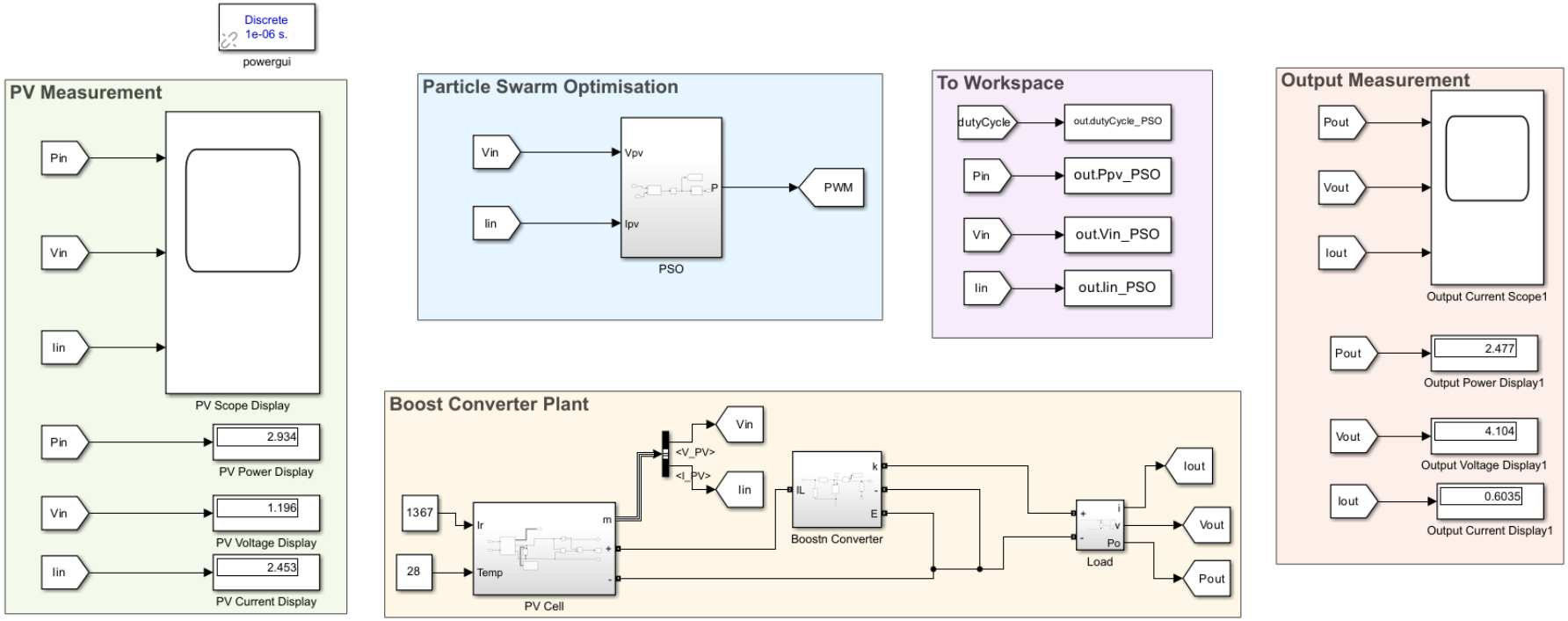

Figure 6. 11: The PSO MPPT Simulink Model at STC

Figure 6.13 depicts the PSO MPPT Simulink Model simulation waveforms for load power, voltage, and current signals. At STC, the irradiation is set to 1367W/m^2 and the temperature to 28°C. The PV output power from Figure 6.12 is 2.934W, the voltage is 1.196V, and the current is 2.453A. The boost converter load power is 2.477W, the voltage is 4.104V, and the current is 0.6035A.

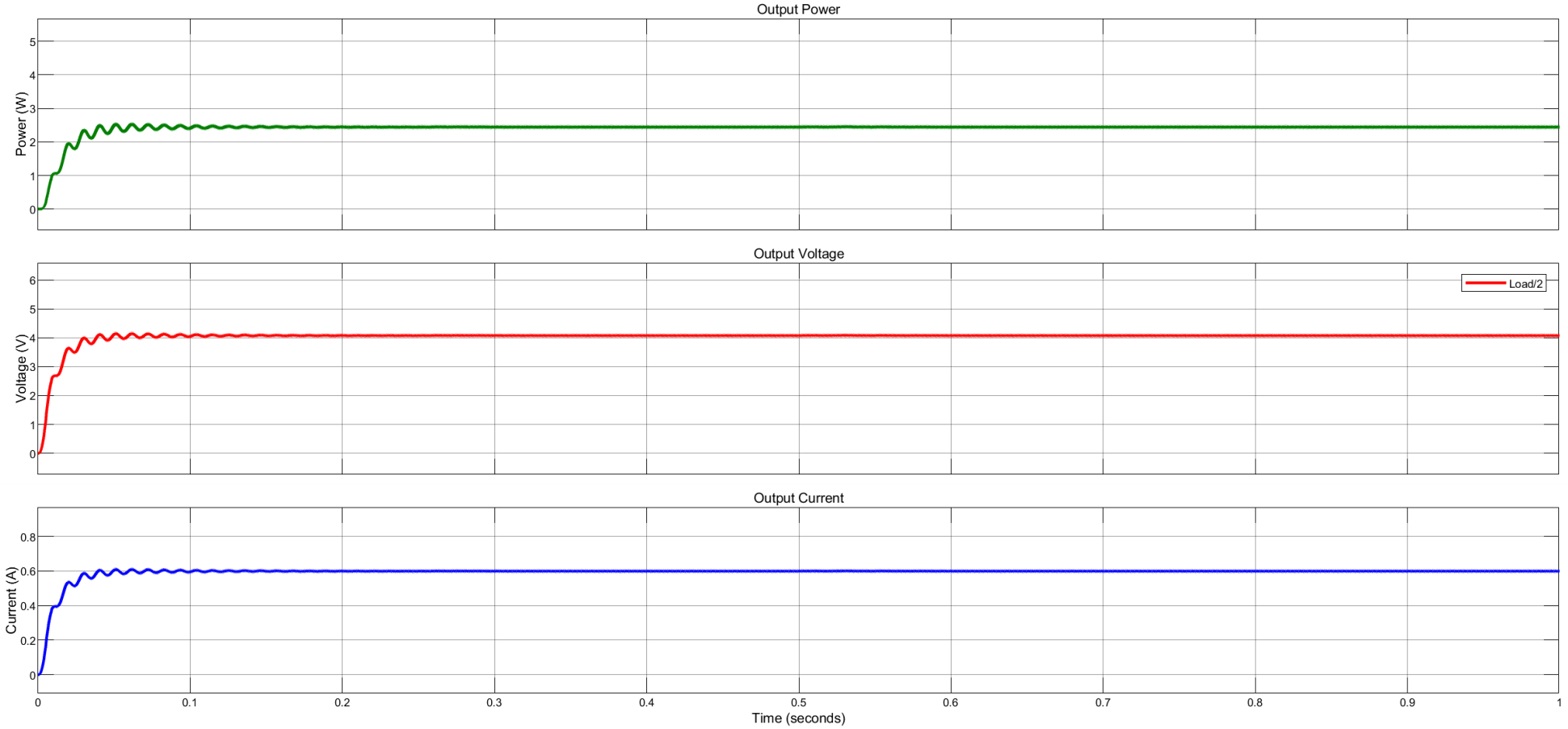

Figure 6. 12: PSO MPPT Simulink Model Simulation Waveforms at STC

To measure the settling time of the output power for the PSO MPPT at STC, the green-line graph of Figure 6.13. which represents the output power of 2.45W is enlarged in Figure 6.14. The settling time is 0.2 seconds.

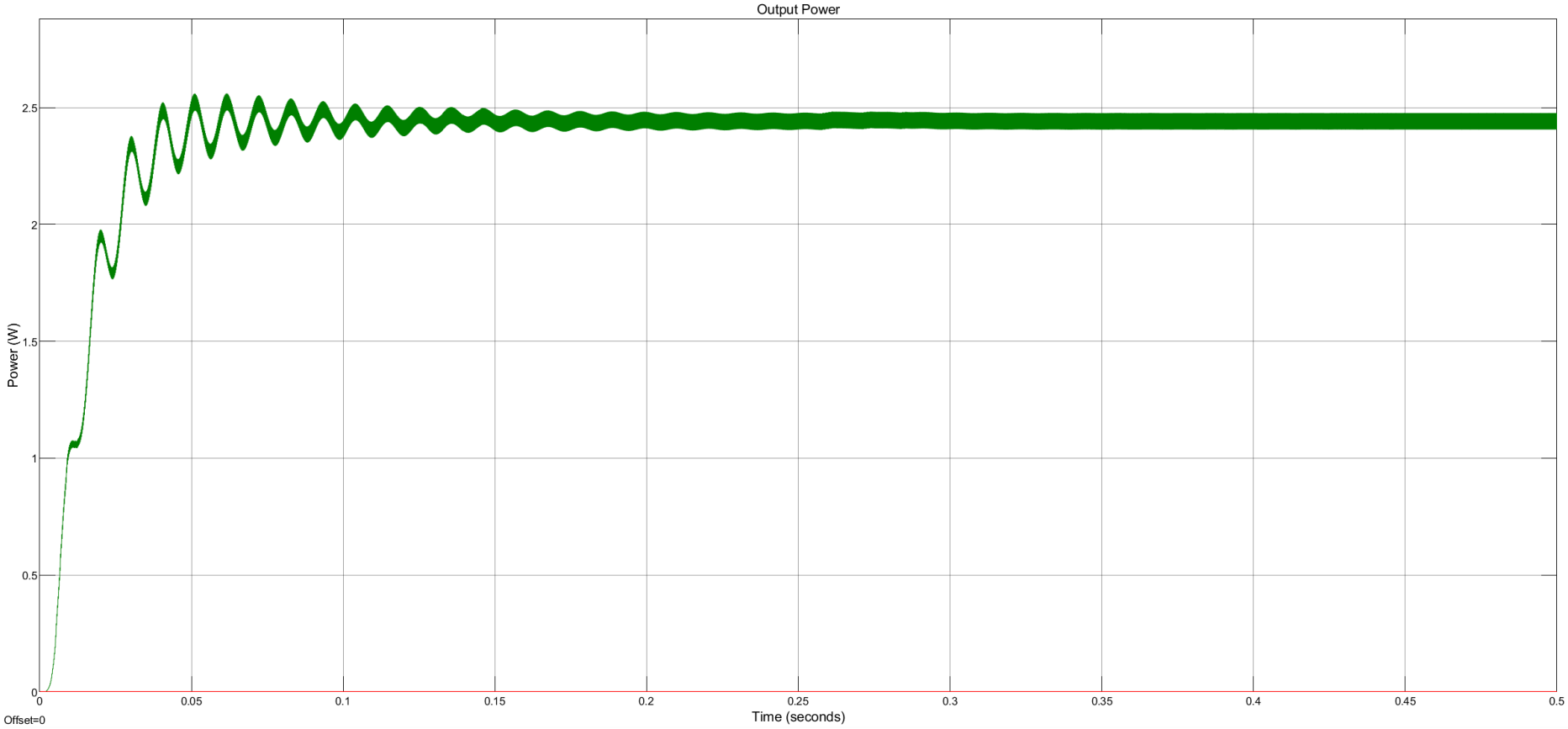

Figure 6. 13: The PSO MPPT settling Time of the Boost Converter Load Power

To measure the oscillations at the GMPP at STC, the green line output power graph of Figure 6.14 is zoomed in between 0.2 seconds and 0.25 seconds, and a sample of pulses at GMPP is taken. The amplitude at GMPP of the sample of pulses is 7.82e-2W peak-to-peak.

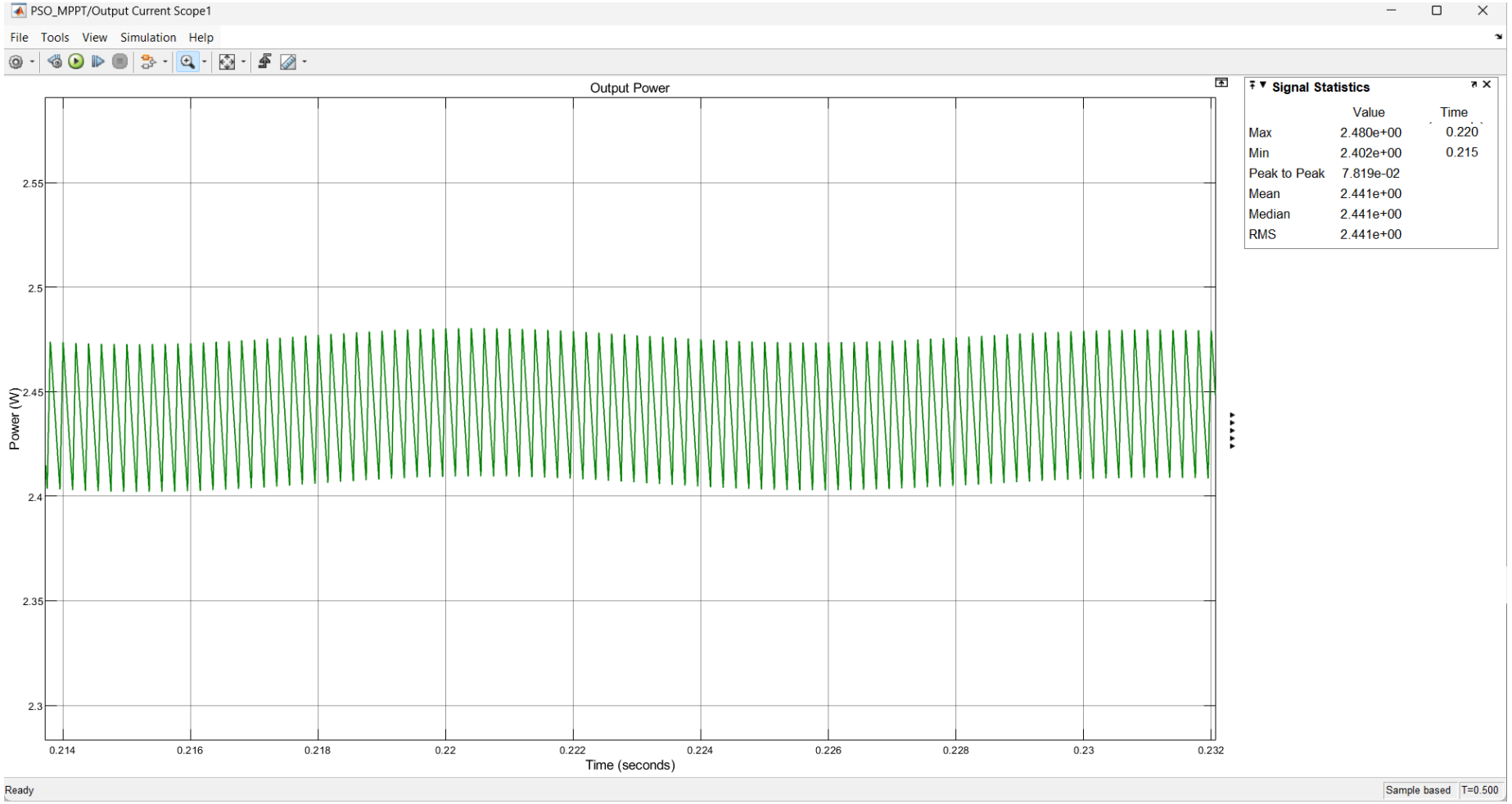

Figure 6. 14: The PSO MPPT oscillations at the GMPP at STC

6.4.4. Particle Swarm Optimisation MPPT at Varying Testing Conditions

The radiation PV input must be kept at 1367W/m2. The temperature PV input must be changed into a dynamic fluctuating input that randomly varies the temperature between -100°C and +120°C. The temperature changes randomly to a value within one second. To measure the average DC voltage at a small sampling time for PSO MPPT and the hybrid MPPT in Figure 6.15 have the sampling time is set to 0.1s, and the simulation time is 1s. The average DC voltage for PSO MPPT is 5.08V in the given simulation time of one second, as seen in the output measurements displayed in Figure 6.16.

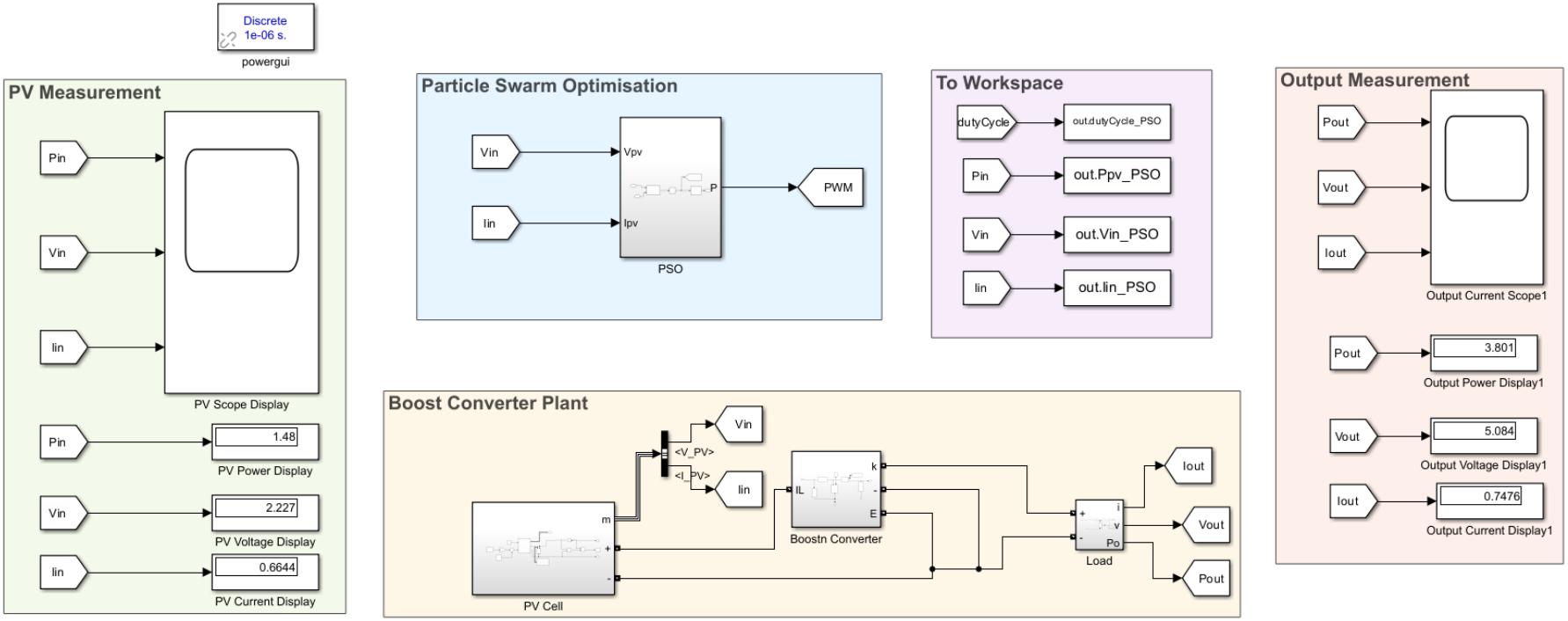

Figure 6. 15: The PSO MPPT Average DC Voltage at a Small Sampling Time

The red line graph in Figure 6.16 is the output voltage of the boost converter load. 5V is the target bus voltage, and as the sampling time changes rapidly within the one-second simulation time, the voltage deviates slightly from the targeted voltage. This slight deviation results in an average harvested voltage within the one-second simulation time, settling at 5.084V. These results are better than the PO MPPT, but the oscillations around the target voltage are substantial and need improvement.

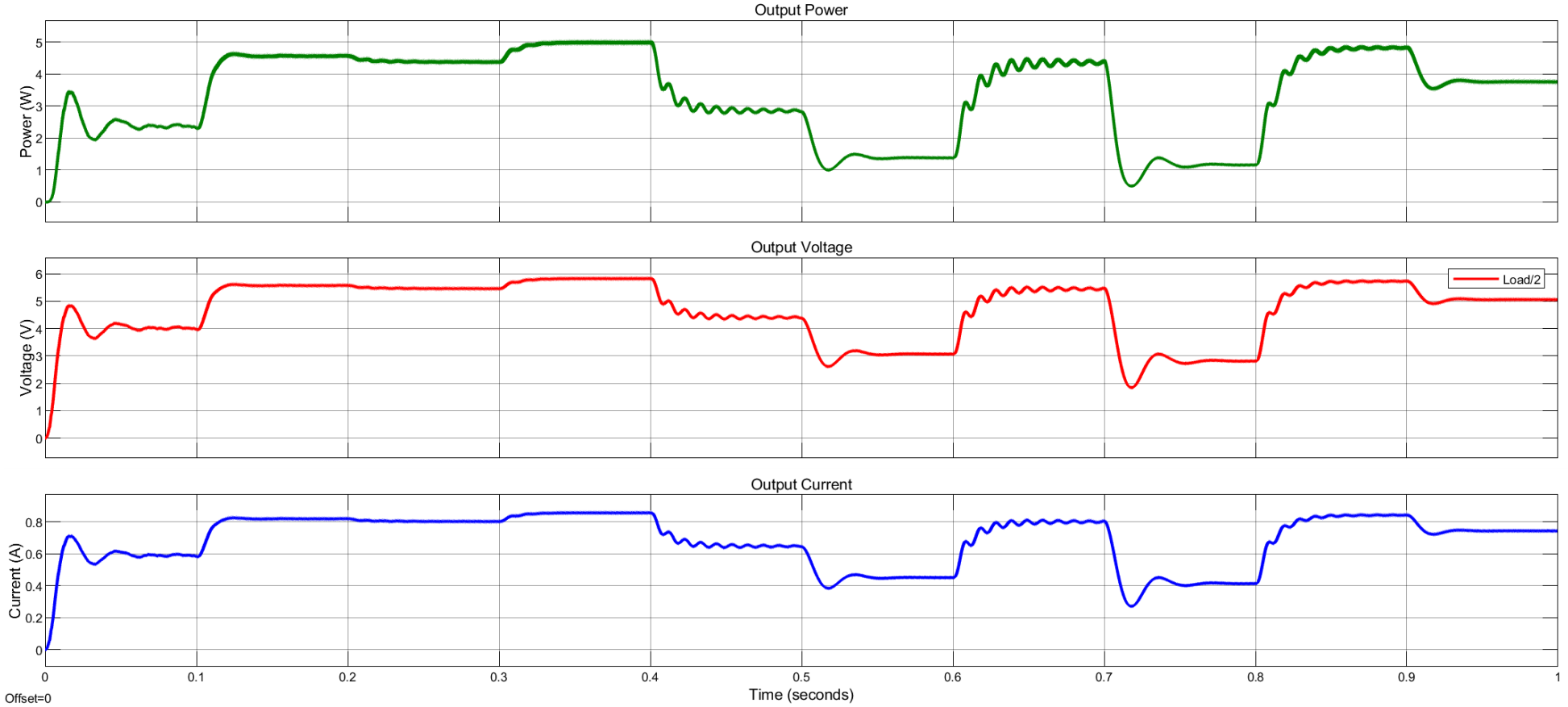

Figure 6. 16: The PSO MPPT Output Waveforms at a Small Sampling Time

6.4.5. Hybrid PO PSO MPPT at Standard Testing Conditions

The hybrid code integrates both the global search capability of PSO and the fine-tuning capability of PO. When the system is close to the optimum (small changes in power), the PO algorithm takes over. Otherwise, the PSO algorithm explores the solution space broadly. The decision to switch between the PO function and the PSO algorithm is based on the magnitude of the change in power output. The hybrid approach mitigates the problem of poor tracking of the GMPP under dynamic environments.

6.4.5.1. Hybrid PO PSO MPPT Function Steps

Step 1: Persistent variables, Particle Initialization, and Delay.

Use the PSO initialization as provided before in section 6.3.2. Initialize variables to track the state of the PO method, using persistent variables to store values between function calls to maintain the algorithm state. Introduce a delay to allow the system to stabilize.

Step 2: Power Calculation and Error Calculation

Use the PSO approach to explore and calculate the power at each duty cycle. Track the previous and current power values.

P = Vpv * Ipv

where:

- Vpv is the photovoltaic (PV) panel voltage
- Ipv is the PV panel current

error = abs(Vout - target_voltage)

where:

- Vout is the output voltage of the boost converter
- target_voltage is the desired output voltage

Step 3: Fitness function and Perturb and Observe

Compute a fitness value based on the inverse of the error.

fitness_value = 1 / (error + epsilon)

perturb and observe function:

if P_new > P_old: Y = Yin + c else: Y = Yin - c

Step 4: Hybrid Decision

If the system detects small changes in power (indicating a steady state), switch to the PO algorithm for finer adjustments. If larger variations in power are detected (indicating potential suboptimal performance), revert to PSO to explore a broader range of duty cycles.

Step 4: Velocity and Duty Cycle Update

The velocity of each particle is updated using the PSO velocity update formula:

v_final = w * v + c1 * rand() * (pbest - d) + c2 * rand() * (gbest - d)

where:

- v_final: Updated velocity
- w: Inertia weight
- v: Current velocity
- c1, c2: Cognitive and social parameters
- pbest: Personal best position
- d: Current duty cycle
- gbest: Global best position

The duty cycle is updated based on the new velocity, ensuring it remains within the bounds [0, 1].

d_final = max(0, min(1, d + v_final))

where:

- d_final: Updated duty cycle
- d: Current duty cycle
- v_final: Updated velocity

Step 5: Return Updated Duty Cycle

Return the updated duty cycle D based on the hybrid logic.

Figure 6.17 shows the Hybrid PO PSO MPPT Simulink model; at the far left are the PV array measurements. The PV output power, voltage, and current are connected to the scope and the display for displaying average DC levels. At the top center is the hybrid PO PSO MPPT MATLAB/Simulink function, which tunes the PWM duty ratio to maximize PV power extraction, and next to it is the ‘To Workspace’ function, which takes the PV voltage and current from the model to the workspace so that the hybrid PO PSO MATLAB function can use them to calculate power. At the bottom center is the boost converter model, which regulates the load voltage. At the far right are the load measurements, where load power, voltage, and current are connected to the scope and displays.

Figure 6.17 depicts the hybrid PO PSO MPPT Simulink Model. At STC, the irradiation is set to 1367W/m^2, and the temperature is set to 28°C. The PV output power is 2.858W, the voltage is 1.165V, and the current is 2.454A. The Boost converter output average power is 2.505W, the output voltage is 4.127V, and the output current is 0.6069A.

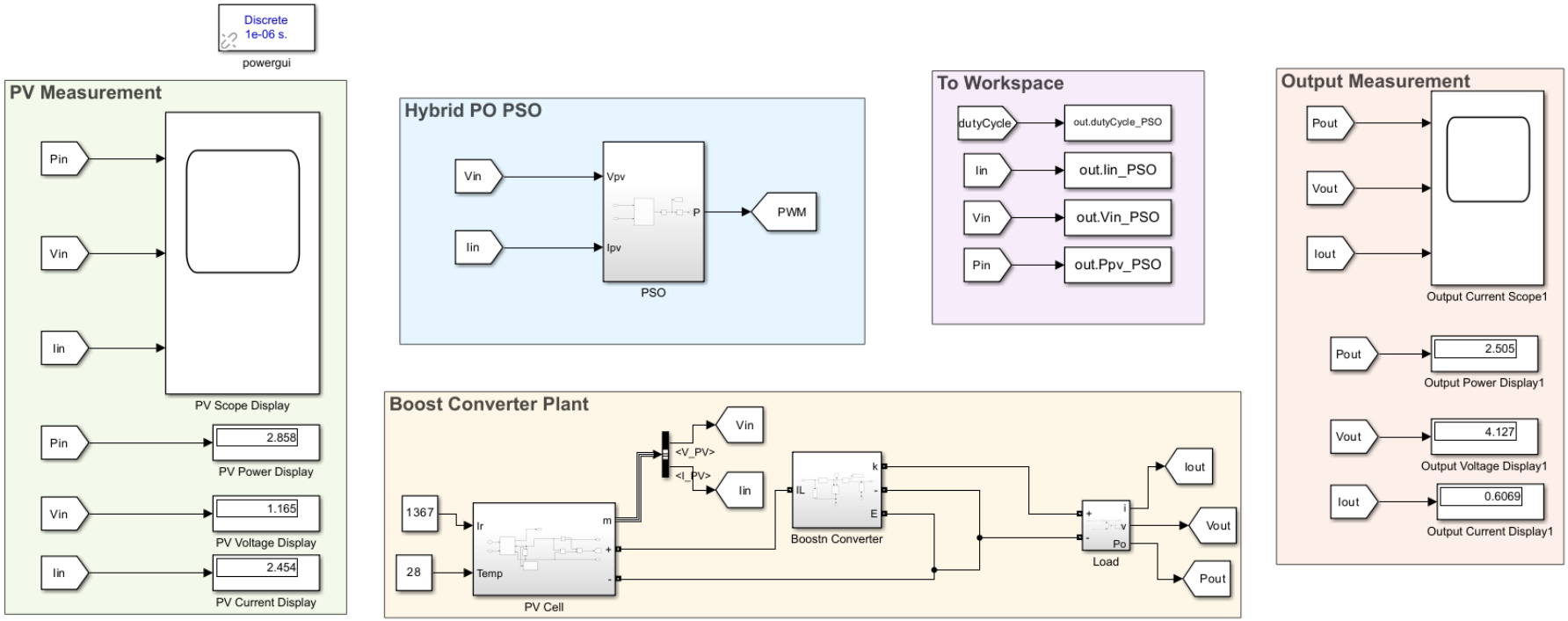

Figure 6. 17: The Hybrid PO PSO MPPT Simulink Model at STC

Figure 6.19 depicts the Hybrid PO PSO MPPT Simulink Model simulation waveforms for load power, voltage, and current signals. At STC, the irradiation is set to 1367W/m^2 and the temperature to 28°C.

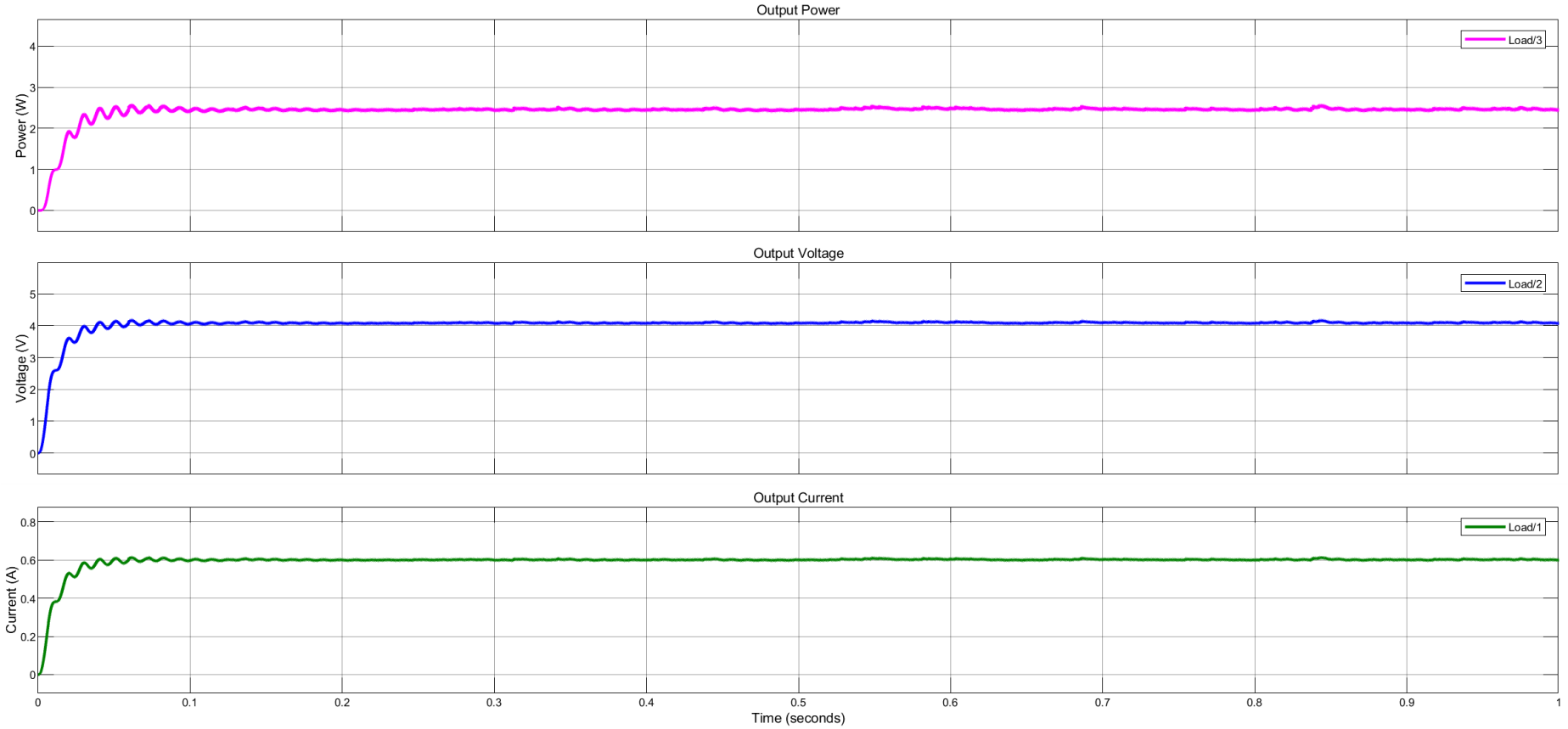

Figure 6. 18: The Hybrid PO PSO MPPT Simulink Model at STC

To measure the settling time of the output power for the hybrid PO PSO MPPT at STC, the pink-line graph of Figure 6.18. which represents the output power is enlarged in Figure 6.20. The settling time is 0.2 seconds.

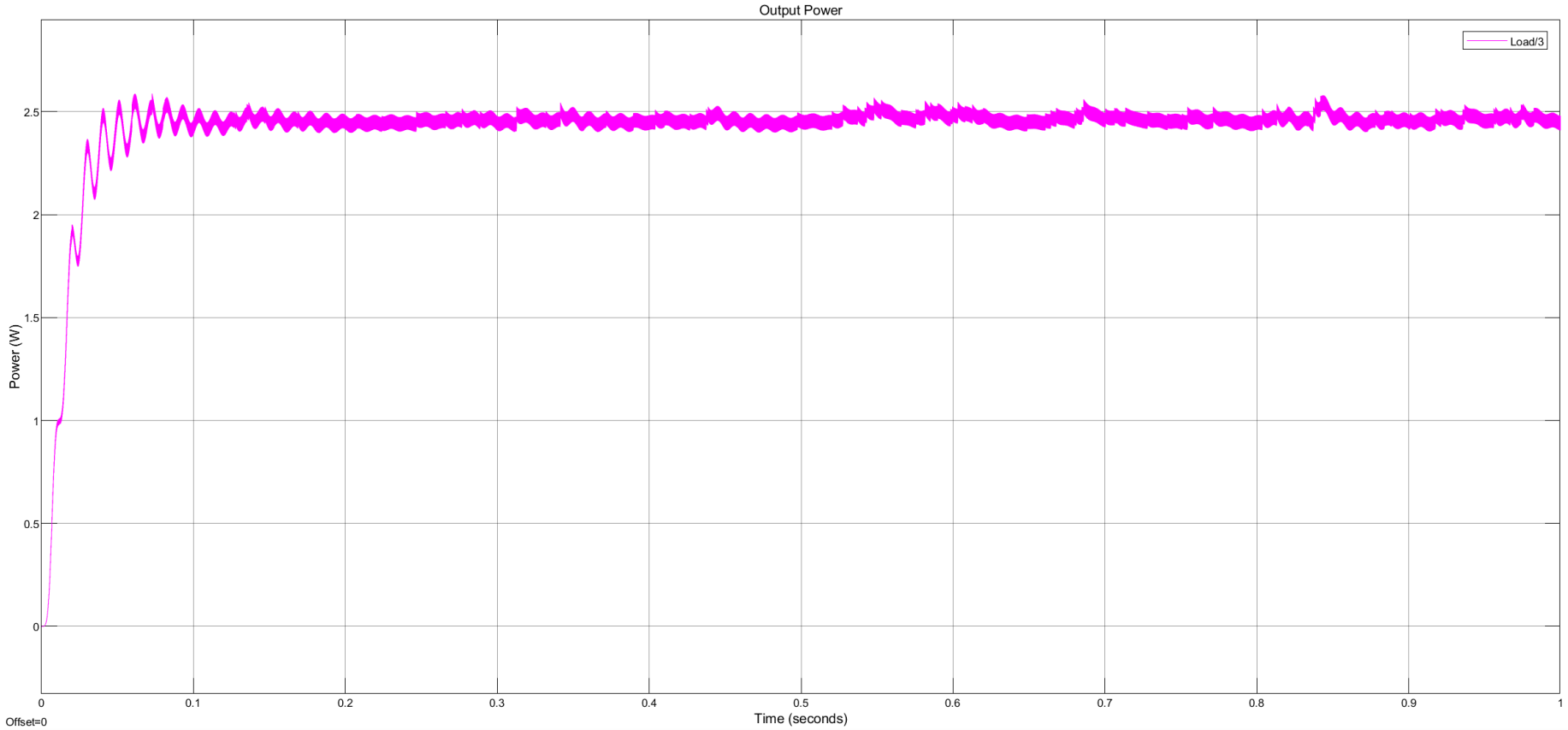

Figure 6. 19: The settling Time of the Boost Converter Load Power

To measure the oscillations at the GMPP at STC, the green line output power graph of Figure 6.20 is zoomed in between 0.2 seconds and 0.25 seconds, and a sample of pulses at GMPP is taken. The amplitude at GMPP of the sample of pulses is 1.022e-1W peak-to-peak.

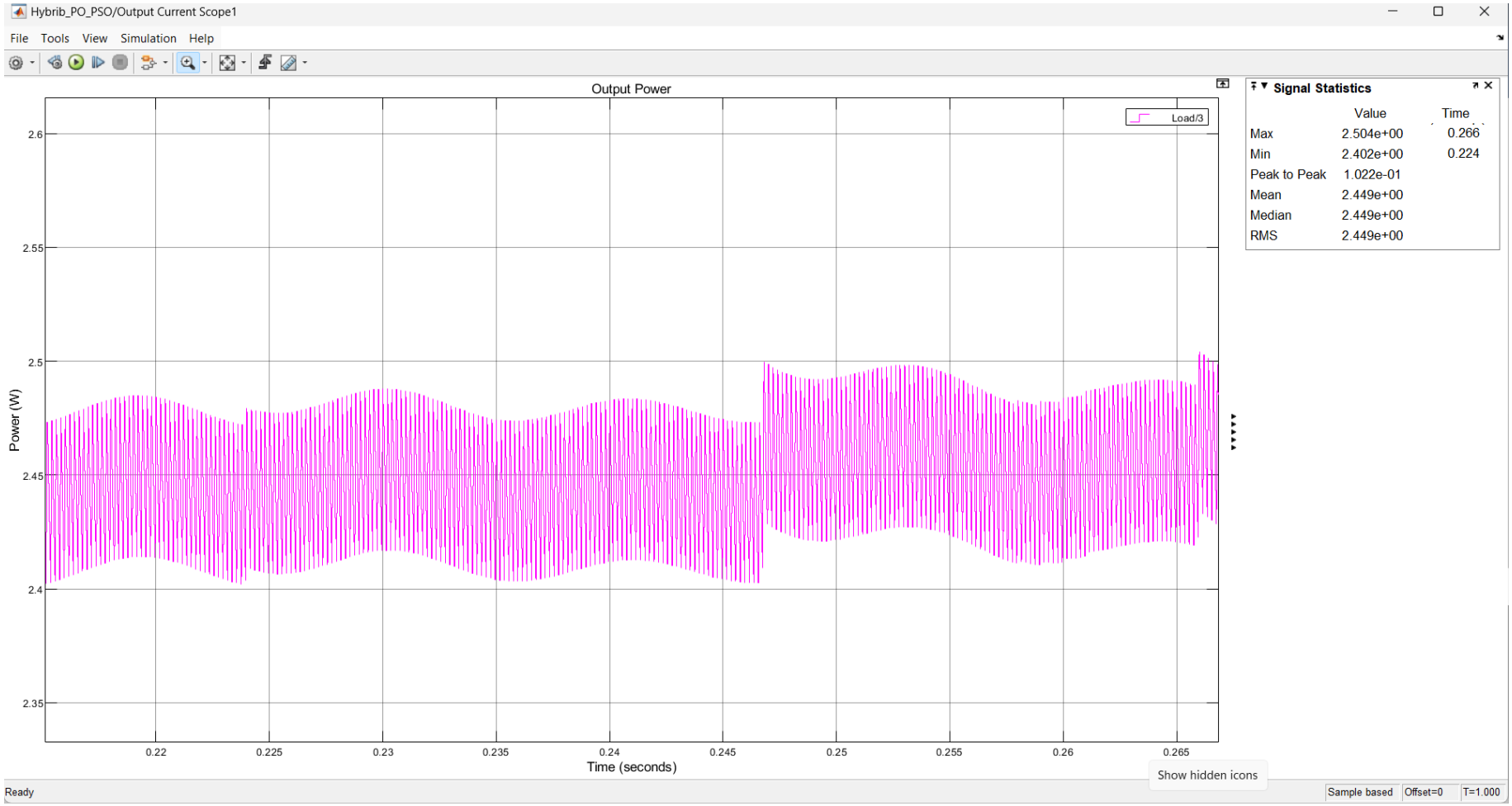

Figure 6. 20: The oscillations at the GMPP at STC

6.4.6. Hybrid PO PSO MPPT at Varying Testing Conditions

The radiation PV input must be kept at 1367W/m^2. The temperature PV input must be changed into a dynamic fluctuating input that randomly varies the temperature between -100°C and +120°C. The temperature changes randomly to a value within one second. To measure the average DC voltage at a small sampling time for Hybrid PO PSO MPPT and the hybrid MPPT, the sampling time is set to 0.1s, and the simulation time is 1s. The average DC voltage for Hybrid PSO MPPT is 5.242V in the given simulation time of one second, as seen in the output measurements displayed in Figure 6.22.

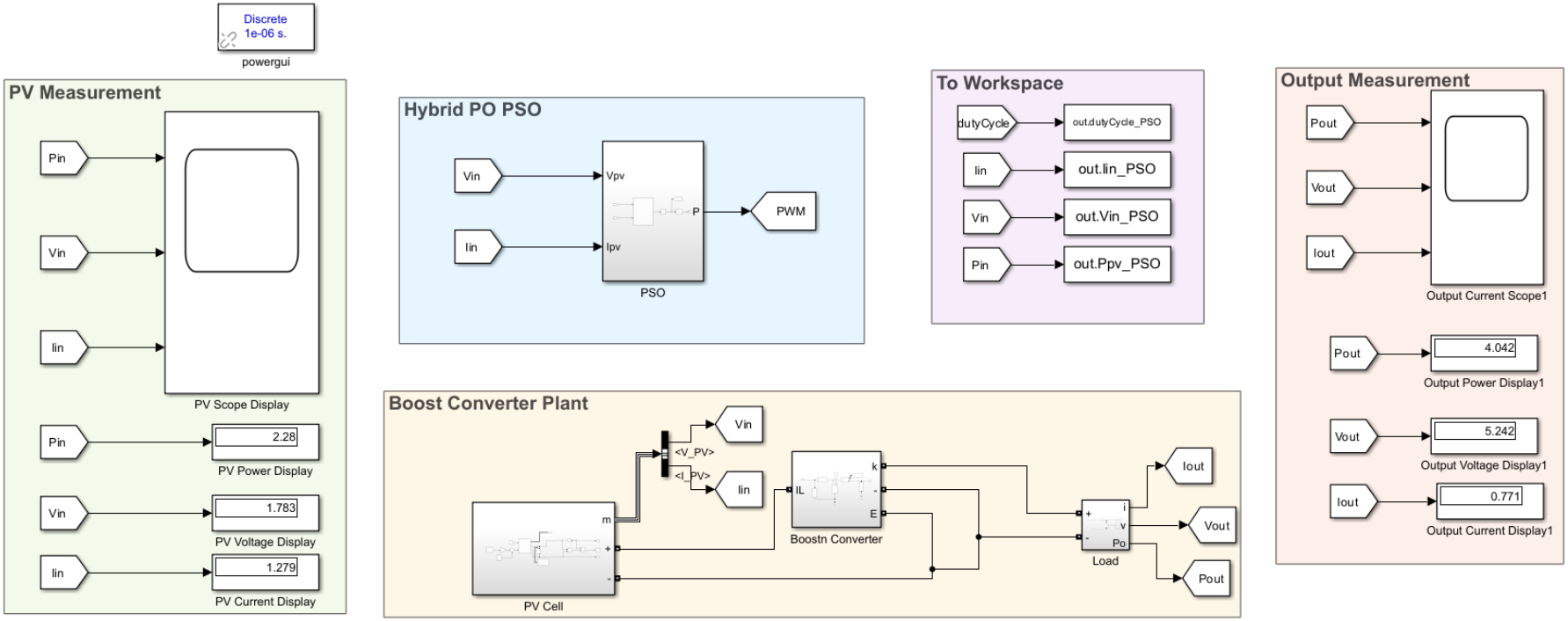

Figure 6. 21: The Hybrid PO PSO MPPT Average DC Voltage at a Small Sampling

The blue line graph in Figure 6.22 is the output voltage of the boost converter load. 5V is the target bus voltage, and as the sampling time changes rapidly within the one-second simulation time, the voltage deviates slightly from the targeted voltage. This slight deviation results in an average harvested voltage within the one-second simulation time, settling at 5.242V. These results are better than the PO MPPT and the PSO MPPT. The oscillations around the target voltage are reduced.

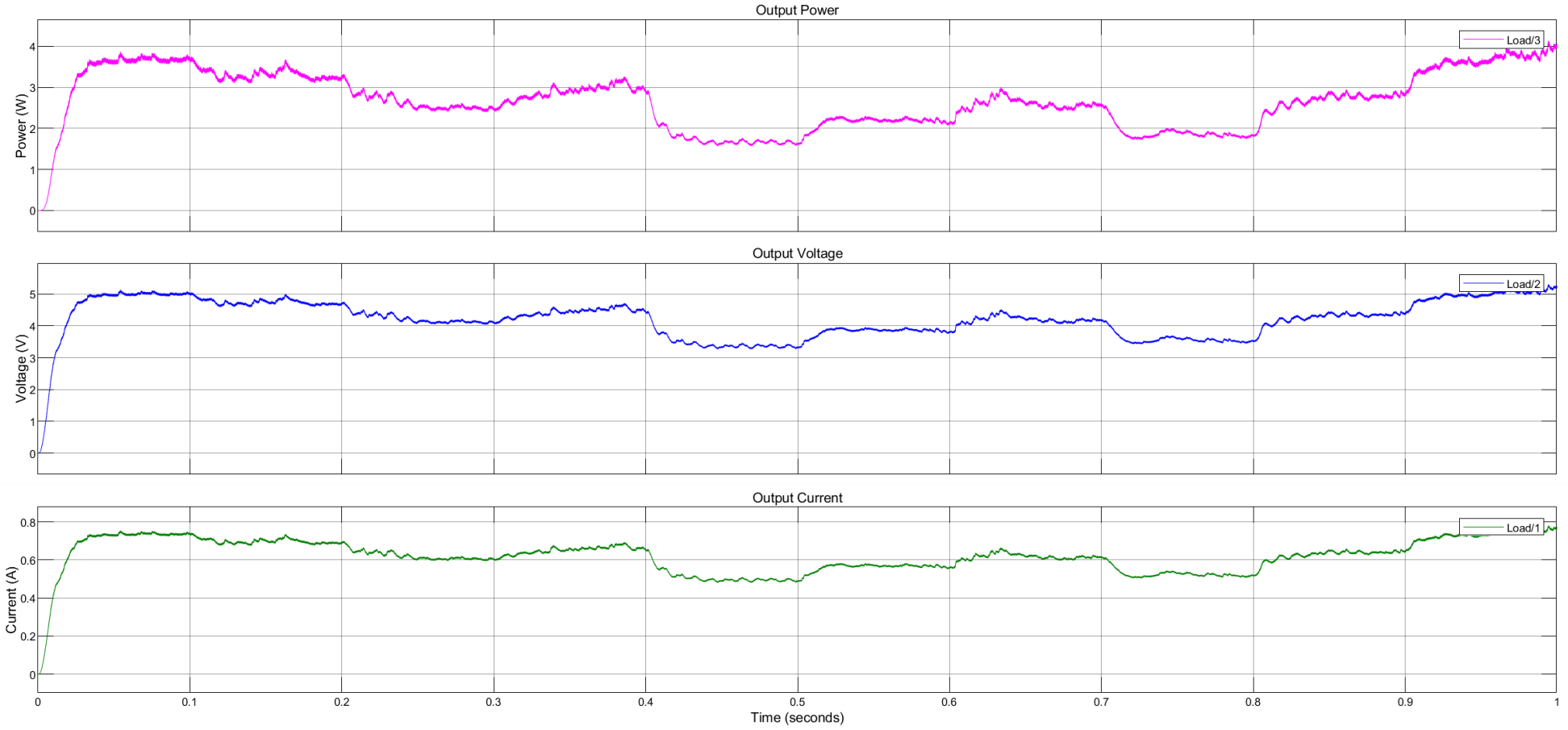

Figure 6. 22: The Hybrid PO PSO MPPT Output Waveforms at a Small Sampling Time

The temperature of the PV input must be kept at 28°C. The radiation PV input must be changed into a dynamic fluctuating input that randomly varies the radiation between 1322W/m^2 and 1414W/m^2. The radiation changes randomly to a value within the specified range every one second. Since the radiation range is not comprehensive and 1367W/m^2 is in between the range, varying radiation simulations will not be simulated in this Thesis. Table 6.2 summarises an output comparison between PO MPPT, PSO MPPT, and the hybrid PO PSO MPPT at STC and varying temperature conditions.

Table 6. 1: Output comparison between PO, PSO & PO PSO MPPTs

At standard Testing Conditions (irradiation = 1367W and Temp = 28°C)				
Outputs	PO MPPT	PSO MPPT	PO PSO MPPT	% Improvement (Between PO & Hybrid PO PSO)
Power	3.044W	2.477W	2.505W	121.52%
Voltage	4.55V	4.104V	4.127V	110.25%
Current	0.6691A	0.6035A	0.6069A	110.25%
At varying Temperature Conditions (Irradiation = 1367W/m^2)				
Outputs	PO MPPT	PSO MPPT	PO PSO MPPT	
Power	2.225W	3.801W	4.042W	55.05%
Voltage	3.89V	5.084V	5.242V	74.21%
Current	0.572A	0.7476A	0.771A	74.19%

6.5. The Hybrid PO PSO MPPT Model benchmark

The Hybrid PO PSO MPPT is the best-performing MPPT function compared to PO MPPT and PSO MPPT under temperature-varying conditions, as seen in Table 6.2, since it uses dual search capability. It starts by using the PSO MPPT function to search a vast solution space, and when it is close to the global maximum power point (GMPP), it switches to the actual seeking PO MPPT function. It smoothens the oscillations at the GMPP and yields the highest power output under temperature-varying conditions.

The graph in Figure 6. 23 shows the performance of the PV system at variable loads and variable temperatures using the six MPPT methods. The six MPPTs in this study are the perturb and observe method (P&O), incremental conductance method (INC), fuzzy logic controller method (FLC), neural network (NN) model, and adaptive neuro-fuzzy inference system method (ANFIS) with the modern approach of the hybrid method (neural network + P&O) for PV systems. The maximum power of the panel is 250W/m^2.

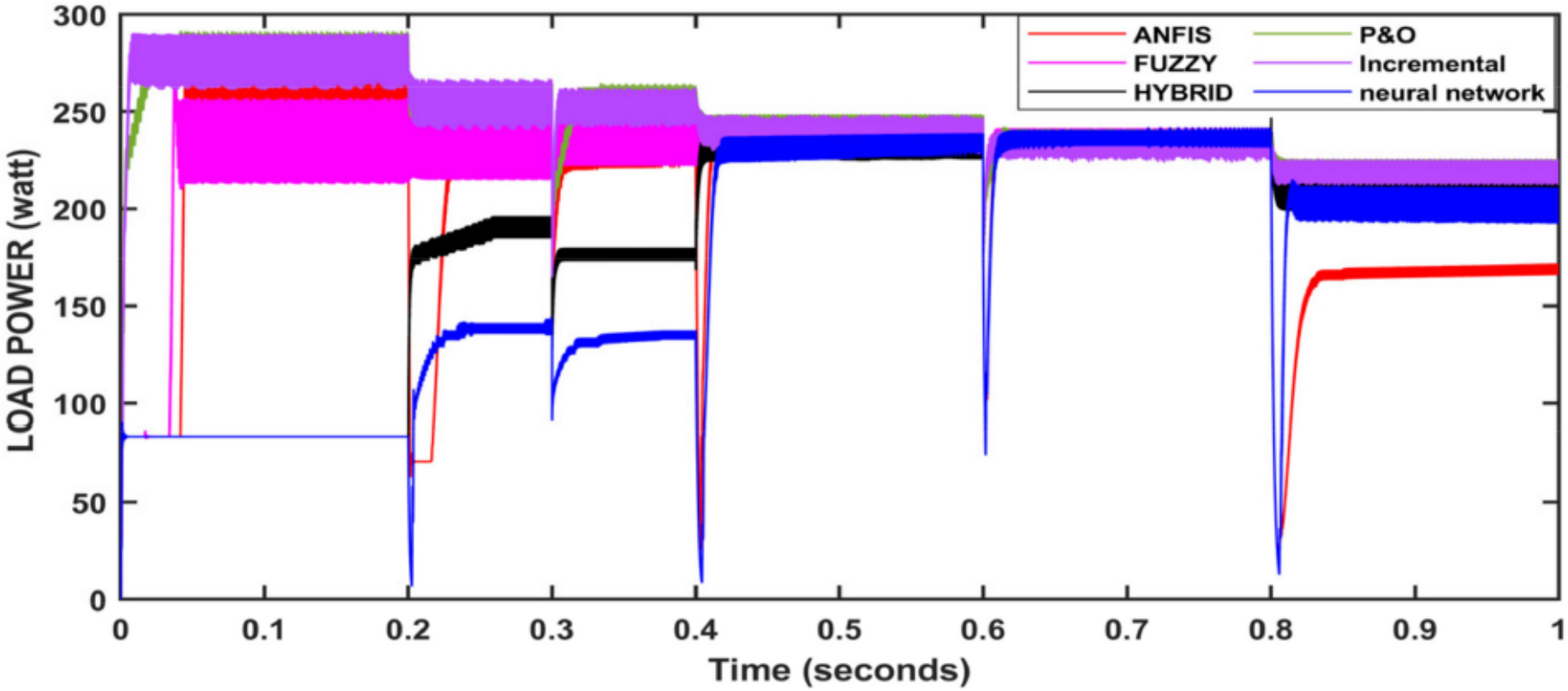

Figure 6. 23: The PO MPPT Benchmark

(Adapted from Devarakonda et. al., 2022)

The results of Figure 6.23 show that at the starting conditions, the output power is more than the panel's maximum output power, and incremental has reached the maximum point first, followed by P&O, ANFIS, and fuzzy. The P&O and incremental algorithms were closer in the initial time, but at a few points, they overlapped. The neural network and hybrid algorithms took some time to track the maximum power point, although up to 0.4 s, these two algorithms' outputs were lower than those of other algorithms. After the load disturbance at 0.3 s, the incremental gained MPP faster but was overtaken by P&O at 0.316 s, followed by fuzzy and ANFIS. After the disturbance at 0.6 s, the fuzzy gained first, closely followed by incremental and hybrid algorithms, and after 0.61 s, all algorithms performed in proximity where P&O, neural network hybrid, and ANFIS were leading.

After 0.8 s disturbance, we observe that P&O, incremental, and fuzzy logic have overlapped in many instances, producing max output, followed by the hybrid algorithm. The neural network has lagged behind all four algorithms, and ANFIS has lagged behind all the algorithms, making the most negligible output. The results of all techniques used in this paper are compared, and examining the obtained results presented in the paper, almost all of the techniques tracked MPP with sufficient accuracy. P&O has a straightforward implementation, but the system response oscillates across the MPP (ringing around) in steady-state operation, resulting in power waste. Based on the given varying parameters, the controllers performed well. The hybrid model has maintained a stable point compared to others, as other controllers suffered from ringing around the MPP, transient disturbances, and a slower settling time than the hybrid model. **(Devarakonda et al., 2022)**

The graphs in Figure 6.24 compare the PO MPPT response with a proposed Look Up Table (LUT) MPPT-based system. Figure 6.24 (a). depicts the voltage fluctuation applied to the converter to evaluate the PO MPPT tracking. PO MPPT duty cycle is shown in Figure 6.24 (b). The controller monitors variations in the input(s), and the duty cycle is adjusted correspondingly to attain the MPP. The proposed Look Up Table (LUT) MPPT-based system was analyzed in a laboratory setting, and findings were achieved. Figure 6.24 compares the PO MPPT response with a proposed Look Up Table (LUT) MPPT-based system. Figure 6.24 (a). depicts the voltage fluctuation applied to the converter to evaluate the PO MPPT tracking. PO MPPT duty cycle is shown in Figure 6.24 (b). The controller monitors variations in the input(s), and the duty cycle is adjusted correspondingly to attain the MPP. The proposed Look Up Table (LUT) MPPT-based system was analyzed in a laboratory setting, and findings were achieved.

The graphs in Figure 6.24 compare the PO MPPT response with a proposed Look Up Table (LUT) MPPT-based system.

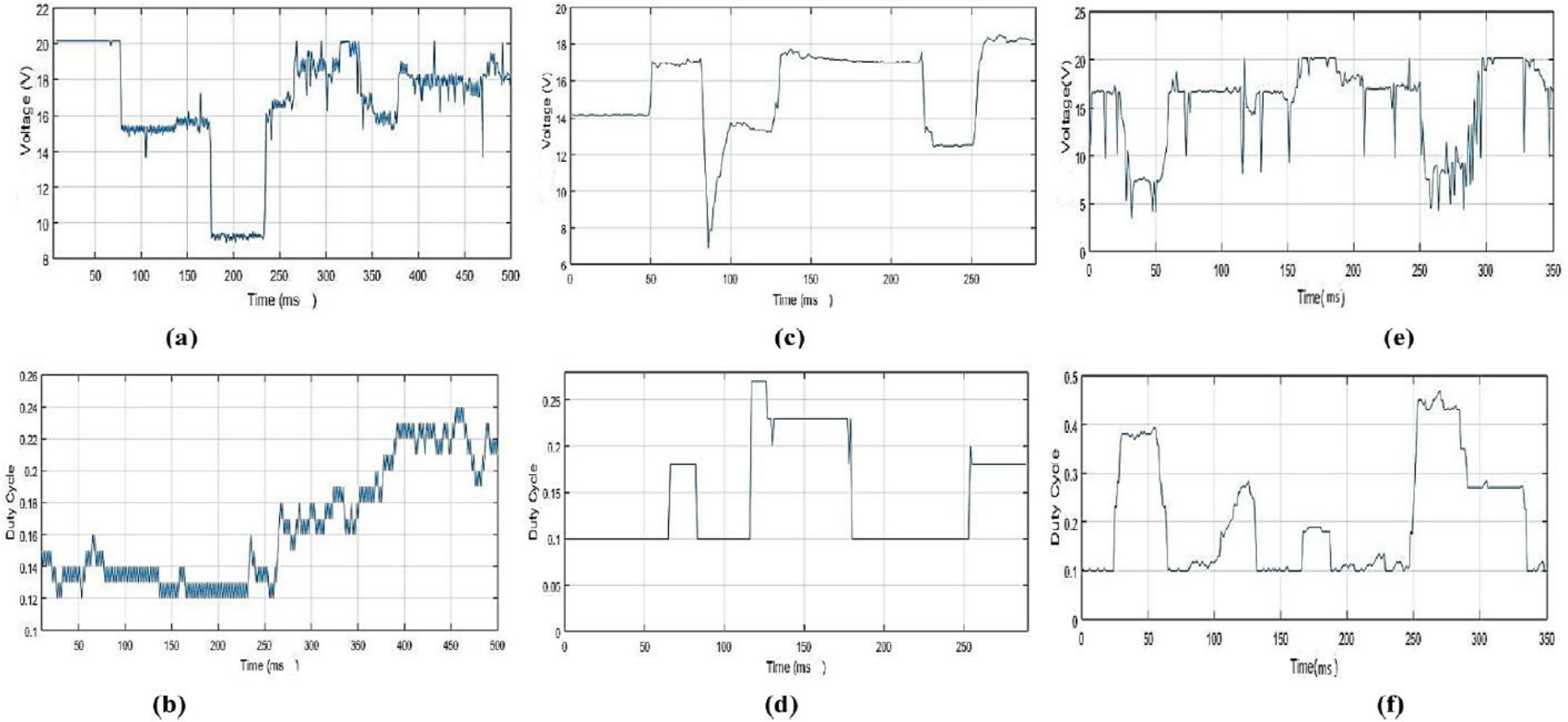

Figure 6. 24: The PO MPPT

(Adapted from Sulthan et al., 2022)

Figure 24 (c) shows the input voltage for the converter using LUT MPPT. Figure 24(d) indicates that LUT MPPT had a fixed duty cycle and responded faster to input variations than PO MPPT. Figure 24 (e) shows the voltage delivered to the PV converter using a suggested two-stage MPP tracking controller. When the controller detects significant changes, the LUT instantly gives the duty cycle information. The P&O algorithm monitors and adjusts the duty cycle to achieve the MPP. Figure 24 (f) depicts the duty cycle response of the proposed MPP tracking controller. This approach is also a hybrid MPPT that combines PO and LUTs.

6.6. Conclusion

Finally, this chapter demonstrated the implementation and effectiveness of a hybrid Perturb and Observe (PO) and Particle Swarm Optimisation (PSO) Maximum Power Point Tracking (MPPT) model explicitly designed for CubeSat power systems. Combining PSO's global search capacity with PO's fine-tuning characteristics, the hybrid strategy successfully overcomes each method's limitations when utilized separately. Specifically, the hybrid model outperformed the independent PO and PSO techniques under normal and dynamically variable space weather conditions, achieving faster convergence to the global maximum power point (GMPP), minimizing oscillations, and producing more power.

This chapter's comparison research discovered that, under changing temperature settings, the hybrid PO-PSO MPPT model outperformed the PO and PSO models alone regarding output power, voltage, and current. These improvements make the hybrid technique especially advantageous for CubeSat missions, where power efficiency is essential due to the scarcity of solar energy in Low Earth Orbit (LEO) conditions. The findings support the hybrid PO-PSO MPPT model as a reliable and efficient solution for CubeSat power systems, ensuring optimal energy harvesting under various space environmental situations.

Future work could focus on injecting the temperature and irradiation inputs of the PV array with real-time low earth orbit space weather data to simulate the PV system response in real time and verify the adaptability of the hybrid PO-PSO MPPT. Chapter seven discusses four technical project deliverables achieved in the thesis work, and these four deliverables are PV array modeling for the CubeSat’s two sides which are exposed to the sun; PO MPPT modeling and simulation; closed loop boost converter transfer function theoretical derivation and MATLAB/Simulink boost converter transfer function linearization generation PID control with GA and PSO PID tuning implementation in MATLAB/Simulink; PSO MPPT function modeling and simulation; and hybrid PO- PSO MPPT modelling and simulation.

CHAPTER 7

CONCLUSION AND FUTURE WORK

7.1. Introduction

Thesis major research work to design a photovoltaic power system for a CubeSat involves careful planning, considering power requirements, solar panel selection, battery systems, power management, integration, testing, and compliance with space regulations. It's essential to balance energy generation and storage to ensure reliable operation throughout the satellite's mission. The CubeSat is envisioned to operate in a sun-synchronous orbit in low earth orbit at an altitude of 6000 km. In a sun-synchronous orbit, the satellite keeps a constant angle with the Sun, passing over the same portions of the Earth at the same local solar time.

This provides for consistent exposure to sunshine. If the CubeSat is stabilized with its solar panels facing the Sun, at least two sides are constantly exposed to the Sun. If the CubeSat spins or its attitude changes, it may reveal up to three sides at different points in its orbit. Depending on the Earth's position relative to the Sun, the CubeSat may pass through its shadow, resulting in an eclipse. During this time, none of the sides would be exposed to sunlight, and a battery storage system must supply power to the CubeSat. Hence, In the models simulated in this Thesis, the PV array design uses four modules that are connected in parallel because in the envisioned 1U CubeSat ($10cm^3$), each adjacent side is mounted with two Azur space modules. The top and the bottom sides are mounted with SPECTROLAB cells.

This thesis has presented the development of a mathematical model for a PV module using the Azur Space datasheet for 3G30C solar cells in MATLAB/Simulink. The 3G30C solar cells are broadly used within the CubeSat community. This thesis has presented the development of a perturb and observe (PO) maximum power point tracking (MPPT) controller, the development of a PID-based closed-loop controller whose gain parameters are tuned by a genetic algorithm (GA) at first and then secondly tuned by PSO algorithm, the development of a particle swarm optimization (PSO) based MPPT, and the development of a hybrid PO PSO MPPT, for application in PV power systems of CubeSat missions. The developed MPPT controllers and the GA/ PSO PID-based closed loop controllers simulation waveforms and output: power, voltage, and current measurements are compared to each other to identify which technique has the best response time, lowest oscillations at the global maximum power point (GMPP), and outputs accurate desired bus power, voltage, and current.

The intention has been to realize a controller with the fastest response time and most minor oscillations at global maximum power point (GMPP) that also outputs accurate power, voltage, and current despite fluctuations in the PV module's input radiation and temperature and converter's load current demands of various CubeSat subsystems. The approach taken was thus to develop a boost converter for four modules mounted on the two adjacent sides of a CubeSat, each adjacent panel side having two Azur Space 3G30C modules connected in parallel and each module having three cells inside it.

Each Azur Space 3G30C module MPP outputs: 2411mV, 442.8mA, operated under STC (1367W/m2, 28°C). Each panel side in the X-configuration or the Y-configuration is fitted with two Azur Space 3G30C modules that are connected in parallel and give a voltage output of 2411mV, a total current output of 885.6mA, at MPP. The two adjacent sides exposed to the Sun are the (+X, +Y) or (-X, -Y) group, which gives a voltage output of 2.4V and a total current of 1.8A. This 4 X 1 array supplies two boost converters: a 5V and a 3.3V boost converter, each connected to its bus line. The chapter presents an introduction in section 7.1, Project Deliverables in 7.2, Applications of the Research Output in 7.3, Future work in 7.4, and Publications in 7.5.

7.2. Project Deliverables

The following subsections briefly discuss the primary outcomes of this research, Subsection 7.2.1. discusses the literature review on the modeling and simulation of the Cube Satellite Power System. Subsection 7.2.2. discusses PV module modeling and the PO MPPT control implementation for a CubeSat power system. Subsection 7.2.3. discusses genetic algorithm (GA) PID tuning and the particle swarm optimization (PSO) PID tuning implementation for CubeSat Power Systems. Subsection 7.2.4. discusses particle swarm optimization MPPT implementation for CubeSat power systems.

7.2.1. Project Deliverable 1: Literature Review on Modelling and Simulation of the Cube Satellite Power Systems

In the literature review of the modeling and simulation of PV solar modules and the modeling and simulation of the power regulation and control system for a CubeSat EPS, the following tasks were accomplished:

- A comprehensive literature focused mainly on this topic:

1. PV solar module mathematical modeling using Simulink.

- A comprehensive and comparative analysis of the literature focused mainly on these topics:

1. MPPT classical functions comparison.

2. PID controllers used to minimize the steady-state error of a closed-loop boost converter transfer function plant, tunned using artificial intelligence (AI) algorithms like particle swarm optimization (PSO), genetic algorithm (GA), fuzzy logic (FL), artificial neural networks (ANN), adaptive neuro-fuzzy inference system (ANFIS), ant colony optimization (ACO), grey wolf optimization (GWO), bee colony optimization (BCO) bacterial foraging optimization (BFO), etc.

3. MPPT functions that use AI algorithms like PSO, GA, FL, etc,

4. MPPT hybrid techniques are implemented as a combination of the MPPT functions like PO, incremental conductance InC, etc., with AI algorithms like PSO, GA, etc.

The contribution to studying how to mathematically model the PV module from first principles using the current equations has been to realize a PV module block in the Simulink library using the Azur space 3G30C solar cell datasheet. The contribution of studying classical MPPT functions has been to ascertain which classical function is ideal for application in CubeSat, considering the limitations of CubeSat volume dimensions, microprocessor computation demand, and weight. The PO function was selected for low computational complexity and easy hardware implementation.

However, the research gap identified was that the PO tracked the GMPP poorly under fast-changing meteorologic conditions. Therefore, a study of low computational AI techniques that are used to improve the tracking accuracy of the PO function under fast-changing meteorologic conditions ensued, and the results of the hybrid PO PSO MPPT function showed improvement in the tracking accuracy of the PO under fast-changing meteorologic conditions.

Also, it was discovered in the literature survey that the mathematical conversion of a closed-loop boost converter into a transfer function using small signal model approximation methods: audio susceptibility, control-to-output transfer functions, and state-space averaging method is inferior to MATLAB/Simulink linearization function since the mathematical derivation methods cannot convert associated control functions connected to the boost converter, like the feedback summing block, PID, pulse width modulator generator block. Hence, the frequency domain control by AI tuning the PID controller that regulates the boost converter closed-loop transfer function plant was

demonstrated using the MATLAB/Simulink generated transfer function. However, the frequency domain analysis is theoretical, and direct implementation is not feasible for CubeSat electrical power generation, regulation, and control circuitry. The PO MPPT function, PSO MPPT function, and the hybrid PO PSO MPPT function are time-domain control functions and can be implemented to extract maximum power from the PV array.

7.2.2. Project Deliverable 2: PV Module Modeling and PO MPPT Control Implementation for a CubeSat Power System

For the one diode/ two resistor (1D/2R) PV model development and simulation, the following tasks were accomplished:

- A mathematical model based on the single-diode and two-resistors (1D/2R) PV model approach was developed using the five algebraic current equations.
- The unknown five parameters were extrapolated from Alverez et al., 2021 work, where they were determined using the analytical fitting of a 1D/2R model equivalent circuit to I-V curves corresponding to data from Azur Space 3G30C solar cells datasheet.
- The mathematical model was implemented using MATLAB/Simulink.
- The temperature and irradiance effects were also incorporated into the model to better approximate the physical PV cell characteristics.
- Conventional MPPT functions for the Maximum Power Point Tracking (MPPT) control of PV generation systems were discussed. The PO MPPT technique was implemented, and the percentage increase in the output power yield was assessed by comparing the output of the MPPT-controlled PV module with that without the MPPT controller.

This project deliverable offers a benchmark for future research in CubeSats concerning the mathematical modeling of solar PV modules used in engineering design. Another contribution is demonstrating a robust maximum power extraction method using a boost converter for two CubeSat's adjacent sides envisaged to be exposed to the Sun in a minimal exposure case. A maximum exposure case is when three sides are exposed to the Sun.

7.2.3. Project deliverable 3: Genetic Algorithm (GA) and PSO PID tuning Implementation for CubeSat Power Systems

For the GA-tuned PID/ PSO-tuned PID controlled transfer function closed loop plant development and design, the following tasks were accomplished:

- A closed-loop boost converter transfer function plant was developed using MATLAB/Simulink linearization.
- The PID controller was placed before the plant to develop a dynamic response and to reduce the steady-state error.
- A steady state error minimization function selected was the integral time absolute error (ITAE). ITAE was chosen because the CubeSat maximum power point (MPP) must be realized in the fastest response time when the satellite transitions from the eclipse zone to the sun zone. The orbit period of the CubeSat in LEO orbit is ninety minutes only. Hence, fast response time in tracking MPP is required to transition from battery to PV power. Thus, the storage battery system is recharged abruptly while the satellite is powered concurrently. Therefore, ITEA offers the best response time and better settling time compared to integral square error (ISE), integral time square error (ITSE), and integral absolute error (IAE).
- The GA/PSO algorithm was implemented in MATLAB/Simulink to search for the best PID gain values that will minimize the steady-state error of the Simulink model.
- After the PID gain values were found, they were applied to the Simulink model, and the manually tuned PID controlled transfer function closed loop plant was compared to the GA/PSO-tuned PID controlled transfer function plant closed loop plant.

This project deliverable demonstrated the GA-tuned and PSO-tuned PID controlled transfer function closed loop plants and identified that the AI-tuned PID controlled transfer function closed loop plant provides faster response and settling time compared to the manually tuned PID controlled transfer function closed loop plant. Also, AI-tuned PID-controlled transfer function closed loop plants produced a 4.6V output voltage, while the manually tuned one produced 0.05664V.

7.2.4. Project Deliverable 4: Particle Swarm Optimization Implementation for CubeSat Power Systems

To coordinate the three transfer functions derived from three distinct methods, namely, the state space averaging derivation method, AC analysis small signal transfer function derivation method, and MATLAB/Simulink linearization methods, the following tasks were accomplished:

- The small signal transfer function derivation approach was implemented to obtain the audio susceptibility transfer function and the boost converter's control-to-output transfer function.
- The averaging method of state space was performed to derive the transfer function from the state space.
- The theoretically derived state space and transfer functions were compared to the linearization Simulink-generated state space and transfer function.

This project deliverable compared the MATLAB/Simulink generated state space with the state space derived from the average method; the deduction was that the software linearised states were three, whereas the calculated states were two. The control-to-output transfer function is a second-order transfer function, and the state space obtained transfer function through the averaging method is a second-order transfer function. However, the value of the multiplying constants is not similar. The Simulink linearisation-generated transfer function is superior to the mathematically derived transfer functions. It is a third-order transfer function because it converts responses of control elements used with the boost converter: PID, closed-loop components, and PWM circuitry.

To implement PSO for CubeSat Power Systems, the following tasks were accomplished:

- The setup of the GA-tuned/ PSO-tuned PID controlled transfer function closed loop plant was used with the ITAE cost function used as the objecting function of the GA/PSO algorithm in a MATLAB script file.
- The GA/PSO algorithm was executed and tuned the PID gain parameters K(1), K(2), and K(3).
- The GA/PSO tunned PID gain parameters values K(1), K(2), and K(3) were entered into the PID of the Simulink model named “PSO_to_theory.slx” and the model was simulated.

This project deliverable demonstrated the frequency domain control by AI tuning the PID controller that controls the MATLAB/Simulink generated boost converter transfer function plant. However, the approach used in this deliverable is the frequency domain analysis, which is theoretical, and direct implementation is not feasible for CubeSat electrical power generation, regulation, and control circuitry.

7.2.5. Project deliverable 5: Development of the hybrid PO PSO MPPT model for implementation in CubeSat power systems

For the Development of the hybrid PO PSO MPPT model, the following tasks were accomplished:

- A PSO MPPT function was developed to adjust the duty cycle D of the boost converter based on the input voltage Vpv and current Ipv of a PV array. The goal is to maximize the power output of the boost converter by finding the optimal duty cycle D using the PSO algorithm.
- A hybrid PO PSO MPPT function was developed. The hybrid code integrates both the global search capability of PSO MMPT and the fine-tuning capability of PO MPPT.
- Case study 1: At standard test conditions (temp = 28°C and irradiation =1367W/m^2), the PO MPPT, PSO MPPT, and the hybrid PO PSO MPPT were tested under these meteorological conditions.
- Case study 2: At a varying temperature (-100°C to +120°C) and fixed irradiations (1367W/m^2), the PO MPPT, PSO MPPT, and the hybrid PO PSO MPPT were tested under these meteorological conditions.
- The PO MPPT, PSO MPPT, and the hybrid MPPT were benchmarked with simulation results from the recent literature.

Under case study 1, the 5V was the target bus voltage, the PO MPPT had a DC average voltage of 4.6V, and the PSO MPPT and the hybrid PO PSO MPPT had an average DC voltage of 4.1V. Under case study 2, the 5V was still the target bus voltage. As the sampling time changed rapidly within the one-second simulation time, the voltage of the PO MPPT deviated significantly from the targeted voltage. This significant deviation results in an average harvested voltage within the one-second simulation time reducing to 3.89V.

For the PSO MPPT, the voltage deviated slightly from the targeted voltage. This slight deviation resulted in an average harvested voltage within the one-second simulation time, settling at 5.084V. These results were better than the PO MPPT, but the oscillations around the target voltage were substantial and needed improvement. In the hybrid PO PSO MPPT, the voltage deviated slightly from the targeted voltage. This slight deviation resulted in an average harvested DC voltage within the one-second simulation time, settling at 5.242V. These results were better than the PO MPPT and the PSO MPPT. The oscillations around the target voltage were reduced.

7.2.6. Software Programs Developed in the Thesis

Table 7. 1: Software Programs Developed

Program description	File type	Appendix
MATLAB function code for PO MPPT	MATLAB script file	A.
MATLAB function code for PSO MPPT	MATLAB script file	B.
MATLAB function code for hybrid PO PSO MPPT	MATLAB script file	C.
MATLAB code GA-tuned PID	MATLAB script file	D.
MATLAB code PSO-tuned PID	MATLAB script file	E.

7.3. Applications of the Research Output

7.3.1. Practical applications

A single OBC executes the 1U CubeSat operations; hence, computational demanding algorithms must be avoided in the CubeSat electrical power system design to relieve the OBC to execute commands for other CubeSat subsystems. The PO was chosen because of its lower computational complexity than incremental conductance and easy hardware complexity compared to fractional open circuit voltage and fractional short circuit current, which require additional sensors to measure open circuit voltage/ short circuit current. Moreover, fractional voltage/current-based MPPT techniques have a simpler structure but suffer from low tracking accuracy due to rough empirical approximations, significant power losses, and difficulty sensing open-circuit and short-circuit currents. MPPTs are typically used when cost is more important than tracking accuracy (Mataifa, 2015). Thus, for practical implementation, it is recommended that PO will be a more suitable tracking MPP technique for CubeSat EPS design.

The problem with PO is tracking under dynamic temperature, irradiance, and oscillations it produces under dynamic conditions. To solve this problem, a literature review of AI techniques was conducted. When comparing Genetic Algorithm (GA), Particle Swarm Optimisation (PSO), Artificial Neural Networks (ANN), Adaptive Neuro-Fuzzy Inference System (ANFIS), and Fuzzy Logic—Fuzzy Logic is widely considered the least computationally complex. However, PSO is typically better suited for accurate and dependable MPPT tracking in standalone PV systems, especially in areas with quickly changing conditions. While fuzzy Logic is more straightforward and faster, it

may not be as precise and adaptable as PSO in optimizing power output from PV systems (Esram, 2007). Thus, a hybrid PO PSO is recommended for a 1U CubeSat EPS design. The PV modeling and simulation of all MPPT techniques researched in this thesis are not practically evaluated. However, the MPPTs recommended for CubeSat implementation consider that the 1 U CubeSat has one OBC, and the complex computational algorithm must be avoided.

7.3.2. Academic/research applications

The comprehensive way the subject matter of this thesis has been treated, with a detailed and systematic presentation of the various fundamental aspects relevant to PV power generation and MPPT conventional and AI comparative analysis, may serve a significant function to students and researchers in the field of designing small satellite and even GEO satellite at large. The results presented here may also be used as a basis for extended research into the effective control and regulation of PV solar-generated power for small satellites, thus improving the theoretical results obtained in this thesis. The theoretical contributions of this thesis can be used as coursework for BENG and MENG satellite degrees and even contribute to a book Chapter for academic purposes.

7.4. Future work

Extensions to the work covered in this thesis could take any one or more of the following directions:

1. Future work recommended is modeling and simulating the top side of PV solar modules and applying the MPPT techniques developed in this research. The bottom side is identical to the top side. Hence, the results of the top-side model will be similar to those of the bottom-side model.

2. Future work recommended is the study of the literature based on modeling and simulating the battery charge regulator and the battery storage system and applying a suitable battery charger and battery system for a CubeSat mission.

3. Future work recommended is mathematically modeling the Spectrolab PV module in Simulink using the Spectrolab datasheet.

4. Also recommended as future work is an actual implementation of either the PO MPPT functions, the PSO MPPT, or the hybrid PO PSO MPPT to a CubeSat ESP that will be launched in orbit.

7.5 Publications

K. Dwaza and S. Krishnamurthy, "Application Perturb and Observe Maximum Power Point Tracking Technique for CubeSat Power Systems," 32nd Southern African Universities Power Engineering Conference (SAUPEC), Stellenbosch, South Africa, 2024, pp. 1-5, doi: 10.1109/SAUPEC60914.2024.10445093.

K.N Dwaza, S. Krishnamurthy and H Mataifa, “Implementation of a Hybrid Perturb and Observe Particle Swarm Optimisation Maximum Power Point Tracking function for CubeSat Photovoltaic Power system,” The paper is planned for submission to the 33rd Southern African Universities Power Engineering Conference (SAUPEC), Tshwane, South Africa, 2025, pp 1-5.

Dwaza, K.N, Krishnamurthy, S and Mataifa, H 2025, ‘A comprehensive study: hybrid classical MPPT and AI MPPT for small satellite PV systems’, The journal paper is planned for submission to the IEEE Transactions on Power Electronics journal.

7.6. Conclusion

This thesis successfully developed and analyzed various Maximum Power Point Tracking (MPPT) controllers explicitly designed for CubeSat power systems. The study investigated and evaluated the performance of various MPPT strategies, such as the Perturb and Observe (PO) method, a PID-based controller optimized with Genetic Algorithms (GA), a Particle Swarm Optimisation (PSO)-based MPPT controller, and a novel hybrid PO-PSO MPPT approach. The comparative analysis found that while standard MPPT methods such as PO are simple and easy to deploy, they fall short in dynamic situations with rapid changes in irradiance and temperature. The GA-optimized PID controller demonstrated better performance in terms of settling time and response accuracy. However, the PSO-based MPPT controller tracked the maximum power point more accurately, with faster response times and fewer oscillations.

The significant contribution of this research is the creation of the hybrid PO-PSO MPPT model, which successfully combines the advantages of both PO and PSO. This hybrid model minimizes the amplitude of oscillations at the global maximum power point (GMPP) and improves tracking accuracy in various meteorological situations, making it ideal for CubeSat applications. The practical applications of this research indicate that the innovative hybrid PO-PSO MPPT model could be a reliable option for CubeSat missions, particularly those with high power precision and efficiency requirements. Although the PV modeling and MPPT techniques were not physically tested, the simulations provided a robust framework for future practical implementations. In

conclusion, this thesis lays the framework for future studies into optimizing power generation and regulation in tiny satellite systems. The discoveries have the potential to considerably improve the design of energy systems in CubeSats, increasing their operational efficiency in space conditions.

REFERENCES

Abdul Zahra, M.M., Sathasivam, K., Al-Azzawi, W.K., Ryadh, A., Shalal, A.A., Hussein, M.A., Zaboun, A.R.T., Garip, I., 2024. Design and Testing of Bidirectional DC-DC Converters for Emergency Lighting. Electr. Power Compon. Syst. 52, 697–708. https://doi.org/10.1080/15325008.2023.2230492

Abdulkadir, M., Yatim, A.H.M., 2014. Hybrid maximum power point tracking technique based on PSO and incremental conductance, in: 2014 IEEE Conference on Energy Conversion (CENCON)., IEEE, Johor Bahru, Malaysia, pp. 271–276. https://doi.org/10.1109/CENCON.2014.6967514

Acharya, S., Alshehhi, F., Tsoupos, A., Khan, O., Elmoursi, M., Khadkikar, V., Zeineldin, H., Al Hosani, M., 2019. Modeling and Design of Electrical Power Subsystem for CubeSats, in: 2019 International Conference on Smart Energy Systems and Technologies (SEST). Presented at the 2019 International Conference on Smart Energy Systems and Technologies (SEST), IEEE, Porto, Portugal, pp. 1–6. https://doi.org/10.1109/SEST.2019.8849042

Agarwal, G., Kumar, A., Nayak, M.M., Agarwal, V.K., 2016. Design of a Student Satellite- PISAT. INCOSE Int. Symp. 26, 276–290. https://doi.org/10.1002/j.2334-5837.2016.00331.x

Aguila-Leon, J., Vargas-Salgado, C., Chiñas-Palacios, C., Díaz-Bello, D., 2023. Solar photovoltaic Maximum Power Point Tracking controller optimization using Grey Wolf Optimizer: A performance comparison between bio-inspired and traditional algorithms. Expert Syst. Appl. 211, 118700. https://doi.org/10.1016/j.eswa.2022.118700

Ahmed, J., Salam, Z., 2016. A Modified P&O Maximum Power Point Tracking Method With Reduced Steady-State Oscillation and Improved Tracking Efficiency. IEEE Trans. Sustain. Energy 7, 1506–1515. https://doi.org/10.1109/TSTE.2016.2568043

Albira, M.E., Zohdy, M.A., 2021. Adaptive Model Predictive Control for DC-DC Power Converters With Parameters' Uncertainties. IEEE Access 9, 135121–135131. https://doi.org/10.1109/ACCESS.2021.3113299

Ali, A.J., Khalily, M., Sattarzadeh, A., Massoud, A., Hasna, M.O., Khattab, T., Yurduseven, O., Tafazolli, R., 2021. Power Budgeting of LEO Satellites: An Electrical Power System Design for 5G Missions. IEEE Access 9, 113258–113269. https://doi.org/10.1109/ACCESS.2021.3104098

Ali, A.N.A., Saied, M.H., Mostafa, M.Z., Abdel- Moneim, T.M., 2012. A survey of maximum PPT techniques of PV systems, in: 2012 IEEE Energytech. Presented at the 2012 IEEE Energytech, IEEE, Cleveland, OH, USA, pp. 1–17. https://doi.org/10.1109/EnergyTech.2012.6304652

Ali, M.B.O.E., Abbaker, A.E.M., Elfaki, S.E.E., 2021. Modeling, Simulation, and Implementation of the Electrical Power System of Cube Satellite Using Matlab and Simulink, in: 2020 International Conference on Computer, Control, Electrical, and Electronics Engineering (ICCCEEE)., IEEE, Khartoum, Sudan, pp. 1–5. https://doi.org/10.1109/ICCCEEE49695.2021.9429573

Ali, Z.M., Vu Quynh, N., Dadfar, S., Nakamura, H., 2020. Variable step size perturb and observe MPPT controller by applying θ-modified krill herd algorithm-sliding mode controller under partially shaded conditions. J. Clean. Prod. 271, 122243. https://doi.org/10.1016/j.jclepro.2020.122243

Allahabadi, S., Iman-Eini, H., Farhangi, S., 2022. Fast Artificial Neural Network Based Method for Estimation of the Global Maximum Power Point in Photovoltaic Systems. IEEE Trans. Ind. Electron. 69, 5879–5888. https://doi.org/10.1109/TIE.2021.3094463

Álvarez, J.M., Alfonso-Corcuera, D., Roibás-Millán, E., Cubas, J., Cubero-Estalrrich, J., Gonzalez-Estrada, A., Jado-Puente, R., Sanabria-Pinzón, M., Pindado, S., 2021. Analytical Modeling of Current-Voltage Photovoltaic Performance: An Easy Approach to Solar Panel Behavior. Appl. Sci. 11, 4250. https://doi.org/10.3390/app11094250

Aminnejhad, H., Kazeminia, S., Aliasghary, M., 2021. Robust sliding-mode control for maximum power point tracking of photovoltaic power systems with quantized input signal. Optik 247, 167983. https://doi.org/10.1016/j.ijleo.2021.167983

Ammar, H.H., Azar, A.T., Shalaby, R., Mahmoud, M.I., 2019. Metaheuristic Optimization of Fractional Order Incremental Conductance (FO-INC) Maximum Power Point Tracking (MPPT). Complexity 2019, 1–13. https://doi.org/10.1155/2019/7687891

Aoughlis, C., Belkaid, A., Colak, I., Guenounou, O., Kacimi, M.A., 2021. Automatic and Self Adaptive P&O MPPT Based PID Controller and PSO Algorithm, in: 2021 10th International Conference on Renewable Energy Research and Application (ICRERA). Presented at the 2021 10th International Conference on Renewable Energy Research and Application (ICRERA), IEEE, Istanbul, Turkey, pp. 385–390. https://doi.org/10.1109/ICRERA52334.2021.9598489

Banakhr, F.A., Mosaad, M.I., 2021. High performance adaptive maximum power point tracking technique for off-grid photovoltaic systems. Sci. Rep. 11, 20400. https://doi.org/10.1038/s41598-021-99949-8

Bani Salim, M., Hayajneh, H.S., Mohammed, A., Ozcelik, S., 2019a. Robust Direct Adaptive Controller Design for Photovoltaic Maximum Power Point Tracking Application. Energies 12, 3182. https://doi.org/10.3390/en12163182

Bani Salim, M., Hayajneh, H.S., Mohammed, A., Ozcelik, S., 2019b. Robust Direct Adaptive Controller Design for Photovoltaic Maximum Power Point Tracking Application. Energies 12, 3182. https://doi.org/10.3390/en12163182

Batarseh, M.G., Za'ter, M.E., 2018. Hybrid maximum power point tracking techniques: A comparative survey, suggested classification and uninvestigated combinations. Sol. Energy 169, 535–555. https://doi.org/10.1016/j.solener.2018.04.045

Bollipo, R.B., Mikkili, S., Bonthagorla, P.K., 2020. Critical Review on PV MPPT Techniques: Classical, Intelligent and Optimisation. IET Renew. Power Gener. 14, 1433–1452. https://doi.org/10.1049/iet-rpg.2019.1163

Chen, Y.-K., Lai, Y.-C., Lu, W.-C., Lin, A., 2021. Design and Implementation of High Reliability Electrical Power System for 2U NutSat. IEEE Trans. Aerosp. Electron. Syst. 57, 614–622. https://doi.org/10.1109/TAES.2020.3028488

Cheon, S.-I., Choi, H., Kang, H., Suh, J.-H., Park, S., Kweon, S.-J., Je, M., Ha, S., 2024. Impedance-Readout Integrated Circuits for Electrical Impedance Spectroscopy: Methodological Review. IEEE Trans. Biomed. Circuits Syst. 18, 215–232. https://doi.org/10.1109/TBCAS.2023.3319212

Da Rocha, M.V., Sampaio, L.P., Da Silva, S.A.O., 2020. Comparative analysis of MPPT algorithms based on Bat algorithm for PV systems under partial shading condition. Sustain. Energy Technol. Assess. 40, 100761. https://doi.org/10.1016/j.seta.2020.100761

Devarakonda, A., Karuppiah, N., Selvaraj, T., Balachandran, P., Shanmugasundaram, R., Senjyu, T., 2022. A Comparative Analysis of Maximum Power Point Techniques for Solar Photovoltaic Systems. Energies 15, 8776. https://doi.org/10.3390/en15228776

Erickson, R.W., Maksimović, D., 2020. Fundamentals of Power Electronics. Springer International Publishing, Cham. https://doi.org/10.1007/978-3-030-43881-4

Esram, T., Chapman, P.L., 2007. Comparison of Photovoltaic Array Maximum Power Point Tracking Techniques. IEEE Trans. Energy Convers. 22, 439–449. https://doi.org/10.1109/TEC.2006.874230

Fahim, K.E., Farabi, S.M., Farhan, S.S., Esha, I.J., Muhtadi, T., 2021. Overview of Maximum Power Point Tracking Techniques for PV System. E3S Web Conf. 242, 01004. https://doi.org/10.1051/e3sconf/202124201004

Fan, Z., Li, S., Cheng, H., Liu, L., 2021. Perturb and Observe MPPT Algorithm of photovoltaic System: A Review, in: 2021 33rd Chinese Control and Decision Conference (CCDC). Presented at the 2021 33rd Chinese Control and Decision Conference (CCDC), IEEE, Kunming, China, pp. 1413–1418. https://doi.org/10.1109/CCDC52312.2021.9602272

Fekik, A., Hamida, M.L., Azar, A.T., Ghanes, M., Hakim, A., Denoun, H., Hameed, I.A., 2024. Robust power control for PV and battery systems: integrating sliding mode MPPT with dual buck converters. Front. Energy Res. 12, 1380387. https://doi.org/10.3389/fenrg.2024.1380387

Garg, A., Mathur, D., Tanwar, H., Joshi, S., 2020. Comparative Analysis of Maximum Power Point Algorithms for Solar PV Applications, in: 2020 21st National Power Systems Conference (NPSC)., IEEE, Gandhinagar, India, pp. 1–6. https://doi.org/10.1109/NPSC49263.2020.9331766

Guter, W., Dunzer, F., Ebel, L., Hillerich, K., Köstler, W., Kubera, T., Meusel, M., Postels, B., Wächter, C., 2017. Space Solar Cells – 3G30 and Next Generation Radiation Hard Products. E3S Web Conf. 16, 03005. https://doi.org/10.1051/e3sconf/20171603005

Harrag, A., Messalti, S., 2015. Variable step size modified P&O MPPT algorithm using GA-based hybrid offline/online PID controller. Renew. Sustain. Energy Rev. 49, 1247–1260. https://doi.org/10.1016/j.rser.2015.05.003

Hassan, A., Bass, O., Masoum, M.A.S., 2023. An improved genetic algorithm based fractional open circuit voltage MPPT for solar PV systems. Energy Rep. 9, 1535–1548. https://doi.org/10.1016/j.egyr.2022.12.088

Hoarca, I.C., 2021. Mathematical modeling and simulation of PV systems Part I: Mathematical modeling and Simulink implementation, in: 2021 International Conference on Applied and Theoretical Electricity (ICATE). Presented at the 2021 International Conference on Applied and Theoretical Electricity (ICATE), IEEE, Craiova, Romania, pp. 1–6. https://doi.org/10.1109/ICATE49685.2021.9465047

Ilyas, A., Khan, M.R., Ayyub, M., 2015. Lookup table based modeling and simulation of solar photovoltaic system, in: 2015 Annual IEEE India Conference (INDICON). Presented at the 2015 Annual IEEE India Conference (INDICON), IEEE, New Delhi, India, pp. 1–6. https://doi.org/10.1109/INDICON.2015.7443268

Jaen-Cuellar, A.Y., De J. Romero-Troncoso, R., Morales-Velazquez, L., Osornio-Rios, R.A., 2013. PID-Controller Tuning Optimization with Genetic Algorithms in Servo Systems. Int. J. Adv. Robot. Syst. 10, 324. https://doi.org/10.5772/56697

Jately, V., Azzopardi, B., Joshi, J., Venkateswaran V, B., Sharma, A., Arora, S., 2021. Experimental Analysis of hill-climbing MPPT algorithms under low irradiance levels. Renew. Sustain. Energy Rev. 150, 111467. https://doi.org/10.1016/j.rser.2021.111467

Jayakumaran, T., Gurunathau, G., Srlkanth, C.V., Shashank, M.K., Venkatesh, R., Ramkiran, B., Neelamegam, P., 2018. A Comprehensive Review on Maximum Power Point Tracking Algorithms for Photovoltaic Cells, in: 2018 Internat2018 International Conference on Computation of Power, Energy, Information and Communication (ICCPEIC)Ional Conference on Computation of Power, Energy, Information and Communication (ICCPEIC)., IEEE, Chennai, India, pp. 343–349. https://doi.org/10.1109/ICCPEIC.2018.8525191

Kabaca, E., Celik, K., Keskin, E., Merzifonluoglu, A., Cakmakci, S., Ozyurt, C.H., Cumhur, M.T., 2015. TUGES, satellite power and energy simulation tool, in: 2015 7th International Conference on Recent Advances in Space Technologies (RAST)., IEEE, Istanbul, pp. 443–448. https://doi.org/10.1109/RAST.2015.7208386

Kamran, M., Mudassar, M., Fazal, M.R., Asghar, M.U., Bilal, M., Asghar, R., 2020. Implementation of improved Perturb & Observe MPPT technique with confined search space for standalone photovoltaic system. J. King Saud Univ. - Eng. Sci. 32, 432–441. https://doi.org/10.1016/j.jksues.2018.04.006

Katche, M.L., Makokha, A.B., Zachary, S.O., Adaramola, M.S., 2023. A Comprehensive Review of Maximum Power Point Tracking (MPPT) Techniques Used in Solar PV Systems. Energies 16, 2206. https://doi.org/10.3390/en16052206

Koushki, B., Jain, P., Bakhshai, A., 2024. Reduced Conduction Loss ZVS Control for Buck-Type Active Filter Operating as Decoupling Circuit. IEEE Trans. Transp. Electrification 1–1. https://doi.org/10.1109/TTE.2024.3392717

Koutroulis, E., Kalaitzakis, K., Voulgaris, N.C., 2001. Development of a microcontroller-based, photovoltaic maximum power point tracking control system. IEEE Trans. Power Electron. 16, 46–54. https://doi.org/10.1109/63.903988

Kumar, P., Patthi, S., Prakhya, R.K., Rao, J.V.G.R., Rayudu, K., 2024. Efficient power conversion with four switch soft-switching boost integrated half-bridge dual-output series resonant converter. J. Eng. Appl. Sci. 71, 173. https://doi.org/10.1186/s44147-024-00501-y

Kumar, P., S, K.H.K., H, A.D., Prabhu, G.K., S, D., Geetha, R.S., 2021. Preliminary Design and Simulation of the Electrical Power System for a CubeSat Using LTspice, in: 2021 7th International Conference on Space Science and Communication (IconSpace)., IEEE, Selangor, Malaysia, pp. 167–173. https://doi.org/10.1109/IconSpace53224.2021.9768770

Larbes, C., Aït Cheikh, S.M., Obeidi, T., Zerguerras, A., 2009. Genetic algorithms optimized fuzzy logic control for the maximum power point tracking in photovoltaic system. Renew. Energy 34, 2093–2100. https://doi.org/10.1016/j.renene.2009.01.006

Lasheen, M., Abdel Rahman, A.K., Abdel-Salam, M., Ookawara, S., 2017. Adaptive reference voltage-based MPPT technique for PV applications. IET Renew. Power Gener. 11, 715–722. https://doi.org/10.1049/iet-rpg.2016.0749

Mahfoud, S., Derouich, A., El Ouanjli, N., Quynh, N.V., Mossa, M.A., 2022. A New Hybrid Ant Colony Optimization Based PID of the Direct Torque Control for a Doubly Fed Induction Motor. World Electr. Veh. J. 13, 78. https://doi.org/10.3390/wevj13050078

Malathy, S., Ramaprabha, R., 2013. Maximum Power Point Tracking Based on Look Up Table Approach. Adv. Mater. Res. 768, 124–130. https://doi.org/10.4028/www.scientific.net/AMR.768.124

Manickam, C., Raman, G.P., Raman, G.R., Ganesan, S.I., Chilakapati, N., 2017. Fireworks Enriched P&O Algorithm for GMPPT and Detection of Partial Shading in PV Systems. IEEE Trans. Power Electron. 32, 4432–4443. https://doi.org/10.1109/TPEL.2016.2604279

Meena, D.C., Devanshu, A., 2017. Genetic algorithm tuned PID controller for process control, in: 2017 International Conference on Inventive Systems and Control (ICISC)., IEEE, Coimbatore, India, pp. 1–6. https://doi.org/10.1109/ICISC.2017.8068639
Mehrotra, S., Ray, R.K., Pandey, D., Naithani, H., 2024. Comparison between State of Art Performance of GaN and SiC Converters for Electric Vehicle Application. Presented at the Symposium on International Automotive Technology, Pune, India, pp. 2024-26–0134. https://doi.org/10.4271/2024-26-0134
Mohamed, H.A., Khattab, H.A., Mobarka, A., Morsy, G.A., 2016. Design, control and performance analysis of DC-DC boost converter for stand-alone PV system, in: 2016 Eighteenth International Middle East Power Systems Conference (MEPCON)., IEEE, Cairo, Egypt, pp. 101–106. https://doi.org/10.1109/MEPCON.2016.7836878
Mohamed, M.A.E., Jagatheesan, K., Anand, B., 2023. Modern PID/FOPID controllers for frequency regulation of interconnected power system by considering different cost functions. Sci. Rep. 13, 14084. https://doi.org/10.1038/s41598-023-41024-5
Mohammed, F.A., Bahgat, M.E., Elmasry, S.S., Sharaf, S.M., 2022. Design of a maximum power point tracking-based PID controller for DC converter of stand-alone PV system. J. Electr. Syst. Inf. Technol. 9, 9. https://doi.org/10.1186/s43067-022-00050-5
Mohammed, I.K., 2024. Design and Simulation of Voltage Control System for Simscape Boost Converter Model With Disturbances. Int. J. Control Autom. Syst. 22, 1707–1716. https://doi.org/10.1007/s12555-023-0311-0
Mohanty, S., Subudhi, B., Ray, P.K., 2017. A Grey Wolf-Assisted Perturb & Observe MPPT Algorithm for a PV System. IEEE Trans. Energy Convers. 32, 340–347. https://doi.org/10.1109/TEC.2016.2633722
Momani, S., El-Khazali, R., Batiha, I.M., 2019. Tuning PID and PIλDδ controllers using particle swarm optimization algorithm via El-Khazali's approach. Presented at the PROCEEDINGS OF THE 45TH INTERNATIONAL CONFERENCE ON APPLICATION OF MATHEMATICS IN ENGINEERING AND ECONOMICS (AMEE'19), Sozopol, Bulgaria, p. 050003. https://doi.org/10.1063/1.5133522
Moradi, M.H., Reza Tousi, S.M., Nemati, M., Saadat Basir, N., Shalavi, N., 2013. A robust hybrid method for maximum power point tracking in photovoltaic systems. Sol. Energy 94, 266–276. https://doi.org/10.1016/j.solener.2013.05.016
Murtaza, A.F., Sher, H.A., Chiaberge, M., Boero, D., De Giuseppe, M., Addoweesh, K.E., 2013. Comparative analysis of maximum power point tracking techniques for PV applications, in: INMIC. Presented at the 2013 16th International Multi Topic Conference (INMIC), IEEE, Lahore, Pakistan, pp. 83–88. https://doi.org/10.1109/INMIC.2013.6731329
Murugesan, D., Jagatheesan, K., Shah, P., Sekhar, R., 2024. PID Controller Trained Using Ant Colony Algorithm for Load Frequency Control Problems on Three Equal-Area Interconnected Thermal Power with Renewable Energy Sources, in: Dey, N. (Ed.), Applications of Ant Colony Optimization and Its Variants, Springer Tracts in Nature-Inspired Computing. Springer Nature Singapore, Singapore, pp. 123–146. https://doi.org/10.1007/978-981-99-7227-2_7
Nkambule, M.S., Hasan, A.N., Ali, A., Hong, J., Geem, Z.W., 2021. Comprehensive Evaluation of Machine Learning MPPT Algorithms for a PV System Under Different Weather Conditions. J. Electr. Eng. Technol. 16, 411–427. https://doi.org/10.1007/s42835-020-00598-0
Noguchi, T., Togashi, S., Nakamoto, R., 2000. Short-current pulse based adaptive maximum-power-point tracking for photovoltaic power generation system, in: ISIE'2000. Proceedings of the 2000 IEEE International Symposium on Industrial Electronics (Cat. No.00TH8543)., IEEE, Cholula, Puebla, Mexico, pp. 157–162. https://doi.org/10.1109/ISIE.2000.930504
Oudrhiri, K., Yang, O., Buccino, D., Kahan, D., Withers, P., Tortora, P., Matousek, S., Lay, N., Lazio, J., Krajewski, J., Klesh, A., 2020. MarCO Radio Occultation: How the First Interplanetary Cubesat Can Help Improve Future Missions, in: 2020 IEEE Aerospace Conference. Presented at the 2020 IEEE Aerospace Conference, IEEE, Big Sky, MT, USA, pp. 1–10. https://doi.org/10.1109/AERO47225.2020.9172734
Panduranga Vittal, K., Bhanja, S., Keshri, A., 2021. Comparative Study of PI, PID controller for Buck-Boost Converter tuned by Bio-Inspired Optimization Techniques, in: 2021 IEEE International Conference on Distributed Computing, VLSI, Electrical Circuits and Robotics (DISCOVER)., IEEE, Nitte, India, pp. 219–224. https://doi.org/10.1109/DISCOVER52564.2021.9663591
Pilakkat, D., Kanthalakshmi, S., 2020. Single phase PV system operating under Partially Shaded Conditions with ABC-PO as MPPT algorithm for grid connected applications. Energy Rep. 6, 1910–1921. https://doi.org/10.1016/j.egyr.2020.07.019
Refaat, M.M., Atia, Y., Sayed, M.M., Fattah, H.A., 2020. Adaptive Fuzzy Logic Controller as MPPT Optimization Technique Applied to Grid-Connected PV Systems, in: Eltamaly, A.M., Abdelaziz, A.Y. (Eds.), Modern Maximum Power Point Tracking Techniques for Photovoltaic

Energy Systems, Green Energy and Technology. Springer International Publishing, Cham, pp. 247–281. https://doi.org/10.1007/978-3-030-05578-3_9
Reza Reisi, A., Hassan Moradi, M., Jamasb, S., 2013. Classification and comparison of maximum power point tracking techniques for photovoltaic system: A review. Renew. Sustain. Energy Rev. 19, 433–443. https://doi.org/10.1016/j.rser.2012.11.052
Robles Algarín, C., Taborda Giraldo, J., Rodríguez Álvarez, O., 2017. Fuzzy Logic Based MPPT Controller for a PV System. Energies 10, 2036. https://doi.org/10.3390/en10122036
Saidi, A.S., Salah, C.B., Errachdi, A., Azeem, M.F., Bhutto, J.K., Thafasal Ijyas, V.P., 2021. A novel approach in stand-alone photovoltaic system using MPPT controllers & NNE. Ain Shams Eng. J. 12, 1973–1984. https://doi.org/10.1016/j.asej.2021.01.006
Salah Hilo Mohammed Al-Attwani, Mustafa Teke, Ethar Sulaiman Yaseen Yaseen, Enes Bektaş, Nurettin Gökşenli, 2024. Enhancing Buck-Boost Converter Efficiency and Dynamic Responses with Sliding Mode Control Technique. J. Tech. 6, 48–57. https://doi.org/10.51173/jt.v6i2.2530
Sharma, S., Chauhan, B.K., Saxena, N.K., 2023. Artificial Neural Network Grid-Connected MPPT-Based Techniques for Hybrid PV-WIND with Battery Energy Storage System. J. Inst. Eng. India Ser. B 104, 1217–1226. https://doi.org/10.1007/s40031-023-00922-y
Sheik Mohammed, S., Devaraj, D., Imthias Ahamed, T.P., 2016. A novel hybrid Maximum Power Point Tracking Technique using Perturb & Observe algorithm and Learning Automata for solar PV system. Energy 112, 1096–1106. https://doi.org/10.1016/j.energy.2016.07.024
Solihin, M.I., Tack, L.F., Kean, M.L., 2011. Tuning of PID Controller Using Particle Swarm Optimization (PSO). Int. J. Adv. Sci. Eng. Inf. Technol. 1, 458. https://doi.org/10.18517/ijaseit.1.4.93
Sulthan, S.M., D., D., B., S.R., O., M.M., Raj, V., 2023. Development and analysis of a Two stage Hybrid MPPT algorithm for solar PV systems. Energy Rep. 9, 1502–1512. https://doi.org/10.1016/j.egyr.2023.07.006
Villegas-Mier, C.G., Rodriguez-Resendiz, J., Álvarez-Alvarado, J.M., Rodriguez-Resendiz, H., Herrera-Navarro, A.M., Rodríguez-Abreo, O., 2021. Artificial Neural Networks in MPPT Algorithms for Optimization of Photovoltaic Power Systems: A Review. Micromachines 12, 1260. https://doi.org/10.3390/mi12101260
Viswambaran, V.K., Anjana, K.V., Zhou, E., Ghani, A., 2017. Performance analysis of FPGA based maximum power point tracking algorithms for photovoltaic applications, in: 2017 International Conference on Electrical and Computing Technologies and Applications (ICECTA)., IEEE, Ras Al Khaimah, pp. 1–4. https://doi.org/10.1109/ICECTA.2017.8252054
Wang, C.-C., Wu, M.-C., Ou, S.-Y., Lin, K.-J., Lin, C.-R., 2010. Analysis and research on maximum power point tracking of photovoltaic array with Fuzzy Logic Control and Three-point Weight Comparison Method. Sci. China Technol. Sci. 53, 2183–2189. https://doi.org/10.1007/s11431-010-4024-2
Wang, L., Luo, Y., Yan, H., 2023. Ant colony optimization-based adjusted PID parameters: a proposed method. PeerJ Comput. Sci. 9, e1660. https://doi.org/10.7717/peerj-cs.1660
Weixiang, S., Hoong, C.F., Peng, W., Chiang, L.P., Yang, K.S., 2011. Development of a mathematical model for solar module in photovoltaic systems, in: 2011 6th IEEE Conference on Industrial Electronics and Applications. Presented at the 2011 6th IEEE Conference on Industrial Electronics and Applications (ICIEA), IEEE, Beijing, China, pp. 2056–2061. https://doi.org/10.1109/ICIEA.2011.5975931
Yin, Z., Du, C., Liu, J., Sun, X., Zhong, Y., 2018. Research on Autodisturbance-Rejection Control of Induction Motors Based on an Ant Colony Optimization Algorithm. IEEE Trans. Ind. Electron. 65, 3077–3094. https://doi.org/10.1109/TIE.2017.2751008
Yuvarajan, S., Shanguang Xu, 2003. Photo-voltaic power converter with a simple maximum-power-point-tracker, in: Proceedings of the 2003 International Symposium on Circuits and Systems, 2003. ISCAS '03. Presented at the ISCAS 2003. International Symposium on Circuits and Systems, IEEE, Bangkok, Thailand, p. III-399-III–402. https://doi.org/10.1109/ISCAS.2003.1205040
Zečević, Ž., Rolevski, M., 2020. Neural Network Approach to MPPT Control and Irradiance Estimation. Appl. Sci. 10, 5051. https://doi.org/10.3390/app10155051

APPENDIX A: MATLAB FUNCTION CODE FOR PO MPPT

```
function[Y,Stage_out,Pold_out]=Perturb_and_Observe_MPPT(P_new,P_old,Delay,Yin,Stag
e_in)
c=0.001;
Pold_out=P_old;
Y=Yin;
Stage_out= Stage_in;
if Delay == 0

if Stage_in==0
if P_new>P_old
Y=Yin+c;
Pold_out=P_new;
elseif P_new<P_old
Y=Yin-c;
Stage_out=1;
Pold_out=P_new;
end
Pold_out=P_new;
end

if Stage_in==1
if P_new>P_old
Y=Yin-c;
Pold_out=P_new;
elseif P_new<P_old
Y=Yin+c;
Stage_out=0;
Pold_out=P_new;
end
Pold_out=P_new;
end

end
```

APPENDIX B: MATLAB FUNCTION CODE FOR PSO MPPT

```
function D = PSO(Vpv, Ipv)

persistent u;
persistent dcurrent;
persistent pbest;
persistent p;
persistent dc;
persistent v;
persistent counter;
persistent gbest;
%initialisation
if(isempty(counter))
    counter = 0;
    dcurrent = 0.5;
    gbest = 0.5;
    p = zeros(3, 1);
    v = zeros(3, 1);
    pbest = zeros(3, 1);
    u=0;
    dc=zeros(3, 1);
    %initial dc for each particle
    dc(1) = 0.2;
    dc(2) =0.4;
    dc(3) = 0.7;
end
%at the 1st time counter=0 is ignored
%delay
if(counter>=1 && counter<300)
    D=dcurrent;
    counter=counter+1;
    return;% return control to the invoking function before it reaches the end of
the function
end
counter=0;% reset counter
% calculate the fitness function (power) of each particle,
% then compare the current value of the function with the previous,
% if the current value is better than the previous. update the value,
%Note: at the first time. this is ignored (u=0)
if(u>=1) && u<=3
    if((Vpv*Ipv)>p(u))
        p(u)=Vpv*Ipv;
        pbest(u)=dcurrent;
    end
end
u=u+1;
% At first, this is excuted because it consists of the condition..
% u==0 initial value of u
if(u==5)
    u=1;
end
if(u==1)
    D=dc(u);
    dcurrent=D;
    counter=1;
    return;
elseif(u==2)
    D=dc(u);
    dcurrent=D;
    counter = 1;
    return;
```

```
elseif(u==3)
    D=dc(u);
    dcurrent=D;
    counter=1;
    return;
elseif(u==4)
    [m,i]=max(p);%finds the indices of the maximum values of P (max power) and
returns them in output vector i
    gbest=pbest(i); % finds the location(duty) of the particle which has max P
    D=gbest;
    dcurrent=D;
    counter=1;
    %update velocity and duty cycle
    v(1)=updatevelocity(v(1),pbest(1),dc(1),gbest)
    v(2)=updatevelocity(v(2),pbest(3),dc(2),gbest)
    v(3)=updatevelocity(v(3),pbest(3),dc(3),gbest)
    %update dutycycle
    dc(1)=updateduty(dc(1),v(1))
    dc(2)=updateduty(dc(2),v(2))
    dc(3)=updateduty(dc(3),v(3))
    return;

else %if u==0
    D=0.1;
end
end

function vfinal=updatevelocity(velocity,pobest,d,gwbest)
%PSO parameters
w=0.4;
c1=1.2;
c2=2;

vfinal = (w*velocity)+(c1*rand(1)*(pobest-d))+(c2*rand(1)*(gwbest-d));
end
function dfinal=updateduty(d,velocity)
dup=d+velocity;
if(dup>1)
    dfinal=1;
elseif(dup<0)
    dfinal=0;
else
    dfinal=dup;
end
end
```

APPENDIX C: MATLAB FUNCTION CODE FOR HYBRID PSO MPPT

```
function D = Hybrid_PSO_PandO(Vpv, Ipv)

persistent u;
persistent dcurrent;
persistent pbest;
persistent p;
persistent dc;
persistent v;
persistent counter;
persistent gbest;
persistent P_old;
persistent stage;
target_voltage = 5.0;  % Desired output voltage
epsilon = 1e-6;  % Small value to prevent division by zero

% Initialize D to a default value
D = 0.5;  % You can choose an appropriate initial value for D

% Initializations (similar to the original PSO code)
if(isempty(counter))
    counter = 0;
    dcurrent = 0.5;
    gbest = 0.5;
    p = zeros(3, 1);
    v = zeros(3, 1);
    pbest = zeros(3, 1);
    u = 0;
    dc = zeros(3, 1);
    P_old = 0;
    stage = 0;
    % Initial dc for each particle
    dc(1) = 0.2;
    dc(2) = 0.4;
    dc(3) = 0.7;
end

% Delay Logic
if(counter >= 1 && counter < 300)
    D = dcurrent;
    counter = counter + 1;
    return;
end
counter = 0;

% Calculate the current power and the error from the target voltage
P_new = Vpv * Ipv;
Vout = Vpv;  % Assume Vout is calculated from the boost converter
error = abs(Vout - target_voltage);
fitness_value = 1 / (error + epsilon);  % Fitness value based on closeness to 5V

% Hybrid Decision: Fine-tune with P&O or explore with PSO
if error < 0.01  % Small error -> Use P&O
    [D, stage, P_old] = Perturb_and_Observe_MPPT(P_new, P_old, 0, dcurrent,
stage);
else  % Larger error -> Use PSO
    if u >= 1 && u <= 3
        if fitness_value > p(u)  % Use fitness_value instead of raw power
            p(u) = fitness_value;
            pbest(u) = dcurrent;
```

```
        end
    end
    u = u + 1;

    if u == 5
        u = 1;
    end

    if u <= 3
        D = dc(u);
        dcurrent = D;
        counter = 1;
        return;
    elseif u == 4
        [m, i] = max(p);
        gbest = pbest(i);
        D = gbest;
        dcurrent = D;
        counter = 1;

        % Update velocity and duty cycle
        for j = 1:3
            v(j) = updatevelocity(v(j), pbest(j), dc(j), gbest);
            dc(j) = updateduty(dc(j), v(j));
        end
        return;
    end
end

% Update the previous power value
P_old = P_new;

end

function vfinal = updatevelocity(velocity, pobest, d, gwbest)
% PSO parameters
w = 0.4;
c1 = 1.2;
c2 = 2;
vfinal = (w * velocity) + (c1 * rand(1) * (pobest - d)) + (c2 * rand(1) * (gwbest
- d));
end

function dfinal = updateduty(d, velocity)
dup = d + velocity;
if(dup > 1)
    dfinal = 1;
elseif(dup < 0)
    dfinal = 0;
else
    dfinal = dup;
end
end

% Definition of the Perturb and Observe function
function [Y, Stage_out, Pold_out] = Perturb_and_Observe_MPPT(P_new, P_old, Delay,
Yin, Stage_in)
c = 0.001;
Pold_out = P_old;
Y = Yin;
Stage_out = Stage_in;
```

```
if Delay == 0
    if Stage_in == 0
        if P_new > P_old
            Y = Yin + c;
            Pold_out = P_new;
        elseif P_new < P_old
            Y = Yin - c;
            Stage_out = 1;
            Pold_out = P_new;
        end
    end

    if Stage_in == 1
        if P_new > P_old
            Y = Yin - c;
            Pold_out = P_new;
        elseif P_new < P_old
            Y = Yin + c;
            Stage_out = 0;
            Pold_out = P_new;
        end
    end
end
end
```

APPENDIX D: MATLAB CODE GA-TUNED PID CONTROLLER FOR BOOST CONVERTER CLOSED-LOOP TRANSFER FUNCTION PLANT

```
clear all
close all
clc

% GA Parameters
nVar = 3;                   % number of variables (Kp, Ki, Kd)
ub = [1000 1000 1000];      % upper Bound
lb = [0 0 0];               % lower bound
popSize = 50;               % population size
maxGenerations = 50;        % maximum number of generations
crossRate = 0.8;            % crossover rate
mutRate = 0.1;              % mutation rate

% Objective function
fobj = @Minie;

% Initialize Population
population = repmat(lb, popSize, 1) + rand(popSize, nVar) .* repmat((ub-lb),
popSize, 1);
fitness = zeros(popSize, 1);

% Main Loop
for gen = 1:maxGenerations

    % Evaluate Fitness
    for i = 1:popSize
        fitness(i) = fobj(population(i, :));
    end

    % Selection
    [~, idx] = sort(fitness);
    population = population(idx, :);
    fitness = fitness(idx);

    newPopulation = population;

    % Crossover
    for i = 1:2:popSize
        if rand < crossRate
            parent1 = population(i, :);
            parent2 = population(i+1, :);

            crossPoint = randi([1, nVar-1]);

            offspring1 = [parent1(1:crossPoint) parent2(crossPoint+1:end)];
            offspring2 = [parent2(1:crossPoint) parent1(crossPoint+1:end)];

            newPopulation(i, :) = offspring1;
            newPopulation(i+1, :) = offspring2;
        end
    end

    % Mutation
    for i = 1:popSize
        if rand < mutRate
            mutationPoint = randi([1, nVar]);
            newPopulation(i, mutationPoint) = lb(mutationPoint) + rand *
(ub(mutationPoint) - lb(mutationPoint));
```

```
        end
    end

    % Evaluate New Population Fitness
    for i = 1:popSize
        fitness(i) = fobj(newPopulation(i, :));
    end

    % Replace Population
    [~, idx] = sort(fitness);
    population = newPopulation(idx, :);
    fitness = fitness(idx);

    % Display Best Fitness
    disp(['Generation# ' num2str(gen) ' Best Fitness = ' num2str(fitness(1))]);

end

% Best Solution
bestSolution = population(1, :);
disp(['Best Solution: Kp = ' num2str(bestSolution(1)) ', Ki = '
num2str(bestSolution(2)) ', Kd = ' num2str(bestSolution(3))]);

% Assign the best PID parameters to the base workspace
assignin('base', 'Kp', bestSolution(1));
assignin('base', 'Ki', bestSolution(2));
assignin('base', 'Kd', bestSolution(3));

% Apply the best PID parameters to the Simulink model
% Assuming the model uses 'Kp', 'Ki', and 'Kd' from the base workspace
sim('GA_Tuned_PID_Boost_C');

% Plot Fitness Curve
plot(fitness);
xlabel('Generation');
ylabel('Fitness');

% Objective Function (ITAE)
function cost = Minie(k)
    assignin('base', 'k', k);
    simOut = sim('GA_Tuned_PID_Boost_C');  % Simulate the model and capture the
output
    ITAE_ts = simOut.get('ITAE');  % Retrieve the ITAE timeseries object from the
simulation output

    % Check if ITAE_ts is not empty and a timeseries object
    if isa(ITAE_ts, 'timeseries') && ~isempty(ITAE_ts.Data)
        ITAE = ITAE_ts.Data;  % Extract the data from the timeseries object
        cost = ITAE(end);  % Assuming ITAE is a vector, take the final value
    else
        cost = inf;  % Assign a high cost if the ITAE is not available or empty
    end
end
```

APPENDIX E: MATLAB CODE PSO-TUNED PID CONTROLLER FOR BOOST CONVERTER CLOSED-LOOP TRANSFER FUNCTION PLANT

```
clear all
close all
clc

% Define the details of the table design problem
nVar = 3;                  % number of variables
ub = [1000 1000 1000]; %upper Bound
lb = [0 0 0];              % lower bound
fobj = @tunning2;          % Objective function Name

% Define the PSO's parameters
noP = 50;                   % number of particles for initialization
maxIter = 50;              % maximum iterations
wMax = 1;
wMin = 0.1;
c1 = 2;
c2 = 2;
vMax = (ub - lb) .* 0.2;
vMin  = -vMax;

% The PSO algorithm

% Initialize the particles
for k = 1 : noP
    Swarm.Particles(k).X = (ub-lb) .* rand(1, nVar) + lb;
    Swarm.Particles(k).V = zeros(1, nVar);
    Swarm.Particles(k).PBEST.X = zeros(1, nVar);
    Swarm.Particles(k).PBEST.O = inf;

    Swarm.GBEST.X = zeros(1, nVar);
    Swarm.GBEST.O = inf;
end

% Main loop
for t = 1 : maxIter

    % Calculate the objective value
    for k = 1 : noP
        currentX = Swarm.Particles(k).X;
        Swarm.Particles(k).O = fobj(currentX);

        % Update the PBEST
        if Swarm.Particles(k).O < Swarm.Particles(k).PBEST.O
            Swarm.Particles(k).PBEST.X = currentX;
            Swarm.Particles(k).PBEST.O = Swarm.Particles(k).O;
        end

        % Update the GBEST
        if Swarm.Particles(k).O < Swarm.GBEST.O
            Swarm.GBEST.X = currentX;
            Swarm.GBEST.O = Swarm.Particles(k).O;
        end
    end

    % Update the X and V vectors
    w = wMax - t .* ((wMax - wMin) / maxIter);

    for k = 1 : noP
```

```
        Swarm.Particles(k).V = w .* Swarm.Particles(k).V + c1 .* rand(1, nVar) .*
(Swarm.Particles(k).PBEST.X - Swarm.Particles(k).X) ...

+ c2 .* rand(1, nVar) .* (Swarm.GBEST.X - Swarm.Particles(k).X);

        % Check velocities
        index1 = find(Swarm.Particles(k).V > vMax);
        index2 = find(Swarm.Particles(k).V < vMin);

        Swarm.Particles(k).V(index1) = vMax(index1);
        Swarm.Particles(k).V(index2) = vMin(index2);

        Swarm.Particles(k).X = Swarm.Particles(k).X + Swarm.Particles(k).V;

        % Check positions
        index1 = find(Swarm.Particles(k).X > ub);
        index2 = find(Swarm.Particles(k).X < lb);

        Swarm.Particles(k).X(index1) = ub(index1);
        Swarm.Particles(k).X(index2) = lb(index2);
    end

    outmsg = ['Iteration# ', num2str(t) , ' Swarm.GBEST.O = ' ,
num2str(Swarm.GBEST.O)];
    disp(outmsg);

    cgCurve(t) = Swarm.GBEST.O;
end

% Display the best PID parameters found
disp('Best PID parameters found:');
disp(['Kp: ', num2str(Swarm.GBEST.X(1))]);
disp(['Ki: ', num2str(Swarm.GBEST.X(2))]);
disp(['Kd: ', num2str(Swarm.GBEST.X(3))]);

semilogy(cgCurve);
xlabel('Iteration#')
ylabel('Weight')

% Objective function
function cost = tunning2(P)
    assignin('base', 'P', P);
    simOut = sim('PSO_Tuned_PID_Boost_C.slx');
    ITAE = simOut.get('ITAE');
    if isa(ITAE, 'timeseries') && ~isempty(ITAE.Data)
        cost = ITAE.Data(end);
    else
        cost = inf; % Assign a high cost if ITAE is not available
    end
end
```